

JAERI - M
92-159

ANNUAL REPORT OF NAKA FUSION RESEARCH ESTABLISHMENT
FOR THE PERIOD OF APRIL 1, 1991 TO MARCH 31, 1992

October 1992

Naka Fusion Research Establishment

JAERI-M レポートは、日本原子力研究所が不定期に公刊している研究報告書です。

入手の問合わせは、日本原子力研究所技術情報部情報資料課（〒319-11茨城県那珂郡東海村）あて、お申しこしてください。なお、このほかに財団法人原子力弘済会資料センター（〒319-11 茨城県那珂郡東海村日本原子力研究所内）で複写による実費頒布をおこなっております。

JAERI-M reports are issued irregularly.

Inquiries about availability of the reports should be addressed to Information Division, Department of Technical Information, Japan Atomic Energy Research Institute, Tokai-mura, Naka-gun, Ibaraki-ken 319-11, Japan.

© Japan Atomic Energy Research Institute, 1992

編集兼発行 日本原子力研究所
印刷 (株)原子力資料サービス

Annual Report of Naka Fusion Research Establishment
for the period of April 1, 1991 to March 31, 1992

Naka Fusion Research Establishment
Japan Atomic Energy Research Institute
Naka-machi, Naka-gun, Ibaraki-ken

(Received October 1, 1992)

Research and development activities at Naka Fusion Research Establishment, JAERI, are reported for the period from April 1, 1991 to March 31, 1992.

JT-60 Upgrade (JT-60U) experiment was commenced in March 1991. After four months in July, deuterium operation was started, and the heating power of perpendicular neutral beams reached 22 MW in August. JT-60 was operated without any serious machine trouble after the upgrading modification. Well controlled equilibrium in the diverted configuration was successfully achieved for $I_p \leq 5$ MA by discharge optimization of elongated plasmas. In JFT-2M, major efforts were put on experiments with intensive divertor biasing and ergodic magnetic limiter. The DIII-D cooperative program was highlighted improved H-mode obtained in boronized-wall experiments.

Concerning theoretical and computational studies, effort was focused on the analyses of the ion temperature gradient mode, MHD relating to the bootstrap current and beta optimization, the MHD mode locking phenomena, and burning plasma characteristics.

As for fusion engineering research, development activities of ceramic turbo-viscous pump and high-resolution mass spectrometer were remarked in the vacuum technology area. High heat flux experiments were carried out with JAERI Electron Beam Irradiation Stand (JEBIS) and Particle Beam Engineering Facility (PBEF), in order to develop plasma facing components. Concerning plasma heating technologies, much effort was devoted to the development of negative ion sources especially on long pulse operation, high energy acceleration and beam optics. The first oscillating test of a 100 GHz-band gyrotron was done using JAERI Gyrotron Test Facility. Major achievements in the superconducting magnet technology were the attainment of high current density of 40 A/mm² in the Demo Poloidal Coil and the successful operation of a hollow-type conductor up to 30 kA at 3 T. Good progress in the development of Nb₃Sn and Nb₃Al strands was also obtained. Concerning the tritium technology, a fuel cleanup system developed and designed by JAERI, was successfully operated with other TSTA components under the joint work with TSTA at LANL. Experiments at Tritium Processing Laboratory were also advanced. R and D activities of reactor structure and blanket technology were performed on design works of ITER and FER.

With the ITER Conceptual Design Activities completed in December 1990, the feasible design concept and the future R and D programs on ITER were successfully developed. Before starting the next-step of ITER, Engineering Design Activities (EDA), Japanese scientific and technical review was finished. Design study of FER was continued in parallel with its related R and D.

Keywords: Fusion Research, JAERI, JT-60U, JFT-2M, DIII-D, Plasma Physics, Fusion Engineering, ITER, FER, Fusion Reactor Design, Annual Report

那珂研究所年報（平成3年度）

日本原子力研究所
那珂研究所

（1992年10月1日受理）

原研・那珂研究所における平成3年度（1991年4月～1992年3月）の研究開発活動について報告する。

改造後のJT-60（JT-60U）実験が、1991年3月開始された。その4ヶ月後の7月には重水素運転がスタートし、8月に垂直入射の中性粒子加熱のパワーが22MWに達した。改造後のJT-60は、重大な装置トラブルもなく稼働した。楕円形プラズマの放電最適化によって、 $I_p \leq 5\text{MA}$ のダイバータ配位において首良く制御された平衡配位を成功裡に達成した。JFT-2Mでは、強いダイバータ・バイアス及びエルゴテック磁気リミターを中心とした実験が行れた。DIII-D協力計画のハイライトは、ボロン化壁実験で得た改良Hモードであった。

理論解析に関する研究では、イオン温度勾配モード、ブートストラップやベータ値最適化に係わるMHD、MHDのモード・ロック現象、及び核燃焼プラズマの特性に関する解析が行れた。

核融合工学の研究に関しては、真空技術の分野でセラミック・ターボ型粗引きポンプと高分解質量分析器の開発が進展した。プラズマ対向機器の開発のために、電子ビーム照射スタンド（JEBS）及び粒子ビーム工学設備（PBEF）を用いた高熱負荷試験が行れた。プラズマ加熱技術では、長パルス運転、高エネルギー加速、及びビーム光学について負イオン源の開発に力を注いだ。また、100GHz帯ジャイロトロン最初の発振テストが、原研ジャイロトロン試験設備を用いて行れた。超電導磁石技術の開発では、実証ボロイダルコイルにおける 40A/mm^2 の高電流密度、及びホロー型導体における3T・30kAの稼働成功が主な成果であった。また、 Nb_3Sn や Nb_3Al 線の開発についても進展を見た。トリチウム技術の開発においては、原研で開発・設計した燃料精製システムが、LANLのTSTAとの協同作業のもとに、TSTAの他機器と共に首尾良く稼働した。また、トリチウム・プロセス棟における実験も進展した。ITERやFERの設計に関して、炉構造及びブランケット工学の研究開発が行れた。

1990年12月に終了したITERの概念設計活動によって、ITERの設計概念及び今後の研究開発計画が首尾良く進展した。ITERの次段階、工学設計活動の開始に先立って、国内の科学技術的レビューを終了した。FERの設計研究を、関連する研究開発と併行して継続した。

FOREWORD

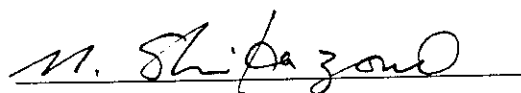
The past fiscal year has brought significant progress in many areas of JAERI Fusion Program.

JT-60 Upgrade (JT-60U) experiment was commenced in March 1991. After four months in July, deuterium operation was started. Well controlled equilibrium in the diverted configuration was successfully achieved for $I_p \leq 5$ MA by discharge optimization of elongated plasmas. The JFT-2M and DIII-D programs were highlighted by the study on confinement properties with divertor biasing and improved H-modes.

With the Conceptual Design Activities, the feasible design concept and the future research and development programs on ITER were successfully developed. JAERI has made many contributions to the program with a conviction that international integration of fusion research and development is essential and ITER can serve as a central project for the next step of fusion research and development.

Continued efforts were laid on the research and development of fusion technologies including superconducting magnet, plasma heating, vacuum technology, tritium handling, high heat flux technology, reactor structure, and blanket technology.

The development of thermonuclear fusion as an energy source is a central element of a national and international energy strategy. With increasing recognition of environmental issues, the features of a fusion power source are even more attractive.



N. Shikazono

Director General

Naka Fusion Research Establishment

JAERI

Contents

I. JT-60 PROGRAM	1
1. Overview	1
2. Operation of JT-60U	2
2.1 Tokamak	2
2.1.1 Operation results of machine components	2
2.1.2 Operation results of plasma facing components	5
2.2 Control system	5
2.2.1 Plasma Control	5
2.2.2 Interlock system for deuterium operation	8
2.2.3 Man/machine interface	8
2.3 Power supply	9
2.4 Neutral Beam Injection System(NBI system)	10
2.5 Radio-frequency system	11
2.5.1 LHCD system	11
2.5.2 ICRF Heating System	12
2.6 Diagnostic systems	14
2.6.1 Neutron yield monitor and its calibration	14
2.6.2 X-ray Crystal Spectrometer	16
2.6.3 Hard X-ray pulse height analysis	17
2.6.4 CO ₂ Laser Interferometer	18
3. Experimental Results and Analysis	19
3.1 Plasma Control and Disruptions	19
3.1.1 Plasma Configuration Control	19
3.1.2 Eddy Current	19
3.1.3 Vertical Stability	20
3.1.4 Plasma Current Ramp-up and Ramp-down	20
3.1.5 MARFE and Detached Plasma	21
3.1.6 Current Quench and Vibration of the Vacuum Vessel in Disruptions	21
3.2 Energy Confinement Properties in Ohmic, L-mode and H-mode	22
3.2.1 Ohmic Confinement	22
3.2.2 L-mode Confinement at High Aspect Ratio	22
3.2.3 Effect of Current Profile on L-mode Confinement	22
3.2.4 Isotope Dependence of L-mode Confinement	23
3.2.5 H-mode Threshold and Confinement	23
3.3 High Poloidal-Beta Confinement	24
3.4 Transport and MHD Studies	26
3.5 Impurity and Divertor Characteristics	28
3.6 Fast ion studies	30
3.6.1 D-D fusion reactivity	30
3.6.2 Fast ion loss by toroidal ripple	30
3.6.3 Triton burnup experiment	31
3.7 LHRF and ICRF Experiments	32
3.7.1 Lower Hybrid Current Drive Experiment	32
3.7.2 ICRF Experiment	33
3.8 Development of Fusion Plasma Analysis Codes	34

3.8.1	Profile Data Handling Code System : SLICE	34
3.8.2	1 1/2 Tokamak Transport Code System : TOPICS	34
3.8.3	Orbit-Following Monte Carlo Code: OFMC	34
3.8.4	Full Equilibrium Identification Code : FEI	35
3.8.5	Current Drive Analysis Code: ACCOME	35
3.8.6	Source Program Organization Tool : SPOT	35
4.	Related Developments and Maintenance	36
4.1	Developments and evaluation tests of B ₄ C-overlaid CFC/graphite	36
4.2	Glow Discharge Cleaning (GDC) System	37
4.3	Related Development in Power supply	38
4.4	Design study of a negative-ion based NBI system for JT-60U	39
4.5	RF development	40
4.5.1	Development of the launcher in LHCD system	40
4.5.2	Analysis of cryogenic window for electron cyclotron heating system	41
II.	JFT-2M PROGRAM	43
1.	Toroidal Confinement Experiments	43
1.1	Overview	43
1.2	Experimental results	43
1.2.1	H-mode studies	43
1.2.2	Divertor biasing experiments	45
1.2.3	Disruption control with EML coils	46
1.2.4	Disruption control with ECH	46
2.	Operation and Maintenance	47
2.1	Introduction	47
2.2	Operation and maintenance	47
2.3	Development of equipments and instruments	47
III.	PLASMA THEORY AND COMPUTATION	49
1.	Introduction	49
2.	Analyses of Confinement and Heating Processes	49
2.1	Confinement scaling for thermal energy in JT-60 L-mode plasmas	49
2.2	Neoclassical theory of fast ions with isotropic velocity distribution function	49
2.3	Ion temperature gradient modes in the neoclassical regime	50
2.4	Particle simulation of the ITG mode in a plasma of a flat density profile	50
2.5	Fast ion transport during ICRF heating	51
2.6	Three dimensional FEL simulation with space-charge effects	51
2.7	Multi-frequency simulation of cyclotron auto-resonance maser (CARM)	52
2.8	Non-canonical Lie perturbation analysis of electron motion in a planar wiggler magnetic field	53
3.	MHD Equilibrium and Stability Analyses	53
3.1	Bootstrap current profiles and scaling in large aspect ratio tokamak	53
3.2	Beta limit and bootstrap current for small aspect ratio tokamak equilibria	53
3.3	Effects of hollow current profiles on the ideal MHD stabilities in high- b_p plasmas	54
3.4	Axisymmetric tokamak simulation by using the TSC code	54

3.5	Comparison of positional instability analyses by TSC and rigid model codes	55
3.6	Velocity shear stabilization of magnetic island in tokamak	55
3.7	Effect of external helical field on rotating magnetic island	56
4.	Analyses of Burning Plasma in Tokamaks	56
4.1	Fusion yield in high-power D-beam injected ^3He plasmas	56
4.2	Effects of spatial diffusion and direct loss on burnup fractions of fast ions	57
4.3	Alpha particle dynamics during the internal disruption	57
4.4	Ripple loss of alpha particles in tokamak reactor with non-circular plasma cross-section	58
5.	Development of Numerical Codes and Plasma Simulator	58
5.1	Numerical experiment of the equilibrium code SELENEJ	58
5.2	Computation of the vacuum magnetic field energy with an arbitrary boundary shape	58
	in the ideal MHD principle	58
5.3	Development of one-dimensional relativistic particle simulation code	59
5.4	Development of toroidal particle code (TPC)	59
5.5	Development of plasma simulator METIS	59
IV.	COOPERATIVE PROGRAM ON DIII-D (Doublet III) Experiment	60
1.	Introduction	60
2.	Highlights of FY1991 research results	60
3.	JAERI collaboration	62
V.	TECHNOLOGY DEVELOPMENT	63
1.	Vacuum Technology and Fuel Injection	63
1.1	Introduction	63
1.2	Progress in ceramic vacuum pump development	63
1.3	Improvement of quadrupole mass spectrometer (QMS)	64
	1.3.1 High resolution QMS using conditions of second stability zone in Mathieu diagram	64
	1.3.2 Fabrication of ceramic quadrupole structure	65
1.4	Large-area Al_2O_3 coatings for ITER in-vessel components	66
1.5	Design of rail-gun system for high-speed fuel pellet injection	67
2.	Superconducting Magnet Development	68
2.1	Introduction	68
2.2	The Demo Poloidal Coil program	68
	2.2.1 Project status	68
	2.2.2 The DPC-TJ experiment	69
2.3	Proto Toroidal Coil project	71
	2.3.1 Development of the Toroidal Model Pancake (TMP) for ITER/FER Toroidal Field Coils	71
	2.3.2 Nb_3Al conductor development	72
2.4	R&D for ITER	74
	2.4.1 Development of super conducting conductor for the central solenoid coil	74
	2.4.2 Cryogenic system for common test facility	75
	2.4.3 Development of Titanium Conduit Conductor	77

3. Beam Technology	78
3.1 Introduction	78
3.2 Negative ion beam technology	78
3.2.1 Long pulse operation	78
3.2.2 High energy acceleration of H^- ions	79
3.2.3 H^- beam optics study	80
3.2.4 D^- production in the joint CEA-JAERI experiment	81
3.2.5 Neutralization and energy recovery experiments of H^-/D^- beam	81
3.3 Application of high current ion beam technology	81
3.3.1 RF plasma generator	81
3.3.2 Development of a high brightness ion source for the proton linear Accelerator	82
3.4 Large scale cryo-sorption pump	82
4. RF Technology	82
4.1 Introduction	82
4.2 Development of the LHRF launcher	82
4.3 Investigation of high power gyrotron and ECH components	83
4.4 Millimeter wave Free Electron Laser	83
4.5 Design study of RF heating and current drive launcher for ITER	85
5. Tritium Technology	85
5.1 Introduction	85
5.2 Development of fuel processing technology under JAERI-LANL(DOE)	86
5.3 Development of tritium processing in TPL (Tritium Process Laboratory)	87
5.3.1 Fuel cleanup	87
5.3.2 Hydrogen isotope separation	88
5.3.3 Tritium analysis and measurement	89
5.3.4 Tritium-materials interaction	89
5.4 Development of tritium safe handling technology	90
5.4.1 Development of tritium confinement using gas separation membrane	90
5.4.2 Development of metal getter(ZrCo) type transport package of tritium	91
5.4.3 Operation of tritium safety systems	92
5.5 Tritium system analysis	92
6. High heat flux technology	93
6.1 Introduction	93
6.2 Activities on divertor plate development	93
6.2.1 Thermal cycling experiments on divertor mock-ups	93
6.2.2 Thermo-hydraulics of the cooling structures	94
6.3 Development of a first wall	96
6.4 Study of plasma surface interaction	96
7. Reactor Structure Development	97
7.1 Introduction	97
7.2 R&D activities for reactor structure	97
7.3 R&D activities for remote maintenance	98

8. Blanket Technology	99
8.1 Introduction	99
8.2 Material-Related R&D	99
8.2.1 Thermo-mechanical durability	99
8.2.2 Material Compatibility	100
8.3 Out-of reactor testing	101
8.4 Design of tritium breeding blanket	102
VI. NEXT STEP FOR JAERI TOKAMAK PROGRAM	104
1. International Thermonuclear Experimental Reactor (ITER)	104
1.1 Introduction	104
1.2 ITER CDA review	104
1.3 ITER Engineering Design Activities (EDA)	106
1.3.1 Physics R&D	106
1.3.2 Technology R&D	107
2. Fusion Experimental Reactor (FER)	108
2.1 Role of FER and ITER	108
2.2 FER Design	110
3. Fusion Reactor Design	110
3.1 Introduction	110
3.2 Steady State Tokamak Reactor (SSTR) Design	111
3.3 Safety Analyses	112
APPENDICES	113
A.1 Publication List	113
A.2 Personnel and Financial Data	124
A.2.1 Change in number of personnel and budget (FY1986-1991)	124
A.2.2 Organization chart (March 31, 1992)	124
A.2.3 Scientific staffs in the Naka Fusion Research Establishment (March 31, 1992)	125

目 次

1. JT-60計画	1
1. 概要	1
2. JT-60の運転	2
2.1 トカマク装置本体	2
2.1.1 主要構成機器の運転結果	2
2.1.2 プラズマ対向機器の運転結果	5
2.2 制御システム	5
2.2.1 プラズマ制御	5
2.2.2 重水素運転のためのインターロックシステム	8
2.2.3 マンマシンインターフェース	8
2.3 電源	9
2.4 中性粒子入射装置	10
2.5 高周波加熱装置	11
2.5.1 LHCDシステム	11
2.5.2 ICRFシステム	12
2.6 計測装置	14
2.6.1 中性子測定装置とその較正	14
2.6.2 結晶分光器	16
2.6.3 硬X線測定装置	17
2.6.4 炭酸ガスレーザ干渉計	18
3. 実験結果と解析	19
3.1 プラズマ制御及びディスラプション	19
3.1.1 プラズマ配位の制御	19
3.1.2 渦電流	19
3.1.3 垂直位置安定性	20
3.1.4 プラズマ電流の立ち上げと立ち下げ	20
3.1.5 MARFEとデタッチド-プラズマ	21
3.1.6 ディスラプション時の電流クエンチと真空容器の振動	21
3.2 オーミック、Lモード及びHモードのエネルギー閉じ込め特性	22
3.2.1 オーミック閉じ込め	22
3.2.2 高アスペクト比でのLモード閉じ込め	22
3.2.3 Lモード閉じ込めでの電流分布の効果	22
3.2.4 Lモード閉じ込めでの同位体依存性	23
3.2.5 Hモード-スレッシュールドと閉じ込め	23
3.3 高ボロイダルベータ閉じ込め	24
3.4 輸送とMHD研究	26
3.5 不純物とダイバータ特性	28
3.6 高速イオンの研究	30
3.6.1 D-D核融合反応率	30
3.6.2 トロイダルリップルによる高速イオン損失	30
3.6.3 トリトン燃焼実験	31

3.7	LHRF及びICRF実験.....	3 2
3.7.1	LHCD実験.....	3 2
3.7.2	ICRF実験.....	3 3
3.8	核融合プラズマ解析コードの開発.....	3 4
3.8.1	分布データ処理コードシステム：SLICE.....	3 4
3.8.2	11/2輸送コードシステム：TOPICS.....	3 4
3.8.3	軌道追跡モンテカルロコード：OFMC.....	3 4
3.8.4	MHD平衡同定コード：FEI.....	3 5
3.8.5	電流駆動解析コード：ACCOMME.....	3 5
3.8.6	ソースプログラム編集ツール：SPOT.....	3 5
4.	関連技術開発および大型装置の保守.....	3 6
4.1	B ₄ C被覆CFCグラファイトの開発と評価.....	3 6
4.2	グロー放電洗浄システム.....	3 7
4.3	電源システムにおける関連開発.....	3 8
4.4	JT-60U用負イオンNBIシステムの開発研究.....	3 9
4.5	RF装置の関連開発.....	4 0
4.5.1	LHCDシステム.....	4 0
4.5.2	ECHシステム.....	4 1
II.	JFT-2M計画.....	4 3
1.	閉じ込め実験.....	4 3
1.1	概要.....	4 3
1.2	実験結果.....	4 3
1.2.1	Hモード研究.....	4 3
1.2.2	ダイバータ・バイアス実験.....	4 5
1.2.3	EMLコイルによるディスラプション制御.....	4 6
1.2.4	ECHによるディスラプション制御.....	4 6
2.	運転とメンテナンス.....	4 7
2.1	はじめに.....	4 7
2.2	運転とメンテナンス.....	4 7
2.3	設備・装置の開発.....	4 7
III.	プラズマ理論と計算.....	4 9
1.	はじめに.....	4 9
2.	閉じ込め・加熱過程の解析.....	4 9
2.1	JT-60のLモード・プラズマにおける熱エネルギー閉じ込め比例則.....	4 9
2.2	等方速度分布を持つ高速イオンの新古典理論.....	4 9
2.3	新古典領域でのイオン温度勾配モード.....	5 0
2.4	平坦な密度分布のプラズマ中のITGモードの粒子シミュレーション.....	5 0
2.5	ICRF加熱時の高速イオン輸送.....	5 1
2.6	空間電荷効果を考慮した三次元FELシミュレーション.....	5 1
2.7	サイクロトロン自動共鳴メーザーの多周波シミュレーション.....	5 2

2.8	平面ウイグラー磁場中の電子運動の非正準リー摂動解析.....	53
3.	MHD平衡と安定性解析.....	53
3.1	大アスペクト比トカマクのブートストラップ電流の分布と比例則.....	53
3.2	小アスペクト比トカマク平衡のベータ限界とブートストラップ電流.....	53
3.3	高 b_p プラズマにおける理想MHD安定性に対する中空電流分布の効果.....	54
3.4	TSCコードによる軸対称トカマク・シミュレーション.....	54
3.5	TSCコードと剛体モデルによる位置不安定性解析の比較.....	55
3.6	トカマクの磁気島の速度シアによる安定化.....	55
3.7	回転磁気島に対する外部ヘリカル磁場の影響.....	56
4.	トカマクにおける核燃焼プラズマの解析.....	56
4.1	高パワー重水素ビーム入射 ^3He プラズマにおける核融合出力.....	56
4.2	高速イオンの燃焼率に対する空間拡散及び直接損失効果.....	57
4.3	内部ディスラプション時におけるアルファ粒子運動.....	57
4.4	非円形断面プラズマ核融合炉におけるアルファ粒子リップル損失.....	58
5.	計算コードとプラズマ・シミュレータの開発.....	58
5.1	平衡コードSELENEJの数値実験.....	58
5.2	理想MHD原理の下での任意境界形状真空磁場エネルギー計算.....	58
5.3	一次元相対論的粒子シミュレーション・コード.....	59
5.4	トロイダル粒子コードTPCの開発.....	59
5.5	プラズマ・シミュレータMRTISの開発.....	59
IV.	DIII-D (ダブレットIII) 実験における研究協力計画.....	60
1.	はじめに.....	60
2.	平成3年度研究成果のハイライト.....	60
3.	原研の協力.....	62
V.	技術開発.....	63
1.	真空技術と燃料注入.....	63
1.1	はじめに.....	63
1.2	セラミック真空ポンプ開発の進展.....	63
1.3	四極子質量分析計(QMS)の改良.....	64
1.3.1	マシユー線図の第II安定領域を利用した高分解能QMS.....	64
1.3.2	セラミック四極子構造の試作.....	65
1.4	ITER炉内構造物用大面積アルミナコーティング.....	66
1.5	レーン銃方式の高速燃料ペレット入射システムの設計.....	67
2.	超電導磁石技術.....	68
2.1	はじめに.....	68
2.2	実証ボロイダル・コイル(DPC)計画.....	68
2.2.1	DPC計画の概要.....	68
2.2.2	DPC-TJ実験.....	69

2.3	原型トロイダル・コイル計画.....	71
2.3.1	ITER/FERトロイダル磁場コイル用トロイダル・モデル・ パンケーキ (TMP) の開発.....	71
2.3.2	Nb ₃ Al 導体の開発.....	72
2.4	ITER R&D.....	74
2.4.1	センター・ソレノイド・コイル用超電導体の開発.....	74
2.4.2	共通試験装置用冷凍機.....	75
2.4.3	チタン・コンジット導体の開発.....	77
3.	ビーム技術.....	78
3.1	はじめに.....	78
3.2	負イオンビーム技術.....	78
3.2.1	長パルス負イオン源の開発.....	78
3.2.2	負イオンビームの高エネルギー化.....	79
3.2.3	ビーム収束性の改良.....	80
3.2.4	日仏共同実験による重水素負イオンビームの生成.....	81
3.2.5	荷電粒子回収に関する日仏共同実験.....	81
3.3	大強度イオンビーム応用技術.....	81
3.3.1	RFプラズマ生成.....	81
3.3.2	高輝度イオン源の開発.....	82
3.4	大容量クライオソーブションポンプ.....	82
4.	RF技術.....	82
4.1	はじめに.....	82
4.2	低域混成波帯アンテナの開発.....	82
4.3	大電力ジャイロトロン及び電子サイクロトロン共鳴加熱用部品の研究.....	83
4.4	ミリ波帯自由電子レーザー.....	83
4.5	ITER用高周波加熱及び電流駆動用アンテナの設計.....	85
5.	トリチウム技術.....	85
5.1	はじめに.....	85
5.2	原研-ロスアラモス国立研究所核融合技術協力における燃料システムの開発.....	86
5.3	トリチウムプロセス技術の開発.....	87
5.3.1	燃料精製.....	87
5.3.2	水素同位体分離.....	88
5.3.3	トリチウム計量管理技術.....	89
5.3.4	トリチウム - 材料相互作用.....	89
5.4	トリチウム安全取扱技術の開発.....	90
5.4.1	ガス分離膜によるトリチウム格納技術の開発.....	90
5.4.2	金属ゲッター (ZrCo) 型トリチウム輸送容器の開発.....	91
5.4.3	トリチウム安全システムの運転、操作.....	92
5.5	トリチウムシステム解析.....	92
6.	高熱負荷受熱機器の開発研究.....	93

6.1	はじめに.....	93
6.2	ダイバータ板要素開発.....	93
6.2.1	ダイバータモックアップの熱サイクル試験.....	93
6.2.2	冷却構造における伝熱流動.....	94
6.3	第一壁の開発.....	96
6.4	プラズマ壁相互作用研究.....	96
7.	炉構造開発.....	97
7.1	はじめに.....	97
7.2	炉構造のR&D活動.....	97
7.3	遠隔メンテナンスのR&D活動.....	98
8.	ブランケット技術.....	99
8.1	はじめに.....	99
8.2	材料関連R&D.....	99
8.2.1	熱機械特性試験.....	99
8.2.2	材料共存性.....	100
8.3	アウトパイル(炉外)試験.....	101
8.4	トリチウム増殖ブランケットの設計.....	102
VI.	原研における次期トカマク開発計画.....	104
1.	国際熱核融合実験炉(ITER).....	104
1.1	はじめに.....	104
1.2	ITER CDAレビュー.....	104
1.3	ITER工学設計活動(EDA).....	106
1.3.1	物理R&D.....	106
1.3.2	工学R&D.....	107
2.	核融合実験炉(FER).....	108
2.1	FERとITERの役割.....	108
2.2	FER設計.....	110
3.	核融合炉設計.....	110
3.1	はじめに.....	111
3.2	定常トカマク炉(SSTR)設計.....	112
3.3	安全解析.....	113
付録	113
A.1	論文リスト(1991年4月-1992年3月).....	113
A.2	人員及び予算に関するデータ.....	124
A.2.1	人員及び年間研究開発予算の推移(1986-1991年度).....	124
A.2.2	組織図(1992年3月31日現在).....	124
A.2.3	研究開発スタッフ・リスト(1992年3月31日現在).....	125

I. JT-60 PROGRAM

1. OVERVIEW

Since November 1989, JT-60 had been shut-down for the modification to JT-60 Upgrade named JT-60U. Construction of JT-60U to allow higher plasma current, deuterium operation and higher heating power was completed in March 1991. JT-60U is capable of producing single-null divertor discharges with plasma current of 6 MA, with high power heating and current drive: neutral beam heating power of up to 40 MW, lower hybrid current drive (LHCD) power of up to 10 MW, and ion cyclotron resonance heating (ICRF) power of up to 5 MW. Features of JT-60U are a high aspect ratio (4.0), a high toroidal field (4 T) and divertor plates with beveled edges. From the viewpoint of divertor heat load, 40 MW of heating power in JT-60U corresponds to alpha heating power in ITER, making ITER-relevant experiments feasible. The main objectives of JT-60U experiments are: (1) confinement improvement, (2) impurity control and divertor studies, (3) steady-state studies, and (4) high energy particle confinement. Through the pursuit of these goals, we aim to contribute to the ITER Physics R&D, and provide data essential for concept development of fusion power reactors like SSTR.

Ohmic experiments with hydrogen gas were initiated at the end of March. Optimizations of break-down, current ramp-up and divertor configuration were performed. Multivariable non-interacting control was adopted to allow independent control over the strong mutual coupling between the ohmic heating coils and the vertical field coils. Well controlled divertor discharges were successfully obtained using this method and discharges with plasma current of up to 4 MA were achieved after only 12 days of operation. After testing and developing the scientific and technical capabilities of the diagnostics and the NBI system, deuterium discharges started in July. After the conditioning of NB injection port, experiments of perpendicular NB beams with power of up to 22 MW started in late August. In October, hydrogen discharges were made before an annual vacuum break in November. Discharges with plasma currents of up to 5 MA have been achieved making the perspective of 6 MA discharges. LHCD experiments with input power of 1.8 MW have also been performed emphasizing the physics understanding of the LHCD. During November and December, the following hardware were installed: the new tangential NB beam system with heating power of 12 MW, the ICRF with a frequency range of 110-130 MHz and a power of 5 MW, and the pellet injector. In January 1992, ICRF experiments started.

The main objective of experiments in 1991 was to study the basic performance of JT-60U and the following experiments have been performed: 1) optimization of plasma control, 2) confinement improvement and studies of its characteristics, 3) MHD and disruption studies, 4) impurity control and divertor studies, 5) studies of ripple loss, high energy particle and D-D reaction product, and 6) LHCD and ICRF experiments.

H-mode experiments were performed in the region of $I_p=1-4$ MA, $B_T=1.7-4$ T, $q_{eff}=3-5$ and $P_{NB}=6-22$ MW. Most of the H-mode data published so far from H-mode tokamaks are in low toroidal field (<3 T) except for those with limiter H-mode in JT-60 (LHCD) and TFTR. In JT-60U, clear L- to H-transitions and density/temperature profiles with steep edge gradients were observed in divertor configuration at 4 T. The maximum enhancement factor of H-mode was 1.5 for the non-steady state case and 1.3 for the quasi-steady state case. The causes of this modest improvement in confinement are discussed. The high- q and high- β_p regime with hot ion enhanced confinement was investigated for concept development of steady-state reactors like SSTR. The maximum β_p reached 2.44, the maximum T_i of 20 keV was achieved and τ_E^{dia} was improved to about 2.9 times as large as that of ITER89-P scaling. The maximum neutron rate of 1.3×10^{16} n/s was also obtained in the highest- β_p discharge. The corresponding Q_{DD} and the equivalent Q_{DT} were 8.9×10^{-4} and ~ 0.20 , respectively. Heat load localized in both toroidal and poloidal directions was shown to be in a good agreement for the first time with calculated heat load profile due to ripple trapped particle loss. The divertor heat flux was analyzed to establish a scaling law on the heat flux peaking factor which is the reciprocal of the scrape-off-layer thickness. Achieved values of the first experiment of the JT-60U LHCD in 1991 were $P_{LH}=1.5$ MW, driven current $I_{RF}=2$ MA, current drive efficiency $\eta_{CD} (\equiv \bar{n}_e R_p I_{RF} / P_{LH}) = 0.25 \times 10^{20} \text{ m}^{-2} \text{ A/W}$ and current driven product CDP ($\equiv \bar{n}_e R_p I_{RF}$) = $3 \times 10^{20} \text{ m}^{-2} \text{ MA}$.

2. OPERATION OF JT-60U

2.1 Tokamak

2.1.1 Operation results of machine components

JT-60U started its operation with Taylor discharge cleaning in late March, 1991. It was operated with hydrogen through April to June with one month inspection stop in May. The calibration work for neutron detectors was performed in the first half of July, then the machine started its first deuterium operation from the middle of July to the end of September. In October it is operated by hydrogen and an annual vacuum open is planned at November.

To attain 6 MA plasma, mechanical performances of the tokamak inevitably comes up as one of the major issues. Under a restricted condition for direct measurement in tokamak operation, efforts have been made to obtain displacements of the vacuum vessel, TFC and its support structure.

The new vessel is made of toroidally continuous double skin structure without bellows and it is operated under the baking temperature of 300°C. Displacement measurement was performed when the vessel was at first baked from RT to 300°C. The horizontal displacement of the vessel was found enough homogeneous and that suggests the good sliding property in the vacuum vessel support. Rapid response displacement detectors with laser system are attached on the lower spacer

H-mode experiments were performed in the region of $I_p=1-4$ MA, $B_T=1.7-4$ T, $q_{eff}=3-5$ and $P_{NB}=6-22$ MW. Most of the H-mode data published so far from H-mode tokamaks are in low toroidal field (<3 T) except for those with limiter H-mode in JT-60 (LHCD) and TFTR. In JT-60U, clear L- to H-transitions and density/temperature profiles with steep edge gradients were observed in divertor configuration at 4 T. The maximum enhancement factor of H-mode was 1.5 for the non-steady state case and 1.3 for the quasi-steady state case. The causes of this modest improvement in confinement are discussed. The high- q and high- β_p regime with hot ion enhanced confinement was investigated for concept development of steady-state reactors like SSTR. The maximum β_p reached 2.44, the maximum T_i of 20keV was achieved and τ_E^{dia} was improved to about 2.9 times as large as that of ITER89-P scaling. The maximum neutron rate of 1.3×10^{16} n/s was also obtained in the highest- β_p discharge. The corresponding Q_{DD} and the equivalent Q_{DT} were 8.9×10^{-4} and ~ 0.20 , respectively. Heat load localized in both toroidal and poloidal directions was shown to be in a good agreement for the first time with calculated heat load profile due to ripple trapped particle loss. The divertor heat flux was analyzed to establish a scaling law on the heat flux peaking factor which is the reciprocal of the scrape-off-layer thickness. Achieved values of the first experiment of the JT-60U LHCD in 1991 were $P_{LH}=1.5$ MW, driven current $I_{RF}=2$ MA, current drive efficiency $\eta_{CD} (\equiv \bar{n}_e R_p I_{RF} / P_{LH}) = 0.25 \times 10^{20} \text{ m}^{-2} \text{ A/W}$ and current driven product $CDP (\equiv \bar{n}_e R_p I_{RF}) = 3 \times 10^{20} \text{ m}^{-2} \text{ MA}$.

2. OPERATION OF JT-60U

2.1 Tokamak

2.1.1 Operation results of machine components

JT-60U started its operation with Taylor discharge cleaning in late March, 1991. It was operated with hydrogen through April to June with one month inspection stop in May. The calibration work for neutron detectors was performed in the first half of July, then the machine started its first deuterium operation from the middle of July to the end of September. In October it is operated by hydrogen and an annual vacuum open is planned at November.

To attain 6 MA plasma, mechanical performances of the tokamak inevitably comes up as one of the major issues. Under a restricted condition for direct measurement in tokamak operation, efforts have been made to obtain displacements of the vacuum vessel, TFC and its support structure.

The new vessel is made of toroidally continuous double skin structure without bellows and it is operated under the baking temperature of 300°C. Displacement measurement was performed when the vessel was at first baked from RT to 300°C. The horizontal displacement of the vessel was found enough homogeneous and that suggests the good sliding property in the vacuum vessel support. Rapid response displacement detectors with laser system are attached on the lower spacer

of TFC as to measure the displacement of the vessel against the lower support structure. The observed vibration frequency of 82 Hz is very close to the calculated fundamental frequency of the vessel. The amplitude increases instantly not changing the primary frequency, then decays with the time constant of 55 to 70 ms. The obtained amplitude and the frequency are within the assumption of design with enough margin.

As a result of the modification for higher plasma current, the estimated overturn force of TFC increased from 440 tons to 600 tons. After one month operation, to get a better adaptation of TFC in April, the neighboring two TFC units were weld for reinforcement[2.1-1]. The displacement was measured before and after welding the pairs of TFC units. To determine the absolute displacement of the upper support structure, displacement detectors were fixed to the neighboring devices such as NBI tanks, RF support and support structure columns. Table I.2.1-1 gives the displacement data of the upper support structure corresponding to 310 tons of TFC overturn force. It indicates that the displacement of the inner radius exceeds that of the outer radius. The effect of the reinforcement of the upper support structure is not clear, because there is no reliable measurement before reinforcement for comparison.

Table I.2.1-1 Displacement data of upper support structure for overturn force of 310 ton

	Radius	Calculation	Measured
RF Supt. Structure	8650	1.25	1.65
NBI Supt. Structure	5720	1.3	2.17
Support Column	8500	1.25	2.1

Figure I.2.1-1 represents the displacement data of a TFC unit (TC-9) measured as a function of the overturn force, comparing before and after the reinforcement welding. It indicates that the reinforcement greatly suppressed the movement of the inboard part of the TFC unit, and the movement of the whole unit as expected in the design calculation.

Dry operation test brought about information relating electro-magnetic properties such as eddy current, one-turn resistance of the vacuum vessel, leak currents through the structures. The one-turn resistance of the vacuum vessel was estimated by observing the currents of the inner and outer Rogowski coils and the voltage responses of the toroidal one-turn coils against the current variation of the OH or V coil. It brought about the result that the vacuum vessel has the one-turn resistance of 0.16 m Ω comparable with 0.2 m Ω predicted in design stage. Until coming up to this value, the voltage responses of the one-turn coils that are laid out properly poloidally has been precisely investigated together with the current outputs of the inner and outer Rogowski coils, and it was found that non-negligible currents run through the neighboring structures besides the vacuum vessel itself.

Figure I.2.1-2 represents differential current values at disruptions with respective operation plasma currents obtained so far. The differential current was taken at the steepest instant during disruption. The machine experienced a disruption of up to 800 MA/s, and it indicates particularly the reliability of the vacuum vessel and its peripherals.

Reference

[2.1-1] T. Kushima et al., Fusion Technology 1990, p. 572.

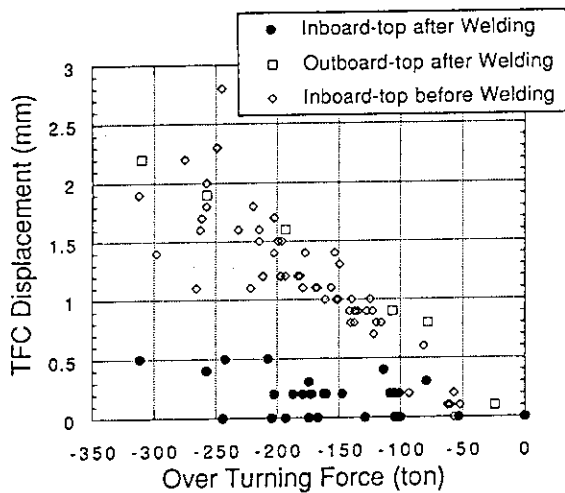


Fig. I.2.1-1 Results of TFC displacement test

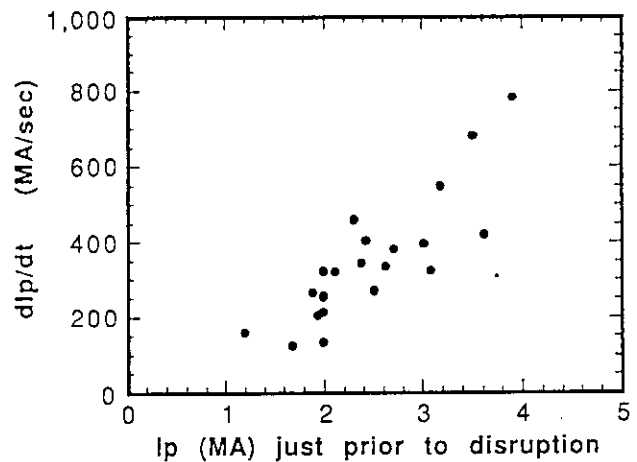


Fig. I.2.1-2 Differential current values at disruptions

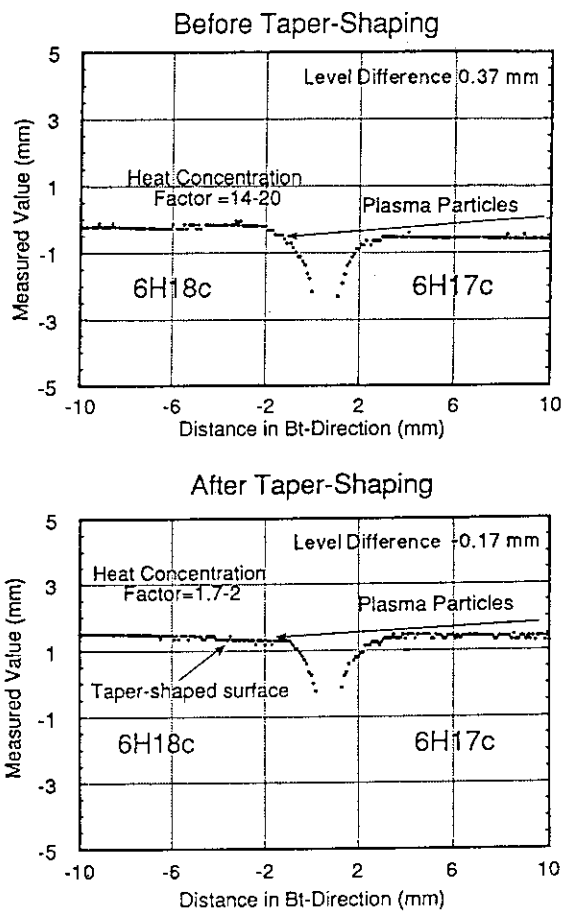


Fig. I.2.1-3 Typical profiles of divertor tile surface before and after taper-shapings

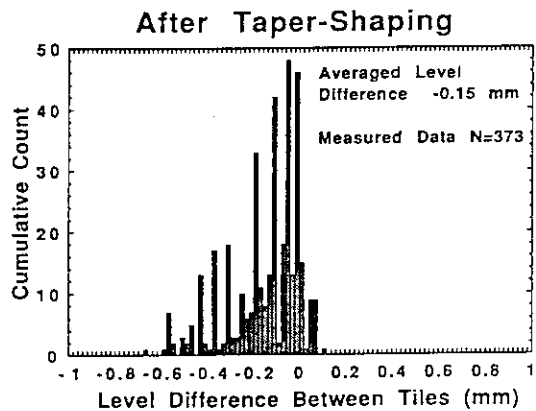
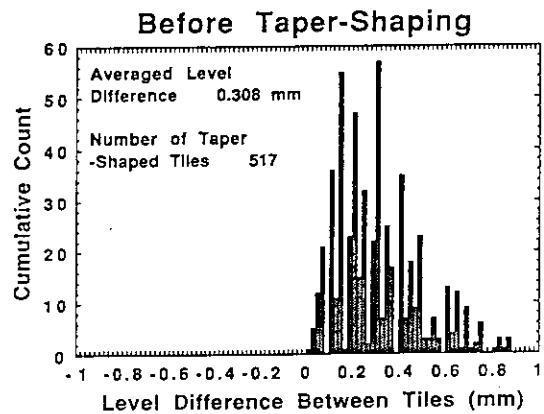


Fig. I.2.1-4 Differences in surface level of divertor tiles before and after taper-shapings

2.1.2 Operation results of plasma facing components

The divertor plate of JT-60U is composed of 2-D felt CFC tiles placed continuously in the toroidal direction. The alignment of the divertor tiles has been improved by the precise adjustment of divertor-base plates and in-situ taper-shaping of CFC tiles to reduce the heat concentration at tile edges. The difference in surface level between adjacent tiles has been measured using 3-D Laser Sensor. As shown in Fig. I.2.1-3, the typical level differences before and after taper-shapings are 0.3 mm and -0.15 mm, respectively. All data on the surface level differences measured before and after taper-shapings are shown in Fig. I.2.1-4. Since July 1991, JT-60U has been operated using deuterium gas with NB heating up to 22 MW for about 2 s. Carbon bursts have not been observed so far. It was found from the post-experiment observation that the erosion of divertor tiles is remarkably reduced and the tile surfaces are coated with glossy redeposited carbon film on the divertor trace zone, and blackened one on the off-trace zones. Broken tiles were not observed. Figure I.2.1-5 shows the divertor tiles after operation from April to October, 1991.

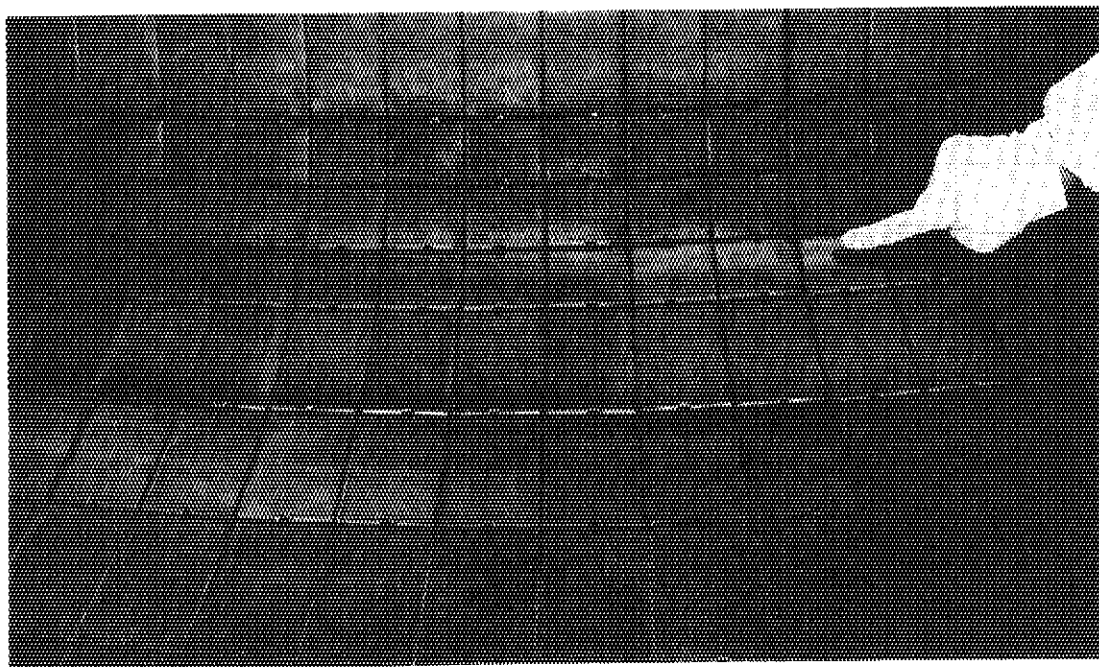


Fig. I.2.1-5 Divertor tiles after operation from April to October, 1991

2.2 Control system

2.2.1 Plasma Control

(1) Plasma position and current control system

We developed a VME multiprocessor system [2.2-1] for plasma position and current control at the JT-60 upgrade (JT-60U). The configuration of the system is shown in Fig. I.2.2-1. Parallel processing with 32-bit RISC processor MC88000 (Motorola Co., USA) in the system makes it possible to calculate the plasma state variables precisely and to execute multivariable

plasma control fast. Parameters of plasma position and X-point are calculated in real-time by the formulas derived statistically from regression analysis based on the equilibrium database. As mutual coupling between the OH-coil and the V-coil and that between the H-coil and D-coil are large respectively, multivariable control with matrix gain was applied for the control of plasma current and positions.

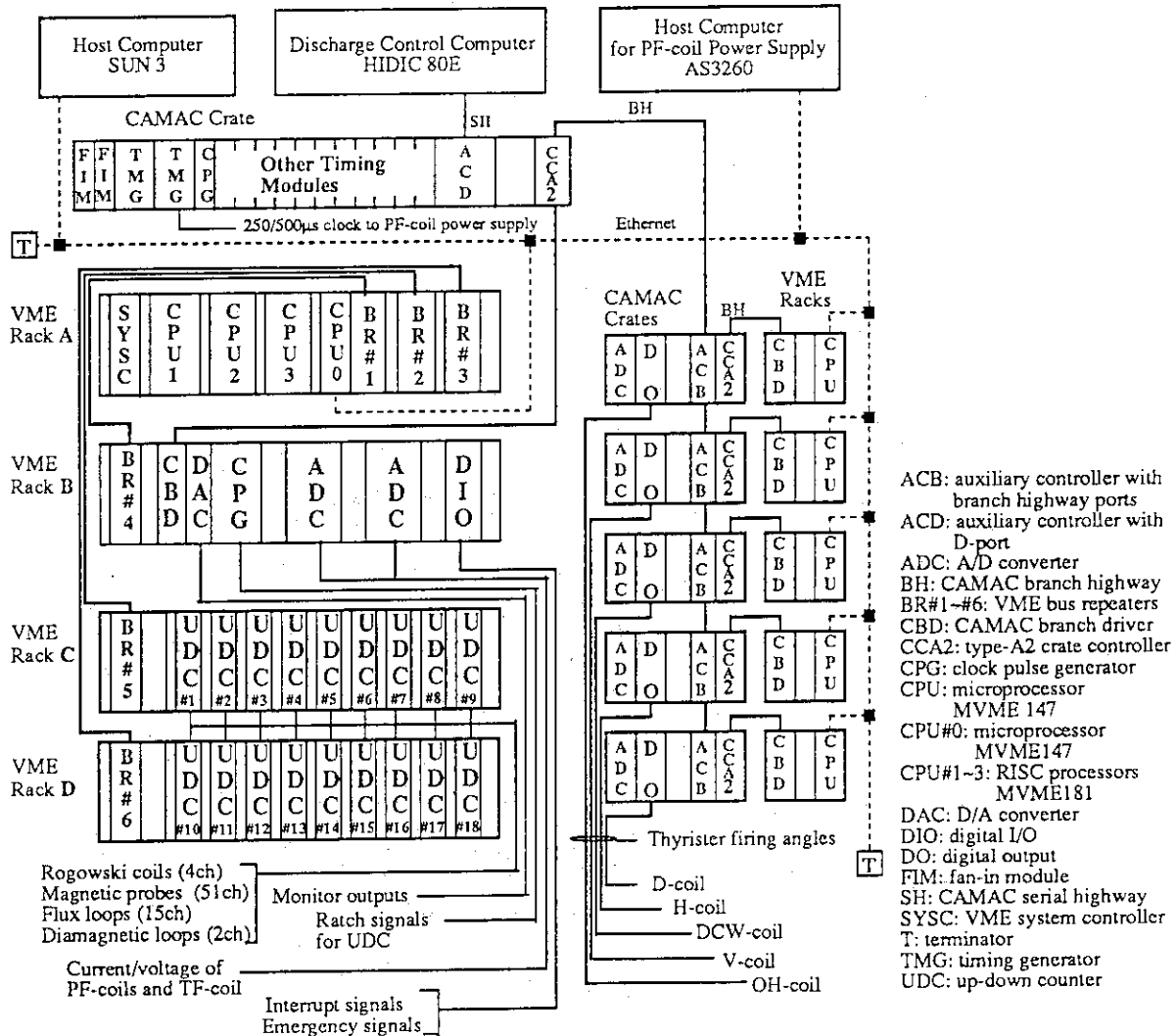


Fig. I.2.2-1 JT-60U Plasma Equilibrium Control System Based on VME Multiple Processors.

The VME system can execute the feedback control with a cycle time of 250 μ s and a delay of 500 μ s for the plasma vertical position control and that with a cycle time of 500 μ s and a delay of 1 ms for the control of the other parameters. Hence, vertical stability margin was effectively increased and stable divertor plasmas with high elongation up to 1.6 were obtained by this fast feedback control. Oscillation of the vertical position was observed in high poloidal beta plasmas over $\beta_p=2.0$ with small current around 1MA, where the decay index $n \cong -1.5$. We were able to

suppress the oscillation by applying the differential control with time constant $\tau_d=6-10\text{ms}$ in addition to the proportional control and to get stable discharges with β_p up to 2.5.

Moreover, in this new control system we have newly introduced "algorithm preprogrammed waveforms", according to which we can dynamically switch the control algorithm at real time. For example, control algorithm of the V-coil can be switched from voltage control and current control proportional to plasma current in the plasma initiation phase to feedback control of the plasma horizontal position in the phases of plasma current ramp-up, flat top and ramp-down.

The control system was fully used to get stable discharges in the JT-60U. Divertor discharges with plasma current up to 4 MA were achieved in only a month after the first plasma of the JT-60U at the end of March 1991 [2.2-2]. In October 1991, discharges with plasma current up to 5 MA have been achieved.

(2) Development of a plasma shape identification method

A new method of plasma shape identification based on the boundary integral equations (BIE) is developed for tokamak plasma control [2.2-3]. Figure I.2.2-2 shows that the BIE method identifies the plasma shape accurately even with a finite number of magnetic sensors in application to JT-60U (elongation factor $k \approx 1.5$) and ITER ($k \approx 2.2$). This method is used to numerically compute the exact analytical solution of the concerned partial differential equation, and if the proper number of sensors are properly located, the shape is definitely and accurately reproduced independently of the size or shape of the tokamak. Several test calculations by the BIE method give the following features:

- (a) The differences in plasma current profile and poloidal beta. β_p has little influence on the accuracy of the shape identification.
- (b) The influence of the change in the hypothetical plasma surface figure on the shape identification is very small.
- (c) The influence of the sensor-plasma distance on the shape identification is comparatively strong. This is because the sensor density is sensitive to the identification accuracy.
- (d) This method is robust against noise in the sensors.

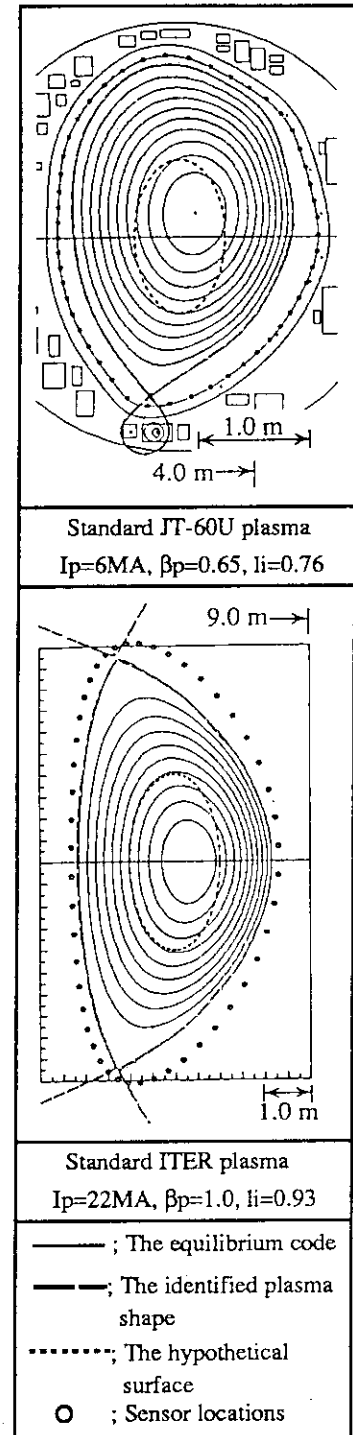


Fig. I.2.2-2 Application to JT-60U and ITER Plasmas.

(e) This method can identify a small circular plasma by the hypothetical plasma surface enclosed within the plasma.

(f) This method can be a useful tool to give a logical determination of sensor locations according to the following logic: The identification errors are produced mainly in the interpolation process. Therefore, if the flux intensity between a pair of adjacent Bt sensors is precisely reproduced using a given interpolation function, the error is minimized. If not, one or more additional sensors are needed between the adjacent sensors. This is in agreement with a natural conviction that many sensors are needed in an area having strong nonlinearity.

2.2.2 Interlock system for deuterium operation

An interlock system on neutron production was prepared for deuterium operation. Two kinds of interlock functions were installed in the discharge control. One is the function on neutron production rate during discharges and the other is that on the amount of neutron production.

Three sets of U^{235} fission chambers in the plasma diagnostic system are used as neutron detectors. The signals of the detectors are put into the plasma monitoring system in the central control system, where the production rate is monitored. When the production rate exceeds the limited value, the interlock signal is transferred to the feedback control computer, which terminates the discharge. The amount of the neutron production per shot is calculated and accumulated in the discharge control computer. When the total amounts of the neutron production per week, three months and year exceed the respective limited values, the discharge control computer locks the next shot of the discharge. The summarized information on the production of neutrons and hard X-rays is stored in the central control computer system for the operation management.

2.2.3 Man/machine interface

A new man/machine interface system in the JT-60 central control system was developed based on Sun-3 workstations connected with a network of Ethernet [2.2-4]. Development of the system was completed in the beginning of April 1991 after its test run during the system integration test of the JT-60U. Improvements on the following points have been made with the new man/machine interface system in the JT-60U operation: (1) the function for setting discharge condition parameters, (2) the functions for monitoring the plant status and discharge results and (3) working environment in the central control room.

References

- [2.2-1] T. Kimura, et al., IEEE Trans. on Nuclear Science 35 (1989) 1554.
- [2.2-2] JT-60 Team presented by T. Kimura, in Proceedings of the 14th Symposium on Fusion Engineering, San Diego, 1991, pp.860-866.
- [2.2-3] K. Kurihara and T. Kimura, JAERI-M 92-075 (1992) (in Japanese).
- [2.2-4] I. Yonekawa, et al., in Proceedings of the 14th Symposium on Fusion Engineering, San Diego, 1991, pp.798-801.

2.3 Power supply

In this fiscal year, the JT-60 poloidal field power supply (PFPS) which was modified to achieve higher plasma currents and so on for JT-60U in the year before [2.3-1] have been operated smoothly and functioned very well. The plasma current of 5MA was performed when the F(OH)-coil power supply delivered the current of +70kA to -105kA, and other V-, H- and D-coil power supplies also controlled the vertical and horizontal positions and the configuration of the plasma as shown in Fig.I.2.3-1.

As the results, we have the prospect of achieving the 6MA-discharge. In order to suppress the vertical instability of plasma, the processing time of a thyristor's computer controller in the H-coil power supply has been reduced to under 0.25 ms by using a 32-bit microcomputer installed on a VME bus system. Experiments on comparison between 0.25ms and 1ms of the processing time showed that the 0.25ms-controlling reduces the vertically oscillatory displacement to 60% than the 1ms-controlling.

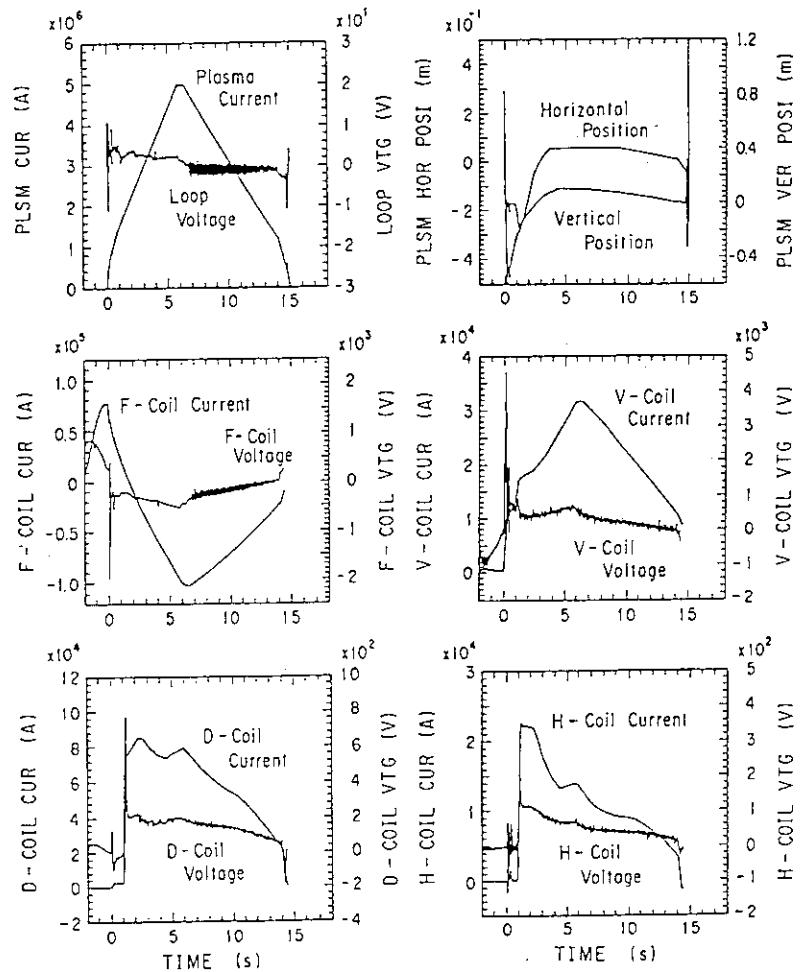


Fig. I.2.3-1 Waveforms of plasma current of 5MA and coils' currents at E14221

The other power supplies, the toroidal field power supply (TFPS) and the motor-generator for the heating system (H-MG) were also operated smoothly. The operating time of TFPS, PFPS and H-MG were 1,496, 1,214 and 1,613 hours, and the number of troubles of each power supply were 84, 165 and 6 times respectively. The main trouble of TFPS is exceeding oscillations of the shaft of the motor-generator. In PFPS, troubles mainly happened relating to the control systems such as phase controllers of the thyristor converters in the H-coil power supply occasionally behave abnormally and overvoltages in the F-coil power supply occurred at the time when the circuit breakers open. H-MG scarcely brought about any troubles.

The utility power distribution facility and the secondary cooling water facility which are operated by power supply group have been operated smoothly. These facilities have been operated

for about ten years from their installation, so not a few parts of the equipment have deteriorated and some of them are desired to be exchanged. In FY 1991, batteries of uninterruptible AC and DC power supplies, which consist of 165 and 102 cells and the ratings of each battery are 1,500 and 300 A-hour/h respectively, were exchanged. In secondary cooling water facility, overhauls of the motors of the pumps were carried out and the cooling tower was painted again.

References

[2.3-1] Y.Matsuzaki et al., Proc. of 16th Symp. on Fusion Technol., London, 1990 p1482

2.4 Neutral Beam Injection System(NBI system)

A quasi-perpendicular injection beamlines composed of ten units out of fourteen NBI units is now under operation and a rest of four units is under modification from the quasi-perpendicular injection to a tangential one, of which two units are co-injection and the others are counter-one.

On the perpendicular NBI, ion source conditioning and beam injections into JT-60U were given with hydrogen by the end of June for taking a hydrogen beam data, with modified acceleration power supplies, ion sources and control system for a higher beam energy operation up to 120keV and for a deuterium beam operation.

A deuterium beam operation started in the middle of July. At first, to estimate beam characteristics with the deuterium, ion source arc efficiency, beam divergence, beam species and power loadings on beamline components and ion source acceleration grids were measured simultaneously with the ion sources conditioning. At same time, the neutral beam power was also measured injecting the beam into a calorimeter. No particular change of the arc efficiency and the beam divergence of the deuterium beam is recognized in comparison with those of hydrogen. The neutral beam species of $D^0(E):D^0(E/2):D^0(E/3)$ is 78:15:7. The neutral beam power is roughly twice compared with hydrogen beam at the same beam energy as shown in Fig.I.2.4-1. In the NBI heating experiments, the power of 23MW with deuterium beam was injected by ten beamlines at the beam energy of 90~95keV.

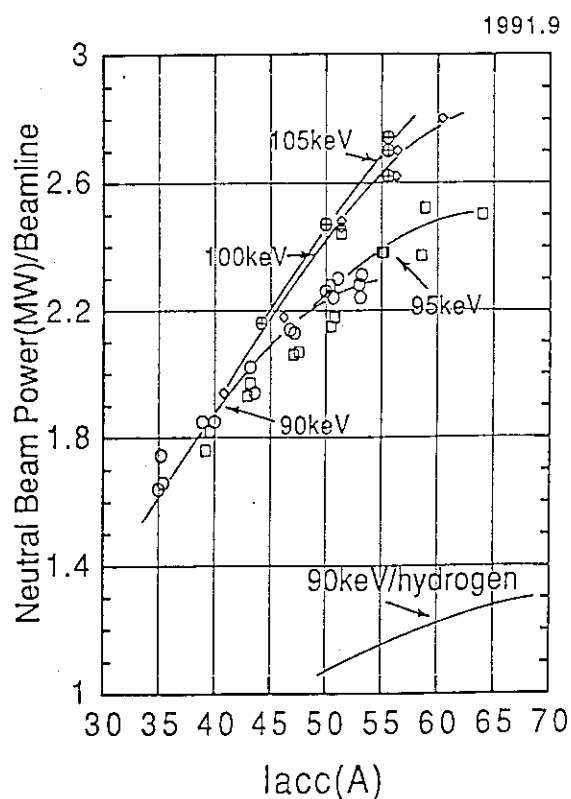


Fig.I.2.4-1 Neutral beam power per beamline with deuterium beam

A measured pumping speed with deuterium gas by a beamline cryopump was $900\text{m}^3/\text{s}$, which is equivalent to about 70% of that with hydrogen gas.

To estimate with accuracy a neutron from a beam dump and a calorimeter in the beamline, a calibration of neutron monitor was done by inserting a specified neutron source (Cf^{252}) into the beamline tank. Followed after the calibration, the neutron dose rate was measured by leading the beam dump and the calorimeter to collide with the beam. The measured value of the neutron dose rate by a beamline was 6×10^9 n/s/ampere (3×10^{11} n/s/beamline) at the beam energy of 100keV. Neutron dose rate increases with the beam energy. Since a beam drift ducts were newly fabricated with JT-60U vacuum vessel, the duct aging was done by injecting a short pulse beam under a stray magnetic field from JT-60U prior to the deuterium beam injected plasma heating. A integrated beam pulse length for the duct aging was in need of about 50 sec to be a reionization loss of below 10%, which was more than three times compared with a former JT-60 duct with hydrogen beam. The reasons why the aging needs a long time in finishing are that the duct cross-section is smaller size than the former and the deuterium gas conductance decreases compared with hydrogen. But the second duct aging that was done in February, 1992, just after two months vacuum break, the required integrated beam pulse length decreased to less than one third, about 15 sec.

For ^3He beams injection that aims at D- ^3He nuclear fusion experiment, a preliminary He gas pumping test by a cryo-sorption with an argon condensed layer has been done using a present JT-60NBI cryopump system. The pumping speed for He gas achieved $400\text{m}^3/\text{s}/\text{beamline}$. After the confirmation of the pumping capability by the test, the cryopumps of six beamline units have been modified to be able to evacuate the He gas.

2.5 Radio-frequency system

2.5.1 LHCD system

The main objective of LHCD experiments in JT-60U is to drive plasma current and to control plasma current profile. To carry out LHCD experiments, a small size launcher has been installed with a injection power level of 2 ~ 3 MW and a large size launcher capable of ~7MW is under construction and will be operated in 1993. The small launcher is composed of 24×4 sub-waveguides and is fabricated by a diffusion bonding method, which is a most promising method to manufacture a LHCD grill with several hundreds number of waveguides for a next fusion device such as ITER. The large one is composed of 48×4 sub-waveguides and is featured by a simple structure which will be mentioned in section 4.5.1.

In 1991, we investigated the power handling capability and the coupling property of the small launcher. A CCD camera was equipped to detect RF breakdowns at the grill mouth, and a double probe was installed at the grill mouth to measure the edge plasma density.

On the initial stage of RF conditioning, RF breakdown was often observed at the grill mouth when the neutral pressure rose at the differential pumping system of the launcher. This the neutral

pressure rise seemed to be induced by a single surface multipactoring discharge because the neutral pressure rise accompanied with a local temperature rise at the transmission vacuum waveguide in the resonance zone. The breakdown was gradually suppressed shot by shot and the maximum injected power reached up to 2.2 MW at the end of this operational run.

It was found that the reflection coefficient ρ was less than $\sim 15\%$ even though the distance (δ) between the outer most magnetic surface and the first wall was about 0.1 m as shown in Fig.I.2.5-1. The degradation of current drive efficiency was not observed at this plasma position. An increment of edge plasma density was observed by injection RF power, and the good coupling characteristic was obtained when the edge plasma density was beyond the cut off density of 2GHz. A good coupling was kept at the distance δ up to 0.15m by combining NBI. This result suggests that edge density control by RF waves may give a solution to couple RF with main plasmas when the plasma position is kept far from the grill.

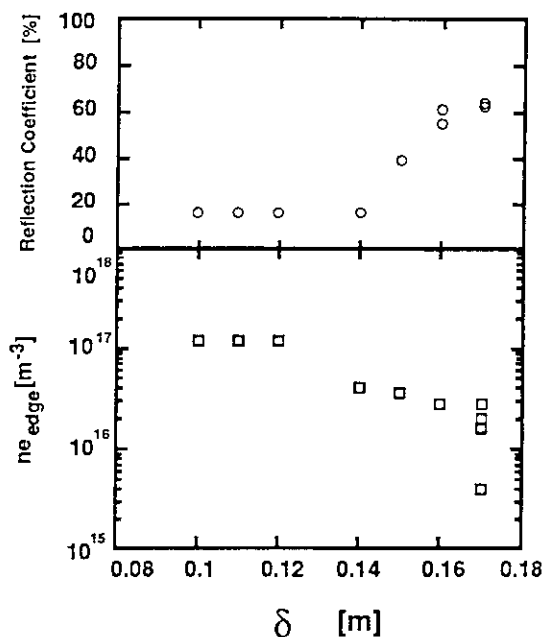


Fig. I.2.5-1 Coupling and edge plasma density as a function of δ .

2. 5. 2 ICRF Heating System

ICRF heating system has been upgraded [2.5-1] accompanied with modification of JT-60 increasing a plasma current up to 6 MA. Figure I.2.5-2 shows an RF skeleton of the upgraded ICRF system. Two antennas had been already installed last fiscal year. Remaining renewed parts of the ICRF system, namely transmission lines, impedance matching system, power and phase measurement system and protection circuits, were installed this fiscal year considering the schedule of JT-60 operation. Number of transmission lines is increased from 4 to 8 lines to be connected with eight loop elements respectively. The impedance matching system is changed from double stub tuners to a combination of a phase shifter and a stub tuner for each line to be able to take impedance matching in a wider range of input antenna impedance. The power and phase measurement system and protection circuits for the antennas and the lines are modified to correspond to increasing antennas and lines.

After the installation the ICRF system has been operated from January 1992. The operation is started with measurements of input antenna impedance for vacuum loading at low power levels of 0.1 W by switching to a network analyzer at the output of the amplifier. Actual impedance matching is taken well and quickly for vacuum loading at high power levels of 200 kW and then for plasma loading in antenna conditioning. Consequently, 1.5 MW injection into a plasma is attained after

three day's antenna conditioning, which is very quick procedure as antenna conditioning in first operation, and it is therefore expected to increase injection power up to 5 MW of maximum rating.

Reference

[2.5-1] T. Fujii, N. Kobayashi, S. Moriyama et al., Proc. 16th Symp. on Fusion Tech., London (1990) 1171.

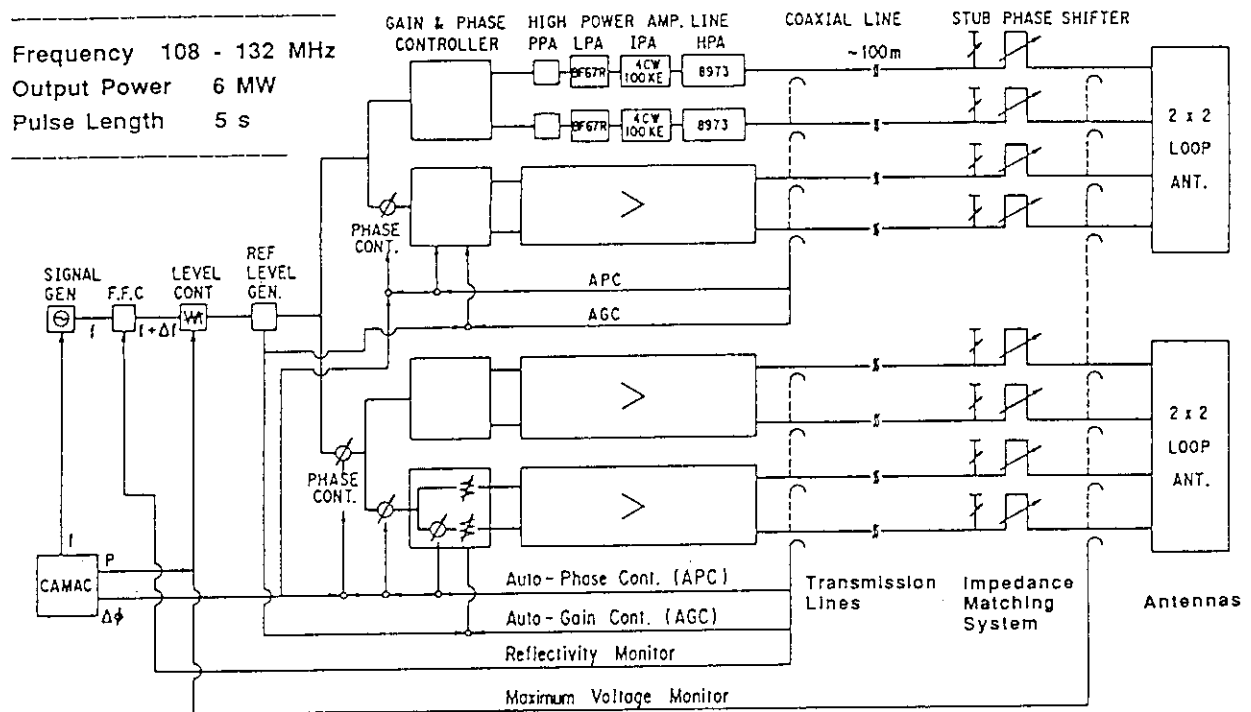


Fig. I.2.5-2 RF skeleton of the upgraded ICRF heating system

2.6 Diagnostic systems

During the period from April 1991 to March 1992, JT-60U had the first experience to operate with deuterium discharge and upgraded plasma current up to 5MA. The diagnostic systems have been arranged, mainly in the previous year, to operate under the new circumstance such as neutron radiation, by remote sensing with fiber optics and suitable shielding of sensors and detectors. Concerning to the diagnostic system operation, in spite of the long interval of JT-60 shut-down, all the diagnostic systems have been started up in satisfactory.

As the newly installed systems in this period, the neutron yield monitor, X-ray crystal spectrometer, hard X-ray pulse height analyzer and tangential CO₂ laser interferometer are described in section I.2.6.1~2.6.4. The JT-60U diagnostic systems and their status at the end of March 1992 are summarized in Table I.2.6-1.

2.6.1 Neutron yield monitor and its calibration

Absolutely calibrated measurements of the neutron yield are important for the evaluation of plasma performance such as the fusion gain Q in D-D operating tokamaks. The time-resolved neutron yield is measured with ^{235}U and ^{238}U fission chambers and ^3He proportional counters in the JT-60U tokamak. Three sets of ^{235}U and ^{238}U fission chambers and a ^3He proportional counter are placed on the torus midplane, just outside the toroidal field coils, at three different toroidal sections. The ^{235}U detector is used in the low and medium neutron yield discharges and the ^{238}U detector is used in the high neutron yield discharges such as high-power NB heating experiments. The ^3He proportional counter has high detection efficiency. This detector can obtain sufficient statistics in the ^{252}Cf source calibration and plays a role of "transfer detector" to cross-calibrate less sensitive detectors using D-D tokamak discharges. We use ^{235}U and ^{238}U fission chambers in both pulse counting mode and Campbell (MSV) mode. The former is suitable for low count rates less than 10^6 cps and the latter is for high count rates more than 10^5 cps. The pair of ^3He detectors are operated in pulse counting mode only.

The *in situ* calibration was performed by moving the ^{252}Cf neutron source toroidally through the JT-60 vacuum vessel. Detection efficiencies of three ^{235}U and two ^3He detectors were measured for 92 locations of the neutron point source in toroidal scans at two different major radii. The total detection efficiency for the torus neutron source was obtained by the averaging the point efficiencies

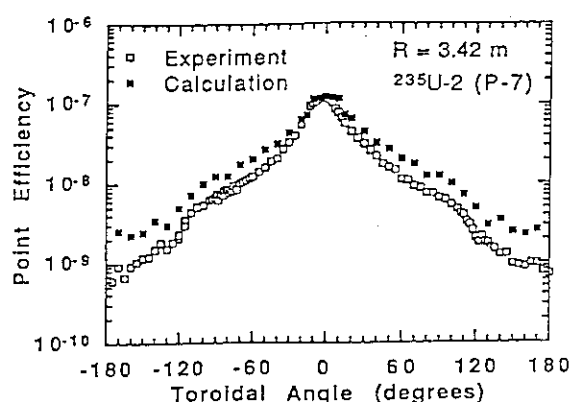


Fig. I.2.6-1 Absolutely calibrated result of ^{235}U fission chamber, which is located at P-7 horizontal port. The experiment data is compared with MCNP calculation.

Table I.2.6-1 Status of JT-60U diagnostic systems

Diagnostic System	Subsystem	Specification	Status Mar.1992
<i>Electron Density</i>	FIR Interferometer	CO ₂ Pumped CH ₃ OH Laser Vertical 2 chords	Operational
	CO ₂ Laser Interferometer	Tangential 1 chord	Under construction
	MMW Reflectometer	2 density points fluctuation	Operational
	Electro-magnetic Wave Scattering	3 points, 50-1.8MHz	Under construction
<i>Electron Temperature</i>	Thomson Scattering	2 Ruby Lasers, 50 points Repetition 4 sec	Operational
	ECE Michelson Interferometer	30 Points $\Delta t \sim 20$ ms	Operational
	ECE Grating Polychromator	20 Points $\Delta \tau \sim 20$ ms	Operational
<i>Ion Temperature</i>	Charge Exchange Recombination Spectroscopy	20 points (tangential) 8 points (perpendicular)	Operational
	Active Beam Scattering	He Beam 200keV, 3.5A 1 point (center)	Operational
	Charge Exchange Neutral Particle Energy Analyzer Array	2 chords (tangential) 2 chords (perpendicular)	Operational
<i>Impurity Measurement</i>	X-ray Crystal Spectrometer (Doppler & Monochromator)	1 chord (vertical) Ti, Ni, Kr-K α Rotating Crystal, 0.1~0.8 nm	Operational
	VUV Spectrometer	1 chord, 0.5~130 nm (Main) 1 chord, 0.5~130 nm (Div.)	Operational
	Light Impurity Spectrometer (Doppler)	1 chord, 100-200 nm (Div.)	Under construction
	Grazing Incidence Monochromator	1 chord, 10-130 nm Absolutely Calibrated VUV	Under construction
	Visible Monochromator	1 chord, 200-700 nm Absolutely Calibrated Visible	Operational
	Visible Spectrometer Periphery	Mirror Scan, 200-700 nm	Under construction
	Visible Spectrometer Divertor	38 points, H α , H β , CII, OII Fiber Optics & Filters	Operational
	Visible Bremsstrahlung (Zeff)	10 points, 523.2 nm Fiber Optics & Filters	Operational
	Motional Stark Spectrometer	1 point for Bp detection	Under construction
<i>Radiation Flux</i>	Soft X-ray PHA	1 chord, 3-110keV	Operational
	H α / D α Arrays	Poloidal 30 chords Toroidal 6 chords Divertor 1 chord Outer Region 1 chord	Operational
	Soft X-ray Arrays	Poloidal 64 chords Outer Region 4 chords	Operational
	Bolometer Arrays	Poloidal 32 chords Divertor 1 chord	Operational
	Hard X-ray PHA	Poloidal 7 chords Co 1 chord, Counter 1 chord	Operational
<i>Neutron</i>	Fission Chamber	3 Points, $\Delta t \sim 10$ ms	Operational
	Neutron Spectrometer (2.45MeV / 14MeV)	1 chord, $\Delta E \sim 2\%$	Operational
<i>Peripheral Plasma & Wall Surface</i>	Infrared TV	Divertor 1 chord 400-500°C	Operational
	Visible TV	Tangential 2 chords	Operational
	High Speed TV	Tangential 1 chord, 1 frame/ms	Operational
	Electro-magnetic Probes (Mirnov Coils)	40 points (Poloidal & Toroidal Arrays)	Operational
	Electro Static Probes	Divertor 40 points	Operational

over the whole toroidal angle. Figure.I.2.6-1 shows the result of *in situ* calibration of the ^{235}U fission chambers, compared with the simulated result by Monte Carlo calculation. The uncertainty of the resulting detection efficiency for the plasma neutrons is estimated to be $\pm 11\%$ [2.6-1].

This system certified the produced fusion neutron rate of 1.3×10^{16} n/s, on the discharge, the ion temperature of which was confirmed to be 20 keV. The time evolution of the plasma parameter is shown in Fig.I.2.6-2.

2.6.2 X-ray Crystal Spectrometer

In order to measure ion temperature from Doppler broadening of X-ray spectra and to observe metal impurity behavior, a X-ray crystal spectrometer has been designed and installed. The schematic view of the spectrometer is shown in Fig.I.2.6-3. The spectrometer has three crystals (Si(220), SiO₂(2243) and Si(660)) and one detector (multi-wire proportional counter, detective area:128x128mm) to measure X-ray spectra of He-like ions of titanium; Ti XXI K α ($\lambda=0.261\text{nm}$), nickel; Ni XXVII K α ($\lambda=0.159\text{nm}$) and krypton; Kr XXXV K α ($\lambda=0.095\text{nm}$), respectively. The resolutions for each line of Ti, Ni

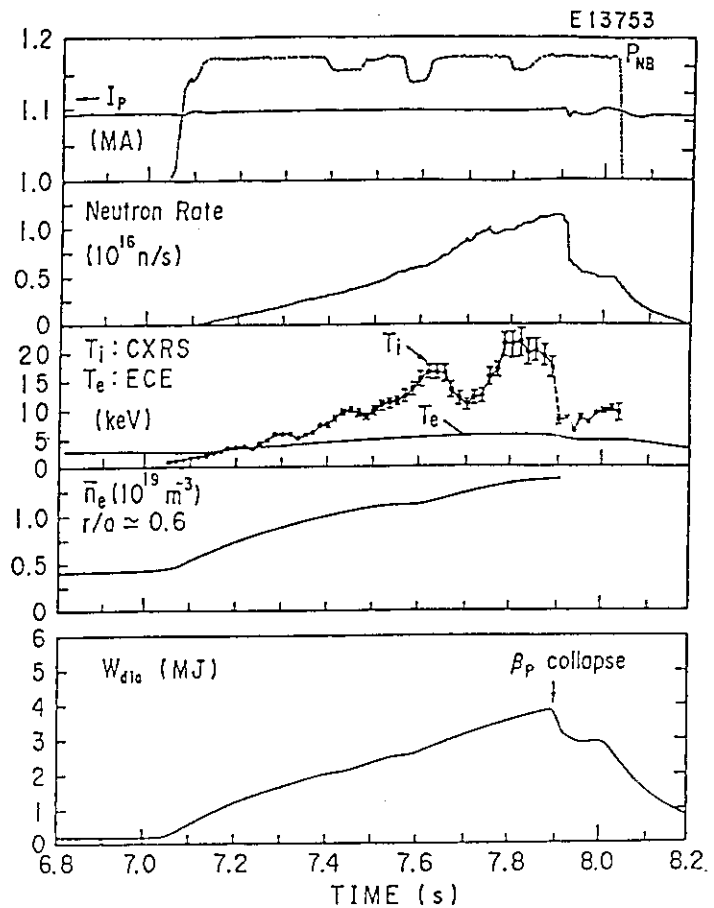


Fig. I.2.6-2 The time evolution of plasma discharge, which show the maximum neutron rate of 1.3×10^{16} n/s.

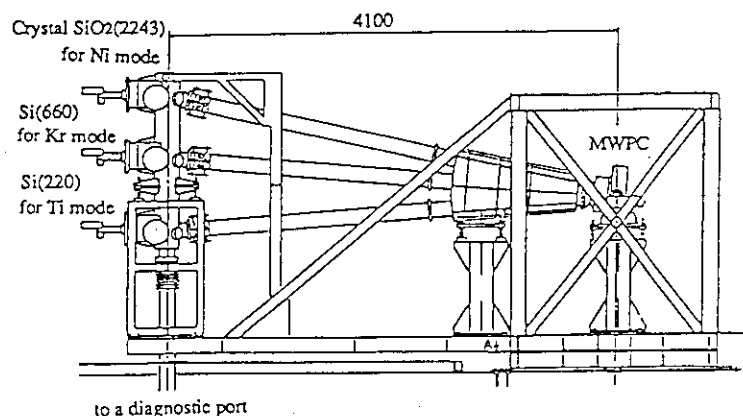


Fig. I.2.6-3 Schematic view of X-ray Crystal Spectrometer for JT-60 Upgrade tokamak. Three crystals are arranged to the X-ray spectra of Ti ($\lambda=0.261\text{nm}$), Ni ($\lambda=0.159\text{nm}$), Kr ($\lambda=0.095\text{nm}$).

and Kr are $\lambda/\Delta\lambda \sim 7600$, 10000 and 9000, respectively. The neutron shield (polyethylene: 650mm^t [max.], 200mm^t [min.]) and γ -ray shield (lead: 250mm^t [max.], 100mm^t [min.]) were installed to prevent the detector from neutron and γ -ray noise, because of the high detective efficiency of the proportional counter. X-ray emitted from these species penetrates through a beryllium window (0.5mm^t), and are diffracted by the Bragg angle on the crystal surface and focused on the detector.

In the LHRF, ICRF experiment and high plasma current ($I_p=4\text{MA}$) OH discharge, X-ray spectra of Ni XXVII $K\alpha$ were measured. It is estimated that the observed metal impurity was originated presumably from LHRF antenna launcher, ICRF antenna and JT-60U wall (diagnostic and NBI port edges).

2.6.3 Hard X-ray pulse height analysis

Distribution function and radial profile of fast electrons produced by the lower hybrid wave are measured by hard X-ray pulse height analysis. The hard X-ray is emitted by electron coulomb collision with ions and we can obtain distribution function of fast electrons by analyzing energy spectrum of the hard X-ray.

Hard X-ray is detected by combination of 8-channel sodium-iodide (NaI(Tl)) and photomultiplier. Seven channels observe radial profile perpendicularly to the magnetic field and the other observes tangentially (Fig.I.2.6-4). The NaI(Tl) detector, which is 5.08cm thick and 5.08cm in diameter with 2 mm aluminum vacuum window, is employed to measure the X-ray energy range of 30keV to 1MeV. Detectors are shielded by 23cm of lead and 50cm of polyethylene against the γ -rays from (n, g) reactions, background X-rays and neutron from D-D reaction. The photomultiplier tubes are shielded against magnetic field by soft iron and μ -metal. The detected X-ray signals are pulse-height analyzed by 256 channels every 50 msec. To measure the fast time evolution, two single-channel-analyzers are used to obtain the hard X-ray count every 1 msec. Radial profiles of the hard X-ray during lower hybrid current drive are obtained. Power deposition profiles of the lower hybrid wave are estimated by using radial profile of the hard X-ray [2.6-2,3].

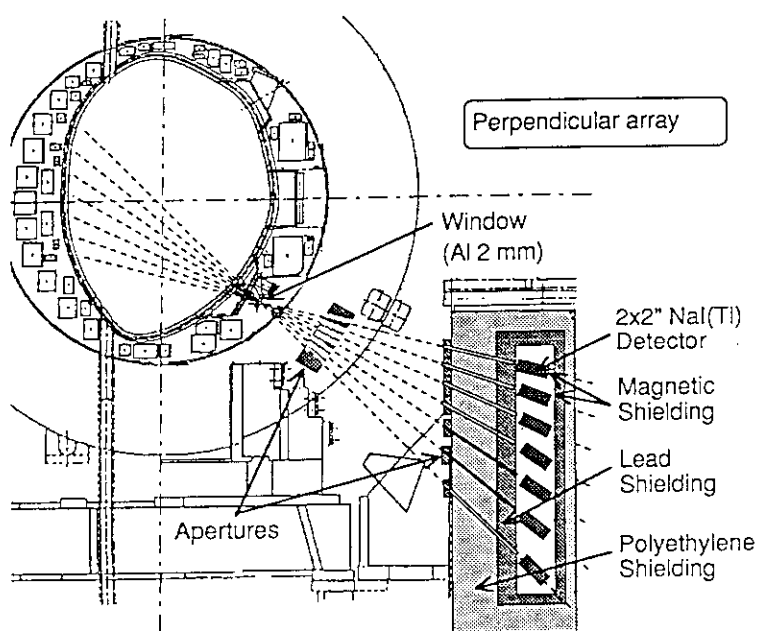


Fig. I.2.6-4 Schematic diagram of the hard X-ray detectors.

2.6.4 CO₂ Laser Interferometer

FIR laser interferometer has been utilized for the time evolution of 2 vertical line densities. Its chords become off-axis from the plasma center, in case of the high ion temperature operation mode, which produces a small size plasma at the inner side of the JT-60 vacuum vessel. This mode is very suitable for the further growing up of ion temperature with NB injection. To ensure to get the density information of the plasma axis, additional interferometer system with CO₂ laser ($\lambda=10.6\mu\text{m}$) is planned to introduce as the tangential viewing chord along the plasma center of the high ion temperature operation mode. The system is designed as a two color interferometer combined with a coaxial HeNe ($\lambda=3.39\mu\text{m}$) laser interferometer to calibrate the mechanical vibration. The schematic diagram of CO₂ interferometer is shown in Fig.I.2.6-5. The first measurement will be performed on Aug.1992.

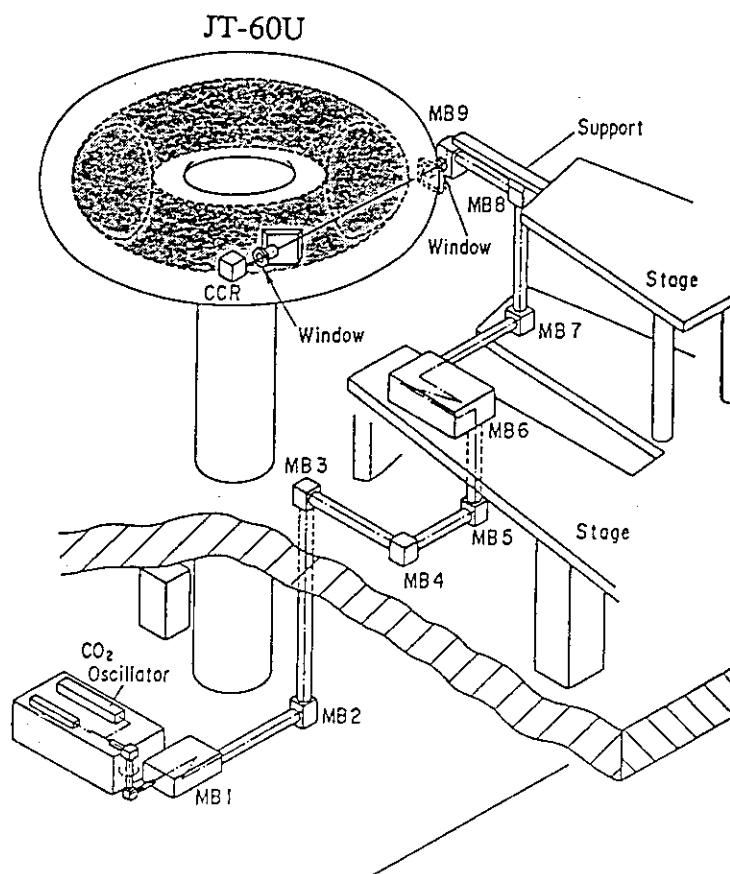


Fig. I.2.6-5 Schematic view of CO₂ laser interferometer. The laser oscillator is located in B1F, and laser beam is guided by a lot of mirror optics. Where MB means mirror containing box.

References

- [2.6-1] T. Nishitani, et al., JAERI-M 91-176
- [2.6-2] T. Kondoh, S. Ide et al., Proc. International Conference on Plasma Physics (Innsbruck, 1992), part II, 969 (1992)
- [2.6-3] T. Kondoh, S. Ide et al., JAERI-M 92-073, 300 (1992)

3. Experimental Results and Analysis

3.1 Plasma Control and Disruptions

3.1.1 Plasma Configuration Control

The control of the plasma configuration is indispensable to get required plasma performances. In JT-60U, four control variables of plasma current (I_p), vertical and horizontal plasma center positions (R_p , Z_p), and height of the null point from the divertor plate (X_p) are selected for a divertor plasma. The measurement formulas for them are derived by regression analysis from calculated database of ~4000 cases. Using these, the start up of JT-60U was carried out successfully[3.1-1].

The poloidal coil system of JT-60U consists of the primary coil (F-coil), the vertical and horizontal magnetic field coils (V-, H-coils), and the divertor coil (D-coil). The mutual inductance between F-coil and V-coil is very large, and is almost the same as the self inductance of F-coil. Thus the control of I_p and R_p have a strong interaction between them. There also exists a large interaction between the control of Z_p and X_p . Then I_p and R_p are controlled by F- and V- coils, and Z_p and X_p are controlled by H- and D-coils. A proportional matrix gain for them is installed in a plasma feedback control computer.

Noninteracting control of I_p and R_p was tested using a matrix gain in a swing of R_p with $\pm 2\text{cm}$ and 10Hz. The large interaction with I_p control, that occurs inevitably in the case of independent control, was suppressed dramatically by a factor 20 using noninteracting control as shown in Fig.I.3.1-1. This method is general and can be applicable to an ITER-like reactor machine [3.1-2].

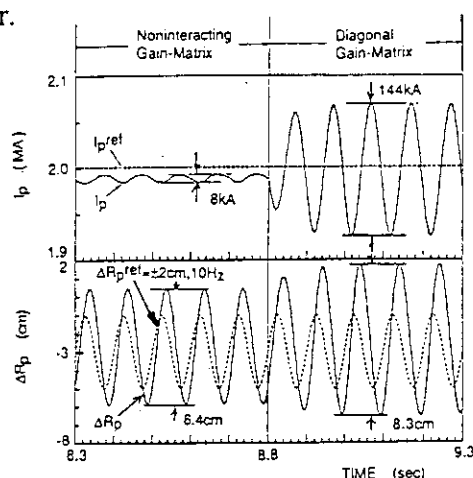


Fig. I.3.1-1 Comparison of the noninteracting control of I_p and R_p with that of independent control.

3.1.2 Eddy Current

The one-turn resistivity of the vacuum vessel of JT-60U was measured as $160\mu\Omega$. A large toroidal current can flow in the vacuum vessel during dynamical phases such as 1)major or minor disruptions, 2)vertically unstable plasmas, and 3)plasma initiation phase. Thus the understanding of eddy current is quite important for the design of an ITER-like reactor machine, because the resistivity of that may be very small (e.g. $\sim 20\mu\Omega$ in ITER).

A magnetic fitting code including vessel eddy currents has been developed to estimate the toroidally symmetric eddy current profile in the vacuum vessel in the plasma breakdown, current ramp-up phase and major disruptions. The measured magnetic data are fairly well reconstructed with the measured current within about 10% error[3.1-3]. This difference suggests that there are other eddy current loops outside the vessel.

3.1.3 Vertical Stability

Vertically elongated JT-60U plasmas ($\kappa \geq 1.6$) require active control of the vertical position. For an investigation of the PD-control of the vertical plasma position, the plasma is modelled by a rigid assembly of axisymmetric current-carrying filaments free to move only in the vertical direction. The dominant up-down antisymmetric mode of the vacuum vessel model alone has a decay time of ~ 10 ms, while that of the vessel and PF-coils together has a decay time of ~ 1 sec.

During the course of several neutral beam-heated shots in high β_p experiment (see section 3.3), β_p became sufficiently high that the preset control gains could not stabilize the plasma. Experimental onset of instability and real growth rate coincide well with the predicted values. This model is applied to the analysis of the expected vertical stability limits for JT-60U, and indicates that $\Lambda \approx 3.0$ is an approximate upper bound to achievable Λ [3.1-5].

3.1.4 Plasma Current Ramp-up and Ramp-down

The plasma current ramp-up rate of 2MA/s has been obtained successfully from I_p of 0.7 to 3.5MA by using newly developed "growing plasma method" as shown in Fig.I.3.1-2. The effective safety factor q_{eff} is reduced below 4.0 with controlled small minor radius just after the plasma initiation at $t \geq 0.25$ s. The plasma internal inductance l_i can be controlled by the choice of the plasma current ramp-up rate and the plasma minor radius. With the constant minor radius, the plasma current ramp-up rate cannot be raised higher than 0.5MA/s owing to locked mode disruptions.

Locked mode disruptions, which are frequently observed in the plasma current ramp-up with low plasma density, can be avoided by this active control of l_i . Thus the stability of the plasma current ramp-up is improved dramatically. Furthermore a systematic study on the locked mode disruption suggests that the error field by D-coil is an essential cause [3.1-6].

In order to get a stable plasma shutdown, a well developed scenario is required to avoid disruptions during the plasma current ramp-down. In JT-60U, the plasma minor radius is reduced during the plasma current ramp-down, in order to avoid tearing type MHD instabilities caused by high l_i with suppressing the peaking of a current profile and to keep the power balance in the plasma peripheral region with raising the joule heating power density. This is named "dwindling plasma method", and has been tried with nearly 100% success. A maximum plasma current ramp-down rate of -4MA/s was obtained from 2MA to 0.5MA.

These experimental results of stable plasma ramp-up and shutdown will supply the technical database for an operation scenario in a fusion reactor.

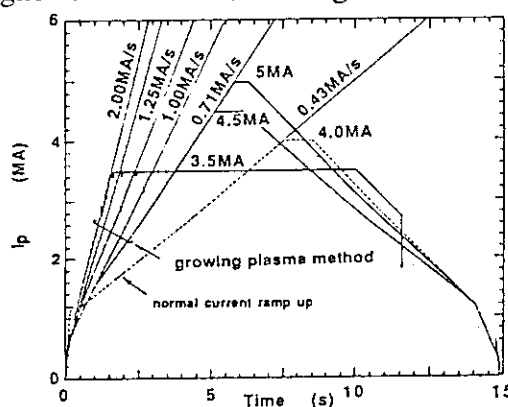


Fig. I.3.1-2 Fast plasma current rise with "growing plasma method".

3.1.5 MARFE and Detached Plasma

Divertor phenomena prior to density limit disruptions have been studied in ohmic and neutral beam heated discharges with power of 7.5-8.5MW. The MARFE occurs when the outer divertor electron temperature falls down to 10eV or less for in either ohmic or neutral beam heated discharges. From the spectroscopic and bolometric observation, it is found that MARFE forms at the outboard side of X-point and just at the inside of the outermost magnetic surface of the main plasma and is accompanied by an increase in particle recycling[3.1-6]. The radiating region changes due to the shift of MARFE, but the divertor radiation loss is saturated as a whole.

Detached plasmas are observed in JT-60U near the the density limit just after MARFE and just before the major disruption. The time delay of the current quench in a major disruption from the start of the detachment becomes long with the increase in q_{eff} and the decrease in I_i [3.1-7]. Disruption-free discharges can be obtained at $q_{\text{eff}} > 7$ with well controlled plasma configuration. Long stable detachment phase of ~ 1 s obtained during the plasma current ramp-up or NB heating suggests the possibility to decrease rapidly the energy flux onto the divertor plate in an emergency such as a loss of coolant for the divertor plate.

3.1.6 Current Quench and Vibration of the Vacuum Vessel in Disruptions

In the current quench of JT-60U, the fastest current decay defined by $I_p/(dI_p/dt)$ is ~ 5 ms, which is almost the same as that in JT-60[3.1-8]. Toroidal eddy currents are generated carrying up to 30-50% of the plasma current just prior to a plasma termination. With typical plasma location and shape ($-0.2 < Z_j < 0.2$ m, $0.72 < a_p < 1.04$ m), the maximum toroidal eddy current increases with the plasma current as shown in Fig.I.3.1-3. It suggests the electromagnetic force from the toroidal eddy current is proportional to $I_{\text{Tor}} \times B_{\text{pol}} \sim I_p^2$.

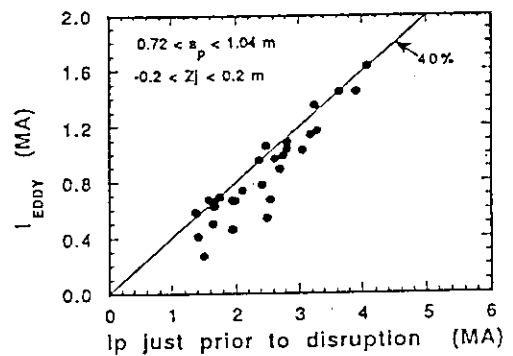


Fig. I.3.1-3 Toroidal eddy current as a function of the plasma current just prior to the current quench.

The displacement of the vacuum vessel has been measured indirectly by laser sensors, that monitors the head of a port. The maximum displacement of the vessel vibration is 0.6mm at 4MA disruption and increases with I_p^2 [3.1-9]. It is consistent with electromagnetic force from the toroidal eddy current. From this scaling the amplitude at 6MA disruption is expected to be 1.3mm, well within the design limit of 2mm.

References

- [3.1-1] M.Matsukawa, et al., JAERI-M 92-073 (1992) p.16-19
- [3.1-2] R.Yoshino, et al., JAERI-M 91-049 (1991)
- [3.1-3] K.Ushigusa, et al., JAERI-M 92-073 (1992) p.20-23, p182-185
- [3.1-4] D.A.Humphreys, et al. JAERI-M 92-069 (1992)
- [3.1-5] R.Yoshino, et al., JAERI-M 92-073 (1992) p.48-51
- [3.1-6] N.Hosogane, et al., 10th PSI, Monterey (1992) C:09
- [3.1-7] R.Yoshino, JAERI-M 92-073 (1992) p.44-47

[3.1-8] JT-60 Team, JAERI-M 89-093 (1989) p.33-37

[3.1-9] Y.Neyatani, et al. , 19th EPS Conf. Innsbruck (1992) I-447

3.2 Energy Confinement Properties in Ohmic, L-mode and H-mode

One of major subjects of the JT-60U confinement study is to clarify feasibility of the H-mode in higher field regime ($B_t \sim 4T$) at relatively high aspect ratio ($A=R/a=4$). Confinement studies of Ohmic and L-mode are also important for better understanding of confinement and transport.

3.2.1 Ohmic Confinement

Energy confinement time of 700ms was obtained in deuterium plasma at $\bar{n}_e=1 \times 10^{19} m^{-3}$, $I_p=1MA$, $B_t=4T$, $q_{eff}=12$ which is close to the Neo-Alcator scaling including $I_p=2MA$ and $3MA$ discharges, consistent with $n_e q$ dependence. Weak isotope mass dependence $\tau_E(D)/\tau_E(H)=1.1-1.3$ was also observed. Ohmic confinement was also studied with ECE T_e profile and ion temperature consistent with measured DD neutron rate. Ion energy confinement decreases ($\sim 0.3s$) with increasing plasma density, consistent with JT-60 result.

3.2.2 L-mode Confinement at High Aspect Ratio

Two types of L-mode confinement studies was made to document D plasma energy confinement in relatively high aspect ratio. One was I_p and power scan for elongated divertor ($A=3.7$) in which we reached maximum plasma stored energy up to 4.4MJ at 4MA, 20MW accompanied by weak H mode transition. Observed energy confinement time was consistent with ITER power law if the current profile is close to the equilibrium for the discharges $q_{95}>3$. Nine channel edge Thomson scattering data shows clear formation of the edge transport barrier even in the L-mode which was thought to be a unique feature of the H-mode. Second was 2MA power scan of small minor radius ($a_p=0.77m$, $A=4$) plasma to reduce ripple loss and improve power deposition profile. The L-mode confinement in this case was 20-30% higher than that from ITER power law and is close to the Goldston scaling (Aachen,1984).

These experimental results shows JT-60U L-mode confinement is close or slightly better than ITER-89P scaling for which average fusion product $\langle nT \rangle \tau_E \sim (I_p A)^2$ (Fig.I.3.2-1).

3.2.3 Effect of Current Profile on L-mode Confinement

After TFTR current ramp down experiment (Zarnstorff,1990), effect of I_i on energy confinement becomes one of new highlights in this field. More

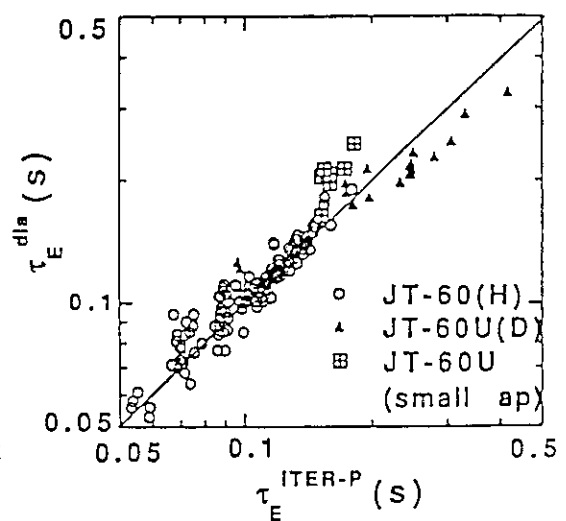


Fig.I.3.2-1 Comparison of measured τ_E and ITER-89P scaling

detailed study was done in JT-60U including the effect of sawtooth on confinement. The confinement enhancement factor (H-factor) increases almost linearly with I_i (Fig.I.3.2-2). But the confinement is also influenced by the sawtooth activities, especially in low q regime. The H-factor increases with increasing sawtooth period.

3.2.4 Isotope Dependence of L-mode Confinement

The effect of ion mass number A_i on the tokamak plasma confinement is still one of unsolved issues. We have compared energy confinement times of $D^0 \rightarrow D^+$ and $H^0 \rightarrow H^+$ plasmas. The ratio of $W_{dia}/(I_i I_p^{0.8})$ for D plasma to H plasma was found to be 1.2-1.3 (Fig.I.3.2-3) while $A_i^{eff}(D)/A_i^{eff}(H)=1.5$ ($A_i^{eff}=(A_i^{eff}(plasma) + A_i^{eff}(beam))/2$) which led to $\tau_E \sim A_i^\alpha$ with $\alpha=0.45-0.65$. Although beam stored energy is two times larger for D beam for the same condition, this difference was not enough to explain the confinement difference.

3.2.5 H-mode Threshold and Confinement

JT-60U is characterized by its high field ($B_t=4T$). And the first wall is almost covered with graphite tiles. These conditions are close to those of experimental reactor. These requires high threshold power and better wall conditioning. Most important subject is thus the H-mode confinement optimization in these conditions.

The threshold power (P_{th}) for L-H transition was studied for various conditions. The P_{th} increases with B_t , consistent with other tokamak experiments. Lowest P_{th} coincides with Nagami's scaling ($P_{th} \sim a^2/k$) including other tokamak results although the wall condition was not good enough. The H-factor over ITER-89P scaling of 1.5 was obtained at $B_t=2.5T$, $I_p=1.7MA$. The transition occurs at $\bar{n}_e \sim 1 \times 10^{19} m^{-3}$ and continuous ELM occurs at $\bar{n}_e \sim 2 \times 10^{19} m^{-3}$. This narrow density window of the ELM-free H-mode is most important issue. At high field, H-mode transition was observed for $P_{abs} \sim 17MW$. Edge electron temperature $T_e(0.95a_p) \sim 1keV$ was obtained at $\bar{n}_e = 5 \times 10^{19} m^{-3}$. The width of the edge transport barrier is $\sim 3cm$ in the outside mid plane. This thickness is ~ 4 times larger than poloidal gyroradius of the bulk ion. Since JT-60U is high poloidal field tokamak, orbit squeezing effect proposed by Shaing is negligibly small. The thickness is close to the slowing down fast ion poloidal gyroradius.

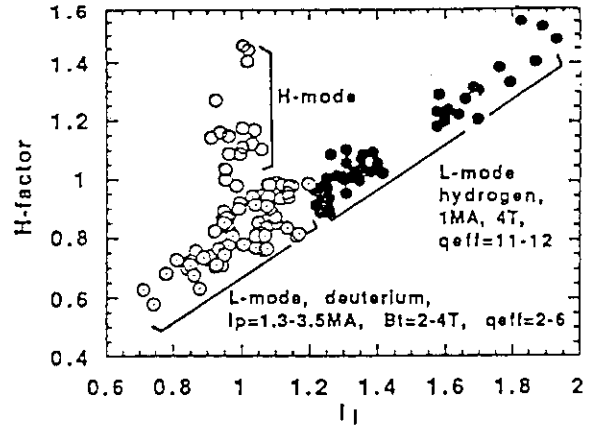


Fig.I.3.2-2 H-factor v.s. I_i (internal inductance)

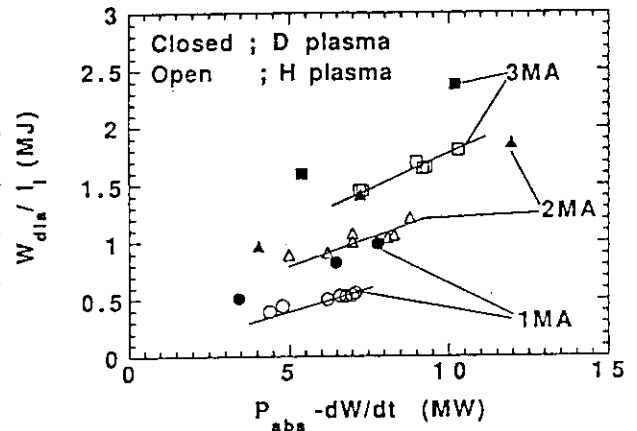


Fig.I.3.2-3 W_{dia}/I_i v.s. net heating power for D and H plasmas

3.3 High Poloidal-Beta Confinement

The goal of high β_p study in JT-60U is to find a realistic view of the high β_p operation for the demonstration of high β_p tokamak reactor concepts such as SSTR and ARIES [3.3-1]. As the JT-60U is capable of operating for a high-field non-circular divertor configuration with a high aspect ratio under high-power auxiliary heating up to 40 MW, the study can be much more reactor-oriented than any other high β_p study attempted before. Succeeding the pioneering work on JT-60 [3.3-2], the high β_p experiment in JT-60U was first carried out in September 1991, in which a highly enhanced regime of plasma confinement was identified.

As the initial results from L-mode and H-mode studies in 1991 did not extrapolate to the first bench mark of the neutron rate (7×10^{15} n/s) in JT-60U, the energetic ion regime was explored in a low current region for increasing it by the beam contributions. On the analogy of the JT-60 high β_p operation, the plasma configuration was chosen to be located inward in the vacuum vessel in order to satisfy the central beam deposition following the vertically inclined beam lines. The resulting small-bore plasma (~ 47 m³) was immune from a fast ion loss due to the significant toroidal field ripple. By scanning the plasma current ($I_p = 1$ -2 MA), a highly enhanced confinement regime was achieved around $I_p \sim 1.1$ MA at a high β_p regime ($\beta_p^{\text{dia}} \sim 2.5$); $3.5 \leq q^* \leq 7.8$ with $B_t = 4.4$ T, where q^* is the cylindrical equivalent safety factor defined as $q^* = \pi(1 + \kappa^2)a^2 B_t / (\mu_0 R_p I_p)$. The discovery of the high β_p enhanced confinement regime spurred the development of a high β_p tokamak reactor and lead to a number of record values in the 1991 run; the neutron rate of 1.3×10^{16} n/s, the ion temperature of ~ 20 keV, the electron temperature of ~ 7 keV, the fusion product of $n_i(0)\tau_E T_i(0) \sim 2 \times 10^{20}$ m⁻³·s·keV and the fusion amplification factor of $Q_{DT} \sim 0.2$.

The high β_p experiments in 1991 spent about four days (63 shots) of the September run. During the early three days, the discharge operation was devoted to searching for optimum plasma current and configuration to increase the neutron rate. The optimized configuration was limited by the inboard clearance (~ 7 cm) and the inside leg of the separatrix placed on the most inner divertor plate; typically, a major radius of $R_p \sim 3.1$ m, a minor radius of $a \sim 0.75$ m, an ellipticity of $\kappa \sim 1.6$ and an aspect ratio of 4.1. Helium TDC (Taylor discharge cleaning) was carried out between shots to obtain a low density degassing discharge; the sequential increase in the target density without shot-by-shot TDC would result in significant deterioration of the confinement enhancement. Under sufficient suppression of deuterium recycling, intense neutral beams up to 21 MW were injected into the low density target plasma.

The enhanced confinement in the high β_p regime strongly depends on the β_p value. As shown in Fig.I.3.3-1, the dependence of the enhancement factor ($H = \tau_E^{\text{dia}} / \tau_E^{\text{L-mode}}$) on the $\epsilon\beta_p$ value would increase the prospects of a future high β_p reactor operating with a high bootstrap current fraction and a high enhancement factor; the L-mode scaling refers to the ITER89 power law. The high β_p plasmas free from sawtooth and $m=1$ activities due to $q > 1$ were characterized by hot-ion mode features ($T_i \sim 3T_e$) with a highly peaked profile of $T_i(0) / \langle T_i \rangle \sim 5$. The confinement

properties were dramatically improved as compared with the high β_p plasmas in the JT-60 hydrogen experiments. It is still an open question whether the difference is attributed to a kind of isotope effect.

The plasma confinement appeared to be most enhanced in the case that frequent D α spikes (FDS's) in the periphery of the plasma were completely suppressed. The FDS-free phase was sustained for ~ 0.8 sec with a low recycling state during beam injection and terminated by the occurrence of a β_p collapse [3.3-3], thereafter large FDS's came out with enhanced recycling. Just before a β_p collapse, high temperature plasmas of $T_i(0) \sim 20$ keV and $T_e(0) \sim 7$ keV (see Fig.I.3.3-2) were attained with high confinement qualities; $H \sim 2.7$ and the Troyon factor $g = \beta_{t \text{ dia}}[\%]/(I_p[\text{MA}]/aB_t) \sim 2.0$ at $P_{\text{abs}} = 17$ MW. The energetic ion regime produced a substantial beam fraction of $\sim 38\%$ to the total stored energy with some pressure anisotropy. The neutron rate increases in proportion to the square of the stored energy as shown in Fig.I.3.3-3, similar to the TFTR supershot regime; the contribution from thermonuclear reaction is $\sim 34\%$ at the maximum neutron rate.

It is apparent that the stability of the high pressure plasmas under a large bootstrap current fraction is crucially important to determine whether such a reactor scenario is workable. While no major disruption was observed, the suppression or avoidance of the β_p collapse became a central issue for the future extension of the high β_p regime.

References

- [3.3-1] Y. Seki, M. Kikuchi, T. Ando et al., in Proc. of the 13th Int. Conf. on Plasma Phys. and Cont. Nucl. Fusion Research, Washington DC, 1990 (IAEA, Vienna, 1991), Vol.3, p.473; R.W. Conn and F. Najmabadi, *ibid.*, p.659.
- [3.3-2] S. Ishida and JT-60 Team, *ibid.*, Vol.1, p.195.
- [3.3-3] S. Ishida, Y. Koide, T. Ozeki et al., Phys. Rev. Lett. **68**(1992)1531.

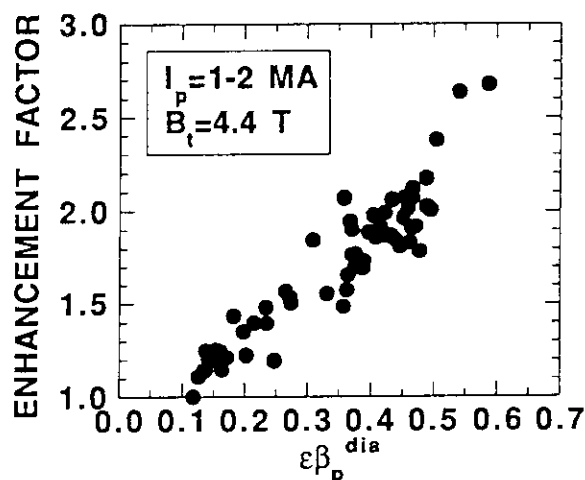


Fig.I.3.3-1 Enhancement factor as a function of $\epsilon\beta_p^{\text{dia}}$

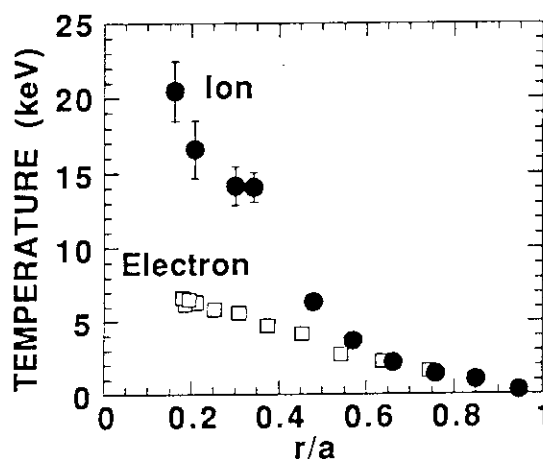


Fig.I.3.3-2 Ion and electron temperature profiles

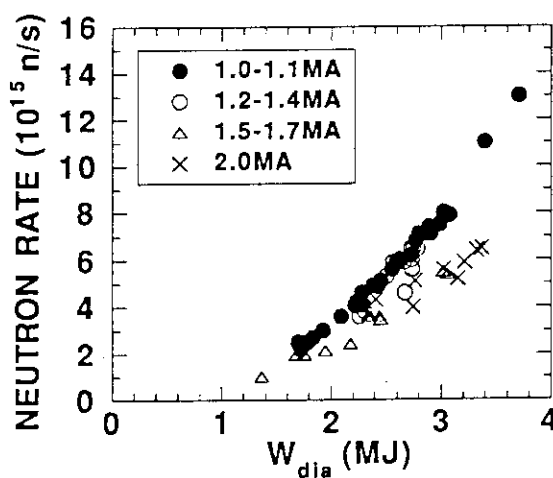


Fig. I.3.3-3 Neutron rate as a function of W_{dia}

3.4 Transport and MHD Studies

The transport properties of JT-60U plasmas have been analyzed in a wide range of plasma parameters. In ohmic plasmas, the particle diffusion coefficient, D , has been evaluated by conducting sinusoidally modulated gas puff into the plasma [3.4-1]. The frequency of gas puff was set between 1 and 7 Hz and the density perturbation level and phase relation were measured. The obtained D is $0.2 \text{ m}^2\text{s}^{-1}$ at the center and $0.8 \text{ m}^2\text{s}^{-1}$ at the edge for $I_p = 2.5 \text{ MA}$.

In ohmic plasmas, the electron thermal diffusivity, χ_e , has been evaluated in the three different way. One is the steady state transport analyses by solving the energy balance equation. We use measured T_e profile, while solve T_i assuming the spatially constant ion thermal diffusivity, χ_i , which is adjusted to reproduce the measured neutron rate and the stored energy measured diamagnetically. Another is to utilize the sawtooth induced heat pulse propagation. The only diagnostics available with enough spatial and time resolution to see the perturbation are the pin diode array which measures the soft X-ray intensity. The perturbation at a specific spatial location can be characterized by the time between the sawtooth crash and the maximum perturbation (ttp = time-to-peak). A plot of the ttp versus spatial location gives information about the transport in the plasma. The other is to conduct gas puff modulation method. The estimated χ_e value at $r = a/2$ is $0.6 \sim 1.0 \text{ m}^2\text{s}^{-1}$ by the steady state calculation. Also steady state calculation with $I_p = 1 \sim 3 \text{ MA}$ plasmas shows no clear I_p dependence of χ_e . The χ_e value by the heat pulse shows $2 \sim 3 \text{ m}^2\text{s}^{-1}$ for $I_p = 3 \text{ MA}$, $B_t = 4 \text{ T}$ plasma, which is about three times larger than that of steady state calculation. The gas puff modulation method shows that the ratio χ_e/D is $5 \sim 10$.

In NBI plasmas, χ_e and χ_i are evaluated from the steady state transport analyses, in which plasma parameter dependence of χ_e and χ_i have been studied. As I_p increases χ_i decrease; $8 \text{ m}^2\text{s}^{-1}$ to $2 \text{ m}^2\text{s}^{-1}$ for $I_p = 1 \sim 4 \text{ MA}$ with $P_{\text{abs}} = 17 \text{ MW}$ and $B_t = 4 \text{ T}$. As P_{abs} increase χ_i increases; $1 \text{ m}^2\text{s}^{-1}$ to $4.5 \text{ m}^2\text{s}^{-1}$ for $P_{\text{abs}} = 8 \sim 20 \text{ MW}$ with $I_p = 3 \text{ MA}$ and $B_t = 4 \text{ T}$. On the other hand, the χ_e value is nearly insensitive to I_p nor P_{abs} , $1 \sim 1.5 \text{ m}^2\text{s}^{-1}$, for the above parameter range. This indicates that the ion transport dominates the overall energy transport. The χ_{eff} value, which is evaluated from one fluid energy balance equation, is almost insensitive to B_t . The χ_e value has been also evaluated by the heat pulse propagation method which shows $0.4 \sim 0.6 \text{ m}^2\text{s}^{-1}$ for $I_p = 3 \text{ MA}$, $P_{\text{abs}} = 17 \text{ MW}$, $B_t = 4 \text{ T}$, which is about one third of steady state calculation. This discrepancy is under investigation.

The anomalous energy transport of JT-60 plasmas have been analyzed from the theoretical point of view. χ_i is evaluated by nonlinear simulation of η_i mode and compared with experimental results. In slab branch, the absolute χ_i values of the mixing length formula of η_i mode and nonlinear result are crucially different, because shear parameter of JT-60 is very small ($S < 0.1$) and the linear mode width of slab η_i mode is broad $\Delta^2 \propto 1/S$ for slab branch. In this weak shear limit, usual mixing length estimate is invalid. In the toroidal branch, the mixing length estimate and nonlinear result are in the same order and both are fairly good in the half way

region of the plasma. However, it cannot explain the anomalous χ_i in the edge region. In Hong / Horton model [3.4-2], the energy is inverse cascading and concentrates in the long wave length region ($k_y \rho_s < 0.1$). In the region $k_y \rho_s > 0.1$, the power spectrum is in the noise level. Improvement of model equations including the trapped electron effect is now undergoing.

The purpose of MHD study in JT-60U is to obtain systematic understandings of MHD instability and clarification of correlation between MHD activities and confinement in tokamak in which safety factor q_{eff} , internal inductance l_i and β are the key parameters. The results for NB heated L-mode discharges with relatively low Toroyon factor (<1.7) are reported as follows.

Based on the ohmic and NB heating experiments, discharge regions related to current driven instabilities are categorized well on the l_i - q_{eff} plane. For a given q_{eff} stable discharges have medium l_i values and disruptive discharges by mode locking appear both in higher l_i and lower l_i . There also exists a boundary of l_i below which sawtooth-free discharges appear. In the sawtooth region, there is another boundary of a profile consistency corresponding to the quasi-stationary current distribution profiles, along which the maximum value of r_{inv}/a (sawtooth inversion radius / minor radius) is almost proportional to $1/q_{\text{eff}}$. (At a given q_{eff} , r_{inv}/a increases with l_i). The sawtooth period τ_{sw} increases with volume averaged electron temperature $\langle Te \rangle$ as $\tau_{\text{sw}} \sim \langle Te \rangle^{3/2}$. This dependence is almost the same as that obtained in [3.4-3].

With increasing β_p , behavior of central MHD changes due to increase in pressure gradient [3.4-4] and bootstrap current. At low β_p , sawteeth accompanied by $m=1$ oscillation are observed. At medium β_p , continuous $m=1$ without sawteeth is observed. At high β_p , both sawtooth and $m=1$ continuous oscillation disappear and central MHD is dominated by higher m/n modes and sometimes large amount of the central energy ($\sim 20\%$ of the total stored energy) is released quickly ($\sim 100\mu\text{s}$) by β_p -collapse (see Sec.3.4). In many cases the β_p -collapse is not followed by major disruption. In JT-60U, fishbone activity is observed when $q_{\text{eff}}\beta_t > 2\sim 3\%$.

Locked modes with rotating precursor at low- l_i have $m \geq 3/n=1$ structure with m/n usually less than q_{eff} , indicating an internal mode. Such locked modes lead to minor disruptions. Locked modes at high l_i (in many cases after detachment) usually exhibit $m=2$ or 3 with $n=1$ and the growth rate ranges from 50 to 500s^{-1} . In case of disruptions preceded by a locked mode with no rotational phase, $m/n=q_{\text{eff}}$, indicating a surface kink mode. In JT-60U, locking occurs when the fluctuation of the poloidal field reaches $\sim 10\text{G}$ ($\sim 0.5\%$ of the equilibrium field) and error fields produced by feeders of divertor coil and primary OH coil seem to affect the locking.

Concerning L-mode confinement, H-factor ($H = \tau_E / \tau_E^{\text{ITER89P}}$) is almost proportional to $l_i^{0.8}$ in the wide range of q_{eff} : $q_{\text{eff}}=2\sim 14$. The degradation of confinement in the low- q region ($q_{\text{eff}} < 4\sim 5$) in L-mode is caused by effects of l_i and sawtooth activity. The maximum value of $H/l_i^{0.8}$ is almost constant in the whole region of q_{eff} . In the low- q region, $H/l_i^{0.8}$ is reduced as sawtooth frequency τ_{sw}^{-1} becomes high and the degradation due to τ_{sw}^{-1} is stronger at lower q_{eff} .

References

- [3.4-1] K. Nagashima et al., in Proc. 19th Eur. Conf. on Controlled Fusion and Plasma Phys., Vol. 1 (1992) 87
- [3.4-2] B. G. Hong and W. Horton, Phys. Fluids B 2 (1990) 978.
- [3.4-3] Y. Kamada et al., GA-A20611, General Atomics 1992.
- [3.4-4] Y. Kamada et al., Phys. Fluids B 4 (1992) 124.

3.5 Impurity and Divertor Characteristics

The activities of impurity and divertor study task force in JT-60U include wall conditioning methods[3.5-1], generation mechanism of carbon impurity[3.5-2], divertor characteristics[3.5-3,4], divertor/sol transport[3.5-5], impurity transport[3.5-6], particle recycling and helium transport[3.5-7] and divertor behaviors prior to disruption[3.5-8]. In this section, we briefly summarize the investigation on carbon impurity generation mechanism[3.5-2], and divertor characteristics[3.5-3].

Fluxes of deuterium ions, oxygen ions and carbon ions in divertor region were measured with spectroscopic diagnostics for the purpose of identification of impurity generation mechanism in ohmically heated deuterium discharges ($I_p=2.0\sim 2.5\text{MA}$) and neutral beam heated discharges ($P_{NB}=5\sim 12\text{MW}$). In order to calculate the carbon influx by sputtering on divertor plates, electron temperature and density profiles near the divertor plates were independently measured. The sputtering yield values were taken from data compiled by Roth[3.5-9]. From the absence of temperature dependence of the measured sputtering yield, the chemical sputtering with deuterium ions has been found to have no effect on the generation of carbon in JT-60U. Fig.I.3.5-1 shows the calculated carbon influx by self-sputtering, physical and chemical sputtering with oxygen ions and physical sputtering (except chemical) with deuterium ions and the measured carbon influx as a function of line averaged electron density in main plasma. The calculated and measured carbon influxes decrease as electron density increases and both dependences on electron density are in good agreement. The carbon influx become large in the low density regime because the energy of ions which bombard divertor plates is high. The discrepancy of a factor of 2.5 between the measured and calculated influxes could arise from profile effects, coarseness of divertor plates [3.5-10], error in estimation of the carbon source by CII line intensity, since some carbon neutrals do not ionize up to CIII. The contributions of the sputtering by carbon, oxygen and deuterium are about 50%, 30% and 20% of total carbon influx in the low density regime ($n_e\sim 1.4 \times 10^{19}\text{m}^{-3}$), respectively. In the high density regime ($n_e\sim 3.4 \times 10^{19}\text{m}^{-3}$), as density of deuterium ions increases, the physical sputtering of deuterium ions occupies the major fraction of total carbon influx.

A dense and cold divertor plasma with an electron density of $n_{ed}=7\times 10^{19}\text{m}^{-3}$ and electron temperature of $T_{ed}=9.5\text{eV}$ was obtained in a high density discharge with a neutral beam power of 8MW. Fully current driven plasmas by LHCD were obtained with main plasma densities of $\sim 1\times 10^{19}\text{m}^{-3}$. With similar heat fluxes to the divertor plates, the electron temperature tend to be higher in LHCD plasmas.

We derived a scaling law of the peaking factor of divertor heat flux that is applicable to beam heated discharges in JT-60U with wide range of plasma parameters. A database was assembled from discharges with $1.2\text{MA} \leq I_p \leq 3\text{MA}$ (plasma current), $1 \times 10^{19}\text{m}^{-3} \leq \bar{n}_e \leq 7 \times 10^{19}\text{m}^{-3}$ (averaged density of main plasma), $1\text{MW} \leq P_{NB} \leq 16\text{MW}$ (NBI heating power), $2.5 \leq q_{eff} \leq 13$ (effective safety factor). The peaking factor Y , defined by $Y = 2\pi R f_{q_{max}} / P_{HEAT}$, is the inverse of the thickness of the scrape-off layer. Here $2\pi R$ is the toroidal circumference, $f_{q_{max}}$ is the maximum heat flux density at the scrape-off layer and P_{HEAT} is the heat flux onto the divertor. Since the peaking factor is dominated by the competing processes of transport along the magnetic field and perpendicular diffusion of particles and heat, it depends on the parameters P_{HEAT} , \bar{n}_e and q_{eff} , which determine the temperature and density in the scrape-off layer and the divertor plasma. From a statistical analysis, we found the peaking factor Y scaled as $P_{HEAT}^{0.49 \pm 0.18} \bar{n}_e^{-0.45 \pm 0.22} q_{eff}^{0.67 \pm 0.18}$ shown in Fig.I.3.5-2. The difference between this scaling and that derived from Harrison's model[3.5-11] ($P_{HEAT}^{5/9} \bar{n}_e^{-7/9} q_{eff}^{4/9}$) could arise from the difference between separatrix density and line-average density.

References

- [3.5-1] M. Shimada et al., in Plasma-Surface Interaction in Controlled Fusion Devices(Proc. 10th Intern. Conf. on Plasma-Surface Interaction in Controlled Fusion Devices, Monterey, 1992), in press.
- [3.5-2] H. Kubo et al., *ibid.*
- [3.5-3] K. Itami et al., *ibid.*
- [3.5-4] N. Asakura et al., *ibid.*
- [3.5-5] K. Shimizu et al., *ibid.*
- [3.5-6] A. Sakasai et al., *ibid.*
- [3.5-7] H. Nakamura et al., *ibid.*
- [3.5-8] N. Hosogane et al., *ibid.*
- [3.5-9] J. Roth, E. Vietzke and A.A. Haasz, Supplement to the Journal Nuclear Fusion, Vol.1 (1991) 63.
- [3.5-10] Y. Hirooka et al., Journal of Nuclear Materials 162-164 (1989) 1004
- [3.5-11] M. Harrison, Analytical Modeling of Divertor and Scrape-Off Layer: ITER-IL-PH-13-9-E12(1989).

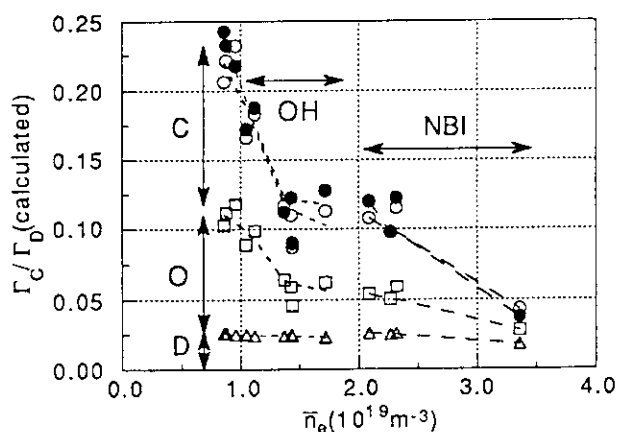


Fig.I.3.5-1 The normalized values of the calculated carbon influx to the measured carbon influx as a function of surface temperature of divertor plates.

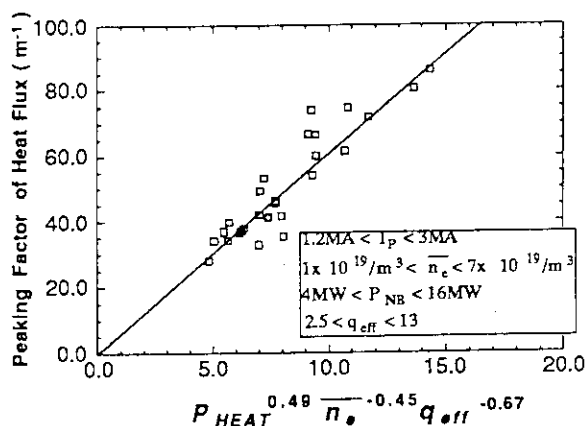


Fig.I.3.5-2 Scaling law of the peaking factor of heat flux in the scrape-off layer. P_{HEAT} , \bar{n}_e and q_{eff} are heat flux to the outer divertor channel, averaged density of the main plasma and effective safety factor, respectively.

3.6 Fast ion studies

3.6.1 D-D fusion reactivity

The initial D-D experiments were undertaken from July 18 to October 4 in 1991. The fusion reactivities of the D-D plasma have been investigated with the neutron monitors employing ^{235}U and ^{238}U fission chambers. In the NB heated discharges, the neutron yield was maximized up to 1.3×10^{16} n/s at relatively low plasma current of 1.1 MA, which associated with low initial target density. In the discharges with $I_p = 1.1$ MA, the neutron yield was limited to be $\sim 7 \times 10^{15}$ n/s in the ELM phase but increased linearly until the β_p collapse occurred. The maximum neutron yield during a pulse increases strongly with the heating power. The upper boundary of the neutron yield varied as $\sim P^{1.8}$ where P is the heating power in the TFTR supershots. In JT-60U, it looks like to vary as $P^{2.5-3}$. It is provably because that the neutron yield has not been maximized in the medium and low heating power regime ($P_{\text{abs}} < 15$ MW). The variation of the neutron yield and the stored energy are well correlated also in the NB heated discharges. When the neutron yield is plotted against the stored energy, the linear dependence of the S_n on W^2 is found for each plasma current.

The neutron production analysis and the projection of the D-T plasma performance have been carried out for the best neutron yield discharge by using a steady-state 1.5 D tokamak code TOPICS. The calculation indicates that for the discharge with the highest Q_{DD} , 27 % of the neutron yield is due to thermal-thermal reactions, 53 % due to beam-thermal and 20 % due to beam-beam reactions. The performance of equivalent D-T discharge was simulated by assuming D^0 beam injecting and 50/50 D/T target plasma using same temperatures and electron density profile, Zeff, beam power, and other parameters as a comparable D-D discharge. The total neutron emission rate is expected to be 1.4×10^{17} n/s in the equivalent D-T discharge, which corresponds to Q_{DT} value of ~ 0.20 .

3.6.2 Fast ion loss by toroidal ripple

The alpha particle loss induced toroidal field ripples is a important problem in the reactor-grade tokamak plasma not only due to the degradation of the alpha heating efficiency but also to the localized heat load on the first wall. The orbit-following Monte Carlo (OFMC) calculation has predicted the ripple loss of alpha particles as well as beam injected ions. The reliability of the calculation, however, has not been confirmed experimentally yet. The JT-60U tokamak is favorable to the ripple loss experiments using neutral beams because JT-60U has 18 toroidal field coils and the ripple magnitude of the full side plasma reaches up to 2.2 % which is near that of ITER and because the neutral beam injection (NBI) lines are near-perpendicular against the magnetic axis. The distribution of the local heat load on the first wall due to the ripple loss has been measured with the toroidal and poloidal arrays of the thermocouple.

Figure I.3.6-1 shows the distributions of the heat load in toroidal direction during NBI heating. The plasma conditions of the shot were plasma current $I_p = 1.7$ MA, neutral beam power

$P_{NB} = 10$ MW, line-averaged electron density $\bar{n}_e = 2.6 \times 10^{19} \text{ m}^{-3}$ and the grad-B ion drift direction oriented downwards. Though the radiation loss and charge exchange loss may be a part of the the heat load onto the first wall, those contributions are negligibly small; those losses are estimated to be as low as 2 W/cm^2 in the considered shot. The heat load on the first wall was localized in both toroidal and poloidal directions; between the toroidal field coils and on the ion drift side. In addition, parameter scan study showed that the heat load increased with the magnitude of ripple δ and/or the effective safety factor q_{eff} . The reason for the increase in heat load is that the ripple well region extends with δ and/or q_{eff} . These experimental observations, the localization of heat load on the ion drift side and the increase in heat load with δ and/or q_{eff} , definitely indicate that the observed heat load is due to fast ion ripple loss.

The ripple loss of the fast ions has been simulated by the orbit-following Monte Carlo code (OFMC). The ripple loss predicted by the OFMC calculation agrees with the experimental results in both toroidal and poloidal distributions within the measurement and calculation uncertainties as shown in Fig. I.3.6-1, which confirms experimentally the validity of the OFMC calculation in a prediction of the alpha particle ripple loss for D-T burning tokamaks.

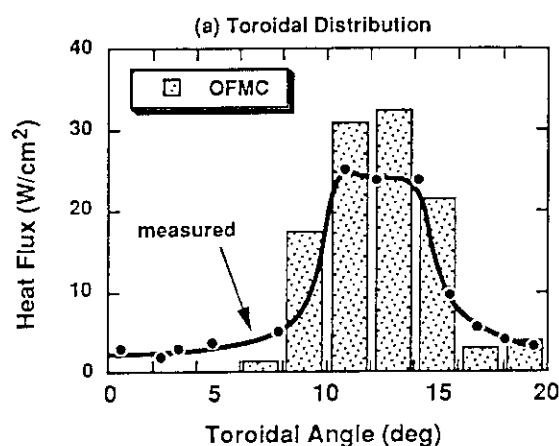


Fig.I.3.6-1 Toroidal distribution of the heat load onto first wall due to the toroidal ripple loss of the beam injected fast ions

3.6.3 Triton burnup experiment

We can estimate the single particle behavior of the alphas in the D-T plasma from the behavior of the 1 MeV toriton produced by $d(d,p)t$ reactions in the D-D plasma because both Larmor radii are almost same. The 1 MeV tritons slow down in the plasma and while doing may burn by $d(t,n)\alpha$ reactions emitting 14 MeV neutron. The confinement and the slowing down of the 1 MeV tritons have been investigated by the time-resolved measurement of the 14 MeV neutrons with a silicon surface-barrier diode positioned outside the vacuum vessel. The time history of the 14 MeV neutron is delayed relative those of the 2.5 MeV neutron produced by the $d(d,n)^3\text{He}$ reactions. The slowing time of the 1 MeV toriton in the NB heated plasma was measured from the delay time of the 14 MeV neutron intensity by perturbing the NB injection power. That in the ohmically heated plasma was measured from the decay time of the 14 MeV neutron intensity after the turn off the NB injection. The measured slowing down times agree with the prediction by the classical theory in both NB and ohmically heated plasmas. The triton burnup ration is in the range 0.2 - 2 % and increases with the plasma current, which indicates that the orbit loss of the 1 MeV toriton decreases with the plasma current.

3.7 LHRF and ICRF Experiments

3.7.1 Lower Hybrid Current Drive Experiment

Steady state operation of the Tokamak Reactor is the most desired scenario for commercial reactor. Development of the non-inductive current drive method is necessary to achieve the steady state operation. In JT-60, Lower Hybrid Current Drive (LHCD) demonstrated notable results of non-inductive current drive of 2 MA, high efficiency $\eta_{CD} (\equiv n_e R_p I_{RF} / P_{LH}) = 0.34 \times 10^{20} \text{ m}^{-2} \text{ A/W}$ and high power LHCD up to $\sim 5 \text{ MW}$ [3.7-1,2], and 80% of the plasma current was driven by the bootstrap current. In JT-60 Upgrade, plasma current is increased up to 6 MA in divertor discharge. LHCD program in JT-60U aims further progress to explore steady state tokamak reactor and study the profile control. In the first campaign, the emphasis of the experiments was placed on the basic understanding of the LHCD, since the expected power level in this period was low around 2 MW.

Maximum LHCD power of $\sim 1.8 \text{ MW}$ has been injected into JT-60U plasma with $B_t = 4 \text{ T}$, $I_p = 1 \sim 2 \text{ MA}$ and hydrogen gas in divertor discharge. In spite of the carbon first wall, density control was easy and very low density plasma far less than $1 \times 10^{19} \text{ m}^{-3}$ was routinely possible in this series of experiment by keeping the wall temperature 150°C and overnight GDC. This enabled driven current of $\sim 2 \text{ MA}$ with 1.1 MW in low density plasma ($\sim 3 \times 10^{18} \text{ m}^{-3}$). The η_{CD} at present is $\sim 0.25 \times 10^{20} \text{ m}^{-2} \text{ A/W}$ and is still low, compared with previous results in JT-60 with the similar launcher. Maximum CDP ($\equiv n_e R_p I_{RF}$) was $0.3 \times 10^{20} \text{ m}^{-2} \text{ MA}$.

Identification of the dispersion relation of the LH wave in tokamak was precisely studied using the NBI as a probe [3.7-3, 4]. The experimental result agrees well with theoretical one and confirmed previous results in JT-60. Rotation of the LHCD plasma is also measured by CXRS. Application of the LHCD drove the plasma slightly to co-direction. Behavior of the fast electrons during LHCD was studied with power modulation. The phase shift of the perpendicular HX signal from the sinusoidally modulated LH power are shown in Fig. I.3.7-1 with various modulation frequencies and they agree well those calculated without the effect of the radial diffusion (solid lines). Therefore, the confinement of the fast electrons in the core plasma is dominated by the slowing down, which is consistent with the energy confinement of the LHCD plasma.

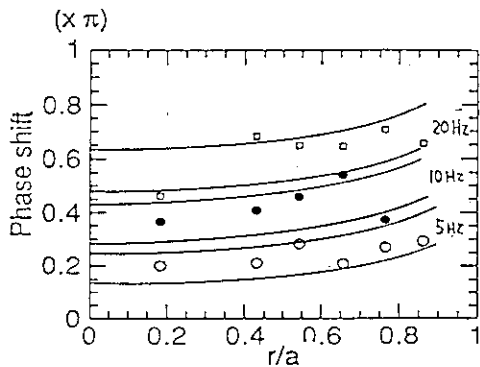


Fig. I.3.7-1 Radial profile of phase delay of the HX signal. Solid lines are calculated ones.

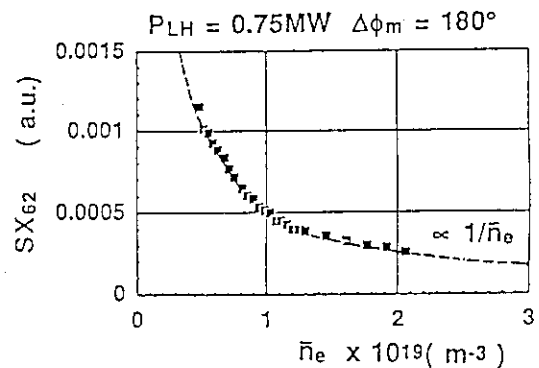


Fig. I.3.7-2 Intensity of SX_{62} vs density. The SX_{62} is proportional to the fast electron loss power to the divertor.

Heat load to the divertor in the presence of the fast electrons produced by the LHCD power is the one of the most interesting engineering topics concerning the ITER/FER design. The effect of the fast electrons to the divertor plate was studied with the Xray signal from divertor plate (SX₆₂). The signal SX₆₂ is inversely proportional to the density as shown in Fig. I.3.7-2. It had been shown previously that energetic electron hitting the thick target radiate Xray and the intensity is proportional to the loss power of the energetic electron. Using this proportionality of the Xray signal, power loss of the fast electrons accelerated by LH wave was estimated. It was found to be small or negligible and again consistent with the confinement of the fast electrons.[3.7-5].

3.7.2 ICRF Experiment

ICRF heating is to be utilized on JT-60U as unique central heating power for confinement study and high energy particle study with coupled power up to 5MW. Specific research items for JT-60U ICRF experiments are as follows: (1) Higher harmonic heating with emphasis on sawtooth stabilization in high density plasmas [3.7-6]. (2) D-³He fusion with fourth harmonic ICRF heating of ³He or deuterium in combination with ³He and deuterium beam injection in high density regimes [3.7-7]. (3) Local current profile control by uni-directional minority ion heating or beam ion acceleration in combination with tangential NBI. (4) More systematic study on synergetic effects between FWEH/CD and LHCD [3.7-8]. In the initial experiments, a good antenna coupling capability with ($\pi,0$) phasing and a small fraction (~ 0.1) of the radiation loss to the injection power have been confirmed. Figure I.3.7-3 indicates antenna coupling resistances as a function of a separatrix-wall distance. It is found that the coupling resistance of the new antennas [3.7-9] are greatly improved from the one of the previous JT-60 antenna.

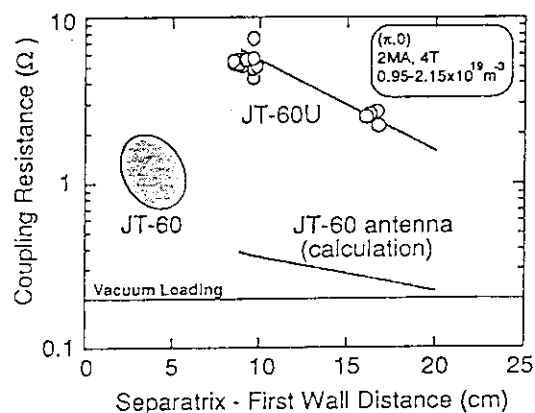


Fig. I.3.7-3 Comparison of antenna coupling resistances between the new JT-60U antennas and the old JT-60 antenna.

References

- [3.7-1] T. Imai, et al., Nuclear Fusion **28**(1988)1341.
- [3.7-2] K. Ushigusa, et al., Plasma Phys. and Contr. Fusion **32**(1990)853.
- [3.7-3] S. Ide, et al., Nuclear Fusion **32**(1992)283.
- [3.7-4] M. Nemoto, et al., Phys. Rev. Lett. **67**(1991)70.
- [3.7-5] K. Ushigusa, et al., to be published.
- [3.7-6] T. Yamamoto et al., Proc. 9th Topical Conf. on Radio-Frequency Power in Plasmas, (Charleston, 1991), AIP, New York, (1991), 243.
- [3.7-7] M. Yamagiwa et al., Nucl. Fusion, **31** (1991) 1519.
- [3.7-8] H. Kimura et al., Proc. IAEA Technical Committee Meeting on Fast Wave Current Drive in Reactor Scale Tokamaks, (Arles, 1991), 261.
- [3.7-9] T. Fujii et al., Proc. 14th Symp. on Fusion Engineering (San Diego, 1991), IEEE, to be published.

3.8 Development of Fusion Plasma Analysis Codes

3.8.1 Profile Data Handling Code System : SLICE

Data from various diagnostics are reconstructed by the profile data handling code system SLICE to physically meaningful profile data consistent with equilibrium calculations by the FBI/SELENE code, which are based on magnetic measurements. SLICE fits the discrete diagnostics data, either local or chord-integrated, to a continuous functional form under constraints which enhance reliability of the fit. The network and data-acquisition functions of the system have been revised to create a flexible and fast interface to the diagnostic data base and the equilibrium data base. Also, the snap-shot analysis function was extended to allow multiple time slices in order to permit analysis of transient phenomena, such as heat-pulse propagation and gas-puff modulation.

3.8.2 1 1/2 Tokamak Transport Code System : TOPICS

For the systematic transport studies in experimental data analysis and theory-based performance analysis, both in steady state and in time evolution, several functions of 1 1/2 tokamak transport code system, TOPICS, have been improved and updated. The major improvements in FY 1991 are the inclusions of the beam-beam contribution in DD and DT reactions, the time-dependent 1D-1V Fokker Planck solver for alpha-particle, the electron-fast ion thermal friction term in the bootstrap current evaluation and the numerical evaluation of trapped particle fraction. The interface with transport and equilibrium data base has been also updated, corresponding to the improvement of each database. The equilibrium analysis consistent with magnetic data and plasma profile data is under way, too, in this code system. The running load module is updated from the system by using the organizing code SPOT for the specified objectives of analysis. Several modules are now running for the steady state and time-evolution analysis of transport properties, verification of fusion reaction rate based on experimental data and the theory-based time dependent analysis of the steady-state tokamak reactor concept.

3.8.3 Orbit-Following Monte Carlo Code: OFMC

The OFMC code to evaluate the particle and energy source profiles was updated for JT-60U experiments with deuterium injection and new vacuum vessel configuration. The non-axisymmetric version of OFMC for studying the ripple loss evaluation includes the module to calculate the effect of radial electric field near the plasma boundary on the ripple trapped particles. The new version has well reproduced the profiles of localized heat deposition resulting from the ripple trapped fast ions. The version to calculate fast ion behaviours in a tokamak with non-cyclic error field has been also developed and the calculation of alpha particle losses with locally rippled toroidal field is under way.

3.8.4 Full Equilibrium Identification Code : FEI

A full equilibrium identification (FEI) code has been developed to analyze MHD equilibrium configurations and the plasma pressure anisotropy in JT-60U. The Grad-Shafranov equation is solved using the SELENE code combined with least-squares minimization techniques to reproduce magnetic data measured outside the plasma. Fifteen one-turn loops have been installed in JT-60U so that the poloidal flux data can be used as constraints for the free boundary problem. Two of the unknown parameters for the plasma current density are determined by specifying I_p and q_0 . The rest two parameters and resulting $\beta_p^{eq} = (\beta_p^{\parallel} + \beta_p^{\perp}) / 2$ and l_i are scanned to minimize the deviations of the calculated poloidal fluxes and magnetic fields from measurements. With this code, β_p^{eq} and l_i are well separated with $\kappa \approx 1.6$ not depending on the assumed q_0 .

3.8.5 Current Drive Analysis Code: ACCOME

The effort of improvement in the numerical code ACCOME for studying the steady state properties of inductive and noninductive current drives in a tokamak was concentrated on the update of MHD equilibrium solver SELENE and the bootstrap current solver. The new version of SELENE includes the various options to determine the plasma boundary, depending on the subject to be solved and increases the flexibility of analysis. Also the numerical accuracy and smoothness of the converged MHD equilibrium solution was improved such that the MHD stability analysis by ERATO-J gives the reliable solution with good convergence character on the radial grid number. The bootstrap current module was improved to include the electron-fast ion thermal friction term and the numerical evaluation of trapped particle fraction. The theoretical efforts to improve the evaluation of fast ion driven bootstrap current are now under going. The new version of ACCOME has been released to LLNL and MIT in U.S.A under the Japan-US collaboration program.

3.8.6 Source Program Organization Tool : SPOT

In order to improve the tractability of NEWORG : the system to control and manage large-size FORTRAN source program, the new version called SPOT has been developed. SPOT was improved to handle more than one include file in addition to several FORTRAN source files. Then SPOT selects necessary subroutines, block data and include members from these files under the guide data, called SPOT DATA, specifying the calculation model, and composes the source FORTRAN program, where unnecessary statements or modules for the model are automatically discarded, and finally creates the load module for running. The man-machine interface to user is also improved in the new version, for the beginner user easily to create his own running code from the large-size programs. The user just prepares the SPOT data and responds to the successive questions from SPOT.

4. RELATED DEVELOPMENTS AND MAINTENANCE

4.1 Developments and evaluation tests of B₄C-overlaid CFC/graphite

We have developed B₄C-overlaid CFC/graphite for plasma facing materials with a low atomic number, high thermal conductivity and high melting point. Surface modification methods employed are three different ones: a conversion method, a chemical vapor deposition (CVD) and a low-pressure plasma-spray (LPPS) method. In the conversion method the surface layer of the substrate graphite is converted into B₄C with chemical reaction between graphite and gaseous boron oxide. On the other hand the other two are the ways in which B₄C-coating are deposited on the substrate graphite.

High heat flux tests in the JAERI electron beam irradiation stand (JEBIS)[4.1-1] reveal that three kinds of B₄C-overlaid CFC have little difference in their surface damage and weight loss up to 12 MW/m² with a time duration of 5 s which is expected to be a maximum heat load for the divertor of JT-60U under normal operation. Under higher heat fluxes with the same duration severe damage such as film exfoliation, film melt and large weight loss are obtained depending on the kinds of prepared materials.

Measurements of deuterium retention characteristics and erosion yields for 1 keV deuterium ion irradiation and of oxygen gettering characteristics for oxygen irradiation have been performed for B₄C-overlaid specimens [4.1-2 ~ 4.1-4]. It was found that the saturation concentration of retained deuteriums is dependent on the irradiation temperature and the release temperature, at which the number of retained deuterium decreases to one half in isochronal annealing, is about 250 K lower for B₄C-overlaid specimens than for graphite as shown in Fig. I.4.1-1. It was also found that the erosion yields of B₄C-overlaid specimens are much lower than that of bare CFC in both chemical sputtering (600-1100 K) and radiation-enhanced sublimation (>1200 K) temperature regions which is shown in Fig. I.4.1-2. Oxygen uptake in B₄C-overlaid specimens is confirmed for 5 keV oxygen ion irradiation at room temperature.

JT-60U in-pile tests reveal that exfoliation and damage of the B₄C-converted divertor tiles are not observed except slight melting at tile edges.

In summary, B₄C-overlaid CFC-graphite has superior characteristics compared to the graphite from view points of surface damage the conversion method is the better way to make B₄C-overlayer on the graphite surface compared with the coating methods.

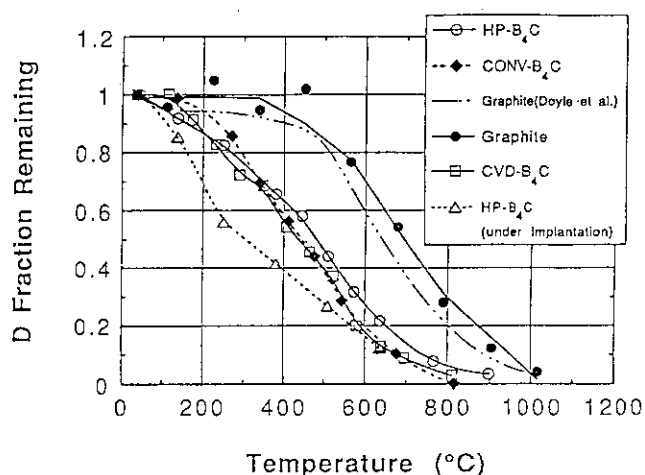


Fig. I.4.1-1 The relative D retention vs. sample temperature in various B₄C specimens and graphite for 1) a saturated sample implanted at room temperature and then isochronally annealed and 2) a sample saturated at the given temperature.

Further developments should be necessary to make thicker B₄C-overlayer and/or carbon fiber reinforced B₄C composite with a good thermal conductivity for the practical use as plasma facing materials in the next step tokamak.

References

- [4.1-1] K. Nakamura et al., to be published in J. Nucl. Mater. (presented at the 10th PSI Conf., Monterey (1992)).
- [4.1-2] R. Jimbou et al., *ibid.*.
- [4.1-3] Y. Gotoh et al., *ibid.*.
- [4.1-4] N. Ogiwara et al., J. Vacuum Soc. Japan 35 (1992) 174.

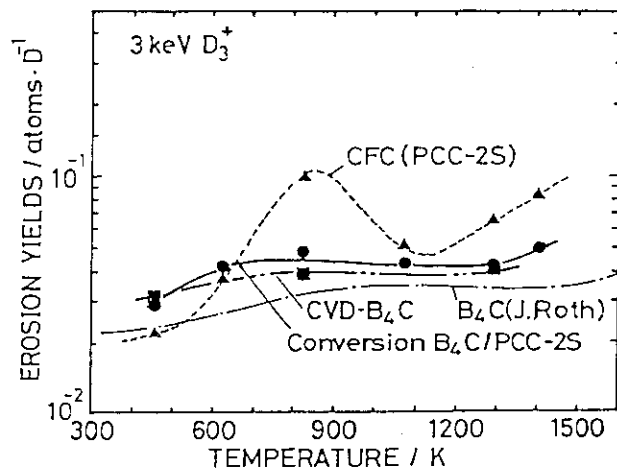


Fig. I.4.1-2 Erosion yields of B₄C-overlaid and CFC specimens for 3 keV D³⁺ irradiation at 6×10^{15} D/cm² in 450 - 1400 K temperature range. The lines are for eye-guide.

4.2 Glow Discharge Cleaning (GDC) System

The modification of GDC system was carried out in May 1991, and a new graphite electrode was installed in JT-60U. Figure I.4.2-2 shows schematic drawing of GDC system. Test operations of GDC system were performed in August through September with conditions shown in Table I.4.2-1, and stable discharges were obtained. The optimization of GDC operation parameters was made until October. During shutdown from November through December, the graphite electrode was replaced by a new one with larger surface area (~4 times) and some monitors were installed as well. From January 1992, a stabilizing resistance was optimized to increase glow current up to ~10 A. Removal rates of gaseous impurities were increased in proportion to glow current as shown in Fig. I.2.2-1.

Table I.4.2-1 Parameters of glow discharge

temperature of vacuum vessel	300 °C
gas	helium
pressure	$\sim 3 \times 10^{-2}$ Pa
pre-ionization	on
glow voltage	600 V
anode voltage	~ 460 V
glow current	~ 1 A

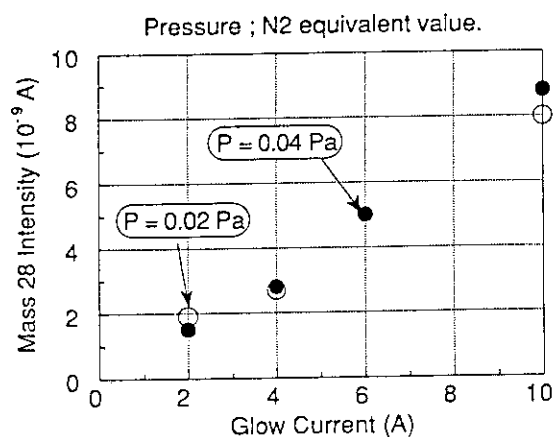
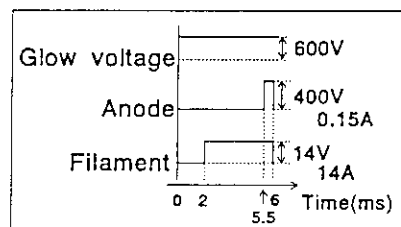
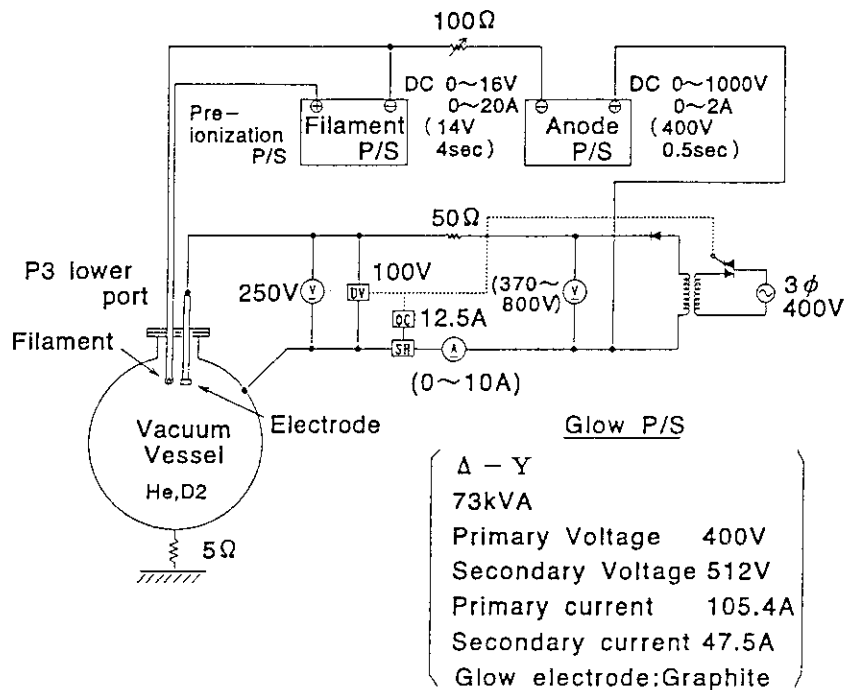


Fig. I.4.2-1 Dependence of mass 28 intensity on glow current



Time chart of pre-ionization

Fig. I.4.2-2 Glow discharge cleaning system of JT-60U

4.3 Related Development in Power supply

A new DDC system which consists of a workstation and microcomputers under VME bus system have been applied to controllers of the thyristor converters [2.3-2]. VME modules, however, were applied only microcomputers, but I/O modules were left as it stands under CAMAC system. In order to process the controllers faster and to simplify the system, we are developing VME I/O modules in hardware and software. We tested some new DI, ADC, DO and VME communication modules with a VME microcomputer in this fiscal year. As test, a measuring the processing time which include an AD converting time by new ADC; ADC05, a calculating time by a microcomputer; MVME 147 SA-2 and a digital output time by a new DO; TMVME 340 was done. The result such as the processing time of 0.23 ms was satisfactory, and this lead us to a plan of replacing the CAMAC I/O modules to the new VME I/O modules.

In order to clean first walls efficiently by the taylor-type discharge cleaning (TD) changing the connection between power supplies and coils by controlling disconnecting

has been investigated. The efficient methods proved are as follows. First, the power supply for TDC deliver the power not only to F-coil, but to V-coil, and the direction of these two coils' currents is converse to each other. This method is preferable to clean the first walls of the outerboard of the vacuum vessel. Second, D-coil forms the short circuit at the point of the disconnecting switches, and so the plasma current of TDC strikes the diverter plates by forces which pull each other between plasma current and induced current on the D-coil. This method is effective in cleaning the diverter plates.

We are investigating on advanced power supply systems of the next step devices such as ITER, JT-60 super upgrade and so on. In this fiscal year, electric energy storage systems were mainly investigated.

References

[2.3-2] T.Aoyagi et al., Proc. of Inter Confer. on accelerator and Large Exp. Phys. Control System, Tsukuba, 1991

4.4 Design study of a negative-ion based NBI system for JT-60U

The negative-ion based NBI system[4.4-1] for JT-60U is required a specification as follows;

- Beam energy: 500keV
- Injection power: 10MW
- Pulse length: 10sec
- Beamline: 1 unit/co-injection
- Beam species: D/H
- Gas influx into tokamak: less than $0.2 \text{ Pa m}^3/\text{s}$

An ion source accelerates the negative deuterium ion beam of 22A (current density: 13 mA/cm^2) at 500keV with a beam divergence of below 5mrad. An multi-cusp type with plasma grid(PG) magnetic filter is adopted as a negative ion generator. An accelerator is a three stages electrostatic acceleration system. An insulator column is made of FRP. A size of the ion source is 2.2 m in diameter and 1.8 m in height. Two sources are mounted on a beamline.

A beamline is composed of an ion source tank, a neutralizer cell tank, an ion dump tank and a drift duct. The ion source tank houses a cryopump for evacuation of gas in the accelerator region to minimize a stripping loss of the negative-ion beam before acceleration.

The ion dump tank houses a positive and a negative ion dumps, an ion beam bending coils, a calorimeter, a set of cryopump and beam limiters. The beamline length from ion source to the drift duct exit is about 24 m. A plane view of the beamline is shown in Fig.I.4.4-1.

An ion source power supply is composed of a pair of negative-ion generator and beam extraction power supplies, and a set of acceleration power supply. The ion generator and the extraction power supplies are mounted on a high voltage table of which potential is floating about 500kV. The high voltage table is placed in a assembly room near the ion source, and its

power is fed by the way of an insulation transformer and a SF₆ gas insulating duct. The acceleration power supply is adopted a high frequency AC side switching using converter/inverter system as a fast cut-off of the current. The capability of the acceleration power supply is 500kV/64A.

The design study of the NBI system has been completed, and its construction will start in 1992.

References

[4.4-1] M.Kuriyama, et al., Design of a Negative-Ion Based NBI System for JT-60U, IEEE 14th Symp.on Fusion Enging.,San Diego(1991)

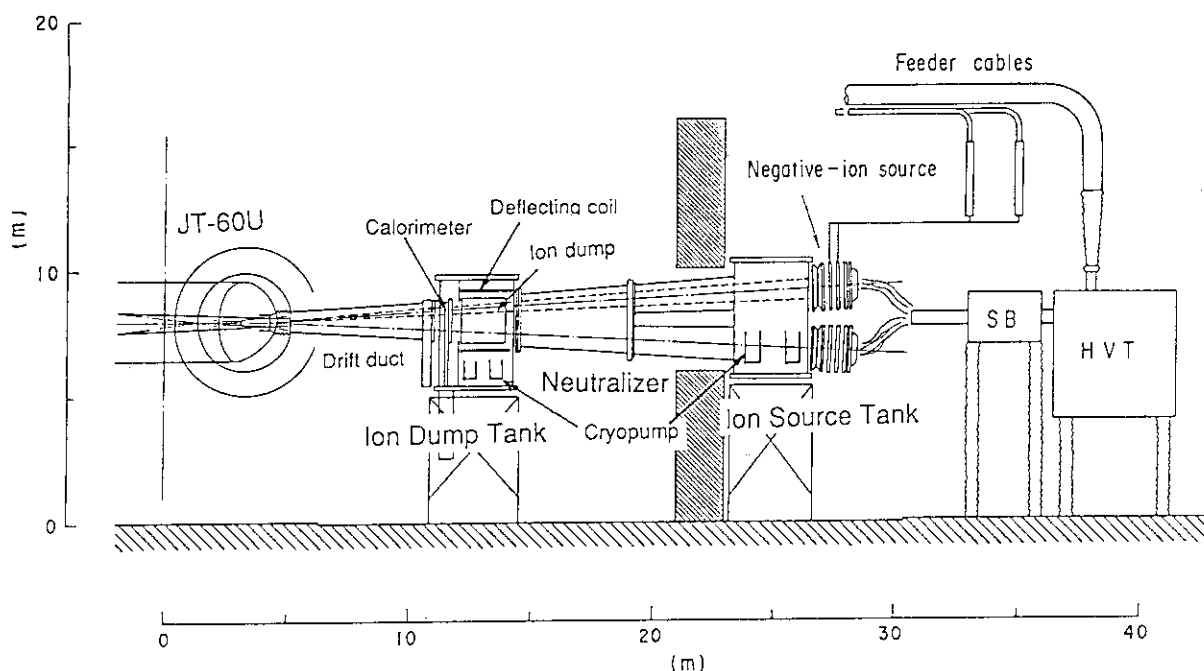


Fig.I.4.4-1 Negative-ion based NBI for JT-60U

4.5 RF development

4.5.1 Development of the launcher in LHCD system

Successful experiments have been carried out by using a multijunction grill on JT-60. In these experiments, it was clearly shown that the coherent wave spectrum improves the current drive efficiency [4.5-1]. On JT-60U, a large size launcher is newly designed to improve wave spectrum by increasing the number of the waveguides up to 192 because a large size port is set for LHCD system on the vacuum vessel.

We optimized the phasing and dividing number to launch a sharp spectrum with a high directivity by using the scattering matrix method, and decided the launcher structure of 4x4 multijunction module, in which RF power is divided into 12 subwaveguides. This new launcher

is expected to improve current drive efficiency by 20~30% compared with the previous launcher on JT-60 [4.5-2]. Figure I.4.5-1 shows the wave spectra of the conventional grill, the old multijunction grill of JT-60 and this new multijunction grill.

The main concern is to fabricate the multijunction module with a large number of subwaveguide. The conventional multijunction launchers have been usually employed

standard sized waveguides to avoid higher modes, however, this requirement makes the construction of the multijunction launcher complicated. To simplify the multijunction launcher with a large number of sub-waveguides, we have adopted oversized taper waveguides and then divided the RF power into multi-subwaveguides at one junction point. We have investigated RF properties of this new type launcher by using a proto-type module, and confirmed that phasing and power dividing rate are well explained by the scattering matrix method without higher modes when the reflection coefficient at the subwaveguides is less than ~10%. Therefore, a high current drive efficiency is expected as far as a good coupling is kept.

This new launcher will be installed on JT-60U at the end of 1992, and be started to operate at the beginning of 1993.

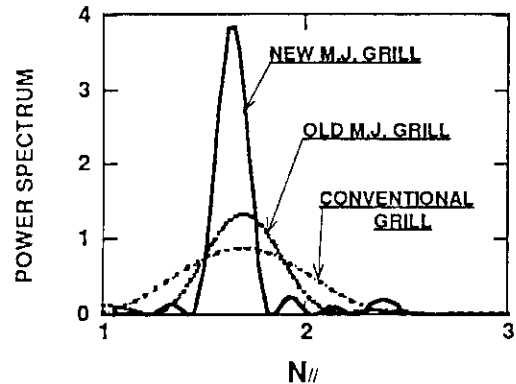


Fig. I.4.5-1 Wave spectra of LHCD grills

4.5.2 Analysis of cryogenic window for electron cyclotron heating system

The preliminary design of 5 MW electron cyclotron heating system was made for JT-60U. The transmission line has closed evacuated corrugated waveguides capable of carrying 1 MW CW RF power in the Gaussian-like HE_{11} mode. In the JT-60U the RF window placed close to torus is needed to avoid spread of tritium and radioactive dust from the tokamak. The evacuated waveguide transmission line adopted makes it ease to employ the cryogenic window. In this section, analysis of the cryogenically cooled window is described from the thermal-mechanical point of view [4.5-3]. At low temperature many parameters of the material used, which determine the window stress, are much improved.

Table I. 4.5-1 Specification for conceptual design of window

Material	Sapphire
Structure	Single disk
Cooling	Edge cooling
Frequency	110 GHz
Transmitted Power	1 MW
RF Mode	HE_{11}
Dia. of Waveguide	60.3 mm
Thickness of Disk	1.33 mm
Pressure in Waveguide	< 0.1 Pa

An edge-cooled single disk window operating at a cryogenic temperature is considered. The specification for design of the window is shown in Table I.4.5-1. The diameter of the disk is 80 mm and its thickness is 1.33 mm corresponding to three half-wavelengths of the microwave in the sapphire. We have calculated the increased temperature and resultant thermal stresses of the disk under the steady state condition. Dielectric heating of the sapphire appears to be the most crucial aspect of the cryogenic window. For the HE_{11} mode the thermal deposited power density has a peak at the center of the disk and most of deposition power concentrates within a radius of 1.7 cm. The heat deposited around the center is conducted to the peripheral region. Total deposited power must be removed at the edge. The thermal conductivity of the sapphire as a function of temperature is also used. Figure I.4.5-2 shows the increased temperature ΔT at the center of the window disk and the deposited RF power on the disk as a function of the edge temperature. It is shown that preferable operation region of the temperature is ranged up to 40K in view of avoiding the thermal runaway. It requires the cooling capability up to 30 W. The increased temperature is less than one degree, which makes thermal stress negligible small comparing with the allowable stress of a sapphire.

A small refrigerator obtained commercially is employed to remove the deposited power at the edge. We approximate the performance of the cooling capability in $T_{\text{edge}} = T_0 + 0.98 P_d$ where T_{edge} is the temperature at the edge of the disk, T_0 the temperature of a cold head of the refrigerator with no thermal load, and P_d is the deposited power on the disk in watt. The edge temperature and the thermal stress at the center as a function of T_0 are plotted in Fig. I.4.5-3. It is clear that the thermal stress is no longer the limiting mechanism at a cryogenic temperature.

References

- [4.5-1] Y. Ikeda, et al., Plasma Devices and Operations, 155 (1991).
- [4.5-2] Y. Ikeda, et al., Proc. of 14th Symp. on Fusion Eng., San Diego, 1991.
- [4.5-3] T. Yamamoto, et al., in Radio-Frequency Power in Plasma (Proc. 9th Top. Conf., Charleston, 1991) p.243.

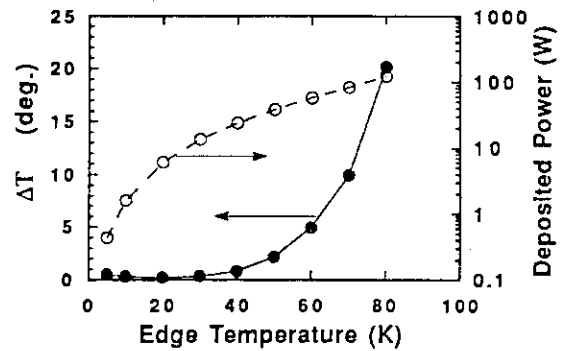


Fig. I. 4.5-2 Increased temperature ΔT at the center of the window disk and deposited RF power as a function of the edge temperature.

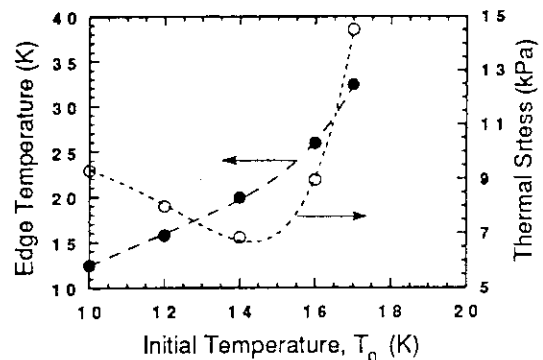


Fig. I.4.5-3 The edge temperature and thermal stress at the center as a function of initial temperature T_0 .

II. JFT-2M PROGRAM

1. Toroidal Confinement Experiments

1.1 Overview

The main progress in JFT-2M program is summarized. For JFY1991, intensive divertor biasing experiments have been performed in order to investigate observed modification of transport properties in scrape-off layer plasmas. The other major efforts have been put on a systematic study of plasma response to externally applied helical magnetic perturbations, produced by the Ergodic Magnetic Limiter coils which were completed and mounted outside on the JFT-2M vacuum vessel in JFY1990(Old type coils; see Fig.II.1.1-1).

In addition, New sets of coils to produce a wide range of helical perturbations have been installed onto the inside wall of the vacuum vessel and brought into operation in this fiscal year(Ladder type coils and saddle type coils; see Fig.II.1.1-2). Experiments with these coils have been performed with much emphasis on transport and MHD characteristics including disruption control.

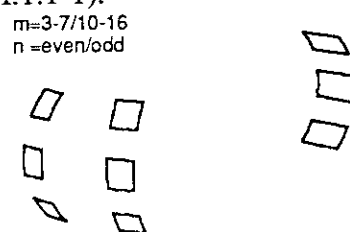
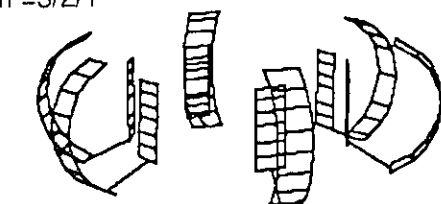


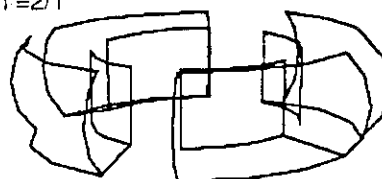
Fig.II.1.1-1 Ergodic Magnetic Limiter Coils (Old type coils)

$m=5/10$
 $n=3/2/1$



Ergodic Magnetic Limiter Coils (Ladder type coils)

$m=2$
 $n=2/1$



Disruption Control Coils (Saddle type coils)

Fig.II.1.1-2 New ergodic magnetic limiter coils installed inside the vacuum chamber in JFY 1991

TV Thomson scattering system(TVTS) has been completed on JFT-2M in a collaboration between JAERI and PPPL.

1.2 Experimental results

1.2.1 H-mode studies

Parameter dependence of radial structure of edge poloidal rotation is studied with spectroscopic measurements for L- and H-mode plasmas in the JFT-2M tokamak. The poloidal rotation velocity profiles and ion temperature profiles at ohmic ($t = 692$ ms), L-mode ($t = 742$ ms) and H-mode ($t = 792$ ms) are shown in Fig.II.1.2-1 and Fig.II.1.2-2. The plasma always rotates in the ion diamagnetic direction outside the separatrix and in the electron diamagnetic direction inside the separatrix. The position, where the plasma does not rotate poloidally, moves

outward as the plasma changes from ohmic to L- and H-mode. The radial electric field profiles are inferred from poloidal/toroidal rotation and ion pressure profiles using the CXRS and emission spectroscopy technique at CVI 5292 Å and the ion momentum balance equation. The electric field becomes more negative in H-mode, corresponding to an increase of poloidal rotation in the electron diamagnetic direction. The gradient of the electric field inside the separatrix, $ds = -1.5$ cm, is positive in ohmic phase, slightly positive in L-mode and becomes negative in the H-mode.

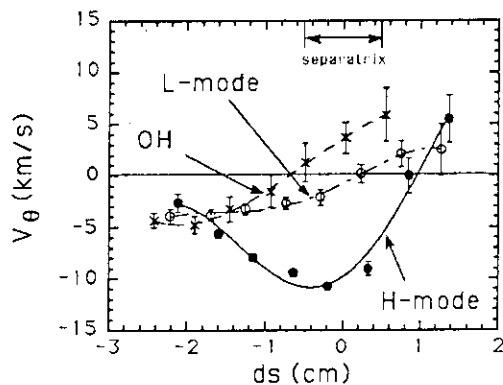


Fig.II.1.2-1 Profiles of poloidal rotation

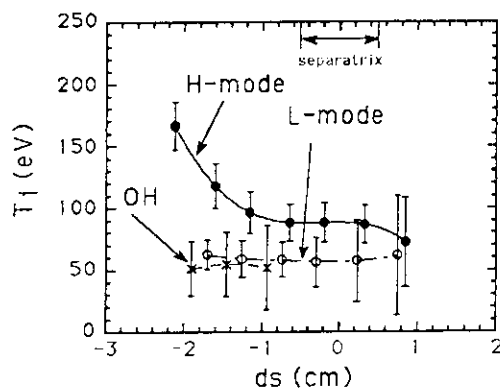
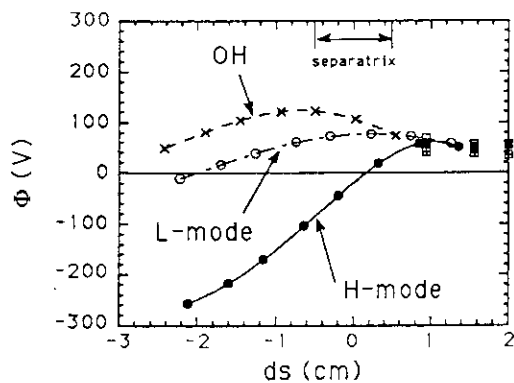
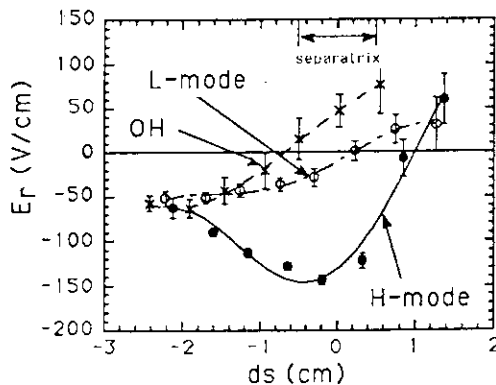


Fig.II.1.2-2 Profiles of ion temperature

The relative space potentials in the plasma are derived by integrating the radial electric field. Combining the measurements of space potential with electric probes, the profiles of space potential for ohmic, L-mode and H-mode are obtained as shown in Fig.II.1.2-3. The space potentials just inside the separatrix are positive in ohmic and negative in H-mode. This negative space potential is -270 V, while the ion temperature is about 170 eV at $ds = -2.1$ cm. These profile measurements indicate that the improvement of thermal transport correlates to the negative $\partial E_r / \partial r$. In conclusion, both E_r and $\partial E_r / \partial r$ become more negative in the thermal barrier, 1-2 cm inside the separatrix, after the L/H transition. Positive $\partial E_r / \partial r$ is observed outside of the separatrix both for L- and H-mode plasmas.



Potential profiles



Radial electric field profiles

Fig.II.1.2-3

1.2.2 Divertor biasing experiments

Effects of divertor biasing have been investigated in relation to transport properties in scrape-off layer plasmas. The JFT-2M divertor biasing system is schematically shown in Fig.II.1.2-4. The bottom inside and outside divertor plates are electrically insulated from the vacuum vessel and both plates are consisted of 16 and 18 toroidally segmented pieces, respectively.

Two types of biasing schemes have been employed; a unipolar biasing scheme in which the inside and outside plates are kept at the same potential with respect to the vacuum vessel, and a differential biasing scheme in which the inside divertor plates are biased with respect to the outside divertor plates. There is a spontaneous current of about 100 A from the outer plates (electron and low field side) to the inner plates (ion and high field side) in case of no biasing.

In recent experiments the negative unipolar biasing has been proved to be effective in reducing the threshold power for L-H transitions. The threshold power is reduced by a factor of two with the negative unipolar biasing of -80V. On the other hand, when the positive differential biasing is applied, the threshold power increases with the biasing voltage. The potential profiles in the scrape-off layer were measured by movable Langmuir probes and shown in Fig.II.1.2-5. The results show that a negative radial electric field is formed just outside the separatrix, suggesting a key role of radial electric field. All relevant physical quantities are now under investigation in order to clarify the phenomena.

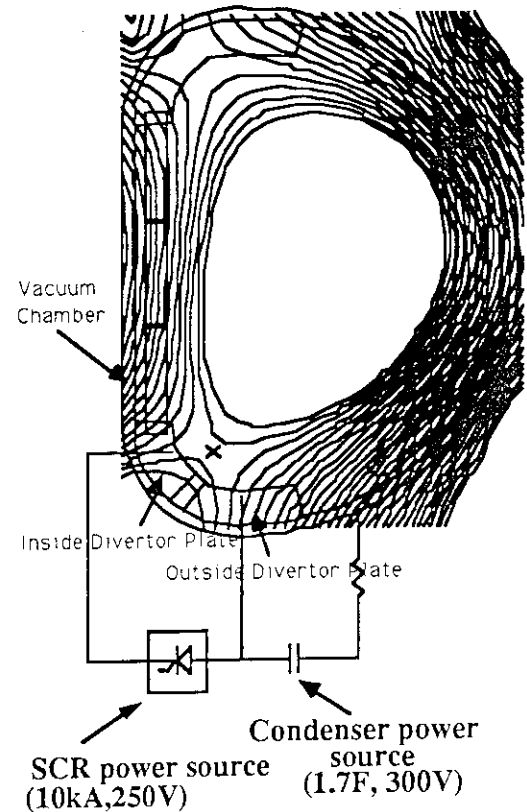


Fig.II.1.2-4 JFT-2M Divertor Biasing System
34 carbon plates can be biased.
(inside divertor plate: 16, outside: 18)

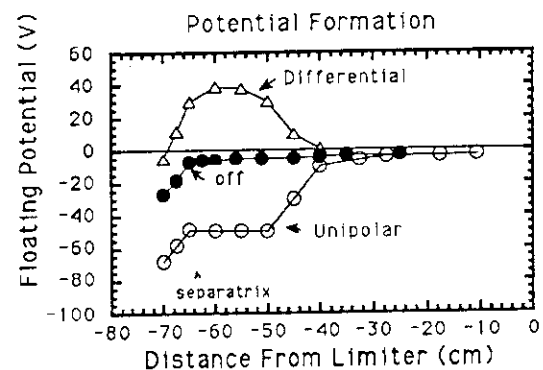


Fig.II.1.2-5 Potential profiles with various divertor biasing schemes.

1.2.3 Disruption control with EML coils

Disruptions during the current ramp-up phase have been shown to be avoided by applying the ergodic magnetic field. A time behavior of the plasma current and magnetic fluctuations are shown in Fig.II.1.2-6. A plasma disruption occurred at 400 msec because of a magnetic fluctuation which began to grow at 150 msec. This fluctuation can be suppressed by a current exceeding 0.5 KA in the Saddle type coils($m=2/n=1$), and as a result the disruptions can be avoided. A duration of more than 50 msec of the ergodic field pulse was necessary to avoid the reappearance of the instability. The magnetic field of Ladder coils ($m=5/n=1$) has also the similar effect on the disruption during the current ramp-up phase.

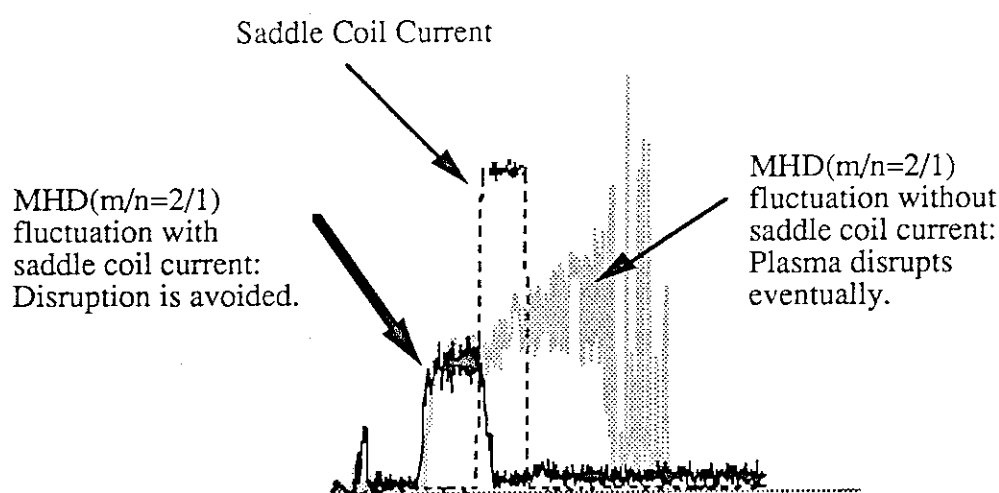


Fig.II.1.2-6 Disruption control with saddle coil coil current

1.2.4 Disruption control with ECH

The typical MHD disruption at safety factor $q_a=3$ has been suppressed by off-central electron cyclotron heating with power of 70-80kW in JFT-2M tokamak. For the suppression the electron cyclotron resonance layer has to be placed radially in a very narrow region of width about 1 cm near $q=2$ surface. The observed narrow suppression window suggests that the basic mechanism responsible for the suppression is direct island heating. Actually time scale of the suppression is much faster than the time scale of the change of overall current profile. Fig.II.1.2-7 shows the suppression of the amplitude of

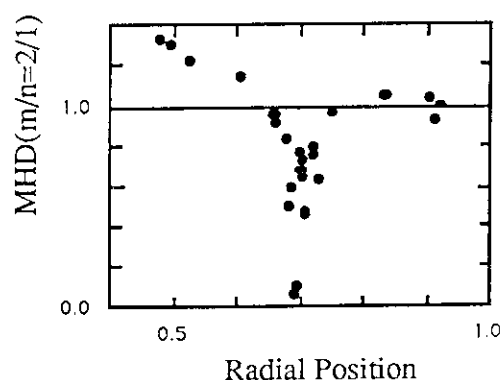


Fig.II.1.2-7 Relative change of MHD amplitude by the application of ECH(140kW).

the MHD instability vs. radial positions of the ECR layer. The suppression occurs only when the ECR layer is located at $r_0/a=0.7$ (r_0 is the radial coordinate of the ECR layer and a is the plasma minor radius). In order to suppress the mode and avoid the disruptions the radial position of the ECR layer should be tuned within 1-2 cm. An enhancement of the mode occurs when the ECR layer is located inside $r_0/a<0.60$.

2. Operation and Maintenance

2.1 Introduction

JFT-2M tokamak has been operated from 1983 by two laboratories (Experimental plasma physics lab. , JFT-2M facility div.). Operation and maintenance of JFT-2M facility and development study of new equipments applicable to JFT-2M tokamak are main parts of facility division. Experimental plan and operation schedule are arranged every week at the group leader meeting. In this fiscal year, each apparatus has been operated smoothly according to the experimental plan, and careful examination of machine status was also carried out daily and periodically. As for development of equipments, new ergodic field coils were installed inside the vacuum vessel to study plasma disruption control .

2.2 Operation and maintenance

Summaries of operation records for main apparatus are listed in Table II.2.2.1. In this fiscal year, two long vent works were carried out first to install two types of disruption-control coil systems inside the vacuum vessel and secondary to repair some troubles in electrical insulators. So two times of long conditioning operation (Baking and TDC) were necessary to start experimental operations and total shot numbers are a little less than that of average years. Main apparatus such as the flywheel motor-generator (MG), JFT-2M machine, neutral beam injection system (NBI), electron cyclotron heating system (ECH) and fast wave current drive system (FW) have been operated smoothly according to experimental plan. Necessary checks and regular examinations of apparatus by each maker were carried out during machine stop phase.

2.3 Development of equipments and instruments

In collaboration with the experimental plasma physics laboratory, development studies have been carried out as follows. As for JFT-2M machine, two types of disruption control coil system were installed inside the vacuum vessel and a fast-chopper power supply was modified to be appropriate to JFT-2M operation specifications. After the experimental operation, some electrical insulators were suffered from plasma arcing and sputtering, then material and structure of insulator were improved not to be injured by the plasma.

The pre-ionization beam system was improved to be usable as a diagnostic neutral beam for the charge exchange recombination measurement. The power supply of arc plasma was

the MHD instability vs. radial positions of the ECR layer. The suppression occurs only when the ECR layer is located at $r_0/a=0.7$ (r_0 is the radial coordinate of the ECR layer and a is the plasma minor radius). In order to suppress the mode and avoid the disruptions the radial position of the ECR layer should be tuned within 1-2 cm. An enhancement of the mode occurs when the ECR layer is located inside $r_0/a<0.60$.

2. Operation and Maintenance

2.1 Introduction

JFT-2M tokamak has been operated from 1983 by two laboratories (Experimental plasma physics lab. , JFT-2M facility div.). Operation and maintenance of JFT-2M facility and development study of new equipments applicable to JFT-2M tokamak are main parts of facility division. Experimental plan and operation schedule are arranged every week at the group leader meeting. In this fiscal year, each apparatus has been operated smoothly according to the experimental plan, and careful examination of machine status was also carried out daily and periodically. As for development of equipments, new ergodic field coils were installed inside the vacuum vessel to study plasma disruption control .

2.2 Operation and maintenance

Summaries of operation records for main apparatus are listed in Table II.2.2.1. In this fiscal year, two long vent works were carried out first to install two types of disruption-control coil systems inside the vacuum vessel and secondary to repair some troubles in electrical insulators. So two times of long conditioning operation (Baking and TDC) were necessary to start experimental operations and total shot numbers are a little less than that of average years. Main apparatus such as the flywheel motor-generator (MG), JFT-2M machine, neutral beam injection system (NBI), electron cyclotron heating system (ECH) and fast wave current drive system (FW) have been operated smoothly according to experimental plan. Necessary checks and regular examinations of apparatus by each maker were carried out during machine stop phase.

2.3 Development of equipments and instruments

In collaboration with the experimental plasma physics laboratory, development studies have been carried out as follows. As for JFT-2M machine, two types of disruption control coil system were installed inside the vacuum vessel and a fast-chopper power supply was modified to be appropriate to JFT-2M operation specifications. After the experimental operation, some electrical insulators were suffered from plasma arcing and sputtering, then material and structure of insulator were improved not to be injured by the plasma.

The pre-ionization beam system was improved to be usable as a diagnostic neutral beam for the charge exchange recombination measurement. The power supply of arc plasma was

Table II.2.2.1 Summary of operation records for main apparatus

Apparatus \ Year		FY 1990	FY 1991				
			Apr-Jun	Jul-Sep	Oct-Dec	Jan-Mar	Total
MG	MG(#1) Operation (hours)	1,004	81	278	60	297	716
	MG(#2) Operation (hours)	1,003	80	278	60	297	715
JFT-2M	Total Operation (hours)	135	4	33	1	27	65
	Discharge Numbers (shots)	6,118	171	1,905	38	1,806	3,920
	Discharge Cleaning (hours)	218	36	13	36	67	152
	Baking (times)	2	1	0	1	0	2
	Pellet Injection (days)	13	0	0	0	0	0
NBI	Total Operation (days)	80	11	29	0	19	59
	Total Injection (times) A	37,365	0	6,955	0	6,576	13,531
	Total Injection (times) B	38,655	0	5,504	0	7,005	12,509
ECH	Total Operation (days)	51	0	5	0	12	17
	Total Injection (times)	157,130	0	6,965	0	4,818	11,783
FW	Total Operation (days)	42	15	19	1	0	35
	Total Injection (hours)	320	109	146	4	0	259

improved to draw 5A beam current. A new ion source with good divergence was installed and test run of total system has started.

As for the pellet injector, development study on a higher repetition and faster speed injector (10 Hz repetition and 2 km/s) was continued. Improvements of the fast acting electro-magnetic valve and the Liq.He cooling capability around the gun barrel were carried out to suppress the high heat road by propellant gas and experimental runs have started.

As for the wall cleaning study, comparison of working gas effect (H₂, He, Ne) in the glow discharge cleaning (GDC) was carried out and it was clearly shown that a sequential procedure of Ne GDC and He GDC is fairly effective to reduce oxygen impurity release. On the other hand, investigation on another boron coating method without handling diboran gas showed that the RF sputtering of boron target is a proper candidate in JFT-2M machine and now production of target material and modifications of RF sputtering system are in preparation.

III. PLASMA THEORY AND COMPUTATION

1. Introduction

During FY1991 the theoretical and computational works were carried out extensively by putting emphases on the following problems.

As for the confinement theory the ion temperature gradient (ITG) mode was studied both analytically and numerically. In relation with the plasma heating several problems relating to the FEL as a high power rf source were studied. Concerning the MHD analyses studies relating to the bootstrap current and beta optimization were carried out for wide ranges of parameters, and positional instability analyses were made. Nonlinear analyses of the mode locking phenomena were also carried out. As for the burning plasma analyses fusion yield in a beam-heated plasma was computed and the loss process of the fast ions in a burning plasma was investigated. Alpha particle dynamics during the internal disruption and the ripple loss of alpha particles were also studied. In preparation for the future large scale computer simulations development of particle codes and the plasma simulator METIS was continued.

2. Analyses of Confinement and Heating Processes

2.1 Confinement scaling for thermal energy in JT-60 L-mode plasmas [2.1-1]

The global energy confinement scaling in tokamak L-mode plasmas plays an important role to guess the transport mechanism as well as to predict the performance of tokamak reactors. To analyze the scaling it should be noted that the fast ion energy component accounts for a certain amount of fraction in the total energy though the thermal energy component is reflected more in the anomalous conductive loss due to plasma turbulence. We analyzed in detail the kinetic database of JT-60 [2.1-2] and obtained an expression for the thermal energy component, $W_{th} \propto (I_p B_t n_e)^{1/2} P_t^{1/3}$, where I_p is the plasma current, B_t the toroidal magnetic field, n_e the electron density and P_t the total heating power. On the basis of this scaling, we reached a presumption that a collisionless or weak-collisional high- β transport dominates the tokamak L-mode plasmas.

References

- [2.1-1] T. Takizuka, Proc. 1992 ICPP, Innsbruck, 1992, Part I, 51.
- [2.1-2] M. Kikuchi, et al., JAERI-M 91-057 (1991).

2.2 Neoclassical theory of fast ions with isotropic velocity distribution function[2.2-1,2.2-2]

Coupled equations of neoclassical friction-viscosity force balance for thermal particles and fast ions resulting from a fusion reaction or additional heatings have been derived. Fast ions are assumed to be isotropic in the velocity space and to have the small banana size in comparison with the plasma radius. First order solution of the drift kinetic equation of fast ion

III. PLASMA THEORY AND COMPUTATION

1. Introduction

During FY1991 the theoretical and computational works were carried out extensively by putting emphases on the following problems.

As for the confinement theory the ion temperature gradient (ITG) mode was studied both analytically and numerically. In relation with the plasma heating several problems relating to the FEL as a high power rf source were studied. Concerning the MHD analyses studies relating to the bootstrap current and beta optimization were carried out for wide ranges of parameters, and positional instability analyses were made. Nonlinear analyses of the mode locking phenomena were also carried out. As for the burning plasma analyses fusion yield in a beam-heated plasma was computed and the loss process of the fast ions in a burning plasma was investigated. Alpha particle dynamics during the internal disruption and the ripple loss of alpha particles were also studied. In preparation for the future large scale computer simulations development of particle codes and the plasma simulator METIS was continued.

2. Analyses of Confinement and Heating Processes

2.1 Confinement scaling for thermal energy in JT-60 L-mode plasmas [2.1-1]

The global energy confinement scaling in tokamak L-mode plasmas plays an important role to guess the transport mechanism as well as to predict the performance of tokamak reactors. To analyze the scaling it should be noted that the fast ion energy component accounts for a certain amount of fraction in the total energy though the thermal energy component is reflected more in the anomalous conductive loss due to plasma turbulence. We analyzed in detail the kinetic database of JT-60 [2.1-2] and obtained an expression for the thermal energy component, $W_{th} \propto (I_p B_t n_e)^{1/2} P_t^{1/3}$, where I_p is the plasma current, B_t the toroidal magnetic field, n_e the electron density and P_t the total heating power. On the basis of this scaling, we reached a presumption that a collisionless or weak-collisional high- β transport dominates the tokamak L-mode plasmas.

References

- [2.1-1] T. Takizuka, Proc. 1992 ICPP, Innsbruck, 1992, Part I, 51.
- [2.1-2] M. Kikuchi, et al., JAERI-M 91-057 (1991).

2.2 Neoclassical theory of fast ions with isotropic velocity distribution function[2.2-1,2.2-2]

Coupled equations of neoclassical friction-viscosity force balance for thermal particles and fast ions resulting from a fusion reaction or additional heatings have been derived. Fast ions are assumed to be isotropic in the velocity space and to have the small banana size in comparison with the plasma radius. First order solution of the drift kinetic equation of fast ion

was solved in terms of pitch-angle scattering eigenfunctions and is valid both in the slowing-down and pitch-angle scattering dominant regimes. By inclusion of the fast ions the self-adjointness of Coulomb collision operator is lost and friction coefficient matrix is no more symmetric in contrast to the case of thermal particles. Also, it was found that viscous forces of fast ions cannot be expressed by the poloidal flows of particle and heat.

References

- [2.2-1] J.P. Wang, et al., JAERI-M 92-087 (1992).
 [2.2-2] J.P. Wang, et al., JAERI-M 92-107 (1992).

2.3 Ion temperature gradient modes in the neoclassical regime [2.3-1]

Four field moment equations for studying the stability of ion temperature gradient (ITG) modes in a fusion plasma with small collision frequency have been derived. Equations consist of temporal evolution for the ion parallel flow, the generalized potential, the ion pressure, and the parallel heat flow. Neoclassical viscosities, the collisionless thermal flow, and the perpendicular compressibility in ion pressure response are included in this formulation and resultant equations are relevant to the banana-platou collisional regime. It was found that the closure condition of neoclassical viscosities is quite important for the energy dissipation and affects the stability of the ITG modes. Also these newly introduced terms were found to have the destabilizing effects in the rare collisional regime.

Reference

- [2.3-1] M. Yagi, et al., submitted to Phys. Fluids B.

2.4 Particle simulation of the ITG mode in a plasma of a flat density profile

Ion temperature gradient (ITG) driven mode and related turbulence in a plasma of a flat density profile ($\eta_i \approx \infty$) is studied by using the toroidal particle code (TPC) [2.4-1]. Below a theoretical threshold value roughly given by $L_T \tau_i / R < 0.1-0.3$, a few poloidally coupled global modes with different frequencies are excited in different radial location of a torus. A temperature relaxation accompanied by the radial movement of the dominant global ITG modes and complex potential vortex reorganization are observed and finally temperature profile approaches the one given by $T(r) \approx T_0 \exp(-cr)$ (c : constant) irrespective of the initial profile, which is similar to those found in a number of toroidal discharges [2.4-2]. The trapped ion mode which plays an important role in a edge region, especially, in a small aspect ratio tokamak ($\epsilon = 0.64$, the trapped particle fraction = 60-90 % except the magnetic axis) is also investigated by the simulation in a collisionless regime. It is found that the wave fluctuation excited by the ITG mode shows the poloidally localized and radially extended strong ballooning structure due to the a deviation of $k_{\parallel} R = [n - m(1 + \cos\theta)]/q(r) = 0$ surface from the flux surface (n and m are toroidal and poloidal mode numbers, respectively).

* In collaboration with the Institute for Fusion Studies, The University of Texas, USA.

References

- [2.4-1] M.J. LeBrun, IFSR #315 (1988).
- [2.4-2] T.K. Kurki-Suonio, R.J. Groebner, and K.H. Burrell, Nucl. Fusion 32 (1992) 133.

2.5 Fast ion transport during ICRF heating

Spatial transport of fast ion produced by the wave-particle resonance with ICRF wave has been studied theoretically and numerically. The particle resonant with ICRF wave gains not only the perpendicular energy but also the parallel momentum when the wave has the finite parallel wavenumber. The resultant change of canonical angular momentum causes both the radial flow and the diffusion of the banana center. Both are in proportion to the energy gain in the perpendicular direction. The diffusion coefficient is proportional to the square of the parallel wavenumber, while the flow velocity is the linear function of it. This means the possibility to control the radial profile of fast ions, like alpha particles. This analytic study has been confirmed by the orbit following Monte-Carlo code with wave-particle resonance.

2.6 Three dimensional FEL simulation with space-charge effects

The three dimensional free electron laser (FEL) code with a rectangular wave guide has been developed and the effect of the space charge field is investigated in high current Raman operation regime with beam energy $E_b = 1-4$ MeV. In the code the electrostatic field $f(x,y,z)$ is solved both for TE and TM wave-guide modes using an expansion technique by the Gould-Trivelpiece (G-T) mode [2.6-1]. Figure III.2.6-1 shows the spatial evolution of the radiation field of 72 GHz TE₀₁ wave-guide mode (Fig.III.2.6-1a) and the expanded space charge field for 25 modes with $(m,n) = (1,1)$ to $(5,5)$ (Fig.III.2.6-1b: only first 9 modes are depicted) in the case of $E_b = 1$ MeV and I_b (beam current) = 200A. The beam cross section for different wiggler positions is shown, where the beam rotation with an elliptic shape induced by the focusing wiggler field and axial field is seen. The dominant mode of the electrostatic field is fundamental $(1,1)$ mode, showing the rapid convergence of the G-T mode expansion. The spatial growth rate $\gamma \approx 28$ db/m which is roughly 3/4 times of the simulation with $\phi = 0$ is obtained. The current dependence of the linear growth rate γ is also investigated and found to be $\gamma \approx I_b^{1/4}$ as in the 1-dimensional model [2.6-2] even in the 3-dimensional configuration. It is also found that TM mode with the longitudinal electric field component is much affected by the space charge field and weakly excited.

References

- [2.6-1] M.A. Krall and A.W. Trivelpiece, *Principle of Plasma Physics*, McGraw-Hill Inc., 1973, p168.
- [2.6-2] Y. Kishimoto, et al., J. Phys. Soc. Jpn., 59 (1990) 118.

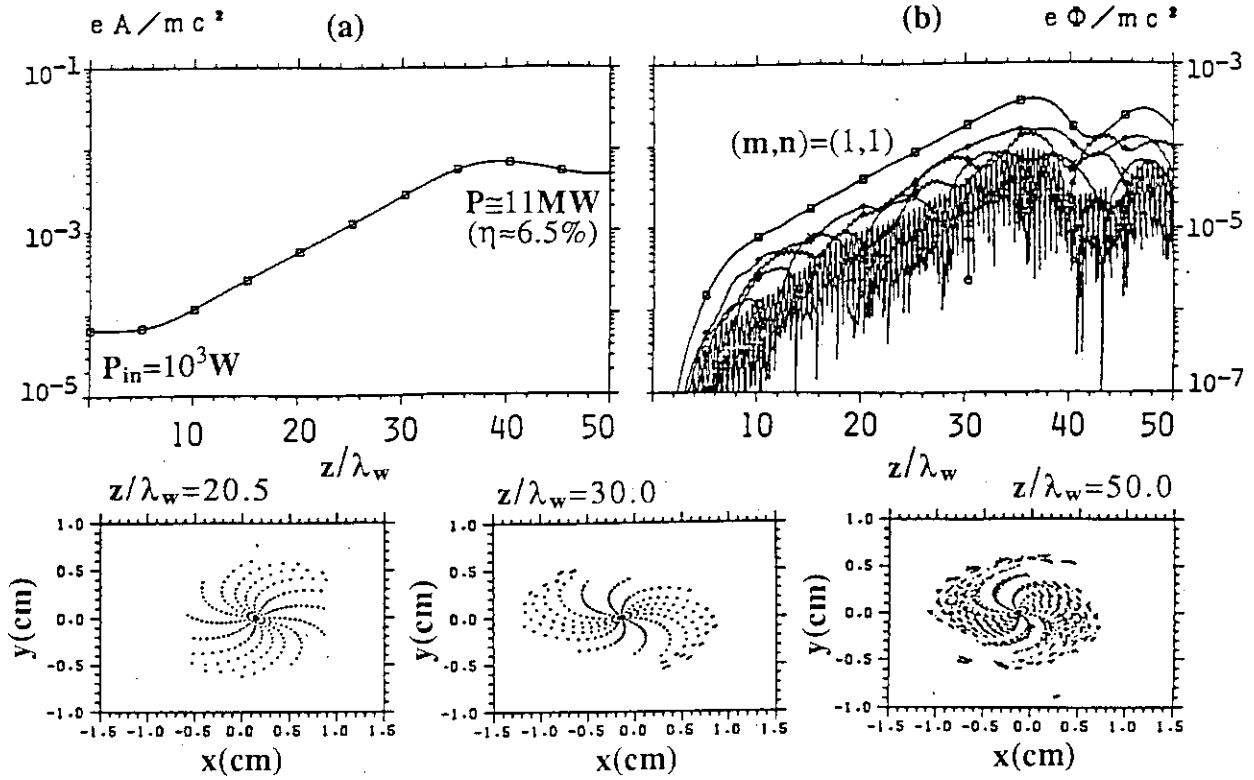


Fig.III.2.6-1 Spatial dependence of the radiation vector field (a) and mode expanded space charge field (b) in the case of $E_b=1MeV$, $I_b=200A$, $\lambda_w=5cm$, $B_w=1kG$, $B_0=1.5kG$. The radiation is 72GHz TE₀₁ mode with $3 \times 2cm^2$ wave guide.

2.7 Multi-frequency simulation of cyclotron auto-resonance maser (CARM)

In order to investigate the mode coupling between linearly excited waves with different frequencies as well as between sideband waves in a nonlinear stage of the cyclotron auto-resonance maser (CARM), a one-dimensional multi-frequency simulation code of the CARM is developed on the basis of the technique developed for the FEL analyses [2.7-1,2.7-2,2.7-3] and the single frequency model [2.7-4]. Since the CARM has rather broad frequency spectrum of the linear growth around the auto-resonance frequency $\omega_r = n\Omega_0/(\gamma(1-\beta_{||}/\beta_p))$, $\Omega_0 = eB_0/mc$, $\beta_{||} = v_{||}/c$, $\beta_p = \omega_r/k_{||}c$, we also observed the mode coupling among linearly growing dominant waves and found that the output frequency spectrum becomes broad especially in the absence of the initial input power. The saturated power is suppressed in a lower level due to the energy partition to many frequency modes. However, the growth of the parasitic wave after

the saturation is slow because there is no instability mechanism corresponding to the sideband instability in the nonlinear trapping stage of FEL.

References

- [2.7-1] Y. Kishimoto, H. Oda, and M. Shiho, Phys. Rev. Lett. **65** (1990) 851.
- [2.7-2] Y. Kishimoto, H. Oda, and M. Shiho, Nucl. Inst. and Meth. **A304** (1991) 632.
- [2.7-3] D. Iracane and J.L. Ferrer, Phys Rev. Lett. **66** (1991) 33.
- [2.7-4] J.K. Lee, et al., Phys. Fluids **31** (1988) 1824.

2.8 Non-canonical Lie perturbation analysis of electron motion in a planar wiggler magnetic field

The motion of a relativistic electron in a planar wiggler field with no guide field has been analyzed by non-canonical perturbation method. This method makes a systematic perturbation analysis possible and the validity of perturbation is clear. By first order perturbation analysis, equation of motion for two-dimensional uncoupled oscillator has been obtained, and it is shown that the electron oscillates slowly around the unperturbed orbit.

3. MHD Equilibrium and Stability Analyses

3.1 Bootstrap current profiles and scaling in large aspect ratio tokamak[3.1-1]

In recent large tokamak experiments bootstrap current is definitely observed to constitute a large fraction of the plasma current, which is naturally taken into account to design a future tokamak reactor. Since this current has intrinsically a hollow profile, a bootstrap current density frequently exceeds a total current density somewhere in a plasma with increasing the fraction of bootstrap currents. This phenomenon is not preferable from the view point of an external current drive. For a tokamak with a large aspect ratio, preferable profiles of total current density and plasma pressure were studied, and it was concluded that a peaked pressure profile and a hollow current profile are desirable. A simple expression for a bootstrap current of a tokamak with a large aspect ratio is proposed;

$$I_{bs}/I_p = \sqrt{\epsilon} \beta_p (1.22 - 1.15\alpha_T/\alpha_p) F(\alpha_p, \alpha_j),$$

where I_{bs} is the bootstrap current, I_p the total plasma current, ϵ the inverse aspect ratio, β_p the poloidal beta, α_T , α_p , and α_j are the profile parameters for temperature, pressure, and current density of the radial profile $(1-\rho^2)^\alpha$. A function $F(\alpha_p, \alpha_j)$ is a simple function of α_p and α_j .

Reference

- [3.1-1] N. Fujisawa and T. Takizuka, JAERI-M 92-064 (1992).

3.2 Beta limit and bootstrap current for small aspect ratio tokamak equilibria[3.2-1]*

the saturation is slow because there is no instability mechanism corresponding to the sideband instability in the nonlinear trapping stage of FEL.

References

- [2.7-1] Y. Kishimoto, H. Oda, and M. Shiho, Phys. Rev. Lett. **65** (1990) 851.
- [2.7-2] Y. Kishimoto, H. Oda, and M. Shiho, Nucl. Inst. and Meth. **A304** (1991) 632.
- [2.7-3] D. Iracane and J.L. Ferrer, Phys Rev. Lett. **66** (1991) 33.
- [2.7-4] J.K. Lee, et al., Phys. Fluids **31** (1988) 1824.

2.8 Non-canonical Lie perturbation analysis of electron motion in a planar wiggler magnetic field

The motion of a relativistic electron in a planar wiggler field with no guide field has been analyzed by non-canonical perturbation method. This method makes a systematic perturbation analysis possible and the validity of perturbation is clear. By first order perturbation analysis, equation of motion for two-dimensional uncoupled oscillator has been obtained, and it is shown that the electron oscillates slowly around the unperturbed orbit.

3. MHD Equilibrium and Stability Analyses

3.1 Bootstrap current profiles and scaling in large aspect ratio tokamak[3.1-1]

In recent large tokamak experiments bootstrap current is definitely observed to constitute a large fraction of the plasma current, which is naturally taken into account to design a future tokamak reactor. Since this current has intrinsically a hollow profile, a bootstrap current density frequently exceeds a total current density somewhere in a plasma with increasing the fraction of bootstrap currents. This phenomenon is not preferable from the view point of an external current drive. For a tokamak with a large aspect ratio, preferable profiles of total current density and plasma pressure were studied, and it was concluded that a peaked pressure profile and a hollow current profile are desirable. A simple expression for a bootstrap current of a tokamak with a large aspect ratio is proposed;

$$I_{bs}/I_p = \sqrt{\epsilon} \beta_p (1.22 - 1.15\alpha_T/\alpha_p) F(\alpha_p, \alpha_J),$$

where I_{bs} is the bootstrap current, I_p the total plasma current, ϵ the inverse aspect ratio, β_p the poloidal beta, α_T , α_p , and α_J are the profile parameters for temperature, pressure, and current density of the radial profile $(1-\rho^2)^\alpha$. A function $F(\alpha_p, \alpha_J)$ is a simple function of α_p and α_J .

Reference

- [3.1-1] N. Fujisawa and T. Takizuka, JAERI-M 92-064 (1992).

3.2 Beta limit and bootstrap current for small aspect ratio tokamak equilibria[3.2-1]*

The stability limit of a very small aspect ratio tokamak, such as TBR2 [3.2-1], with an aspect ratio of 1.6 has been studied by using the critical pressure criterion for the ballooning stability. The β -limit has its maximum value at elongation of 1.7. With increasing the triangularity the β -limit values increase, while the elongation corresponding to the maximum beta value stays at the same value. It is found that even at low temperature as 600 eV the transport is already in banana regime and that the bootstrap current may account for a significant part (about 30 %) of the total plasma current.

* In collaboration with Instituto de Fisica, UNICAMP, Brazil

Reference

[3.2-1] P.H. Sakanaka and S. Tokuda, IAEA TCM on Research Using Small Tokamaks (Hefei, China 1991).

3.3 Effects of hollow current profiles on the ideal MHD stabilities in high- β_p plasmas[3.3-1]

The ideal MHD stabilities on high β_p plasmas with hollow current profile, resulting from large bootstrap current, are studied using the MHD stability codes, ERATO-J and BETA. For a parabolic-like pressure profile, ideal MHD modes are unstable in the wide regime of the $(\epsilon\beta_p, q_0)$ space: the growth rate of the kink-ballooning mode is larger in the high beta regime ($\epsilon\beta_p > 0.5$) than that in a plasma with parabolic current, and the mode is unstable even in a higher q_0 region ($q_0 > 2$). In a low beta regime ($\epsilon\beta_p < 0.5$), the infernal modes are destabilized by the weak magnetic shear region. These ideal MHD modes in a plasma with the hollow current profile were found to be stabilized by controlling the pressure profile such that the maximum pressure gradient is located inside of the radius with pitch minimum and the importance of profile control was stressed especially in a high plasma with large bootstrap current.

Reference

[3.3-1] T.Ozeki, et al., Proc. of 33th Annual APS/DPP Meeting (1991).

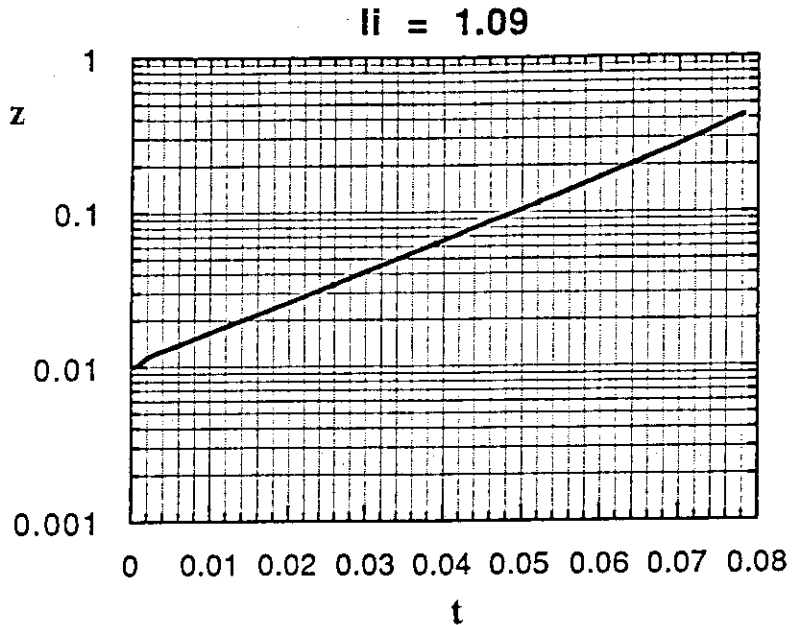
3.4 Axisymmetric tokamak simulation by using the TSC code

The growth rate of axisymmetric instability in highly elongated ITER plasma ($\kappa=1.96$) was obtained by using the tokamak simulation code (TSC). The results of the simulation show that the growth time is less than half of L/R time (~ 50 msec) of conductive shell (Fig.III.3.4-1), and the significant effect of plasma deformation during instability process should be important to optimize control accuracy [3.4-1]. Since the computer simulation by TSC code is very time consuming, an attempt to improve simulation speed was made. For this purpose FFT (fast Fourier transform) algorithm is adopted for the FACR (Fourier analysis and cyclic reduction) solver in which DFT (discrete Fourier transform) was used.

Reference

[3.4-1] M. Azumi, et al., JAERI-M 92-041 (1992).

Fig. III.3.4-1 Time evolution of magnetic axis (z) during axisymmetric instability in ITER plasma ($\kappa=1.96$, $l_i=1.09$). Linear growth time is evaluated to be 21 ms, which is less than half of L/R time of conductive shell.



3.5 Comparison of positional instability analyses by TSC and rigid model codes

The effect of current profiles on the positional instability in ITER has been studied by using TSC and rigid model codes. The results of both the codes agree well for l_i (internal inductance) > 0.9 and the growth rate increases with the increase of l_i . For $l_i < 0.8$ TSC shows that the growth rate decreases while the rigid model gives the opposite result.

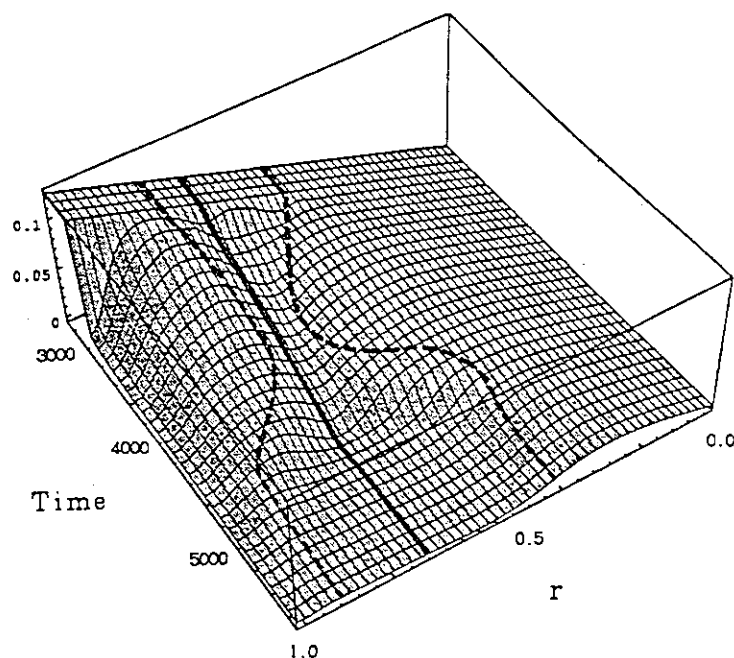
3.6 Velocity shear stabilization of magnetic island in tokamak

Effects of shear flow on plasma stability were studied in cylindrical geometry. We consider the plasma perturbation with a wavenumber $\mathbf{k} \equiv (m/r)\mathbf{e}_\theta + (n/R)\mathbf{e}_\phi$, where m and n are poloidal and toroidal mode numbers and r and R are the minor and major radii, respectively. If there exist a magnetic surface with $\mathbf{k} \cdot \mathbf{B} = \mathbf{k} \cdot \mathbf{V} \neq 0$ (\mathbf{B} : equilibrium magnetic field, \mathbf{V} : plasma flow velocity: in normalized unit with Alfvén velocity of unity), stability of plasma is strongly modified by the plasma flow and Kelvin-Helmholtz type MHD stability must be considered with inclusion of plasma inertia and viscosity terms. If $\mathbf{k} \cdot \mathbf{B}$ and $\mathbf{k} \cdot \mathbf{V}$ become 0 simultaneously at the resonant surface, stability problem is reduced to Δ' stability analysis of the marginal equation as usual tearing mode stability. When a plasma flow velocity has sufficiently large dip at resonant surface, size of magnetic island is reduced and tearing mode can be stabilized by the sheared plasma flow.

3.7 Effect of external helical field on rotating magnetic island

Nonlinear MHD calculations of the $m/n=2/1$ tearing mode in a low β cylindrical tokamak are carried out by taking account of the plasma rotation with the effect of magnetic field induced by external helical current. Rotation of a magnetic island is locked to external helical field through $J_{h\phi} \times B_{h\rho}$ damping torque, where $B_{h\rho}$ is radial component of external helical field and $J_{h\phi}$ is plasma current induced by the helical field and the plasma rotation. When rotating flow speed is high enough, this damping torque produces strong velocity shear near the resonant surface until locking of the magnetic island occurs. After the mode locking, width of magnetic island becomes larger than that without helical field due to phase matching between the external helical field and the locked magnetic island (See Fig.III.3.7-1). The stabilization effect can be sustained by keeping the transient state of the velocity profile by applying an external helical field with alternating directions. This method also releases the magnetic island from mode locking induced by other mechanisms such as interaction with a resistive shell or an error field, which is often followed by major disruptions.

Fig.III.3.7-1 Radial velocity profile versus time normalized to poloidal Alfvén transit time. External helical field is turned on at $t=3000$, and mode locking of magnetic island to external field occurs at $t=4500$. Positions of resonant surface (solid bold line) and magnetic island width (broken line) are also shown.



4. Analyses of Burning Plasma in Tokamaks

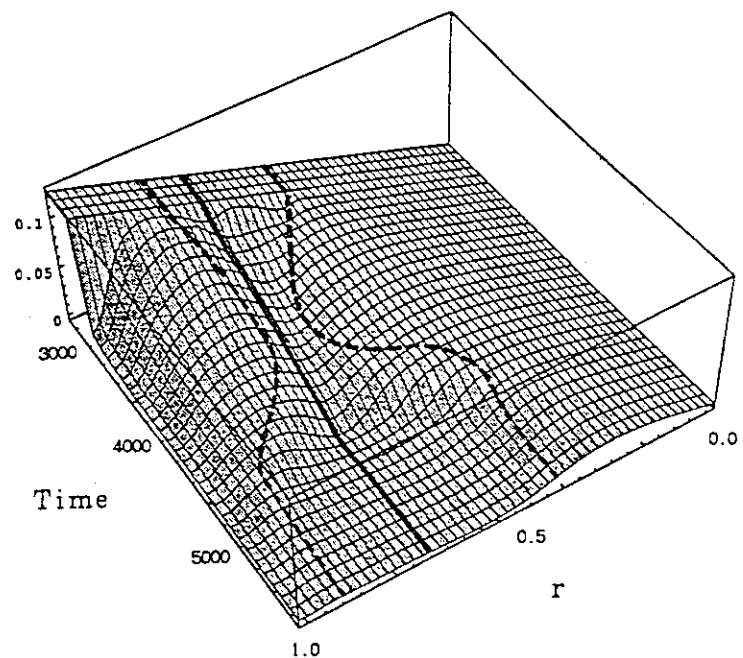
4.1 Fusion yield in high-power D-beam injected ^3He plasmas [4.1-1]

Fusion yield in ^3He plasmas sustained by injection of 10-MW 500-keV deuteron(D)-beam and by injection of 120-keV D-beam up to 30-MW was studied by taking global energy confinement into account. The global energy confinement time, τ_E , defined by the ratio of the

3.7 Effect of external helical field on rotating magnetic island

Nonlinear MHD calculations of the $m/n=2/1$ tearing mode in a low β cylindrical tokamak are carried out by taking account of the plasma rotation with the effect of magnetic field induced by external helical current. Rotation of a magnetic island is locked to external helical field through $J_\phi^h \times B_\rho^h$ damping torque, where B_ρ^h is radial component of external helical field and J_ϕ^h is plasma current induced by the helical field and the plasma rotation. When rotating flow speed is high enough, this damping torque produces strong velocity shear near the resonant surface until locking of the magnetic island occurs. After the mode locking, width of magnetic island becomes larger than that without helical field due to phase matching between the external helical field and the locked magnetic island (See Fig.III.3.7-1). The stabilization effect can be sustained by keeping the transient state of the velocity profile by applying an external helical field with alternating directions. This method also releases the magnetic island from mode locking induced by other mechanisms such as interaction with a resistive shell or an error field, which is often followed by major disruptions.

Fig.III.3.7-1 Radial velocity profile versus time normalized to poloidal Alfvén transit time. External helical field is turned on at $t=3000$, and mode locking of magnetic island to external field occurs at $t=4500$. Positions of resonant surface (solid bold line) and magnetic island width (broken line) are also shown.



4. Analyses of Burning Plasma in Tokamaks

4.1 Fusion yield in high-power D-beam injected ^3He plasmas [4.1-1]

Fusion yield in ^3He plasmas sustained by injection of 10-MW 500-keV deuteron(D)-beam and by injection of 120-keV D-beam up to 30-MW was studied by taking global energy confinement into account. The global energy confinement time, τ_E , defined by the ratio of the

total stored energy to the input power was taken to be inversely proportional to the square root of the input power. Higher fusion yield is produced in the regime of lower n_e and higher T_e , unless the reduction of the ^3He density due to the increase of the non-thermal deuteron population is too significant. The hot ion mode of $T_i=2T_e$ assumed for high-power 120-keV D-beam injection was found not to be preferable to the $T_i=T_e$ mode under the same τ_E . The fusion yield is decreased significantly by accumulation of the thermal deuterons.

Reference

[4.1-1] M. Yamagiwa, Plasma Phys. Contr. Fusion **34** (1992) 715.

4.2 Effects of spatial diffusion and direct loss on burnup fractions of fast ions [4.2-1]

Effects of spatial diffusion and of direct loss of fast ions on their burnup fractions were studied by solving a Fokker-Planck equation including a diffusive loss or a direct loss. Almost the same time evolution of the triton burnup fraction as obtained by introducing spatial diffusion can be reproduced by adjusting the loss time. However, the 14-MeV neutron emission profile in the case with spatial diffusion is broader than that with the direct loss. As to the ^3He burnup fraction, the difference between the cases with spatial diffusion and direct loss was found to be relatively large. The diffusive loss can become important even for ^3He burnup. Effects of charge-exchange loss on the triton burnup fraction were also examined. It was found that the reduction of the burnup fraction by half the value with no loss assumed can occur for a reasonable value of the neutral density in beam injected plasmas.

Reference

[4.2-1] M. Yamagiwa, to be published in Plasma Phys. Contr. Fusion.

4.3 Alpha particle dynamics during the internal disruption [4.3-1]

A hybrid code of fast ion particle model and MHD model is under development and, using the code, behavior of alpha particles during the internal disruption has been studied. Guiding center equations with perturbed magnetic and electric fields have been solved in cooperation with evolution of MHD activities. While $\mathbf{E} \times \mathbf{B}$ drift is dominant for low energy ions and expels them with the fluid flow, alpha particles show different behaviors for passing and trapped particles. Passing alpha particles follow the change of magnetic topology and are expelled from the region with q less than 1, mainly along magnetic field lines, while the combination of $\mathbf{E} \times \mathbf{B}$ drift with toroidal precession drift randomizes trapped alpha orbits and flattens their radial profile after the internal disruption.

Reference

[4.3-1] M. Azumi, et al., JAERI-M 92-073 (1992), p170

4.4 Ripple loss of alpha particles in tokamak reactor with non-circular plasma cross-section

Geometrical effect of noncircular cross-section on the loss of alpha particles induced by toroidal field ripple is investigated theoretically and numerically by using an orbit-following Monte-Carlo code. The ripple-enhanced banana drift, the critical field ripple for ergodic orbit, and the ripple well region are all very sensitive to the elongation. The effect of triangularity on these parameters is not so important as that of elongation. The ripple-enhanced banana-drift loss shows a drastic decrease with plasma ellipticity. As the banana-drift loss is reduced with ellipticity, the ripple trapping begins to dominate the total loss and shows a sharp increase with ellipticity. The resulting beneficial effect of elongation to reduce ripple-enhanced losses is weakened. Geometrical effect is very important not only for the basic loss mechanisms but also for the global ripple losses of alpha particles in connection with the distribution of field ripple. The total ripple loss in vertically elongated O-shaped TF coils shows a moderate decrease with ellipticity. In contrast with the results in O-shaped TF coils, the total loss increases with ellipticity in realistic D-shaped TF coils. The total loss in D-shaped TF coils decreases with triangularity more strongly than that in O-shaped TF coils.

5. Development of Numerical Codes and Plasma Simulator

5.1 Numerical experiment of the equilibrium code SELENEJ[5.1-1]

Numerical experiments of MHD equilibrium code SELENEJ in which the profile of surface average parallel current $\langle \mathbf{J} \cdot \mathbf{B} \rangle$ is specified were carried out. Especially, the convergence property of the iterative solution method in the semi-fixed boundary condition was examined. The usual simple iteration method gives only an approximate solution with low accuracy but not converged solution, where the coil currents are determined by least square fitting and vary with the movement of the plasma vacuum boundary at each iteration. It was found that convergence is improved excellently if the coil currents are fixed when fairly good convergence with respect to the plasma boundary position was attained.

Reference

[5.1-1] M. Nakamura and S. Tokuda, Proceedings of 1991-Workshop on MHD Computations (1991).

5.2 Computation of the vacuum magnetic field energy with an arbitrary boundary shape in the ideal MHD principle

A new version of ERATO-2S has been developed which can compute the vacuum magnetic field energy for the configuration with an arbitrary boundary shape expressed by a single-value function. The vacuum energy is expressed by radial displacements on the plasma

4.4 Ripple loss of alpha particles in tokamak reactor with non-circular plasma cross-section

Geometrical effect of noncircular cross-section on the loss of alpha particles induced by toroidal field ripple is investigated theoretically and numerically by using an orbit-following Monte-Carlo code. The ripple-enhanced banana drift, the critical field ripple for ergodic orbit, and the ripple well region are all very sensitive to the elongation. The effect of triangularity on these parameters is not so important as that of elongation. The ripple-enhanced banana-drift loss shows a drastic decrease with plasma ellipticity. As the banana-drift loss is reduced with ellipticity, the ripple trapping begins to dominate the total loss and shows a sharp increase with ellipticity. The resulting beneficial effect of elongation to reduce ripple-enhanced losses is weakened. Geometrical effect is very important not only for the basic loss mechanisms but also for the global ripple losses of alpha particles in connection with the distribution of field ripple. The total ripple loss in vertically elongated O-shaped TF coils shows a moderate decrease with ellipticity. In contrast with the results in O-shaped TF coils, the total loss increases with ellipticity in realistic D-shaped TF coils. The total loss in D-shaped TF coils decreases with triangularity more strongly than that in O-shaped TF coils.

5. Development of Numerical Codes and Plasma Simulator

5.1 Numerical experiment of the equilibrium code SELENEJ[5.1-1]

Numerical experiments of MHD equilibrium code SELENEJ in which the profile of surface average parallel current $\langle \mathbf{J} \cdot \mathbf{B} \rangle$ is specified were carried out. Especially, the convergence property of the iterative solution method in the semi-fixed boundary condition was examined. The usual simple iteration method gives only an approximate solution with low accuracy but not converged solution, where the coil currents are determined by least square fitting and vary with the movement of the plasma vacuum boundary at each iteration. It was found that convergence is improved excellently if the coil currents are fixed when fairly good convergence with respect to the plasma boundary position was attained.

Reference

[5.1-1] M. Nakamura and S. Tokuda, Proceedings of 1991-Workshop on MHD Computations (1991).

5.2 Computation of the vacuum magnetic field energy with an arbitrary boundary shape in the ideal MHD principle

A new version of ERATO-2S has been developed which can compute the vacuum magnetic field energy for the configuration with an arbitrary boundary shape expressed by a single-value function. The vacuum energy is expressed by radial displacements on the plasma

surface by solving the integral equation for the scalar magnetic potential. The growth rates (eigenvalues) obtained by this version and those by the hybrid finite element method (ERATO-2V) agree well.

5.3 Development of one-dimensional relativistic particle simulation code

A one-dimensional relativistic particle simulation code has been developed to study the interaction between relativistic electrons and intense electromagnetic waves in a fusion plasma as well as in an FEL. In the code ions are also simulated by option. The cloud in cell (CIC) method is used to compute the charge and the current densities.

5.4 Development of toroidal particle code (TPC)

A diagnostic module has been developed in the toroidal particle code (TPC). The module supplies color graphics and uses PLPLOT graphic library which can be installed on a workstation. A solver which solves field equations in the nonlinear gyrokinetic simulation code in a torus is under developing. In this solver the general metrics of the toroidal coordinates can be chosen such as those of straight field line coordinates. Two- and three-dimensional δf codes have been developed and investigated the validity of them by studying the Landau damping, the behavior of a cold plasma and beam plasma instability.

5.5 Development of plasma simulator METIS

Conceptual design work of a plasma simulator METIS dedicated for the calculations of the alpha-particle loss analysis and the nonlinear MHD simulation was continued from the last year on. In this fiscal year, a proto-type debugging system for METIS was developed. A benchmark test of the code to analyze ripple-losses of alpha particle "SLWALF" was made on the proto-type plasma simulator ProtoMETIS. Calculation results agree well with those from the same code on a general use scalar machine FACOM M780/10S.

IV. COOPERATIVE PROGRAM ON DIII-D (Doublet III) Experiment

1. Introduction

The DIII-D tokamak program is now demonstrating advanced tokamak operating modes transiently and plans in future experiments to sustain these improved confinement, stability, and divertor modes with non-inductive rf current drive. To date, the DIII-D tokamak has demonstrated understanding of:

- # Tokamak operating features such as plasma control, wall conditioning, plasma heating and disruption phenomena.
- # Plasma stability through demonstration of increased first stability regime limit and tokamak operation in the second stability regime with plasma betas which exceed those needed for a reactor.
- # High quality plasma confinement regimes (H-mode, VH-mode, high inductance H-mode) that lead to smaller and less expensive reactors.
- # Radio frequency heating and current drive techniques that can provide reactor profile control and steady-state operation, and
- # Divertor heat load reduction as well as method of impurity control which are important steps toward steady-state reactors.

The DIII-D long range research program focuses on divertor and advanced tokamak issues.

The goal is to provide an integrated demonstration of well-confined high-beta divertor plasma with non-inductive current drive.

2. Highlights of FY1991 research results

A new confinement regime has been discovered in the DIII-D tokamak following boronization. Thermal energy confinement times are up to 1.8 times higher than in a typical H-mode, as shown in Fig.IV.2-1. Both plasma temperatures and densities are higher than in H-mode discharges with similar auxiliary heating, and these discharges have lower impurity content and radiated power. The internal inductance is also higher indicating a more peaked current profile and suggesting that current profile control may be a key element in improving confinement in these discharges. This mode has energy confinement time 3.5 times that predicted by ITER89P L-mode scaling and has doubled the best

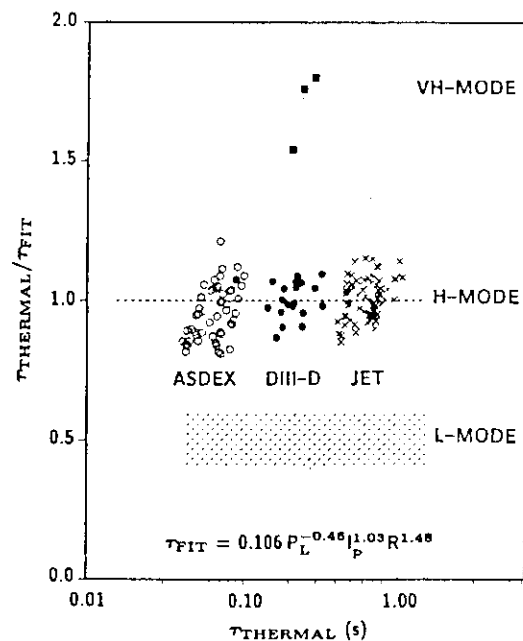


Fig.IV.2-1 Thermal confinement of DIII-D VH-mode improve a factor of 1.8 over the DIII-D/JET H-mode scaling result.

IV. COOPERATIVE PROGRAM ON DIII-D (Doublet III) Experiment

1. Introduction

The DIII-D tokamak program is now demonstrating advanced tokamak operating modes transiently and plans in future experiments to sustain these improved confinement, stability, and divertor modes with non-inductive rf current drive. To date, the DIII-D tokamak has demonstrated understanding of:

- # Tokamak operating features such as plasma control, wall conditioning, plasma heating and disruption phenomena.
- # Plasma stability through demonstration of increased first stability regime limit and tokamak operation in the second stability regime with plasma betas which exceed those needed for a reactor.
- # High quality plasma confinement regimes (H-mode, VH-mode, high inductance H-mode) that lead to smaller and less expensive reactors.
- # Radio frequency heating and current drive techniques that can provide reactor profile control and steady-state operation, and
- # Divertor heat load reduction as well as method of impurity control which are important steps toward steady-state reactors.

The DIII-D long range research program focuses on divertor and advanced tokamak issues.

The goal is to provide an integrated demonstration of well-confined high-beta divertor plasma with non-inductive current drive.

2. Highlights of FY1991 research results

A new confinement regime has been discovered in the DIII-D tokamak following boronization. Thermal energy confinement times are up to 1.8 times higher than in a typical H-mode, as shown in Fig.IV.2-1. Both plasma temperatures and densities are higher than in H-mode discharges with similar auxiliary heating, and these discharges have lower impurity content and radiated power. The internal inductance is also higher indicating a more peaked current profile and suggesting that current profile control may be a key element in improving confinement in these discharges. This mode has energy confinement time 3.5 times that predicted by ITER89P L-mode scaling and has doubled the best

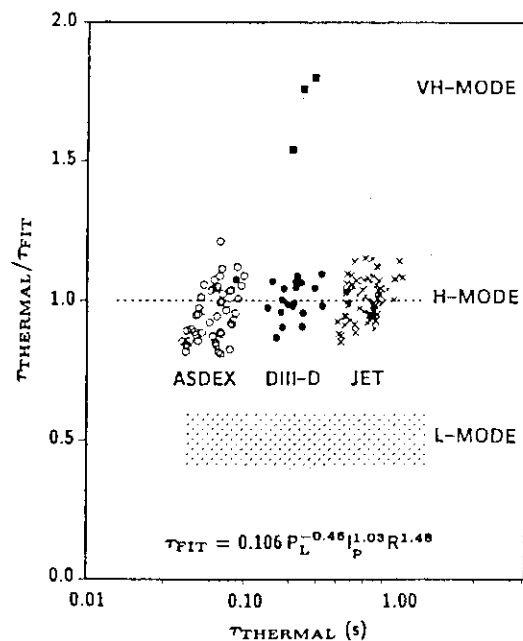


Fig.IV.2-1 Thermal confinement of DIII-D VH-mode improve a factor of 1.8 over the DIII-D/JET H-mode scaling result.

DIII-D triple product to $n_D(0)\tau_E T_i(0)$ to $2 \times 10^{20} \text{m}^{-3} \text{skeV}$. This very high confinement mode is referred as the VH-mode [2-1].

The normalized beta and normalized energy confinement time can be increased by plasma current profile peaking. Normalized beta values have reached $B/(I/aB)=6.5$ and L-mode confinement has been doubled by peaking the current profile (Fig.IV.2-2). In high beta discharges with an inverted central q-profile with negative shear, the plasma interior has entered the second stability regime with central beta values reaching 42 %, as shown in Fig.IV.2-3.

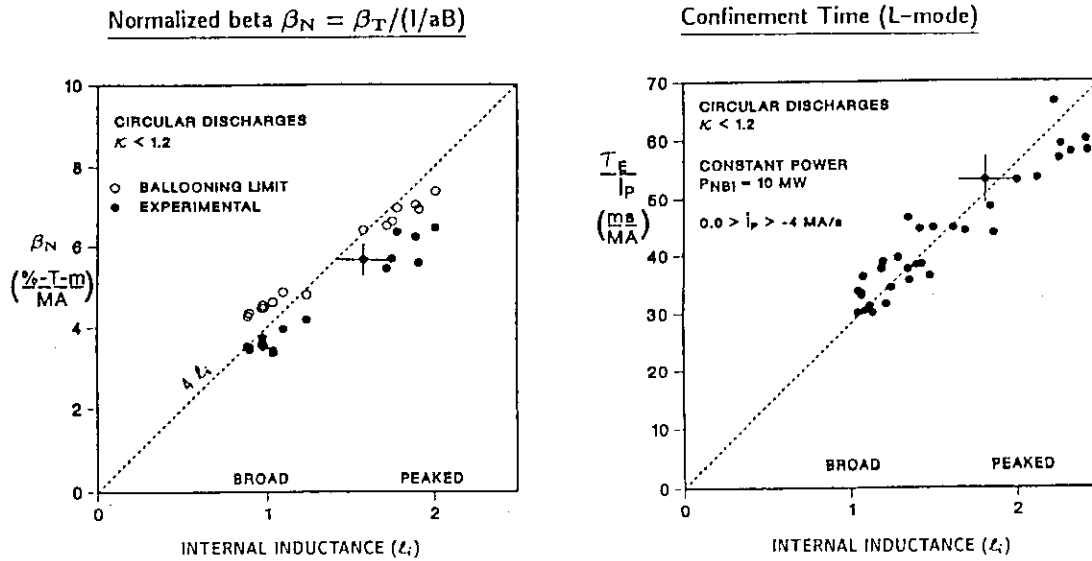


Fig.IV.2-2 Current profile control improves normalized beta and confinement, suggesting the importance of localized non-inductive current drive to improve tokamak performance.

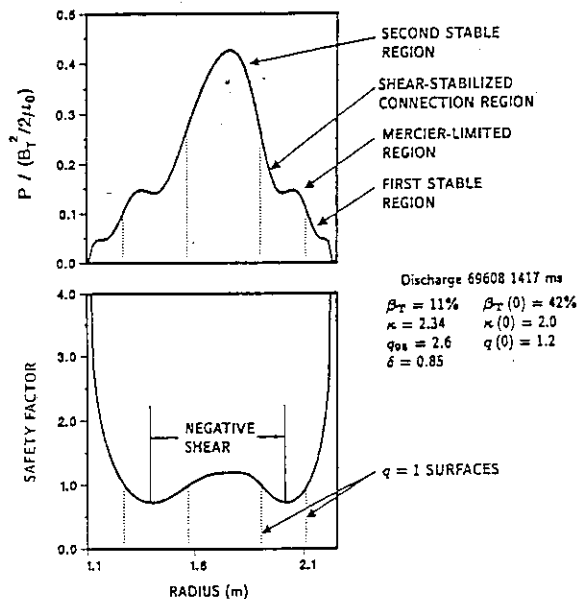


Fig.IV.2-3 Second stability of the DIII-D central core (42% beta) is achieved with reversed central q-profile. The pressure profile is obtained from measured kinetic profiles plus a calculated beam ion contribution and is confirmed by soft x-ray and external magnetics. The q-profile is from magnetics, SXR($q=1$) and motional Stark effect.

Divertor studies form a key element of the DIII-D research program. In collaboration with other laboratories and universities, an extensive set of divertor diagnostics has become operational on DIII-D and a divertor/edge data base is being assembled. Now transport diagnostics are operational and detailed L- to H-mode physics studies are underway. In 1992 a cryopump will be installed for particle pumping to obtain H-mode density control and to operate DIII-D with higher temperature for improved current drive efficiency. Future plans could include the implementation of a divertor more specific to ITER R&D needs.

Fast wave electron heating and current drive experiments have been carried out with a four element phased array antenna. Efficient electron heating was observed in plasmas with electron temperatures above 1.5 keV. Fast wave heating efficiency was similar to neutral beam heating but fast waves generated H-mode with lower power than with neutral beams. Fast wave current drive experiments, with ECH plasma electron preheating, showed a loop voltage drop indicating current drive was independent of the antenna directional phasing relative to the ohmic current. However, sawtooth behavior and experiments in progress are aimed at explaining these results.

3. JAERI collaboration

During JFY 1991, two full time on site JAERI scientists made substantial contributions to the productivity and progress of the DIII-D experimental program. Their research has supported both the DIII-D and JAERI program efforts in the areas of H-mode physics, ECH, fast wave and tokamak diagnostics. Perturbative particle transport analysis using modified ONETWO code at giant ELMs indicated that inward particle pinch has found to be insignificant in the edge region of the H-mode plasma[3-1]. The result is consistent with present understanding of H-mode physics, i.e. a decrease of diffusive transport in the edge resulting from suppression of edge turbulence. Soviet x-ray diagnostics has been improved and an extensive measurements has been done on the electron energy distribution during rf current drive experiments in DIII-D. In addition to the profile evolution of high energy electrons, a difference in the energy spectrum has been observed between co- and counter- directed fast wave phasing relative to the ohmic current[3-2]. Steady-state condition of the H-mode on DIII-D has been summarized from a view point of the wall conditioning and contributed to ITER physics/design options workshop.

The continuation of the DIII-D collaboration for another four years until Aug. 1996 has been agreed with both sides and will be signed in near future.

References

- [2-1] T.C. Simonen, J. of Fusion Energy, **10**(1991)263.
- [3-1] H. Matsumoto et al., Bull. Am. Phys. Soc. **36**(1991)2476.
- [3-2] H.Kawashima et al., GA-A20957(1992)

Fast wave electron heating and current drive experiments have been carried out with a four element phased array antenna. Efficient electron heating was observed in plasmas with electron temperatures above 1.5 keV. Fast wave heating efficiency was similar to neutral beam heating but fast waves generated H-mode with lower power than with neutral beams. Fast wave current drive experiments, with ECH plasma electron preheating, showed a loop voltage drop indicating current drive was independent of the antenna directional phasing relative to the ohmic current. However, sawtooth behavior and experiments in progress are aimed at explaining these results.

3. JAERI collaboration

During JFY 1991, two full time on site JAERI scientists made substantial contributions to the productivity and progress of the DIII-D experimental program. Their research has supported both the DIII-D and JAERI program efforts in the areas of H-mode physics, ECH, fast wave and tokamak diagnostics. Perturbative particle transport analysis using modified ONETWO code at giant ELMs indicated that inward particle pinch has found to be insignificant in the edge region of the H-mode plasma[3-1]. The result is consistent with present understanding of H-mode physics, i.e. a decrease of diffusive transport in the edge resulting from suppression of edge turbulence. Soviet x-ray diagnostics has been improved and an extensive measurements has been done on the electron energy distribution during rf current drive experiments in DIII-D. In addition to the profile evolution of high energy electrons, a difference in the energy spectrum has been observed between co- and counter- directed fast wave phasing relative to the ohmic current[3-2]. Steady-state condition of the H-mode on DIII-D has been summarized from a view point of the wall conditioning and contributed to ITER physics/design options workshop.

The continuation of the DIII-D collaboration for another four years until Aug. 1996 has been agreed with both sides and will be signed in near future.

References

- [2-1] T.C. Simonen, J. of Fusion Energy, **10**(1991)263.
- [3-1] H. Matsumoto et al., Bull. Am. Phys. Soc. **36**(1991)2476.
- [3-2] H.Kawashima et al., GA-A20957(1992)

V. TECHNOLOGY DEVELOPMENT

1. Vacuum Technology and Fuel Injection

1.1 Introduction

Vacuum Technology is one of the most important elements of technology for the operation and maintenance of the current fusion devices. In addition, development of innovative vacuum components and techniques is essential for realization of a fusion experimental reactor like ITER. The technology area includes vacuum pumps, gauging, vacuum materials processing, components, sealing and leak hunting.

For this fiscal year, the development activities of ceramic turbo-viscous pump and high-resolution quadrupole mass spectrometer should be remarked. Development of the Al_2O_3 coatings for ITER in-vessel components and the new vacuum flange/gasket systems was also advanced. Concerning the flange/gasket improvement, a novel copper gasket shown in Fig. V.1.1-1 was found to have excellent performance and durability during high temperature baking.

Besides vacuum technology development, a design study of the rail-gun system for high-speed fuel pellet injection was started in this fiscal year as a part of the fuel cycle program for the ITER EDA.

1.2 Progress in ceramic vacuum pump development

The conditions needed for the torus pumping system of the nuclear fusion reactor are large pumping speed, high throughputs, and the robustness against radiation, tritium and high magnetic fields. To establish

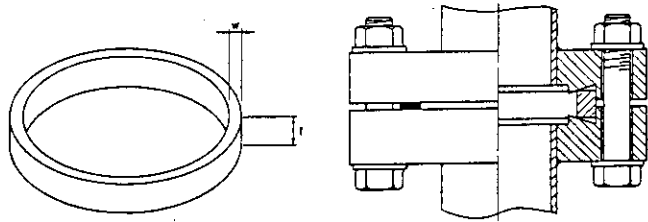


Fig. V.1.1-1 A novel copper gasket (left) and the cross section of the gasket held between two flanges(right).

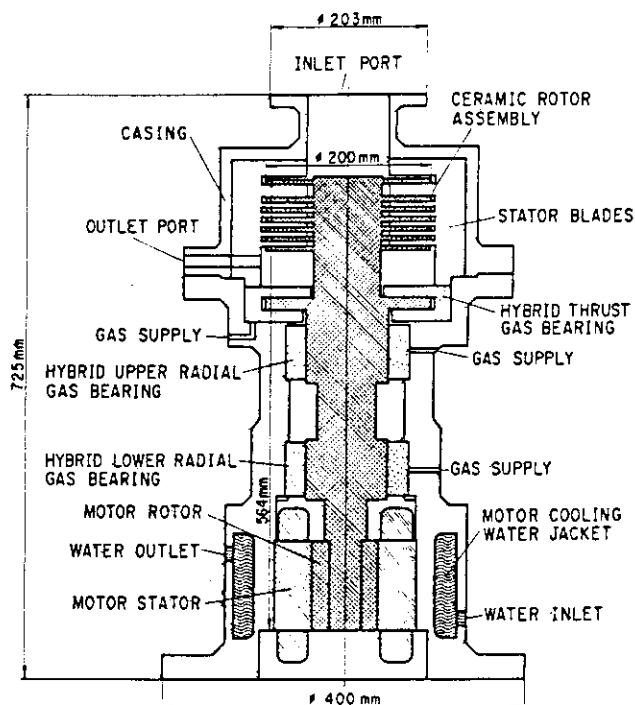


Fig. V.1.2-1 Cross-sectional view of the large-size ceramic turbo-viscous pump.

such a system by using dynamic oil-free pumps, two types of ceramic pumps, ceramic turbomolecular pump and ceramic turbo-viscous pump, were proposed and developed.

In this fiscal year, emphasis was laid on the development of a large-size turbo-viscous pump whose rotor assembly consisted of eight rotor disks, seven for pumping and one for thrust gas bearing, 200 mm in diameter. The main design features differing from those of the previous medium-size pump are the adoption of a hybrid gas bearing, Consisting of static and dynamic gas bearing, and an electric motor instead of a gas turbine (see Fig. V.1.2-1).

The performance test has shown that the pump works in a wide pressure range from atmospheric pressure to 10^{-3} Pa and has a maximum pumping speed of $2.8 \text{ m}^3/\text{min}$ for nitrogen at around 20,000 rpm.

1.3 Improvement of quadrupole mass spectrometer (QMS)

1.3.1 High resolution QMS using conditions of second stability zone in Mathieu diagram [1.3-1]

In this fiscal year, stresses were laid on a detailed ion orbit analysis in a quadrupole electric field using the second stability zone (zone II) in the Mathieu diagram and a demonstration of $^4\text{He}^+ - \text{D}_2^+$ separation.

Figure. V.1.3-1 shows the zone II where the parameter λ 's or g s correspond to mass correspond

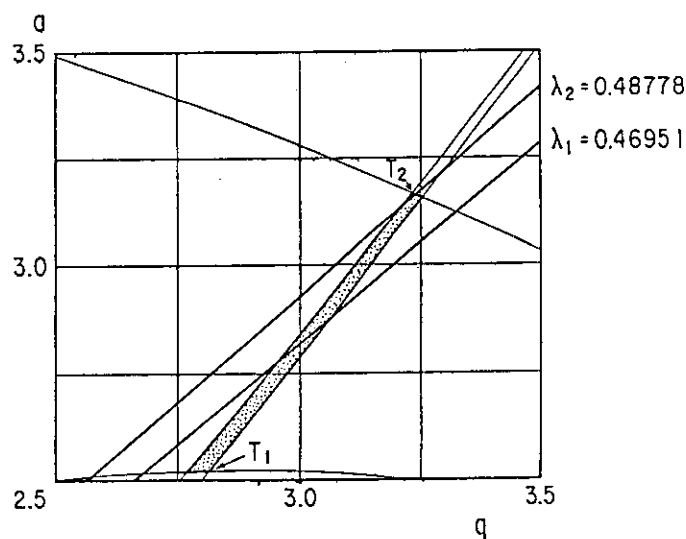


Fig. V.1.3-1 Partial view of the Mathieu diagram in which the dotted area shows the second stability zone, where $a = (8eU)/mr_0^2 \omega^2$ and $q = (4eV)/mr_0^2 \omega^2$, (U : dc voltage; V : rf voltage, m : mass of ion, e : charge of ion, r_0 : inner radius of quadrupole electrodes, ω : angular frequency.) λ_1 and λ_2 represent some values $a/2q$, T_1 and T_2 indicate the tips of zone II.

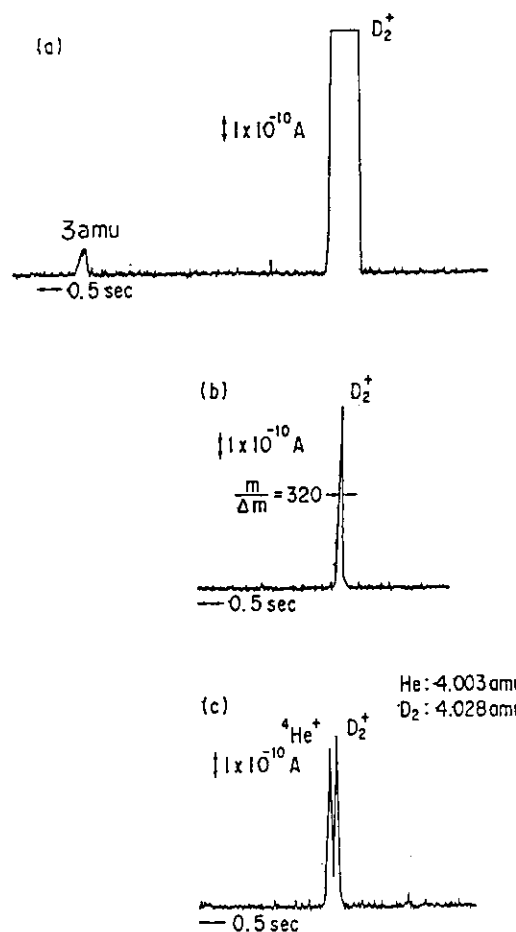


Fig. V.1.3-2 Measured mass spectra. (a) fat D_2^+ peak, (b) highly-resolution D_2^+ peak, $m/\Delta m = 320$ at half height, and (c) $^4\text{He}^+$ and D_2^+ peaks appeared separately, with the same resolution as in (b).

to mass scan lines. λ defined by $\lambda = a/2q$ is related to the dc to rf voltage ratio, U/V . The inner diameter and the length of the quadrupole electrode tested were 4.0 mm and 200 mm, respectively. The minimum resolution ($m/\Delta m$) needed for the separation of $^4\text{He}^+$ and D_2^+ is 161 at D_2^+ peak. When λ was adjusted to λ_1 which crossed the center of zone II, a fat D_2^+ peak was obtained as shown in Fig. V.1.3-2(a). Then, λ was carefully increased to λ_2 . Although the peak height drastically decreased, a highly resolved D_2^+ peak for which a value of $m/\Delta m = 320$ at the half height is obtained as shown in Fig. V.1.3-2(b). While maintaining this condition, ^4He gas was slowly mixed to D_2 . A $^4\text{He}^+$ peak separately appeared at the lower mass side of the D_2^+ peak. [see Fig. V.1.3-2(c)].

1.3.2 Fabrication of ceramic quadrupole structure [1.3-2]

In the course of the QMS improvement, a novel QMS was developed by using a ceramic single-piece quadrupole. The quadrupole structure was made of silicon nitride. The four hyperbolic surfaces were coated with metal thin films about 10 μm thick to form electrodes. A cross-sectional view of the ceramic quadrupole and a QMS head assembled with the quadrupole are shown in Fig. V.1.3-3(a) and (b), respectively. Mass spectra were successfully obtained

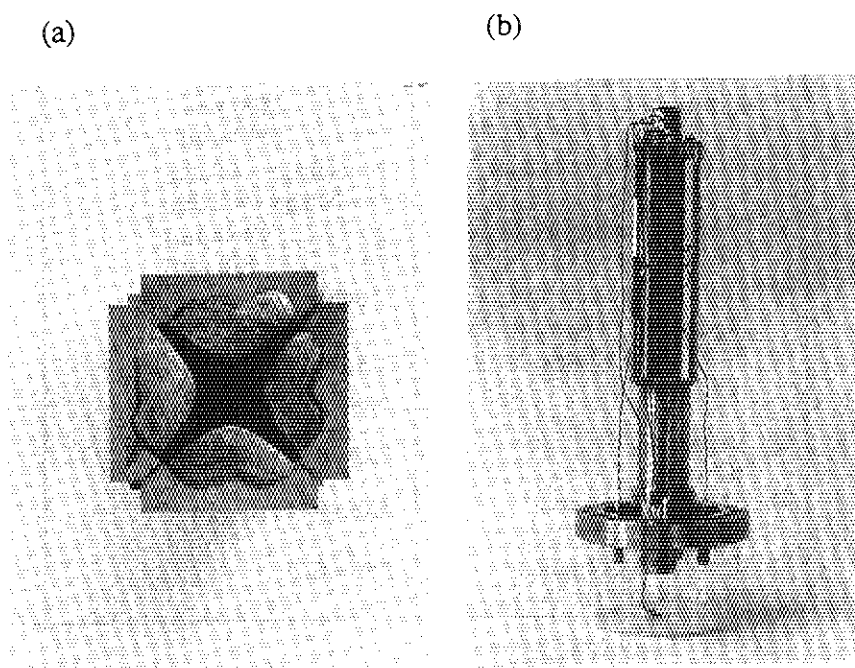


Fig. V.1.3-3 (a) Cross-section view of Si_3N_4 quadrupole structure having $r_0 = 4.3$ mm and $l = 200$ mm (b) QMS head consisting of a Si_3N_4 single-piece quadrupole, a Nier-type ion source and of secondary electron multiplier. For the electrical wiring ceramic-insulated wires composed of SiO_2 -coated nickel-clad copper [1.3-3] are used.

by using the conditions of the second stability zone in the Mathieu diagram. It seems that there are no differences in sensitivity and resolution between the two QMS's with ceramic quadrupole and conventional metal one of the same dimensions.

References

- [1.3-1] S.Hiroki, T.Abe and Y.Murakami, to be published in Rev. Sci. Instrum. 63 (1992).
- [1.3-2] S.Hiroki, T.Abe, et al., to be published in Vacuum 43 (1992).
- [1.3-3] Annual report of the Naka Fusion Research Establishment, JAERI-M 91-159.

1.4 Large-area Al₂O₃ coatings for ITER in-vessel components

The in-vessel components of a fusion reactor like ITER will be placed in severe operation conditions such as high temperatures and large electromagnetic forces induced by plasma disruptions. To reduce the disruption-induced effects on the components, it is useful to coat the surface of the components with ceramic materials with adequate electrical conductivity and abrasion resistance property.

In the previous year, Al₂O₃ was selected as an insulation coating material for the stainless steel components because it showed a little nuclear transmutation effect on the electrical properties and good abrasion resistance. In this fiscal year, large-area Al₂O₃ coatings, 300 × 100 mm, were

Table V.1.4-1 Experimental Results of Insulation Coating Films

Properties	Al ₂ O ₃ Plasma spraying	ITER Requirement
1) Tensile Strength (kgf•mm ⁻²)	0.9 (590 μm) 1.4 (590 μm) 1.2 (620 μm)	>0.5
2) Thermal shock resistance	No damage (200 μm) No damage (660 μm)	>10 Cycles (RT = 77 °K)
3) Tolerant bending angle (°)	30 (260 μm) 20 (580 μm)	-
4) Thermal conductivity (J•cm ⁻¹ •°C ⁻¹ •sec ⁻¹)	0.0465	>2.5×10 ⁻⁴
5) Break down voltage (V)	2.5×10 ³ (210 μm) 5.0×10 ³ (580 μm)	>10 ³
6) Resistivity (Ω•cm)	3.5×10 ⁸	>2.0×10 ³
7) Abrasion Resistance (cycles; 50MPa, 350°C)	5.0×10 ³ (410 μm)	>10 ⁴
8) Coefficient of friction (RT ~ 350°C)	0.6 ~ 0.7	-

- (1) Environment : N₂ gas atmosphere
- (2) Sample Temperature : 350 (°C)
- (3) Contact pressure : 50 (MPa)
- (4) Cycle Speed : 50 (mm•sec⁻¹)
- (5) Cycle pattern : See below

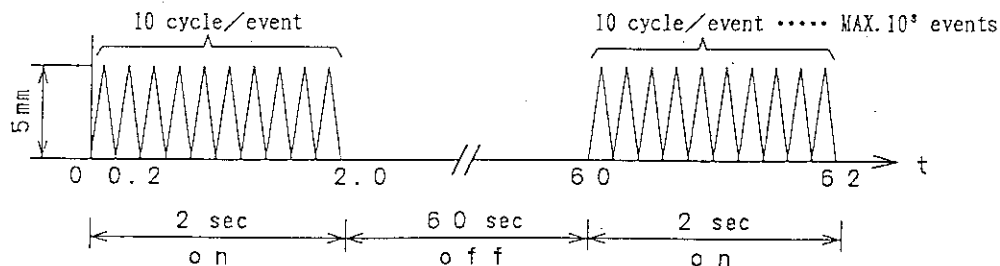


Fig. V.1.4-1 Experimental conditions for abrasion test of Al₂O₃ coatings.

successfully carried out by using the plasma spray method. A Ni/Cr layer was inserted in between stainless steel and Al_2O_3 to increase the bonding strength as well as to release the thermal stresses in the coatings.

Figure V.1.4-1 shows the experimental conditions for abrasion test, which are chosen by considering the operation conditions of ITER. Table V.1.4-1 shows some test results of the Al_2O_3 coatings with ITER requirements

1.5 Design of rail-gun system for high-speed fuel pellet injection

Considerable attention has been devoted to the efficient fueling of near-ignition tokamaks. Achieving deep penetration of solid hydrogen-isotope pellets into the plasma is very important to obtain the reduced transport and enhanced reaction rate resulting from highly peaked density profiles. High speed pellets have been demonstrated by using single-stage gun, two-stage gun, electromagnetic rail-guns and so on for deep fueling.

In this fiscal year, the rail-gun system was designed to develop the repeating pellet injection technology with a repetition rate of 1-2 Hz and technology to change pellet velocity from 1.5 to 5 km/s during repeating injection. On this system, a pellet is accelerated initially by a single-stage pneumatic gun. The rail-gun is used as the second accelerator. The rail length is 1-3 m, and a diameter of rail bore is 3-4 mm. A pellet diameter is 3-4 mm without a sabot. Main results of the rail-gun system design are as follows.

- (1) A laser-produced plasma (He or H_2) armature, which is used to accelerate a pellet, is better than a spark plasma armature from the view point of reproducible production of the plasma armature.
- (2) In order to reduce the rail damage, it is necessary that a rail current is low, less than several kA, and a voltage between rail conductors is very low. The designed rail current and voltage are 30 kA and 1 kV at maximum, respectively.
- (3) A insulator with high dielectric constant is better to reduce the accumulation of the electric field near the rail edge which causes the rail damage.

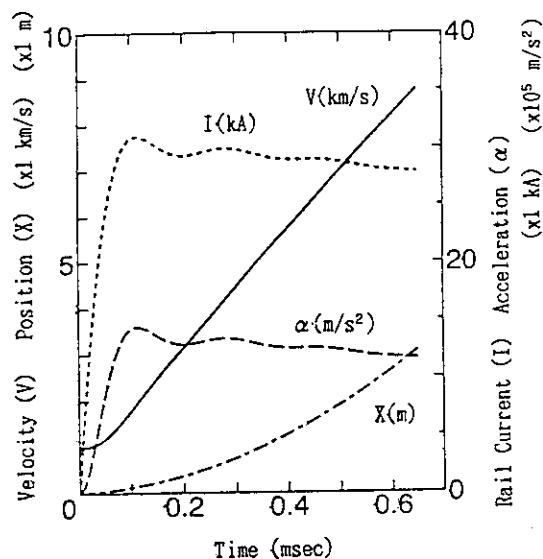


Fig. V.1.5-1 Time variations of pellet speed (V), rail current (I), acceleration (α) and pellet position (X). On this calculation, the classical rail is used. Capacity of the condenser is 3.75 mF and the charged voltage is 1 kV. The pellet size is 3 mm $\phi \times$ 3 mmL (mass=1.83 mg).

- (4) Materials of W-Y203 is more excellent than Cu, W, etc., as the rail conductor from the view point of low damage.
- (5) From the calculation of the pellet acceleration, the speed of more than 5 km/s can be achieved by using the classical rails of 1 m length (rail current=30 kA) as shown in Fig. V.1.5-1. However, the augmented rail is much better than the classical rail. The 1-2 Hz repeating pellet-injection with 1-5.5 km/s will be possible by using the above-mentioned rail-gun system.

In the present plan, the rail-gun system will be constructed in the next fiscal year.

2. Superconducting Magnet Development

2.1 Introduction

JAERI has been systematically developing superconducting fusion magnet technologies, composed of advanced technologies for 1) toroidal coils [DC operation, 12 T, large coil with a height of 15 - 20 m], 2) central solenoid coils [pulsed operation, 13 T, 3-4-m ID], 3) outer ring coils [pulsed operation, 5-7 T, 5-20-m ID], and 4) a large cryogenic system [30 kW x 4 at 4 K].

In the Demo. Poloidal Coil (DPC) Program, the third test coil (DPC-TJ) and the fourth one (Toroidal Model Pancake) were tested in conjunction with the back up coils at the DPC test facility (DPCF). In parallel, JAERI has developed advanced Nb₃Sn strands for the Scalable Model Coil of the central solenoid coils and a Nb₃Al strand for the Model Coil of the toroidal field coils. These coils will be fabricated and tested under the Engineering Design Activity (EDA) of the ITER project. Major achievements obtained in the FY1991 are as follows.

- (a) Demonstration of new conductor concept (Preformed armor) by the DPC-TJ
- (b) Achievement of high average current density [40 A/mm²] by the DPC-TJ
- (c) The first charging of a hollow type conductor up to 30 kA at 3T by the Toroidal Model Pancake.
- (d) Achievement of high critical current density [800 A/mm²] at 12T by newly developed Nb₃Sn strands with low pulsed loss for a Scalable Model Coil to be developed under the ITER R&D project.
- (e) Detailed design of an 8-kW refrigerator of the ITER common test facility.
- (f) The first achievement of large current Nb₃Al conductor [40 kA at 12T]
- (g) Confirmation of much less critical current degradation of Nb₃Al compared to that of the Nb₃Sn. A typical degradations at 0.4-% strain are -5% and -30% for Nb₃Al and Nb₃Sn strands, respectively.

2.2 The Demo Poloidal Coil program

2.2.1 Project status

- (4) Materials of W-Y203 is more excellent than Cu, W, etc., as the rail conductor from the view point of low damage.
- (5) From the calculation of the pellet acceleration, the speed of more than 5 km/s can be achieved by using the classical rails of 1 m length (rail current=30 kA) as shown in Fig. V.1.5-1. However, the augmented rail is much better than the classical rail. The 1-2 Hz repeating pellet-injection with 1-5.5 km/s will be possible by using the above-mentioned rail-gun system.

In the present plan, the rail-gun system will be constructed in the next fiscal year.

2. Superconducting Magnet Development

2.1 Introduction

JAERI has been systematically developing superconducting fusion magnet technologies, composed of advanced technologies for 1) toroidal coils [DC operation, 12 T, large coil with a height of 15 - 20 m], 2) central solenoid coils [pulsed operation, 13 T, 3-4-m ID], 3) outer ring coils [pulsed operation, 5-7 T, 5-20-m ID], and 4) a large cryogenic system [30 kW x 4 at 4 K].

In the Demo. Poloidal Coil (DPC) Program, the third test coil (DPC-TJ) and the fourth one (Toroidal Model Pancake) were tested in conjunction with the back up coils at the DPC test facility (DPCF). In parallel, JAERI has developed advanced Nb₃Sn strands for the Scalable Model Coil of the central solenoid coils and a Nb₃Al strand for the Model Coil of the toroidal field coils. These coils will be fabricated and tested under the Engineering Design Activity (EDA) of the ITER project. Major achievements obtained in the FY1991 are as follows.

- (a) Demonstration of new conductor concept (Preformed armor) by the DPC-TJ
- (b) Achievement of high average current density [40 A/mm²] by the DPC-TJ
- (c) The first charging of a hollow type conductor up to 30 kA at 3T by the Toroidal Model Pancake.
- (d) Achievement of high critical current density [800 A/mm²] at 12T by newly developed Nb₃Sn strands with low pulsed loss for a Scalable Model Coil to be developed under the ITER R&D project.
- (e) Detailed design of an 8-kW refrigerator of the ITER common test facility.
- (f) The first achievement of large current Nb₃Al conductor [40 kA at 12T]
- (g) Confirmation of much less critical current degradation of Nb₃Al compared to that of the Nb₃Sn. A typical degradations at 0.4-% strain are -5% and -30% for Nb₃Al and Nb₃Sn strands, respectively.

2.2 The Demo Poloidal Coil program

2.2.1 Project status

The Demo Poloidal Coil (DPC) program was initiated in 1985 to develop forced-cooled large-current superconducting coils and coil systems for future thermonuclear fusion machines. In this project, two Nb-Ti 30-kA pulsed coils (DPC-U1 and -U2) were fabricated and tested first [2.2-1]. Using these coils as background field coils, two Nb₃Sn pulsed coils (DPC-EX and US-DPC) were already tested successfully in the previous reporting period starting from April 1991 [2.2-2, 2.2-3]. In this period, the DPC-TJ coil was set between the DPC-U1 and -U2 coils and been tested as the third Nb₃Sn test coil of this program.

2.2.2 The DPC-TJ experiment

2.2.2.1 Outline of the DPC-TJ coil

The DPC-TJ coil was fabricated under the joint-research contract between JAERI and Toshiba Corporation. It demonstrated a new technology of the large-current high-rigidity high-field superconducting coil with high-current-density of 40 A/mm² by its fabrication and test [2.2-4]. Figure V.2.2-1 shows the DPC-TJ coil whose dimensions were the inner diameter of 1.0 m, the outer diameter of 1.8 m and the axial length of 0.11 m. Its conductor was a (NbTi)₃Sn cable-in-conduit forced-cooled type and its design condition was 24 kA, 12 T at 4.2 K [2.2-5]. The feature of the DPC-TJ coil is the preformed-armor method devised in this work, where the heat-treated Nb₃Sn conductor with thin conduit was put in the thick strong armor as shown in Fig. V.

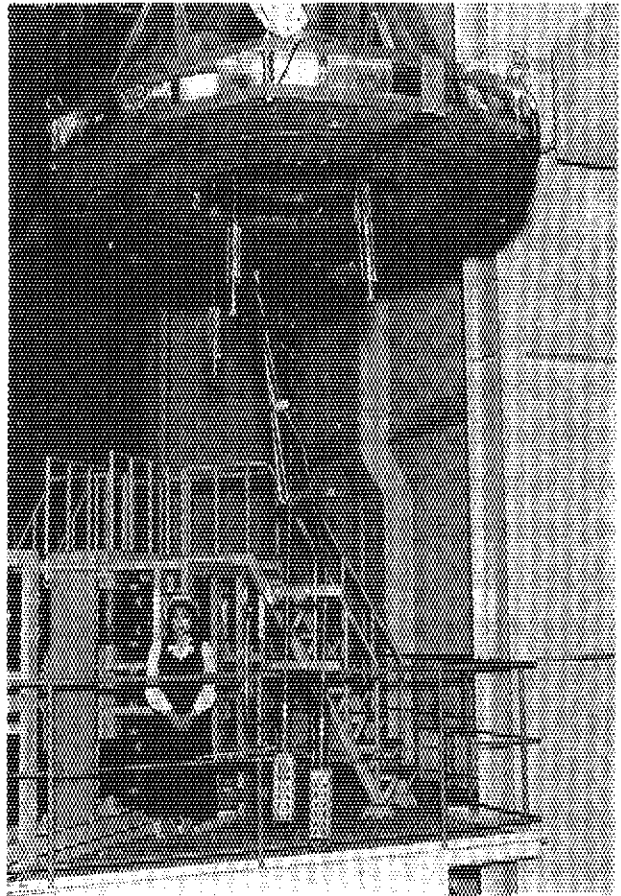


Fig.V.2.2-1 The DPC-TJ coil, a 1.0 m I.D.-1.8 m O.D. forced-cooled 24 kA-40 A/mm² (NbTi)₃Sn test coil.

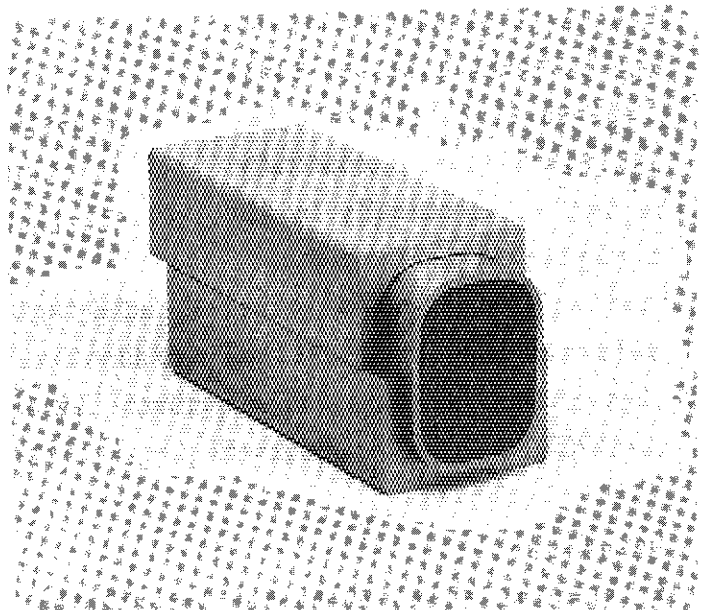


Fig.V.2.2-2 The preformed-armor cable-in-conduit type DPC-TJ conductor. 486 strands are covered with a inner gastight conduit and the outer strong armor.

2.2.2 which was formed into the coil shape in advance. High-rigidity high-current-density coils can be fabricated by this new method without any technical difficulties.

2.2.2.2 Main achievements from the DPC-TJ experiment

The DPC-TJ coil was installed between the DPC-U1 and -U2 coils and was tested for about two months. In this test, the DPC-TJ coil was charged up to its rated current of 24 kA together with the DPC-U1/U2 coils without any training quenches, and reached the maximum magnetic flux density of 7.6T, with a stored energy of 31MJ in the coil system and the average current density of 40 A/mm² in the winding part at the coolant temperature of 4.2K. In a single coil charging test, the DPC-TJ was operated at 30kA stably with 4.5 K-coolant and also with 10 K-heated coolant. The load lines of the DPC-TJ coil are shown in Fig.V.2.2-3. The critical current of the conductor at 4.2 K estimated from critical currents measured at 11 K or higher was around 41 kA at 12 T, which was the largest current capacity that had ever been achieved by the superconductors in the coils. Moreover, the DPC-TJ coil was proved to be stable mechanically as well as electrically by its extremely few wire movement

and AE signals and by its smooth radial-expansion due to electromagnetic force. Designed performances of the DPC-TJ coil were almost confirmed and a lot of valuable data could be obtained in this experiment [2.2-6, 2.2-7, 2.2-8, 2.2-9]. As the final investigation, the DPC-TJ coil was cut into several pieces and its winding quality was confirmed visually.

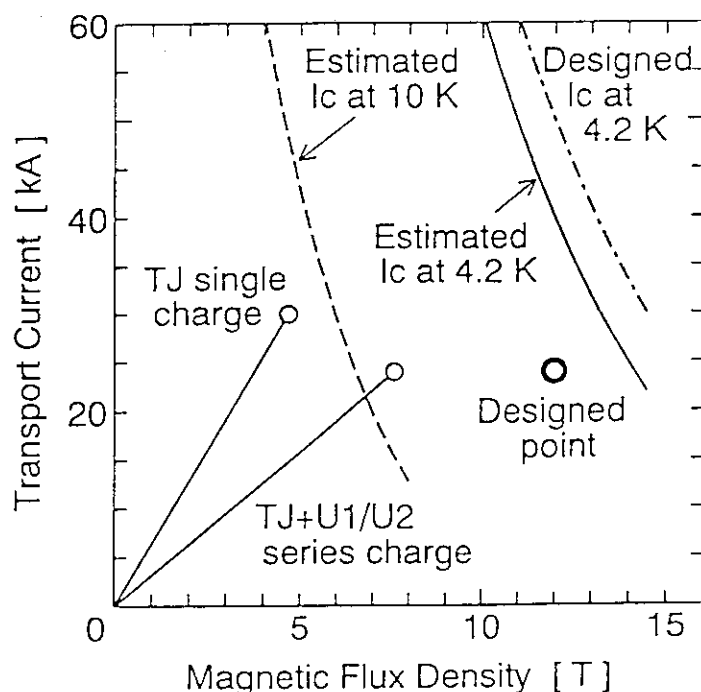


Fig.V.2.2-3 The load lines of the DPC-TJ coil and its estimated critical currents (I_c). 24 kA-7.6 T-4.2 K and 30 kA-4.7T-10K were achieved.

References

- [2.2-1] H.Tsuji, E.Tada, K.Okuno, et al., Proc. of 11th Int. Conf. on Magnet Technology (1990) 806
- [2.2-2] Y.Takahashi, K.Yoshida, T.Ando, et al., Cryogenics, Vol.31 (1991) 640
- [2.2-3] M.M.Steeves, M.Takayasu, T.A.Painter, et al., Advances in Cryogenic Engineering, Vol.37A (1991) 345
- [2.2-4] M.Nishi, T.Ando, H.Tsuji, et al., Cryogenic Engineering, Vol.27 (1992) 207

- [2.2-5] N.Aoki, T.Ogaki, I.Noguchi, et al., Cryogenic Engineering, Vol.27 (1992) 221
- [2.2-6] M.Ono, H.Mukai, M.Shimada, et al., Cryogenic Engineering, Vol.27 (1992) 226
- [2.2-7] N.Koizumi, K.Yoshida, T.Isono, et al., Cryogenic Engineering, Vol.27 (1992) 233
- [2.2-8] M. Sugimoto, T.Kato, K.Kawano, et al., Cryogenic Engineering, Vol.27 (1992) 239
- [2.2-9] Y. Wachi, H.Mukai, M.Ono, et al., Cryogenic Engineering, Vol.27 (1992) 245

2.3 Proto Toroidal Coil project

2.3.1 Development of the Toroidal Model Pancake (TMP) for ITER/FER Toroidal Field Coils

The development of the Toroidal Model Pancake (TMP) has been carried out since 1988 [2.3.1-1,2.3.1-2,2.3.1-3]. TMP was designed and manufactured as one of test coils in the DPCF at JAERI. Hollow cooling, monolithic conductors are candidate conductors for toroidal field (TF) coils in fusion reactors because of their small degradation of critical current, small mechanical disturbance, and considerable manufacturing experience. However, the monolithic conductor had to be optimized to decrease its large AC loss and to increase its stability.

TMP has a hollow cooling, monolithic Nb_3Sn conductor (TMC-FF), and its inner diameter and conductor length are 1m and 90m, respectively. A view of the TMP is shown in Fig.V.2.3-1. TMP was designed for DC coils, aiming at the application to TF coils. The design specification of the TMP is 30kA and 12T.

An optimization of the bronze ratio and tin density in the $(\text{NbTi})_3\text{Sn}$ strand was carried out. The maximum critical current density at 4.2K, 12T was 404A/mm².

The measured time constants of the coupling current in parallel and perpendicular fields were 4ms and 400ms, respectively.

The stability test of a 1/23 scale sample was also carried out and its results showed stability margin of full size conductor would be 40mJ/cc-metal at the nominal operating point.

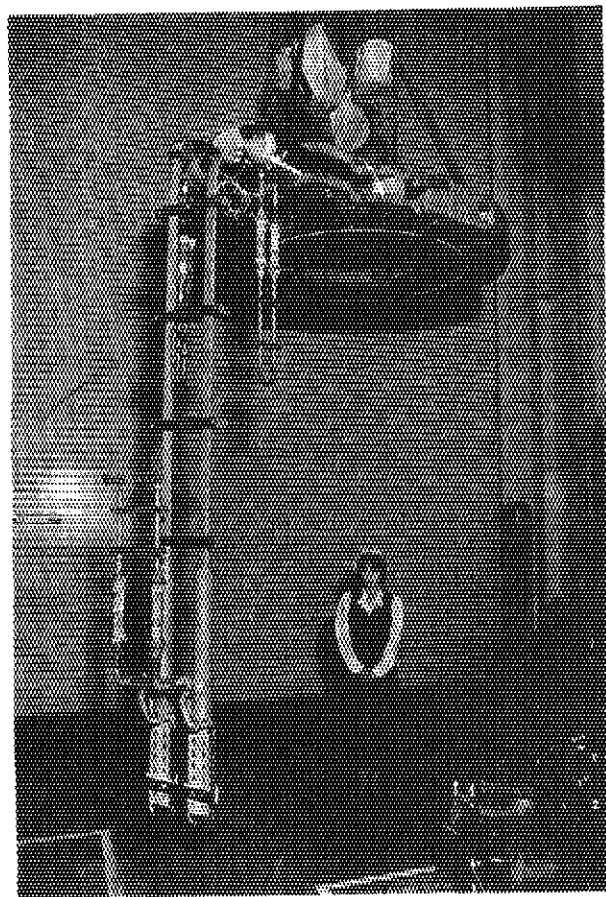


Fig.V.2.3-1 View of the Troidal model pancake.

The critical current of full size conductor was measured at 13 T and 4.2 K. The measured critical current of 24kA should be no degradation of the critical current when compared with the results of the straight sample before cabling[2.3.1-4].

A 90m length conductor was manufactured in April, 1991, and TMP construction was completed August 1991. TMP was installed between DPC-U1 and U2. Performance tests of TMP were carried out for one month from January 1992.

The total cooling weight was 23 tons including TMP, DPC-U1, U2 and supporting structures. And cooldown was completed within 150 hours. TMP was charged up to the design current of 30-kA without magnet quench. Maximum charging current of the TMP reached 41kA by the dumping of the DPC-U1,U2 coils. The rated current of a hollow cooling, monolithic Nb₃Sn conductor was scaled up to 30kA that was operating current for the next fusion machine (ITER/FER).

References

- [2.3.1-1] K.Yoshida, M.F.Nishi, Y.Takahashi, et al., IEEE Trans. Mag., vol.25, 1989, pp1488-1491
- [2.3.1-2] M.F.Nishi, Y.Takahashi, T.Isono, et al., Proc of 13th Fusion Eng., IEEE Catalog No. 89CH2820-9, 1989, pp.780-783
- [2.3.1-3] M.Sugimoto, T.Isono, N.Koizumi, et al., IEEE Trans. Mag., vol.28, 1992, pp.218-221
- [2.3.1-4] T.Isono, Y.Takahashi, K.Yoshida, et al., IEEE Trans. Mag., vol.27, 1991, pp.1839-1842

2.3.2 Nb₃Al conductor development

JAERI is carrying out the development of Nb₃Al cable-in-conduit conductors for fusion magnets. The Nb₃Al strands were made by a jerry roll process. The effect of axial strain on the critical current density of a cable-in-conduit conductor and hysteresis losses were investigated in 1991.

2.3.2.1 Effect of axial strain on the critical current density of a Nb₃Al cable-in-conduit conductor

The effect of axial strain on the critical current of a Nb₃Al cable-in-conduit conductor was measured jointly at KfK in Germany at a magnetic field of 12 T. The conductor consisted of 36 strands which was inserted into a circular stainless steel conduit with 30 % void fraction and then heat-treated. The diameter of the strand was 1.02 mm. The conductor exhibited a maximum of the critical current at around 0.7 % strain, but the degradation of the critical current at 0 % strain and 12 T was only 20% for Nb₃Al. This result is compared to a 50-% degradation of Nb₃Sn cable-in-conduit conductor at the same strain condition. Furthermore, the critical current versus strain characteristic behaves completely reversible under both loaded and unloaded conditions up to the measured strain of 1.7 %. Figure V.2.3-2 shows the relation between the critical current and the axial strain for a Nb₃Al cable-in-conduit conductor in comparison with a Nb₃Sn cable-in-conduit conductor.

2.3.2.2 Hysteresis losses of a Nb₃Al strand

Hysteresis losses in a multi-filamentary Nb₃Al /Cu composite strand was examined by means of measuring magnetization. The Nb₃Al strand consists of 397 Nb₃Al filaments, whose diameter was 21 μm , embedded in the copper matrix. The non-copper critical current density was 510 A/mm² at 12 T which was at the same level as that of commercial Nb₃Sn strands. Magnetization measurements of the Nb₃Al strand were performed in the parallel and perpendicular fields. For the field perpendicular to strand length, it was shown that effective filament diameter was almost equal to the actual filament diameter 20 μm . On the other hand, the hysteresis loss for the parallel field was around one-fourth as large as that for perpendicular, corresponding to effective filament diameter of approximately 8 μm . The reason for this result is considered that the Nb₃Al layer produced between Al and Nb sheets after reaction was in a whirlpool state, and it shows that the Nb₃Al conductor was fully available for application to magnets in fusion machines such as ITER. Figure V.2.3-3 shows the hysteresis losses as a function of magnetic field for a Nb₃Al strand in the parallel and perpendicular fields.

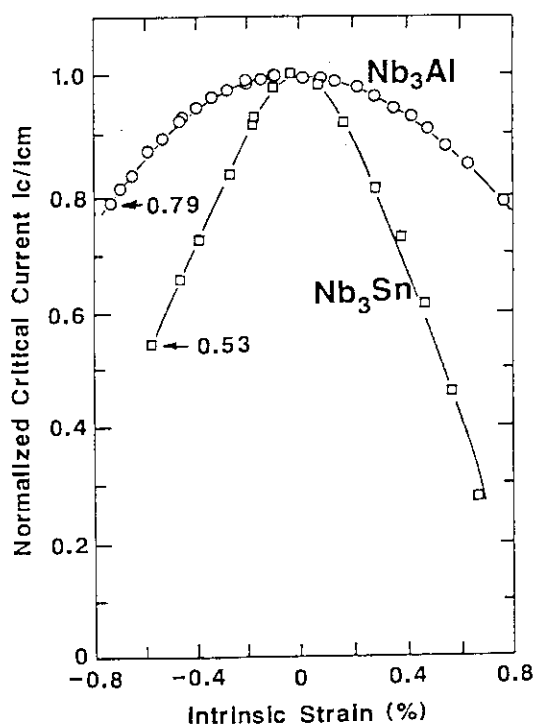


Fig.V.2.3-2 Relation between the critical current and the axial strain for a Nb₃Al cable-in-conduit conductor in comparison with a Nb₃Sn cable-in-conduit conductor.

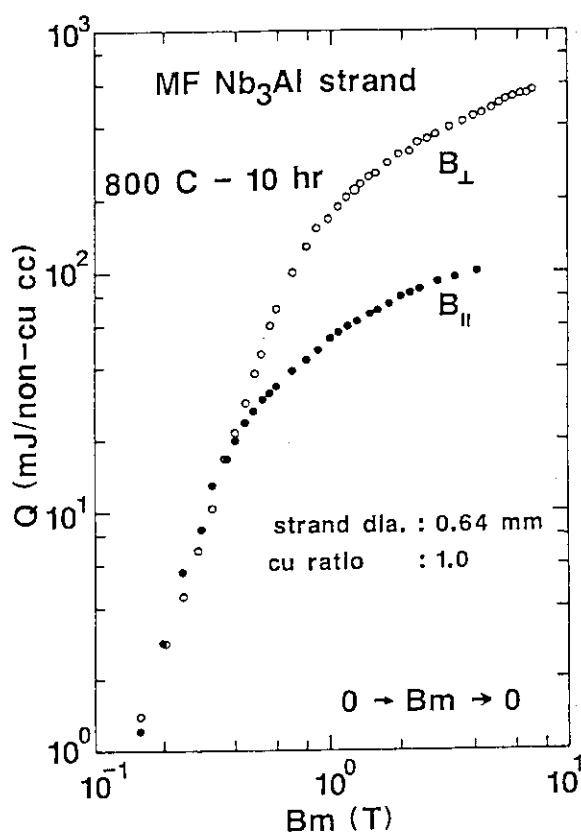


Fig.V.2.3-3 Hysteresis losses as a function of magnetic field for a Nb₃Al strand in the parallel and perpendicular fields.

2.4 R&D for ITER

2.4.1 Development of super conducting conductor for the central solenoid coil

The super conducting poloidal field coils consist of eight central solenoid coils, two divertor coils and four outer ring coils[2.4.1-1]. The requirements of the central solenoid coil were found to be the most difficult by the conceptual design activity (CDA)[2.4.1-2] as follows:

- | | |
|----------------------------|------|
| (1) Maximum magnetic field | 13T |
| (2) Operating Current | 40kA |
| (3) Field change | 2T/s |

The requirements of central solenoid coils are beyond present technology level in super conducting magnet.

A model for the central solenoid coils (CS scalable model coil) were designed to simulate the critical performance of ITER CS coils. The 2-m inner bore of the CS scalable model coil corresponds to 3.4 m inner bore of the real central coils. The conductor is Nb₃Sn cable-in-conduit type to satisfy above operating condition. The strand diameter is required to be less than 1 mm in order to let heat flux density small. Also low hysteresis losses are required. The target of super conducting wire was specified in CDA as follows:

- | | |
|--|-------------------------|
| (1) Current density at non-copper area | > 800 A/mm ² |
| (2) Effective filament diameter | < 10 μm |

The development of super -conducting wires as shown in Fig.V.2.4-1 for ITER CS coil were planed from three manufacturing processes, bronze, internal tin, tube, available in Japan. The thickness of Tantalum barrier and Tin contents of bronze, and arrangement of Niobium filament were modified to increase the critical current in the bronze process. The local ratio of Copper / Niobium, location of Tin were modified to decrease effective filament diameter in the internal tin process. The CuNi matrix in Niobium tube included tin inside was selected to improve drawing performance.

Finally, the bronze process was success to reach requirement of ITER super conducting wire as shown in Fig.V.2.4-2. The critical current density averaged over non-copper area was 765 and 841 A/mm² at compressive and tensile condition at 4.2 K, respectively. The effective filament diameter is 6μm measured by inductive

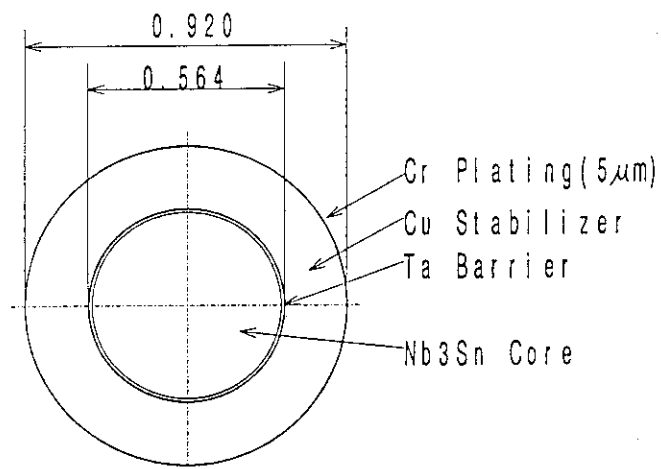


Fig.V.2.4-1 Super conducting wire for ITER Center Solenoid coil.

magnetization. The development of wire was completed by satisfying the ITER requirement.

The trial manufacturing of full scale conductor is now under way to make a critical current sample, a stability measurement and AC loss measurement. The about 600 superconducting wires are bundled in the pure titanium conduit selected to avoid thermal shrinkage from 1000 K to 4 K during heat treatment. The preformed armor developed in the DPC-TJ coil is selected to support magneto electric forces. The trial manufacturing of full size conductor will be completed in end of 1992.

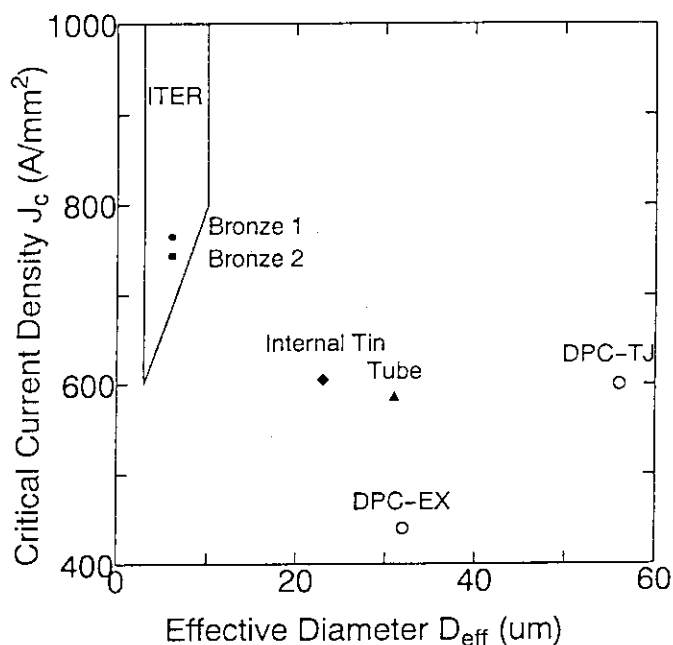


Fig.V.2.4-2 Critical current density vs. Effective diameter of superconducting wire for the central solenoid coils.

References

- [2.4.1-1] "ITER MAGNET", ITER Documentation Series, No.26, IAEA, Vienna, 1991
- [2.4.1-2] "Research and Development Needs for ITER Engineering Design", ITER Documentation Series, No.20, IAEA, Vienna, 1991

2.4.2 Cryogenic system for common test facility

An 8-kW helium refrigerator is planned to be constructed within coming three years, in order to cool and test CS scalable model coils which will be fabricated in the ITER-EDA. The refrigerator is not only a significant model of ITER refrigerator, which is supposed to be an unit of around 30-kW refrigerator, but also a test facility for the cryogenic machinery such as large-scale turbo-expander, cryogenic pump, and cold compressor of the ITER.

In this period, the design work has been completed and the system configuration and the capacities are determined as shown in Fig.V.2.4-3 and Table.V.2.4-1, respectively. The system consists of cryogenic pump unit, helium refrigerator unit, liquid helium tank, compressors, helium gas supply and purification units and other equipments. Helium refrigerator unit is shown in Fig.V.2.4-4, where the supercritical helium turbo-expander is added to the conventional Claude cycle with two JT valves in order to improve the efficiency of the refrigerator, leading to high Figure Of Merit of more than 1/300 (FOM: here, defined as refrigeration rate of

Table V.2.4-1 Cryogenic system capacities

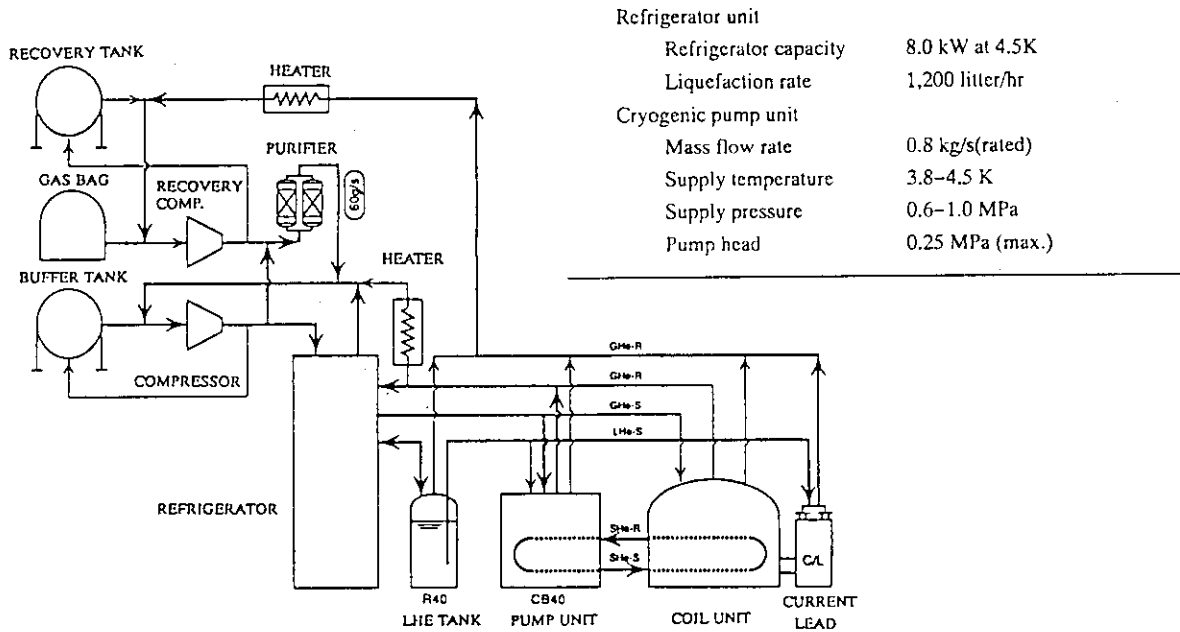


Fig.V.2.4-3 System configuration of the cryogenic system for ITER common test facility.

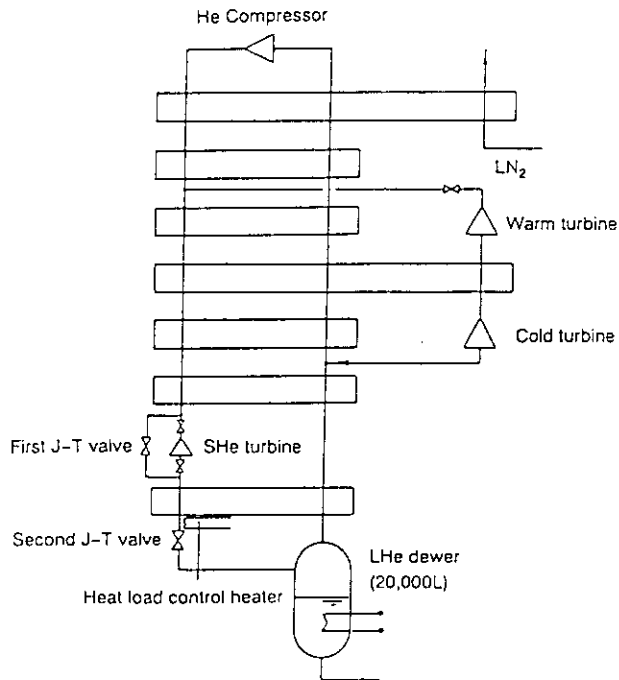


Fig.V.2.4-4 Helium refrigerator unit flow diagram.

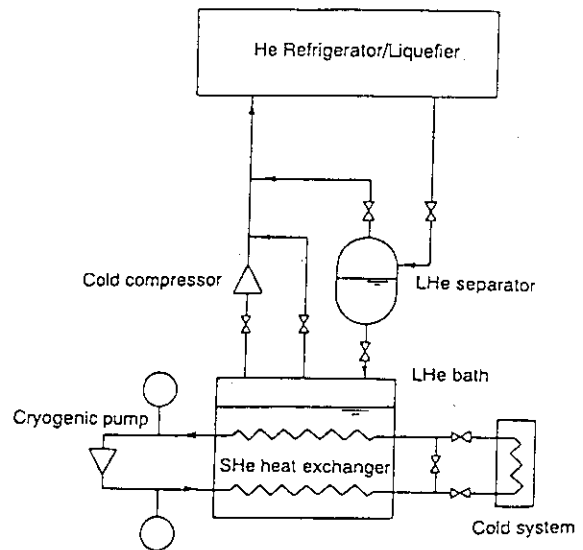


Fig. V.2.4-5 Cryogenic pump unit flow diagram.

required compressor work and liquid nitrogen consumption). Cryogenic pump unit is shown in Fig.V.2.4-5, where supercritical helium is supplied to the coil in the closed circulation loop with the cryogenic pump. The heat load of the coils is absorbed through the heat exchangers immersed in liquid helium bath.

2.4.3 Development of Titanium Conduit Conductor

Degradation of critical current due to difference of thermal expansion between a stainless steel conduit and a Nb_3Sn superconducting material is one of serious problems in cable-in-conduit conductor. Titanium, a low coefficient of thermal expansion material, was applied to a conduit in order to reduce the degradation of critical current because the thermal expansion of titanium is nearly equal to that of Nb_3Sn . Figure V.2.4-6 shows the ratio of critical current of a stainless steel conduit conductor, $I_c(304\text{SS})$, to critical current of a titanium conduit conductor, $I_c(\text{Ti})$, as a function of magnetic field. It was demonstrated that Ti conduit brought about twice as large critical current as stainless steel conduit at 12 T.

On the other hand, conduit material is required to have high mechanical performance at

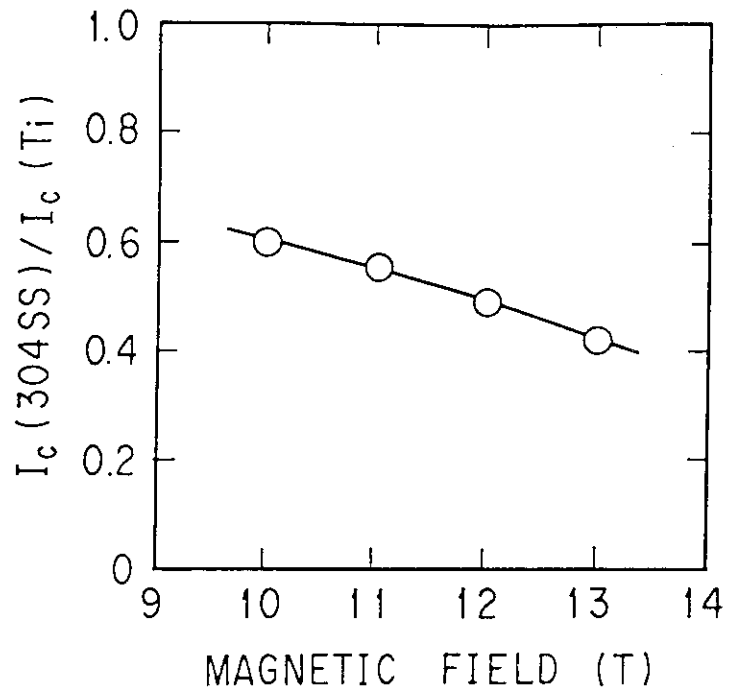


Fig.V.2.4-6 The ratio of critical current of a stainless steel conduit conductor, $I_c(304\text{SS})$, to critical current of a titanium conduit conductor, $I_c(\text{Ti})$, as a function of magnetic field.

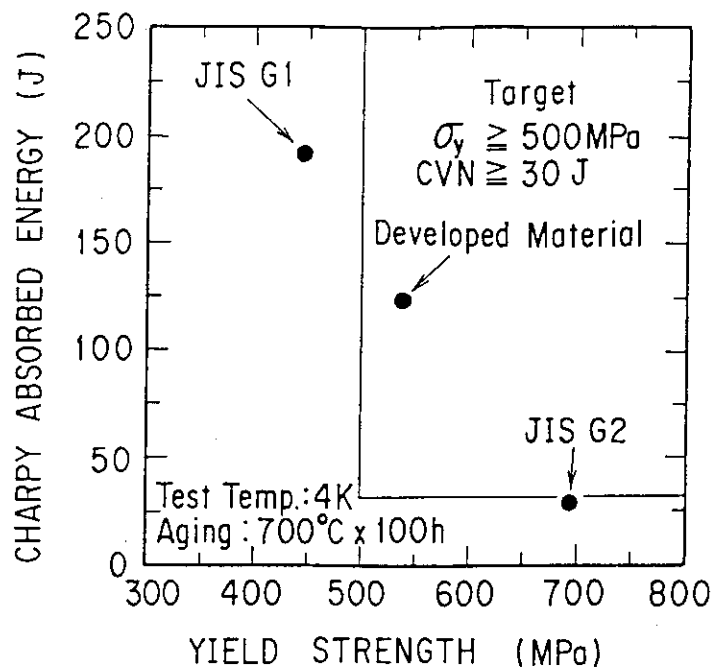


Fig.V.2.4-7 Relation between Charpy absorbed energy and yield strength of Ti material at 4K.

cryogenic temperature after Nb₃Sn reaction heat treatment. Requirements on mechanical properties after aging are both Charpy absorbed energy of more than 30 J and yield strength of more than 500 MPa. At first, two kinds of commercial titanium, JIS G1 and JIS G2, were tested to evaluate cryogenic mechanical properties. Figure V.2.4-7 shows relation between Charpy absorbed energy and yield strength at 4 K. JIS G1 had higher absorbed energy and lower yield strength compared with the target. JIS G2 had lower absorbed energy and higher yield strength compared with the target. Therefore, new Ti material which has intermediate properties between JIS G1 and JIS G2 has been developed successfully to satisfy the requirements. This material is being modified to get higher strength without degradation of Charpy absorbed energy.

3. Beam Technology

3.1 Introduction

Beam technology oriented to neutral beam (NB) injector has been advanced mainly in a negative ion source R&D. After succeeding in 10 A negative hydrogen ion beam production, the efforts are concentrated on long pulse operation, high energy acceleration, beam optics study, production of negative deuterium ion beam and energy recovery of the negative ion beams. R&D's on positive ion beam technology have also been continued for a long life plasma generator and high brightness ion source for accelerator applications.

3.2 Negative ion beam technology

3.2.1 Long pulse operation

Continuous production of the negative ion beam is one of the crucial subjects to realize a steady state tokamak reactor. In the ITER, for example, continuous operation of up to two weeks is desired for the current drive by the NB system.

The pulse length of the H⁻ beam production was short, so far, because of the restriction on power supplies. We have designed a new plasma generator and extractor, where all elements of the source are effectively water cooled. Each grid has expansion mechanism (bellows structure) in the peripheral region of the grid for the thermal expansion.

Using this ion source, continuous operation for 1000 s was demonstrated at H⁻ ion beam of 50 keV, 0.52 A (14 mA/cm²). A power flow diagram is shown in Fig. V.3.2-1. It was demonstrated that heat loadings in the ion source grids were very stable and low enough for the long pulse operation. Then the ion source was operated for longer pulse duration of up to 24 h. The arc current was 140 A and the initial H⁻ ion current was 0.3 A at 50 keV. In this operation, about 100 mg of cesium was seeded before the operation and there was no additional cesium injected during the pulse. Although the H⁻ ion current slightly decreases with time; e.g. 20 % reduction at t = 10 h, the cesium effect lasted for 24 h. Hence the consumption rate of the cesium

cryogenic temperature after Nb₃Sn reaction heat treatment. Requirements on mechanical properties after aging are both Charpy absorbed energy of more than 30 J and yield strength of more than 500 MPa. At first, two kinds of commercial titanium, JIS G1 and JIS G2, were tested to evaluate cryogenic mechanical properties. Figure V.2.4-7 shows relation between Charpy absorbed energy and yield strength at 4 K. JIS G1 had higher absorbed energy and lower yield strength compared with the target. JIS G2 had lower absorbed energy and higher yield strength compared with the target. Therefore, new Ti material which has intermediate properties between JIS G1 and JIS G2 has been developed successfully to satisfy the requirements. This material is being modified to get higher strength without degradation of Charpy absorbed energy.

3. Beam Technology

3.1 Introduction

Beam technology oriented to neutral beam (NB) injector has been advanced mainly in a negative ion source R&D. After succeeding in 10 A negative hydrogen ion beam production, the efforts are concentrated on long pulse operation, high energy acceleration, beam optics study, production of negative deuterium ion beam and energy recovery of the negative ion beams. R&D's on positive ion beam technology have also been continued for a long life plasma generator and high brightness ion source for accelerator applications.

3.2 Negative ion beam technology

3.2.1 Long pulse operation

Continuous production of the negative ion beam is one of the crucial subjects to realize a steady state tokamak reactor. In the ITER, for example, continuous operation of up to two weeks is desired for the current drive by the NB system.

The pulse length of the H⁻ beam production was short, so far, because of the restriction on power supplies. We have designed a new plasma generator and extractor, where all elements of the source are effectively water cooled. Each grid has expansion mechanism (bellows structure) in the peripheral region of the grid for the thermal expansion.

Using this ion source, continuous operation for 1000 s was demonstrated at H⁻ ion beam of 50 keV, 0.52 A (14 mA/cm²). A power flow diagram is shown in Fig. V.3.2-1. It was demonstrated that heat loadings in the ion source grids were very stable and low enough for the long pulse operation. Then the ion source was operated for longer pulse duration of up to 24 h. The arc current was 140 A and the initial H⁻ ion current was 0.3 A at 50 keV. In this operation, about 100 mg of cesium was seeded before the operation and there was no additional cesium injected during the pulse. Although the H⁻ ion current slightly decreases with time; e.g. 20 % reduction at t = 10 h, the cesium effect lasted for 24 h. Hence the consumption rate of the cesium

was estimated to be less than 4 mg/h.

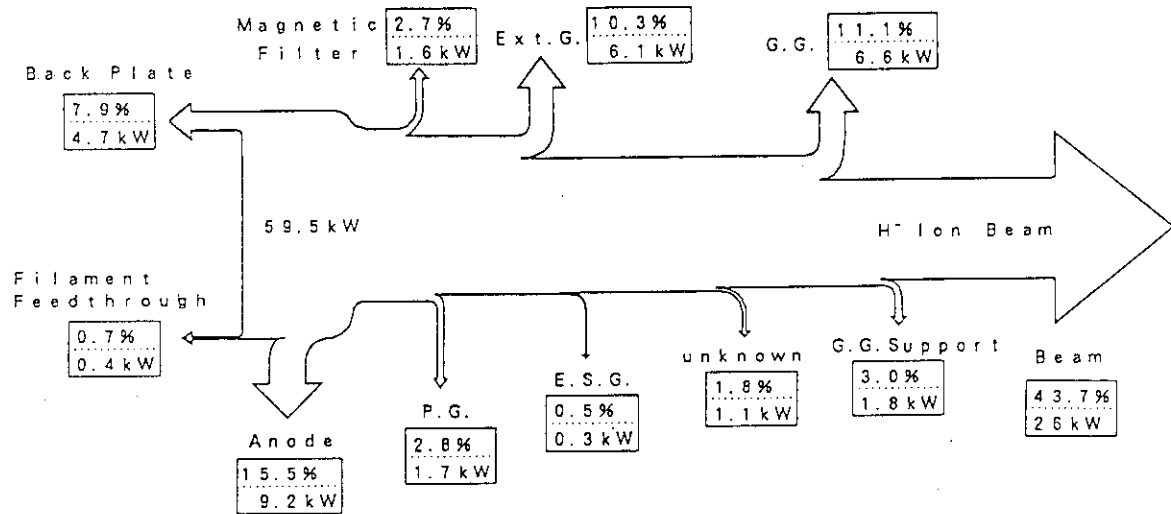


Fig. V.3.2-1: A power flow diagram at the long pulse operation for 1000 s.

3.2.2 High energy acceleration of H^- ions

Beam acceleration characteristics have been investigated using a 350 keV negative ion source. A schematic of the ion source is shown in Fig. V.3.2.-2. The source consists of a cylindrical plasma generator, whose inner dimensions are 22 cm in diameter and 17 cm in depth, and an electrostatic accelerator. The accelerator has an extraction gap of 5.7 mm and a two stage acceleration gaps of 83 mm and 57 mm. Diameters of the apertures in the extractor and the accelerator are 14 mm and 16 mm, respectively.

A H^- beam of 300 keV, 17 mA, 5 s, 5.5 mrad was produced in a cesium seeded operation with the single aperture accelerator. Divergence of the negative ion beams was compared for the

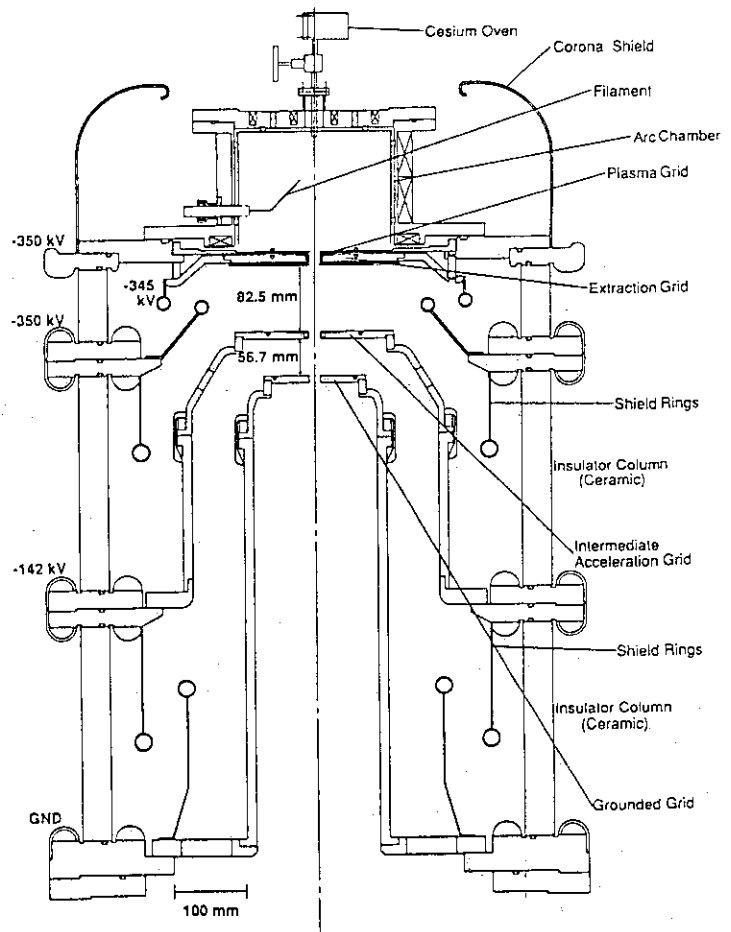


Fig. V.3.2-2: A schematic of the 350 keV high energy ion source. The source is composed of a cesium seeded volume type plasma generator, an electrostatic extractor, and a two-stage high energy accelerator.

operations with and without cesium seeding. The results showed that it was possible to obtain a good beam divergence in the cesium seeded source as well as in the pure volume source when a perveance is kept to be constant.

Experiments on multi-beamlet acceleration was started using a multi-aperture accelerator to demonstrate a high energy, high current H^- beam production. The accelerator has 9 holes within an area of 6 cm x 6 cm. Each aperture is the same size as that of the single aperture accelerator. A H^- beam of 304 keV, 57 mA, 1.5 s was produced.

3.2.3 H^- beam optics study

As a part of the beam optics study, steering of H^- beamlet was carried out by displacing apertures in ESG and/or GG(3rd and 4th grids). The experimental results are summarized as follows: 1) The aperture displacement up to 3 mm was tested for various extraction /acceleration voltages. The steering angle of up to 50 mrad was obtained. Significant beam divergence growth or direct interception due to the displacement was not observed. (See Fig. V.3.2-3) 2) It was confirmed that the beamlet steering angle is proportional fairly well to the aperture displacement. 3) The beamlet steering by the aperture displacement is independent of the deflection by the magnetic field produced by the dipole magnets for the electron suppression. It was confirmed that the steering technique is very useful for compensation of beam deflection caused by the magnetic field, and beamlet focussing of multi-aperture accelerator.

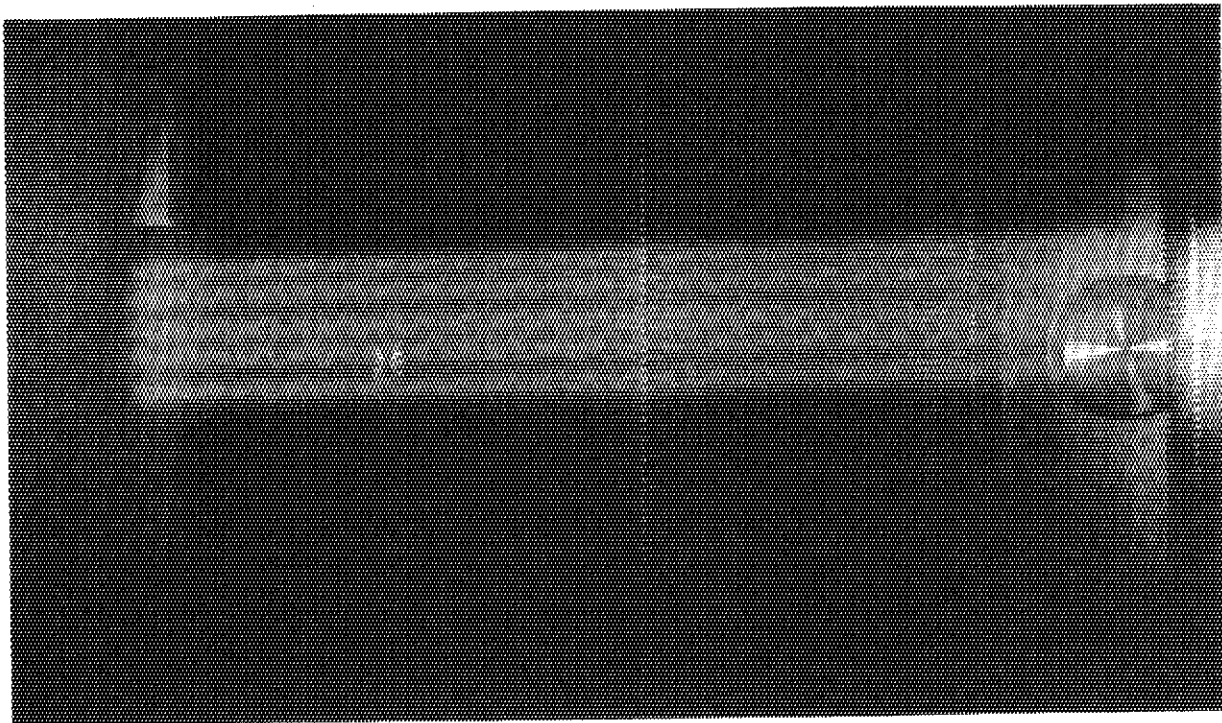


Fig. V.3.2-3: A picture of the beam (side view) taken at about 1 m downstream from the source. The five lines of beamlets corresponding to that produced from five lines of apertures are easily distinguished. The beamlets are steered in the horizontal direction.

3.2.4 D⁻ production in the joint CEA-JAERI experiment

In order to produce high current D⁻ ion beam, a large Cs-seeded plasma generator developed by JAERI was utilized and tested in a CEA-JAERI joint experiment. The plasma generator has a semi-cylindrical cross section, whose dimensions are 34 cm in diameter and 129 cm in length. By installing strong permanent magnets around the wall of the plasma generator, plasma confinement is improved for enhancing the negative ion yield.

By injecting a small amount of cesium, a high current D⁻ beam of 2.2 A, 100 keV was stably produced for 5 seconds. The current density was about 10 mA/cm², which almost satisfies the values required for future NB systems for JT-60U and ITER. Further, the optimum gas pressure giving the highest beam current was as low as 0.4 Pa in the plasma generator. The ion source could be operated at a pressure of 0.05 Pa with a small reduction of the H⁻ ion beam current. These values were low enough to reduce the striping losses of H⁻ ions in the accelerator.

The isotope effect on D⁻/H⁻ ions in the cesium-seeded ion source was also investigated. Major results are as follows;

- (1) The beam current ratio (I_{D^-}/I_{H^-}) was around 0.8, which is higher than the root of mass ratio.
- (2) The optimum gas pressure in the D₂ gas operation was nearly same in the H₂ operation.
- (3) The electron current extracted with negative ions was suppressed to almost zero by biasing the plasma grid positively with respect to the plasma generator both in H₂ operation and in D₂ operation. Required bias voltage in the D₂ operation was higher by 2V than that in the H₂ operation.

3.2.5 Neutralization and energy recovery experiments of H⁻/D⁻ beam

Neutralization and energy recovery experiments of high current H⁻/D⁻ beams have been conducted for the first time in a negative ion based neutral beam injector under the joint CEA-JAERI collaboration. A new type of energy recovery system was utilized. This allows: 1) to separate electrostatically the neutrals and charged components of the beam at the exit of the neutraliser; 2) to decelerate the residual unneutralised negative ions; 3) to prevent secondary emission of electrons from the negative ion collector by means of electrostatic trapping. Beam components, which were separated at the exit of neutralizer, measured by calorimeter as a function of neutraliser gas target thickness. The neutralization efficiency was around 60 % at the beam energy of 100 keV. This result agrees well with the theoretical prediction. When the primary D⁻ beams was 102 keV, 1.2 A, the residual negative ions have been decelerated down to 8 keV with high efficiency. Taking into account the additional power consumption of the electrostatic deflector, we concluded that 81 % of the residual negative ions power was recovered.

3.3 Application of high current ion beam technology

3.3.1 RF plasma generator

In order to develop a long life ion source and a plasma neutralizer, a RF plasma generator that has no filaments is being tested. By introducing 2MHz radio frequency into a bucket source, whose dimensions are 20 cm in diameter and 17 cm in length, via an antenna, high density hydrogen plasma was generated. Under an operating pressure of 0.5 Pa and an RF power of 20 kW, the ion saturation current density was as high as $6 \times 10^{11} \text{ cm}^{-3}$. Produced plasma was uniform over the field free region of the bucket source, i.e. 12 cm in diameter. It indicates that the RF plasma generator is applicable to the long life source and the plasma generator.

3.3.2 Development of a high brightness ion source for the proton linear Accelerator

A prototype ion source has been designed and tested for the 10 MeV, 10 mA, CW proton linear accelerator called Basic Technology Accelerator (BTA), which is to be constructed at JAERI. The ion source consists of a multicusp plasma generator and a two-stage extractor, and is expected to produce a 100 keV, 120 mA proton beam with a normalized emittance of as low as 0.5 nmm.mrad. First experiment was conducted using a 60 kV Test Facility, where hydrogen ions were extracted from a single aperture of 8 mm in diameter, accelerated to the maximum energy of the Test Facility, and transported to the multi-channel calorimeter located at 2 m downstream of the ion source. A convergent hydrogen ion beam of 60 keV, 56 mA, of which perveance is higher than that of 100 keV, 120 mA proton beam, was produced continuously with an e-folding half-width divergence of 10 mrad. Assuming the beam diameter is 4 mm at the exit of the ion source, we estimate the normalized emittance is about 0.45 nmm.mrad (90%). The proton ratio was measured by a Doppler-shifted spectroscopy and found to be 76 % at 50 mA. Since the proton yield is increasing with the beam current, more than 80 % proton ratio will be achievable.

3.4 Large scale cryo-sorption pump

In fusion reactor, it is required to evacuate not only hydrogen isotopes but also helium gas. By applying know-how accumulated in R&D's of JT-60 NB injector cryopump, we have developed a large scale cryo-sorption pump using SF₆ condensed layer, and basic data of the cryo-sorption pump using Ar and N₂ condensed layer pump have been obtained.

4. RF Technology

4.1 Introduction

Following the completion of the power supply and the control systems on the JAERI Gyrotron Test Facility in April 1991, the first oscillating test of a short pulse, 0.5 MW gyrotron named E 3960 was done using this Test Facility in summer, 1991. The manufacturing and preliminary short pulse test of the E 3971 gyrotron at 110 GHz for the ECH test stand also has been completed. Long pulse test is to be made in 1992.

In order to develop a long life ion source and a plasma neutralizer, a RF plasma generator that has no filaments is being tested. By introducing 2MHz radio frequency into a bucket source, whose dimensions are 20 cm in diameter and 17 cm in length, via an antenna, high density hydrogen plasma was generated. Under an operating pressure of 0.5 Pa and an RF power of 20 kW, the ion saturation current density was as high as $6 \times 10^{11} \text{ cm}^{-3}$. Produced plasma was uniform over the field free region of the bucket source, i.e. 12 cm in diameter. It indicates that the RF plasma generator is applicable to the long life source and the plasma generator.

3.3.2 Development of a high brightness ion source for the proton linear Accelerator

A prototype ion source has been designed and tested for the 10 MeV, 10 mA, CW proton linear accelerator called Basic Technology Accelerator (BTA), which is to be constructed at JAERI. The ion source consists of a multicusp plasma generator and a two-stage extractor, and is expected to produce a 100 keV, 120 mA proton beam with a normalized emittance of as low as 0.5 nmm.mrad. First experiment was conducted using a 60 kV Test Facility, where hydrogen ions were extracted from a single aperture of 8 mm in diameter, accelerated to the maximum energy of the Test Facility, and transported to the multi-channel calorimeter located at 2 m downstream of the ion source. A convergent hydrogen ion beam of 60 keV, 56 mA, of which perveance is higher than that of 100 keV, 120 mA proton beam, was produced continuously with an e-folding half-width divergence of 10 mrad. Assuming the beam diameter is 4 mm at the exit of the ion source, we estimate the normalized emittance is about 0.45 nmm.mrad (90%). The proton ratio was measured by a Doppler-shifted spectroscopy and found to be 76 % at 50 mA. Since the proton yield is increasing with the beam current, more than 80 % proton ratio will be achievable.

3.4 Large scale cryo-sorption pump

In fusion reactor, it is required to evacuate not only hydrogen isotopes but also helium gas. By applying know-how accumulated in R&D's of JT-60 NB injector cryopump, we have developed a large scale cryo-sorption pump using SF₆ condensed layer, and basic data of the cryo-sorption pump using Ar and N₂ condensed layer pump have been obtained.

4. RF Technology

4.1 Introduction

Following the completion of the power supply and the control systems on the JAERI Gyrotron Test Facility in April 1991, the first oscillating test of a short pulse, 0.5 MW gyrotron named E 3960 was done using this Test Facility in summer, 1991. The manufacturing and preliminary short pulse test of the E 3971 gyrotron at 110 GHz for the ECH test stand also has been completed. Long pulse test is to be made in 1992.

4.2 Development of the LHRF launcher

A new type of the multi-junction grill, which consist of six element multi-junctions with a tapered waveguide from the standard sized waveguide to the over sized waveguide at 2 GHz, has been applied to the LHCD launcher for JT-60U LHRF system.

A conceptual design on the lower hybrid antenna module has been studied to perform the experiment to provide data on RF outgassing from the waveguide antenna under high power, long pulse operation. A preliminary discussion between JAERI and CEA-Cadarache has started to conduct a collaborative program on the LHRF antenna module.

4.3 Investigation of high power gyrotron and ECH components

Research and development of a 100 GHz band gyrotron have been carried out at JAERI for the application to an electron cyclotron resonance heating (ECH) for a fusion reactor.

The oscillation mode of the gyrotron named E3960 is measured using a wave number spectrometer (k-spectrometer). The 120 GHz gyrotron of a waveguide coupling type is used for measurement. The output power is extracted from the top of the gyrotron with the oscillation mode through a tapered waveguide and a ceramic window. The wave number spectrometer is installed on the top of the gyrotron as illustrated in Fig.V.4.3-1 and the precise measurement of the mode number was carried out. Figure V.4.3-2 shows data of the wave number spectrometer. The detected mode numbers are indicated in the figure. A frequency is 120.18GHz for all modes. It is concluded that considering the frequency the oscillation

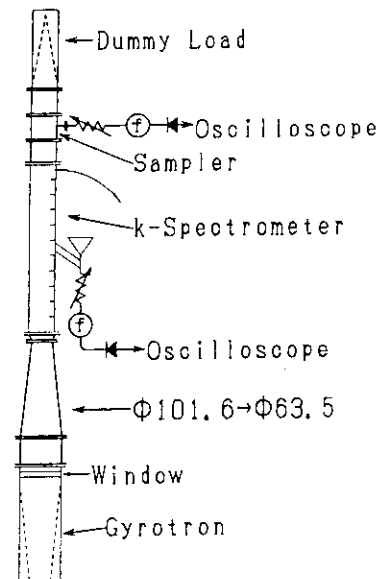


Fig.V.4.3-1
Schematic view of mode measurement system.

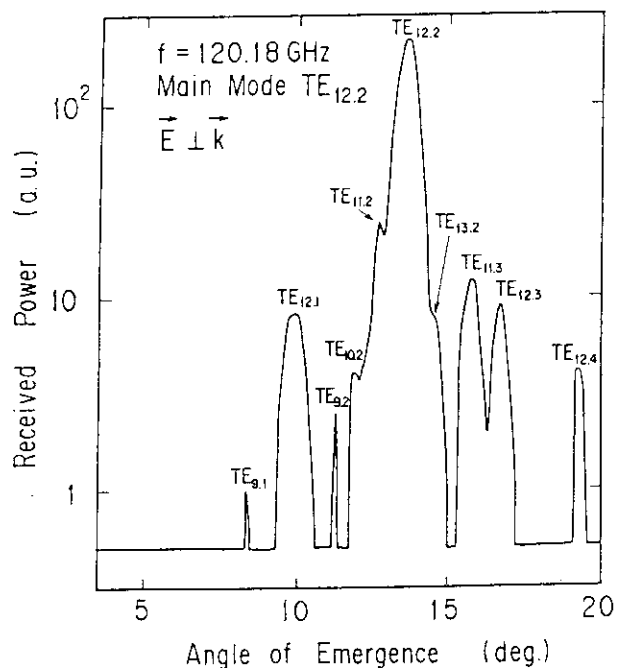


Fig.V.4.3-2
Experimental result of mode measurement.
Vertical axis is a received power by a horn antenna of the wave number spectrometer.

mode is only $TE_{12,2}$ whispering gallery mode at 120.18GHz and the other measured mode appeared by the mode conversion at the tapered waveguide and the gap between the waveguide.

The development of the long pulse gyrotron of 110 GHz was made. To expand a cavity size to decrease a heat load on a cavity wall, the whispering gallery mode $TE_{22,2}$ is used as an oscillating mode. Consequently, a long pulse operation more than 1sec. at 500kW become possible. The configuration of gyrotron E3971 is illustrated in Fig.V.4.3-3. The Vlasov type quasi-optical mode converter is installed inside the gyrotron. The output power is extracted as a Gaussian beam through double ceramic

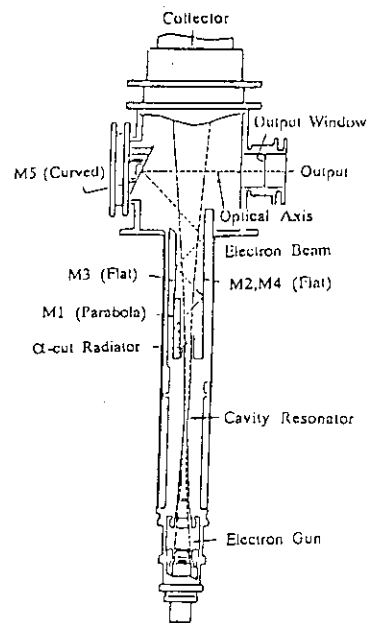


Fig.V.4.3-3 Configuration of gyrotron (E3971).

windows mounted at the side of the gyrotron. The preliminary test was carried out using a newly constructed test facility [4.3-1], the power generation of more than 300kW at 110GHz was confirmed. The strong magnetic field imposed on the gyrotron is supplied by a newly developed super-conducting magnet coil. This coil has a persistent current mode, in which the circuit of coil is isolated from the outer power supply. Consequently, the thermal invasion into the cryogenic section is significantly reduced and the consumption rate of a liquid helium is decreased up to 0.1~0.3 liter/hr. The configuration of the magnetic field is controlled using auxiliary coils .

References

- [4.3-1] M.Tsuneoka, et al., Proc.of the 14th IEEE/NPSS Symp. on Fusion Engineering, Vol.1, p.497, CA Oct.(1991).

4.4 Millimeter wave Free Electron Laser

Millimeter wave Free Electron Laser (FEL) has been experimentally investigated using 1MeV, 3kA induction linac. A focusing wiggler has been used; a surface of each wiggler magnet is parabolically curved which suppress the electron beam divergence when passing through the wiggler. The wiggler pitch is 45mm and the total pitch number is 33.[4.4-1] From 30GHz to 60GHz, FEL amplification were studied. Figure V.4.4-1 shows a typical result at 45GHz. The closed circles indicate the result when an input power is 10W. The high gain of

52dB is obtained. Furthermore, when the input power is increased up to 200W, the power saturation is observed at 6MW. The maximum spatial growth rate was 56dB/m.

References

[4.4-1] K.Sakamoto, et al., Proc. of Int. school of Plasma Phys., High power Microwave generation and Applications, p.597 (1991).

4.5 Design study of RF heating and current drive launcher for ITER

Improve design of the LHRF

and ICRF launchers on ITER has been made. In the LHRF launcher design we have applied to the reference design of ITER CDA [4.5-1] the concept of the replacement of the launcher mouth separately by remote handling tools from inside the torus. By adopting the new multi-junction developed for the JT-60U launcher a better RF contact of the choke type between the mouth part and the rest of the RF plug has been realized. In the ICRF antenna design a concept of ceramics-free antenna feeder using the ridged waveguide is studied in the frequency range of 15-80 MHz and within the constraint of ITER. This scheme is attractive for the ITER ICRF system, because it can eliminate the problem of ceramics and enhance a reliability of the antenna system in a reactor environment.

References

[4.5-1] V. V. Parail et al., ITER CURRENT DRIVE AND HEATING SYSTEM, ITER DOCUMENTATION SERIES, No.32, IAEA, VIENNA 1991.

5 Tritium Technology

5.1 Introduction

Research and development for tritium technology are being carried out for the purpose of the establishment of the tritium processing, tritium safe handling, and related technologies for fusion reactor. The major activities in the F.Y. 1991 are summarized as follows. For the joint operation of the Tritium Systems Test Assembly (TSTA) at Los Alamos National Laboratory (LANL) under Annex IV, full loop experiments and components testing were performed by using

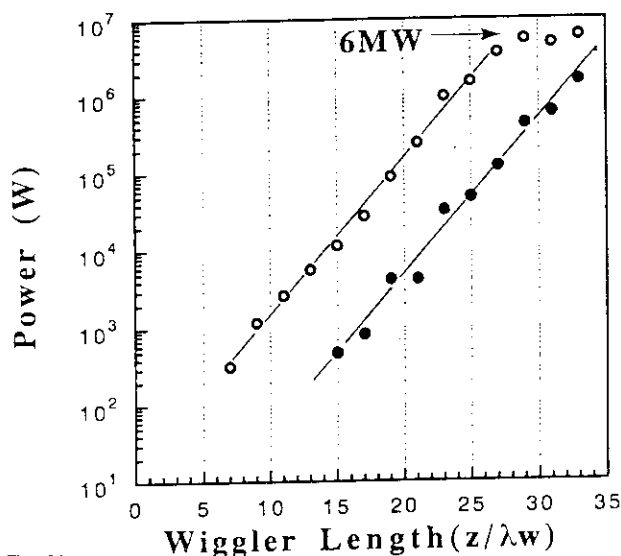


Fig.V.4.4-1

Experimental data of power amplification at 45GHz. Closed and Open circles indicate the results for input power $P_{in}=10W$ and $200W$, respectively.

52dB is obtained. Furthermore, when the input power is increased up to 200W, the power saturation is observed at 6MW. The maximum spatial growth rate was 56dB/m.

References

[4.4-1] K.Sakamoto, et al., Proc. of Int. school of Plasma Phys., High power Microwave generation and Applications, p.597 (1991).

4.5 Design study of RF heating and current drive launcher for ITER

Improve design of the LHRF

and ICRF launchers on ITER has been made. In the LHRF launcher design we have applied to the reference design of ITER CDA [4.5-1] the concept of the replacement of the launcher mouth separately by remote handling tools from inside the torus. By adopting the new multi-junction developed for the JT-60U launcher a better RF contact of the choke type between the mouth part and the rest of the RF plug has been realized. In the ICRF antenna design a concept of ceramics-free antenna feeder using the ridged waveguide is studied in the frequency range of 15-80 MHz and within the constraint of ITER. This scheme is attractive for the ITER ICRF system, because it can eliminate the problem of ceramics and enhance a reliability of the antenna system in a reactor environment.

References

[4.5-1] V. V. Parail et al., ITER CURRENT DRIVE AND HEATING SYSTEM, ITER DOCUMENTATION SERIES, No.32, IAEA, VIENNA 1991.

5 Tritium Technology

5.1 Introduction

Research and development for tritium technology are being carried out for the purpose of the establishment of the tritium processing, tritium safe handling, and related technologies for fusion reactor. The major activities in the F.Y. 1991 are summarized as follows. For the joint operation of the Tritium Systems Test Assembly (TSTA) at Los Alamos National Laboratory (LANL) under Annex IV, full loop experiments and components testing were performed by using

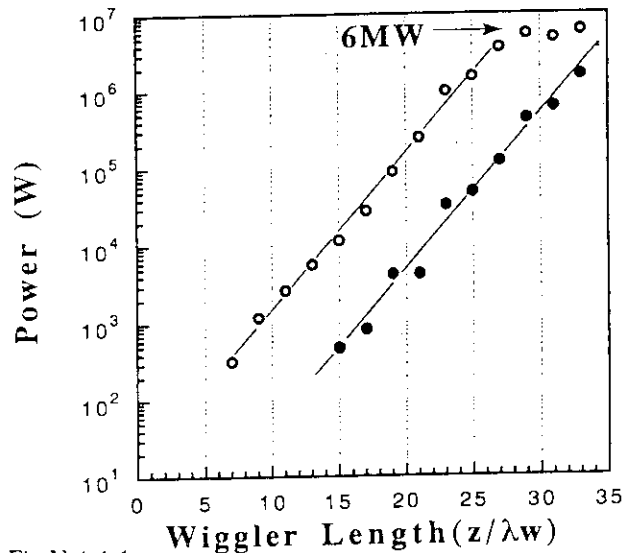


Fig.V.4.4-1

Experimental data of power amplification at 45GHz. Closed and Open circles indicate the results for input power $P_{in}=10W$ and $200W$, respectively.

1 ~ 100 g level tritium. Especially, JAERI Fuel Cleanup System (JFCU), which is developed and designed by JAERI, was successfully operated with the other TSTA components. For the tritium processing and related technologies, experimental studies for fuel cleanup and hydrogen isotope separation were carried out using about 1.5 g tritium. Research and development associated to tritium analysis and measurements, and tritium waste reduction were accomplished. Metal getter type tritium transport package was designed and tested under the IAEA's transportation regulations. The safety systems of Tritium Process Laboratory were fully in tritium service for the above mentioned experiments, and were successfully operated without off-normal tritium release.

5.2 Development of fuel processing technology under JAERI-LANL(DOE)

Joint operation of TSTA at Los Alamos National Laboratory (LANL) under Annex IV projected a number of important scheduled milestones to conclude the 5 year collaborative program on the development of fusion fuel cycle. The JAERI Fuel Cleanup System (JFCU), which is a full-scale fuel loop subsystem that processes simulated plasma exhaust and developed and designed by JAERI, was performed its tritium operation several times. "Loop runs" - experimental campaign of the integrated TSTA loop - demonstrated the operation of simulated fusion fuel cycle using realistic DT mixed gases with wide range of impurities. Documentation, training and many of the operational procedures were modified to meet the newer DOE requirements that are becoming more and more strict.

The JFCU completed the first tritium test in July, 1991. Major component's functions to purify and recover hydrogen isotopes from mixture and compounds, as well as safety feature of the JFCU were verified with a gram of tritium. Interface with TSTA safety systems such as Tritium Waste Treatment, Process Evacuation and computer systems were successful. Integrated loop test of the JFCU with the Isotope Separation System was performed in October. JFCU supplied pure DT mixture to the distillation columns stably from 2 l/min to 10 l/min of throughput range, that exceeds the designed capacity. Interconnection of the systems, stabilizing effect against the flow/pressure perturbation, and removal of helium impurity

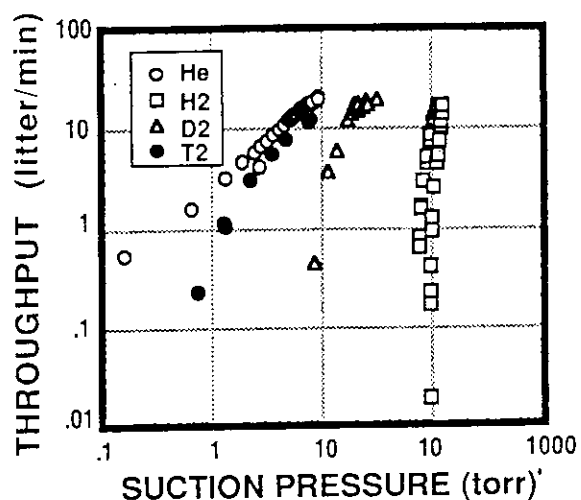


Fig. V.5.2-1 Pumping characteristics of Normetex Scroll Pump in the JFCU flow process obtained with various gases. Pump showed poor compression for hydrogen isotopes.

were major advantages of the JFCU verified in the test. In the later experimental campaign, JFCU demonstrated the processing of methane, ammonia, nitrogen, water, helium and their mixture as impurities. Experiment of JFCU with pure tritium of 10 gram level revealed the characteristics of the components. Figure V.5.2-1 shows the characteristics of the Normetex Scroll Pump with various gases. As seen in the figure, marked difference was observed among the gases. A metal bellows pump was added to improve the compression of light species in the JFCU.

Operation of the isotope separation system made a significant improvement in stability and the purity of product. Raman spectroscopy system was installed to analyze the species from various points in the distillation columns. Figure V.5.2-2 shows an example of the spectra obtained in the dynamic measurement of the column. Improved stability, more frequent measurement and combined numerical simulation enabled the understanding of both real time profile and dynamic change of the distillation columns.

Facility of TSTA has ceased the operation from April to June, 1991 in order to improve safety of the operation. Training, operation procedure and their documentation were reviewed, modified and approved so that the operation of TSTA meets the new DOE regulation on the nuclear facilities. The experience of JAERI to be involved in the activity will be beneficial for the future fusion research collaboration where foreign nuclear regulation will be involved.

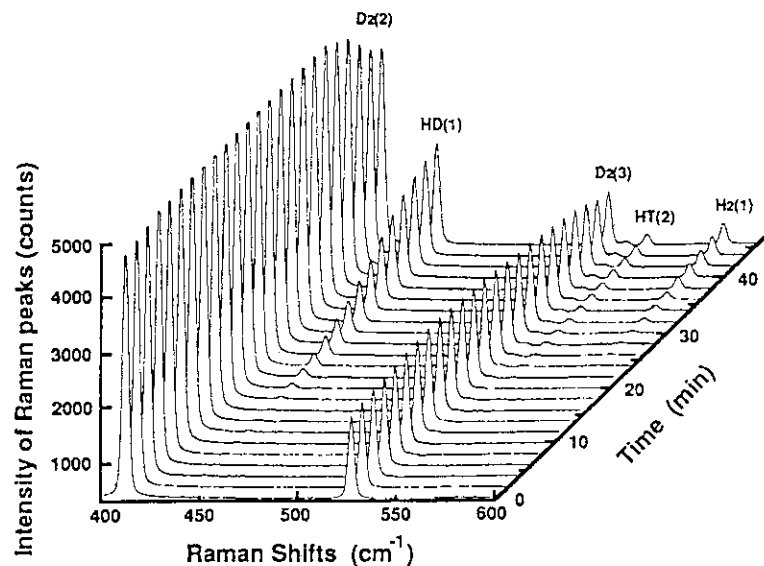


Fig. V.5.2-2 Dynamic behavior of hydrogen isotope spectra in the distillation column measured by laser Raman spectroscopy

5.3 Development of tritium processing in TPL (Tritium Process Laboratory)

5.3.1 Fuel cleanup

The experiment of fuel clean up system (FCU) was continued. Poor trapping of tritiated water vapor at the cold traps that have been observed in last year is still under investigation. Additional molecular sieve beds were installed in order to minimize the loss of tritium to the

effluent. Process was configured to avoid the generation of tritiated water and handle the tritiated impurities in batch process. This test will continue in the next year.

5.3.2 Hydrogen isotope separation

Experimental studies for cryogenic distillation have been continued with H-D-T system (1.5 g of tritium). The columns used were different in inner diameters (1 cm and 2 cm) and the sizes of packing. The larger column was packed with 3 mm Dixon Ring, and 1.5 mm Dixon Ring was used for the smaller column. The experimental observations were in close agreement with calculated results for both the columns. We propose distillation columns that have feed back streams and equilibrators for the isotope separation system in the fusion cycle. In the fusion reactor blanket system, the produced tritium is accompanied by protium. Numerical analysis shows that protium and tritium can be separated by a single column with a feed back stream and a catalytic equilibrator. Experimental studies have been initiated to discuss the separation characteristics of the columns having the feed back streams.

Another separation system of hydrogen isotope mixtures at TPL consists of four thermal diffusion columns. Some separation experiments with tritium verified that the system could meet designed performance. The optimum operating procedure was also established through the experiments. The system will be fully operated to recover tritium from hydrogen isotope mixtures in the next fiscal year.

Several theoretical studies pointed out that separation factors of the thermal diffusion columns could be remarkably

enhanced by refrigerating outer walls of columns to cryogenic temperature. We have designed and constructed an experimental apparatus of the 'cryogenic-wall' thermal diffusion column. Figure V.5.3-1 shows a schematic flow diagram of the experimental apparatus. The apparatus consists of a thermal diffusion column, a cryostat, and a liquid nitrogen supply system. The column is 29.4 mm in inner diameter and 2000 mm in height. Figure V.5.3-2 shows the dependence of separation factor on column pressure measured in the total reflux experiments. The hot wire temperature is 1273 K. The maximum separation factor (9.1) was obtained at 94 kPa for the

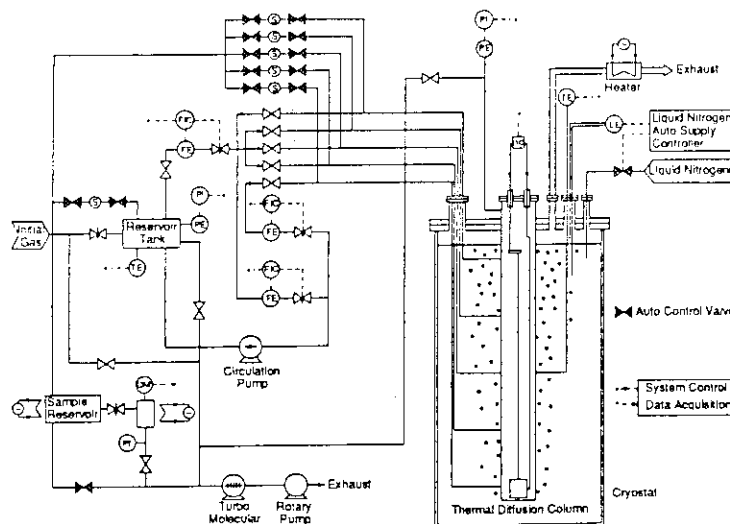


Fig. V.5.3-1 Schematic flow diagram of 'cryogenic-wall' thermal diffusion system

'water cooled-wall' column. On the other hand, the factor was 112.7 at 30 kPa for the 'cryogenic-wall' column. It was thus demonstrated that the separation factor was appreciably enlarged by using the 'cryogenic-wall' column.

5.3.3 Tritium analysis and measurement

To establish system control and tritium inventory accounting in fusion fuel processing systems, analytical method for processing gases should be developed. From this viewpoint we have continued development of a real time and in-situ process gas analyzer using laser Raman spectroscopy. To accumulate basic data for the analysis of various gases expected in plasma exhaust, Raman spectra of hydrogen isotope including tritium and deuterated methane and ethane had already measured by the last fiscal year. In this fiscal year, our attention was focused on measurement of tritiated methane spectrum. Figure V.5.3-3 shows the Raman spectra for tritiated methane.

5.3.4 Tritium-materials interaction

Tritium permeation into first wall coolants could be a serious problem from a viewpoint of tritium safety in D-T fusion reactors. To simulate tritium permeation behavior and estimate tritium permeation rate through candidate materials for first wall, ion driven permeation of deuterium implanted into Al-Li and Fe-Ti with low incident energy, ranging from 100 to 2000 eV, have been studied. The experimental results show that the deuterium permeation rates through both alloys decreased due to trapping effects of Li and Ti for deuterium, compared with that through pure Al and Fe.

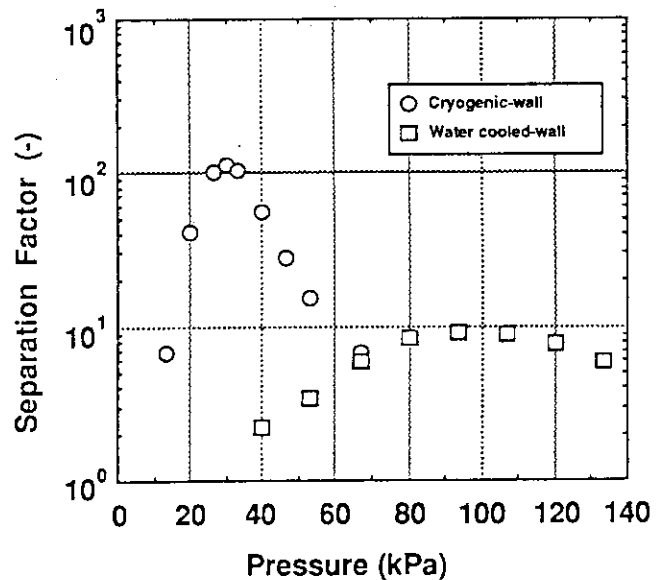


Fig. V.5.3-2 Separation factor as a function of column pressure

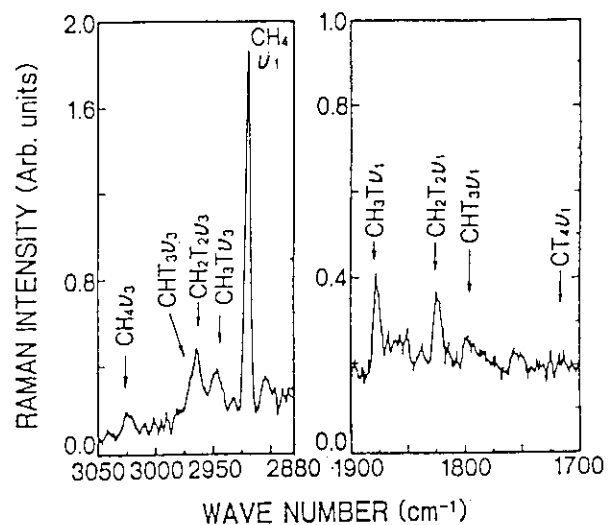


Fig. V.5.3-3 Raman spectrum of isotopic methane observed in $\text{CH}_4 : \text{T}_2 = 1 : 2$ mixed gas. Pressure, 60 kPa ; Elapsed time, 320 h ; Resolution, 5 cm^{-1}

In order to evaluate the long-term reliability and safety of zirconium-cobalt (ZrCo) alloy as a tritium (T) getter, the release behavior of decay helium from ZrCo tritide has been investigated for two years by the application of radio-gas chromatography. The release fractions of the total decay helium in ZrCo tritide are still less than 3 % and are almost constant for 24 months under the operating temperatures = 293 ~ 425 K, the ratios of tritium and alloy (T/ZrCo) = 0.3 ~ 1.4, and the number of hydrogenation-dehydrogenation cycles before tritiation = 1 ~ 10.

5.4 Development of tritium safe handling technology

5.4.1 Development of tritium confinement using gas separation membrane

It is important to establish a compact and cost-effective tritium confinement system, because a fusion facility such as ITER will require large tritium safety system. Polyimide membrane has a selective permeability for hydrogen gas and water vapor. The polyimide gas separation module process will be potentially applicable for volume reduction of tritium contaminated gas. For process demonstration, feasibility studies with a small scale polyimide gas separation module contains hollow filament membrane shown in Fig. V.5.4-1 have been carried out at TPL with a small amount of tritium. Figure V.5.4-2 shows flow diagram of experimental set up for the separation of tritium in glovebox gas (dry nitrogen gas). The feed gas

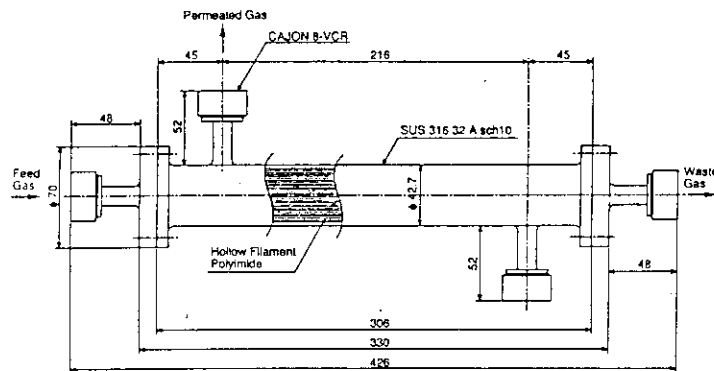


Fig. V.5.4-1 Structure of the gas separation module

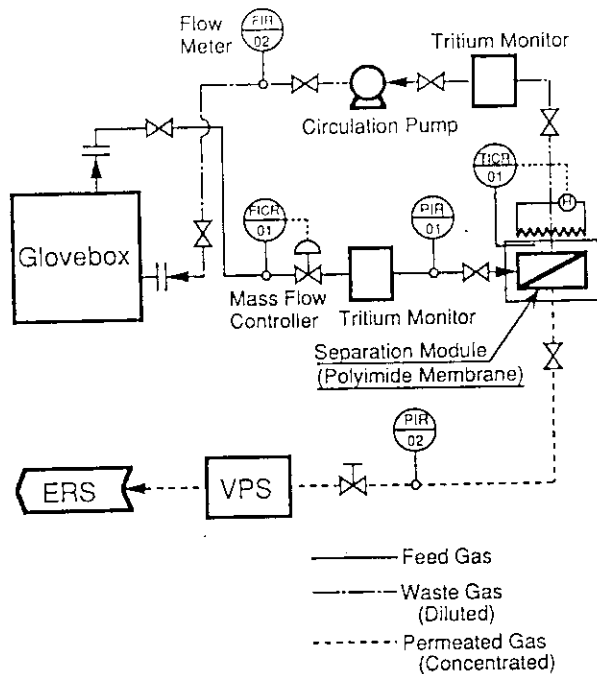


Fig. V.5.4-2 Flow diagram for tritium removal experiment with the module

was supplied from a glovebox to the gas separation module by the circulation pump. The waste gas that did not permeate the membrane was recycled to the glovebox. Tritium concentration of the feed and the waste gases was measured by ion chambers. Permeated side was pumped by the Vacuum Pumping System (VPS) of TPL which consists of oil-free vacuum pumps. Exhaust gases of VPS was sent to the Effluent tritium Removal System (ERS). A typical experimental

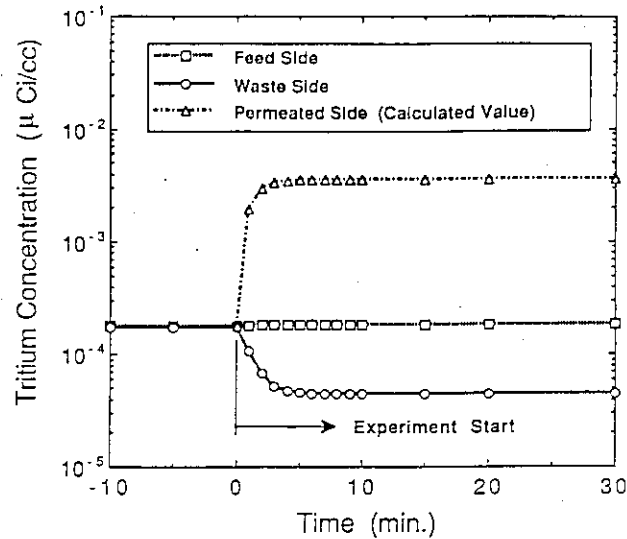


Fig. V.5.4-3 Extraction of tritium from the Glovebox gas through the separation module

Feed gas : Glovebox Atmosphere gas,
 Temperature of module : 87 deg.C,
 Flow rate of feedgas : 1.00NL/min.,
 Flow rate of waste gas : 0.96NL/min.,
 Pressure at feed side : 440 Torr,
 Pressure at permeated side : 1.1 Torr

result for separation of tritium in glovebox gas was shown in Fig. V.5.4-3. Tritium concentration in waste gas decreased immediately and was stabilized at approximately 1/5 of that of feed gas, on the other hand, the permeated stream concentrated tritium to factor of 20. It is concluded that the gas separation module is applicable to separate tritium from dry nitrogen stream.

5.4.2 Development of metal getter (ZrCo) type transport package of tritium

The purpose of development of this package (name of the package is TPL-92Y-450K) is to transport the tritium (25 g in the maximum) produced and refined in Canada or U.S.A., as a form of ZrCo tritide, to TPL.

This package is designed to meet the transport requirements of Safety series No. 6, "Regulations for Safe Transport of radioactive Materials" 1985 Revised edition, International Atomic Energy Agency (IAEA). Conceptual figure of the package is shown in Fig. V.5.4-4. In order to verify that this package complies with the requirements as BU package under the accident test condition regulated in IAEA transport regulations, the demonstration test (9 m drop test, 1 m puncture test, and 1073 K thermal test) have been performed using prototype module of the package. To confirm the integrity of the containment boundary, the leak tests were carried out before and after the demonstration tests. Results of the tests showed that this package complied with all requirements contained in IAEA transport regulations.

5.4.3 Operation of tritium safety systems

The safety systems which composed of Glovebox, Glovebox gas Purification system (GPS), Effluent tritium Removal System (ERS), Air Cleanup System (ACS) etc., were fully in tritium service without off-normal tritium release.

Figure V.5.4-5 shows monthly release of tritium from TPL stack. Total tritium release to environment was less than 0.12 Ci in this period.

5.5 Tritium system analysis

The stage model is used for simulation of the cryogenic distillation columns, since it is suitable for a multi-component system. In addition, the model allows us to simulate dynamic behavior of columns. The HETP is a key parameter of the model. Although the model has the above - mentioned advantages, the HETP is hardly estimated by theoretical analysis. To overcome this problem, we have developed simulation codes, and examined relation between the HETP and the mass and heat transfer mechanism within the columns. The code estimate the mass and heat transfer rates on the basis of the laminar boundary layer theory and the Chilton-Colburn analogy theory. The numerical analysis results indicated that the overall mass transfer rate

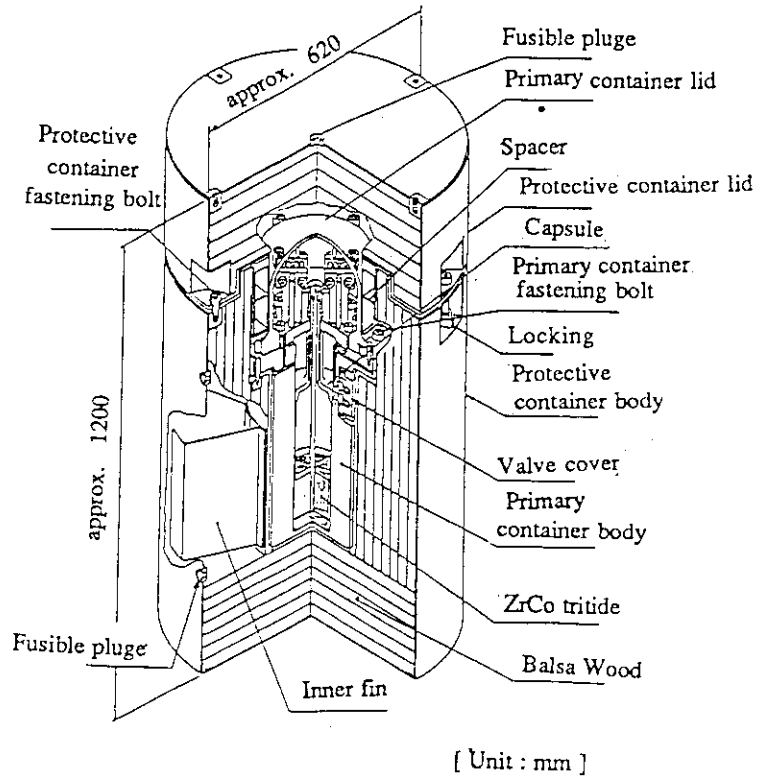


Fig. V.5.4-4 Illustration of TPL-92-Y-450K Package
Total weight of package : 450 kg

Specification of content	
Material of radioactive isotope	: Tritium (Form of ZrCo tritide)
Total weigh of radioactive isotope (Tritium)	: Max. (2.5 g/Package)
Total Activity	: Max. 9.25 (PBq/Package)
Total heat generation rate	: Max. 25 (W/Package)

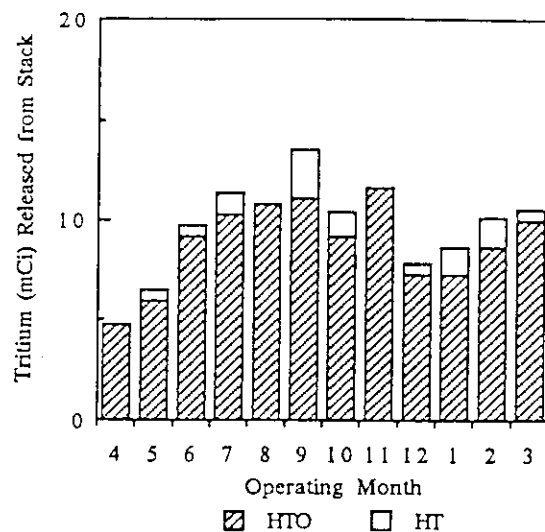


Fig. V.5.4-5 Monthly release of tritium from TPL stack (FY 1991)

increased with the vapor flow rate proportionally. The HETP was therefore unchanged against the vapor flow rate.

From tritium safety point of view, it is very important to establish tritium accountability systems in fusion reactors. In this fiscal year we initiated a conceptual design study for tritium accountability systems in the experimental fusion reactor (ITER).

6 High heat flux technology

6.1 Introduction

Since it is essential for the next step large devices, such as ITER, to develop plasma facing components (PFCs), JAERI has carried out the experimental and analytical studies on PFCs. Our major effort has been concentrated to develop the divertor plate and first wall for ITER. To develop the promising divertor plate and the first wall for ITER, there are many experimental and developmental issues, i.e., material selection, joining technique, element and component characterizing tests for the promising cooling structures and bonds, evaluation of erosion, and so on. To clear off these issues, two types of high heat flux facilities have been utilized at JAERI. One is a hydrogen ion beam irradiation system, called the Particle Beam Engineering Facility (PBEF), and the other is an electron beam irradiation test system, called the JAERI Electron Beam Irradiation System (JEBIS). Further, three types of particle irradiation facilities, MSP, SSP and Pre-DIPES, have been utilized for evaluation of erosion.

With respect to the evaluation of the erosion during the off-normal event such as the plasma disruption, the JEBIS can deliver intense electron beam which can simulate a heat load onto the surface of PFCs during plasma disruption. Japan - European Community collaborative experiments has also been performed in the JEBIS and JUDITH at KfA in Germany.

6.2 Activities on divertor plate development

Developing efforts on the divertor plate for ITER have experimentally been made in PBEF and JEBIS. The divertor plate is subjected to heat fluxes of 15 to 30 MW/m². Carbon based materials are primary candidate of the armor tiles in the physics phase of ITER, and metal armor materials are proposed in the technology phase. One of the key technologies for developing the divertor plate is the joining technique of the armor tiles to the metal cooling structure. To evaluate joining properties, three types of the divertor mock-ups have been fabricated and tested. Based on their results, 1 m long divertor mock-ups have been designed and fabricated. Heat removal experiments of various types of the cooling structures have also been performed for the design of the divertor plate.

increased with the vapor flow rate proportionally. The HETP was therefore unchanged against the vapor flow rate.

From tritium safety point of view, it is very important to establish tritium accountability systems in fusion reactors. In this fiscal year we initiated a conceptual design study for tritium accountability systems in the experimental fusion reactor (ITER).

6 High heat flux technology

6.1 Introduction

Since it is essential for the next step large devices, such as ITER, to develop plasma facing components (PFCs), JAERI has carried out the experimental and analytical studies on PFCs. Our major effort has been concentrated to develop the divertor plate and first wall for ITER. To develop the promising divertor plate and the first wall for ITER, there are many experimental and developmental issues, i.e., material selection, joining technique, element and component characterizing tests for the promising cooling structures and bonds, evaluation of erosion, and so on. To clear off these issues, two types of high heat flux facilities have been utilized at JAERI. One is a hydrogen ion beam irradiation system, called the Particle Beam Engineering Facility (PBEF), and the other is an electron beam irradiation test system, called the JAERI Electron Beam Irradiation System (JEBIS). Further, three types of particle irradiation facilities, MSP, SSP and Pre-DIPES, have been utilized for evaluation of erosion.

With respect to the evaluation of the erosion during the off-normal event such as the plasma disruption, the JEBIS can deliver intense electron beam which can simulate a heat load onto the surface of PFCs during plasma disruption. Japan - European Community collaborative experiments has also been performed in the JEBIS and JUDITH at KfA in Germany.

6.2 Activities on divertor plate development

Developing efforts on the divertor plate for ITER have experimentally been made in PBEF and JEBIS. The divertor plate is subjected to heat fluxes of 15 to 30 MW/m². Carbon based materials are primary candidate of the armor tiles in the physics phase of ITER, and metal armor materials are proposed in the technology phase. One of the key technologies for developing the divertor plate is the joining technique of the armor tiles to the metal cooling structure. To evaluate joining properties, three types of the divertor mock-ups have been fabricated and tested. Based on their results, 1 m long divertor mock-ups have been designed and fabricated. Heat removal experiments of various types of the cooling structures have also been performed for the design of the divertor plate.

6.2.1 Thermal cycling experiments on divertor mock-ups

The thermal cycling experiments of monoblock and saddle type divertor mock-ups have been performed in JEBIS. Figure V.6.2.1-1 shows cross sectional views of both of the divertor mock-ups tested. The saddle type has an advantage on having a possibility of in-situ repair of the armor tile compared with that of the monoblock type. Tubes with a twisted tape insert are applied to the cooling tubes because of its superior heat transfer properties.

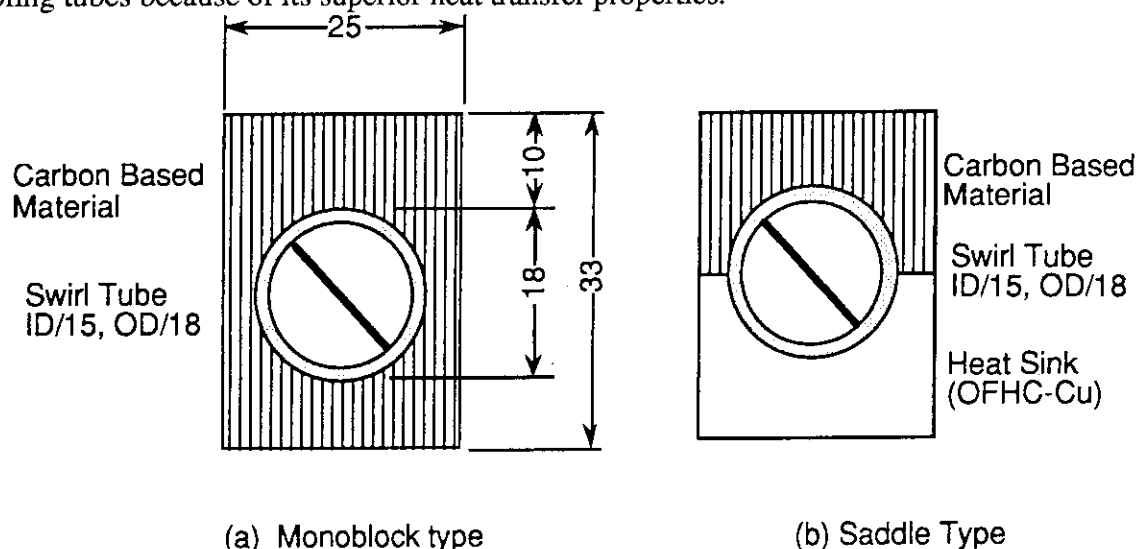


Fig. V.6.2.1-1 Cross Sectional Views of the Divertor Mock-ups

The monoblock type divertor mock-ups are tested at heating conditions of 15 MW/m^2 for 20 to 50 s, which is longer enough than the thermal constant of the divertor mock-up. After 1000 thermal cycles, no cracks and no fatal damages are found in the CFC/OFHC-Cu bonding structures [6.2-1]. Furthermore, the saddle type divertor mock-up has endured 20 MW/m^2 with 20 to 50 s for more than 1000 thermal cycles without temperature increase of the armor surface.

To evaluate effects of sweeping heat loads on the divertor plate in ITER, JEBIS has been trying a simulation of the sweeping heat loads and can successfully operate a sweeping condition in which sweeping frequency and sweeping distance are up to 1.0 Hz and $\pm 10 \text{ cm}$ at a peak heat flux of 30 MW/m^2 [6.2-2].

6.2.2 Thermo-hydraulics of the cooling structures [6.2-3]

From thermo-hydraulics point of view, it is very important to predict the critical heat flux (CHF) with the highly subcooled flow and the CHF margin of the cooling structure for the divertor plate. Though one side of the divertor plate is exposed to tokamak plasma, no CHF correlations and few CHF data are available for the prediction of CHF under one-sided heating condition. For this purpose, CHF experiments of various types of the tubes have been performed in PBEF. Figure V.6.2.2-1 summarizes incident CHF values of various types of the cooling

1. Straight and Smooth Tube for reference



CHF: 19.3

CHF unit : MW/m²

2. Outer Diameter Dependence



CHF: 21.5



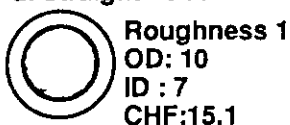
CHF: 19.3



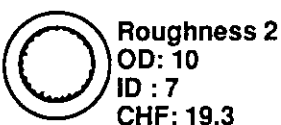
CHF: -

3. Dependence of Inner Wall Roughness

a. Straight Tube



CHF: 15.1



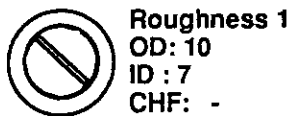
CHF: 19.3



CHF: 21.0

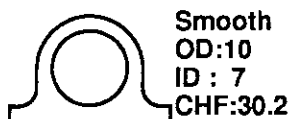
b. Swirl Tube (tape twist ratio $y=2.5$)

CHF: 27.0

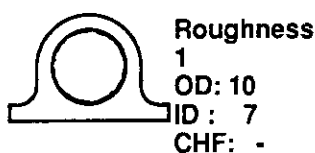


CHF: -

c. Externally-Finned Tube (external fin width = 15 mm)



CHF: 30.2



CHF: -



CHF: -

d. Externally-Finned Swirl Tube (tape twist ratio $y=2.5$, external fin width = 15 mm)

CHF: 38.5



CHF: -



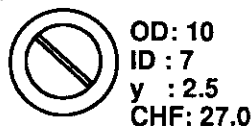
CHF: -



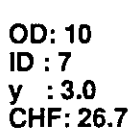
CHF: -

4. Dependence of Tape Twist Ratio

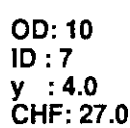
a. Swirl Tube



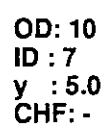
CHF: 27.0



CHF: 26.7



CHF: 27.0

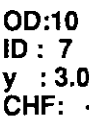


CHF: -

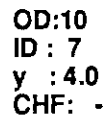
b. Externally-Finned Swirl Tube



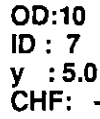
CHF: 38.5



CHF: -



CHF: -



CHF: -

Figure V.6.2.2-1 Incident CHF Values of Various Types of the Cooling Structures
In the figure, CHF value is defined at the tube outer surface, because of one side heating condition.

tubes under the cooling condition for the flow velocity of 10 m/s with the inlet pressure of around 0.9 MPa. In particular, tubes with a twisted tape insert have higher CHF values.

Experimental data which were obtained under one sided heating condition have been evaluated by various existing CHF correlations which are based on a condition for uniform circumferential heating. Experimental CHF data of the straight tube show relatively good agreement with some correlations within an accuracy of -20 to +10 %, but no correlations are available in the CHF prediction of the other types of the cooling structures. Further experiments are necessary to evaluate the applicability of the existing CHF correlations under the condition for one side heating.

References

- [6.2-1] S. Suzuki, *et al.*, *Fusion Technol.*, **21** (1992) 1858.
- [6.2-2] M. Araki, *et al.*, to be published to the 17th Symp. on Fusion Technol.
- [6.2-3] M. Araki, *et al.*, *Fusion Technol.*, **21** (1992) 1835.

6.3 Development of a first wall

The first wall is subjected to heat fluxes of 0.2 to 0.6 MW/m². The radiatively cooled first wall is used in high heat flux area (0.6 MW/m²) such as NB armor plates, and conductively cooled first wall is used in low heat flux area (0.2 MW/m²). The attachment structure of the radiatively cooled first wall was improved and thermal tests were carried out at 0.6 MW/m² in JEBIS. Problems such as loose of the bolts was not observed.

6.4 Study of plasma surface interaction

Erosion of divertor plates has mainly caused by plasma particles from the scrape off layer and by disruptive heat load. The effect of non-uniform magnetic field was investigated in order to control the scrape off layer plasma. Experimental data qualitatively corresponded with the theoretical results[6.4-1]. High density plasma production was tried for measurement of erosion yield of PFC materials such as C/C composites, and the hydrogen plasma density of 7×10^{13} ions/cm³ was obtained in small volume. Hydrogen ion beam device (MSP) for sputtering yield measurement was improved, and hydrogen ion beam of 1 keV, 20 mA was obtained.

High heat flux experiments (5-40 MW/m², 5 s and 550 MW/m², 5-10 ms) in JEBIS have been carried out on three kinds (convesion, CVD and plasma spray methods) of B₄C-overlaid C/C composites, on which B₄C is overlaid with thickness of 100-250 μ m. It turned out that the conversion method is the best of the three methods applied in the present tests, because no exfoliation has occurred even under the simulated disruptive heat load.[6.4-2]

Under Japan-EC collaboration, disruptive heat load, up to 2000 MW/m², experiments were carried out on carbon based materials and tungsten in JEBIS. No cracks occur at high temperature region in tungsten.

References

- [6.4-1] S. Tanaka, et al., to be published to J. Nucl. Mater.
- [6.4-2] K. Nakamura, et al., to be published to J. Nucl. Mater.

7. Reactor Structure Development

7.1 Introduction

The reactor structure of tokamak machine is composed of plasma vacuum vessel, tritium breeding blanket, divertor system and vacuum chamber for superconducting magnet system. As to the next generation machine, the reactor structure components would be inevitably large scaled sizes and massive. The major task of the reactor structure R&D is to establish the manufacturing technology and the remote assembling/disassembling technology.

7.2 R&D activities for reactor structure

The vacuum vessel is a key containment structure to provide the first barrier of tritium. In addition, the vacuum vessel has to provide one-turn toroidal resistance and nuclear shielding functions, and should be sufficiently tough against the electromagnetic loads. The double walled structure reinforced by the toroidal and poloidal ribs, and the toroidally uniform resistance were employed as the most promising concept. The 1m x 1m sized segments with a total wall height of 300 mm and a wall thickness of 20 mm have been fabricated and tested under the internal pressure, in-plane shear, compression and bending loads. The test results show that the fabrication error due to welding can be controllable and that the double wall structure has sufficient mechanical toughness as well as large margin for plastic yield load.

A hydro-driven cotter system was selected and designed as the locking mechanism for supporting in-vessel replaceable components. Two different types of the cotter driver have been developed, namely piston/cylinder type for the divertor support and metallic balloon (dilatation tube) type for the blanket support. The cotter driving metallic balloon with a flat race-track cross section has been fabricated successfully by using super plasticity process, and its driving capabilities of more than several tens ton/m has been examined. The titanium alloy (Ti-6Al-4V) has been selected for the metallic balloon material because it has excellent super plasticity at elevated temperature and because of its high specific strength. The single-layered and triple-layered balloons were formed. Since the triple-layered balloon reduces bending stress which is induced during loading, reliability as well as driving force has been improved than the single-layered balloon. On the other hand, the piston/cylinder type with a long stroke (170 mm) has also been fabricated with particular attention to the selection of material combination for pressure ring and its guide. The cotter itself has survived 1000 operation cycles without any adhesive and

References

- [6.4-1] S. Tanaka, et al., to be published to J. Nucl. Mater.
- [6.4-2] K. Nakamura, et al., to be published to J. Nucl. Mater.

7. Reactor Structure Development

7.1 Introduction

The reactor structure of tokamak machine is composed of plasma vacuum vessel, tritium breeding blanket, divertor system and vacuum chamber for superconducting magnet system. As to the next generation machine, the reactor structure components would be inevitably large scaled sizes and massive. The major task of the reactor structure R&D is to establish the manufacturing technology and the remote assembling/disassembling technology.

7.2 R&D activities for reactor structure

The vacuum vessel is a key containment structure to provide the first barrier of tritium. In addition, the vacuum vessel has to provide one-turn toroidal resistance and nuclear shielding functions, and should be sufficiently tough against the electromagnetic loads. The double walled structure reinforced by the toroidal and poloidal ribs, and the toroidally uniform resistance were employed as the most promising concept. The 1m x 1m sized segments with a total wall height of 300 mm and a wall thickness of 20 mm have been fabricated and tested under the internal pressure, in-plane shear, compression and bending loads. The test results show that the fabrication error due to welding can be controllable and that the double wall structure has sufficient mechanical toughness as well as large margin for plastic yield load.

A hydro-driven cotter system was selected and designed as the locking mechanism for supporting in-vessel replaceable components. Two different types of the cotter driver have been developed, namely piston/cylinder type for the divertor support and metallic balloon (dilatation tube) type for the blanket support. The cotter driving metallic balloon with a flat race-track cross section has been fabricated successfully by using super plasticity process, and its driving capabilities of more than several tens ton/m has been examined. The titanium alloy (Ti-6Al-4V) has been selected for the metallic balloon material because it has excellent super plasticity at elevated temperature and because of its high specific strength. The single-layered and triple-layered balloons were formed. Since the triple-layered balloon reduces bending stress which is induced during loading, reliability as well as driving force has been improved than the single-layered balloon. On the other hand, the piston/cylinder type with a long stroke (170 mm) has also been fabricated with particular attention to the selection of material combination for pressure ring and its guide. The cotter itself has survived 1000 operation cycles without any adhesive and

abrasive wear on the cotter surface. Furthermore, full scaled divertor support structure has been fabricated as shown in Fig.V.7.2-1.

7.3 R&D activities for remote maintenance

From viewpoint of maintenance scheme, all the reactor components are classified into three categories: scheduled maintenance components, unscheduled maintenance components and permanent components. The classification and the maintenance concept have been developed.

The in-vessel vehicle system was selected for the scheduled maintenance components such as plasma facing components. In the rail-mounted vehicle maintenance system, the rail is expanded sequentially and supported by four arms from the respective 90-degree horizontal ports so as to provide stable and reliable operation. The half torus model of the rail-mounted vehicle system in one fifth scale was manufactured, and the basic tests of the rail mounting and the divertor plate substitution has been successfully carried out. As the next step, the full scaled vehicle with end effector (handling manipulator) has been manufactured as shown in Fig.V.7.3-1. The full scaled divertor assembling test shall be carried out by using this apparatus and the above mentioned full scaled divertor support structure shown in Fig.V.7.2-1.

The typical unscheduled maintenance component, the tritium breeding blanket is the largest (15 m) and the heaviest (80 ton) among the in-vessel components. The cask-type twin manipulator system with double seal door was employed for replacing the blanket module through the narrow upper port. The design concept of the blanket handling was developed and a one fifth

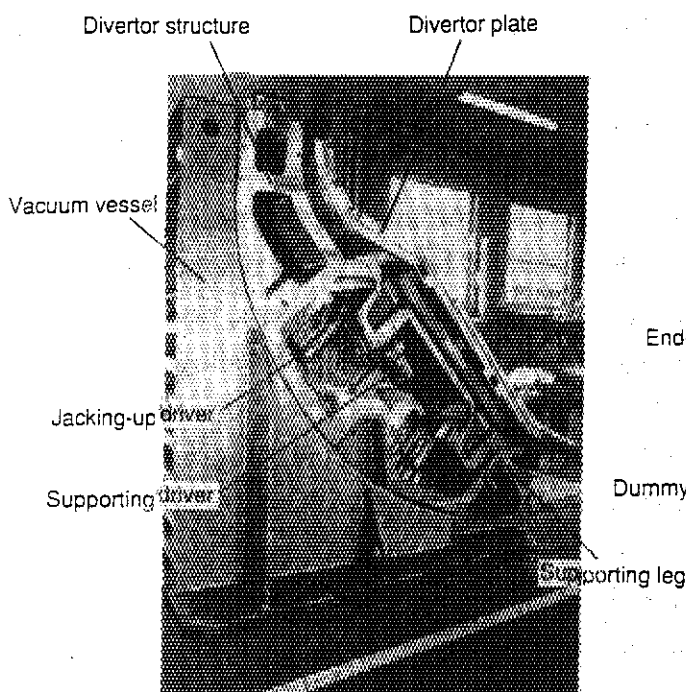


Fig.V.7.2-1 Full scaled model of divertor support structure system

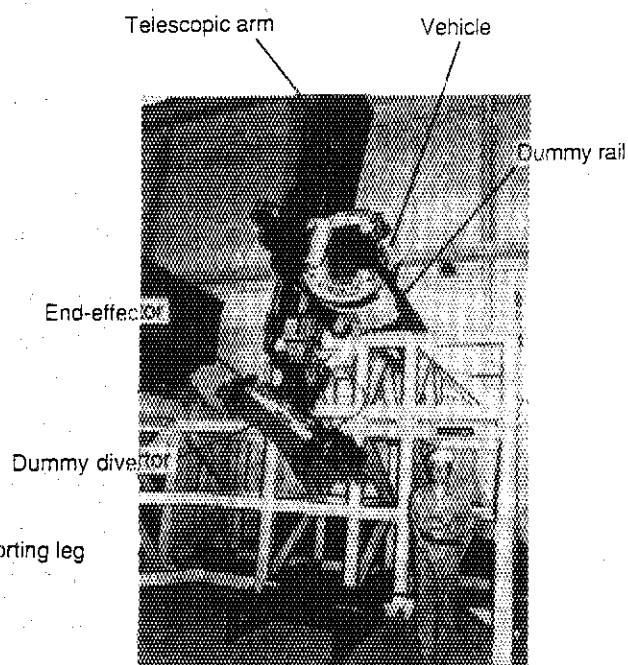


Fig.V.7.3-1 Full scaled model of divertor handling vehicle

scale model was fabricated and tested. The major results are (i) The blanket handling in the narrow space has been successfully demonstrated with computer posture control by twin manipulator system., and (ii) Feasibility of slide and seal/lock mechanisms of the double seal door has been established.

As the widely common technology, the welding and cutting procedures for the cooling pipes of the in-vessel replaceable components should be established. The internal-access concept for welding/cutting pipes was employed because of the pipes being in close order. The welding /cutting head with CO₂ laser beam, which consists in a vehicle mounted with a traveling mechanism along the pipe and a focusing lens, has been manufactured and applied to 200A(Sch40) SUS pipe. The feasibility of this concept has been demonstrated.

8. Blanket Technology

8.1 Introduction

Blanket is a component which generates tritium, fuel gas of thermonuclear reaction, and to change kinetic energy of neutrons to thermal energy, and is one of the key components for energy producing fusion reactors. In ITER, the blanket is scheduled to be installed from the beginning of its operation and is utilized mainly for tritium production.

During ITER/EDA, a variety of R&Ds are to be developed so as to establish fabrication technology of blanket modules and to evaluate their performances under the anticipated ITER operation conditions. These R&Ds are categorized into four groups; material development, box structure development, out-of-reactor tests and in-reactor tests.

Material development covers development of fabrication technology of breeding and multiplier materials, and irradiation and non-irradiation tests of these materials. Box structure development aims at development of fabrication technology of the blanket box structure and its thermo-mechanical tests. Out-of-reactor and in-reactor tests are to be developed to evaluate performances of blanket modules under non-nuclear and nuclear environments, respectively.

In this fiscal year preliminary R&Ds have been developed on material developments and out-of-reactor tests. Much efforts have been made on design works of ITER driver blanket and test modules for in-reactor tests. For in-reactor tests JMTR is scheduled to be utilized for functional tests and Russian reactors for lifetime tests.

8.2 Material-Related R&D

Experimental works related to material tests have been performed on the thermo-mechanical durability and material compatibility using industrially-produced microspheres of breeder (lithium ceramics) and multiplier (Be).

scale model was fabricated and tested. The major results are (i) The blanket handling in the narrow space has been successfully demonstrated with computer posture control by twin manipulator system., and (ii) Feasibility of slide and seal/lock mechanisms of the double seal door has been established.

As the widely common technology, the welding and cutting procedures for the cooling pipes of the in-vessel replaceable components should be established. The internal-access concept for welding/cutting pipes was employed because of the pipes being in close order. The welding /cutting head with CO₂ laser beam, which consists in a vehicle mounted with a traveling mechanism along the pipe and a focusing lens, has been manufactured and applied to 200A(Sch40) SUS pipe. The feasibility of this concept has been demonstrated.

8. Blanket Technology

8.1 Introduction

Blanket is a component which generates tritium, fuel gas of thermonuclear reaction, and to change kinetic energy of neutrons to thermal energy, and is one of the key components for energy producing fusion reactors. In ITER, the blanket is scheduled to be installed from the beginning of its operation and is utilized mainly for tritium production.

During ITER/EDA, a variety of R&Ds are to be developed so as to establish fabrication technology of blanket modules and to evaluate their performances under the anticipated ITER operation conditions. These R&Ds are categorized into four groups; material development, box structure development, out-of-reactor tests and in-reactor tests.

Material development covers development of fabrication technology of breeding and multiplier materials, and irradiation and non-irradiation tests of these materials. Box structure development aims at development of fabrication technology of the blanket box structure and its thermo-mechanical tests. Out-of-reactor and in-reactor tests are to be developed to evaluate performances of blanket modules under non-nuclear and nuclear environments, respectively.

In this fiscal year preliminary R&Ds have been developed on material developments and out-of-reactor tests. Much efforts have been made on design works of ITER driver blanket and test modules for in-reactor tests. For in-reactor tests JMTR is scheduled to be utilized for functional tests and Russian reactors for lifetime tests.

8.2 Material-Related R&D

Experimental works related to material tests have been performed on the thermo-mechanical durability and material compatibility using industrially-produced microspheres of breeder (lithium ceramics) and multiplier (Be).

8.2.1 Thermo-mechanical durability

To validate thermal cycle durability of the Be spheres, thermal cycling test was conducted under the conditions of temperature range of 200-700°C, 5-minute interval on each cycle and up to the number of 1000 cycles. Cracks were observed in some of the spheres which were exposed over 10 cyclic operations [8.2-1] as shown in Fig.V.8.2-1. In order to prevent crack formation, improvement of current fabrication technology and further examination may be required.

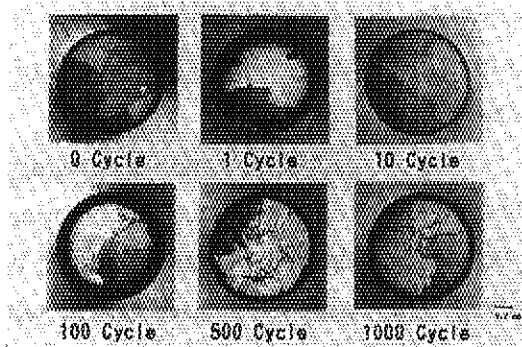


Fig V.8.2-1 Photographs of Be Sphere after heat cycle

8.2.2 Material Compatibility

It is a critical issue for the multi-layered pebble bed blanket design to clarify the material interaction phenomena such as compatibility among the materials composing the blanket under the real blanket environment.

8.2.2.1 Test between Lithium Ceramics and Austenitic Stainless Steel [8.2-2]

Compatibility test among lithium ceramics (Li_2O , Li_4SiO_4 , Li_2ZrO_3) and austenitic stainless steel (316SS, PCA(Primary Candidate Alloy)) has been carried out under the following conditions; temperature range between 350°C and 750°C, exposure time of 150 and 500 hours, moisture content of 1, 200 and 2000 vppm in the helium gas. After the reaction test for compatibility, several specimens of austenitic stainless steel were examined in terms of tensile strength and elongation at the room temperature.

In the case of Li_2O and 316SS, compatibility is good enough under the conditions of temperature below 550°C and moisture content below 200 vppm in He. This is interpreted as attribution of the formation of LiCrO_2 protective layer. Under the conditions of temperature above 550°C and moisture content of 2000 vppm in He, the modified 316SS(PCA) reacted more with Li_2O forming double layers of Li_5FeO_4 and LiCrO_2 . Elongation of PCA under the moisture content of 2000 vppm decreased more steeply than the case of 200 vppm moisture. It was confirmed that Li_4SiO_4 and Li_2ZrO_3 have less reactivity with PCA than the Li_2O under the

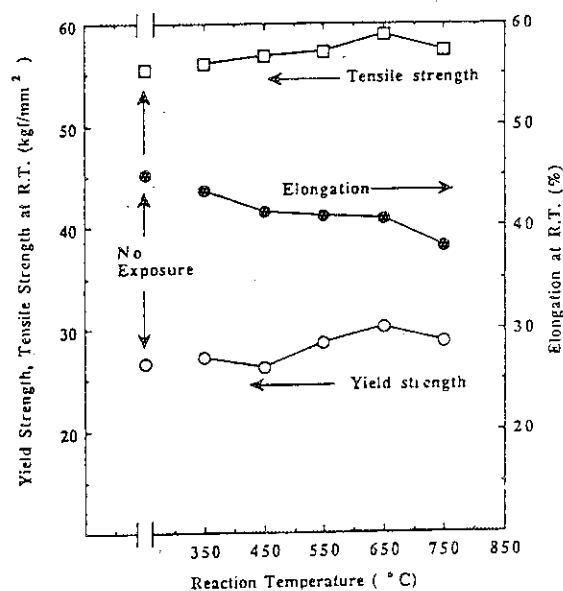


Fig.V.8.2-2 Temperature dependence of mechanical properties of PCA with H_2O

representative conditions.

Especially, Li_2ZrO_3 showed no reaction with PCA under the examined conditions.

As shown in Fig.V.8.2-2, mechanical strength of PCA was not degraded severely by co-existence of Li_2O and moisture (200 vppm) under the test temperatures examined. Although elongation slightly decreased with temperature increase, this tendency was similar with that in the case of no contact with Li_2O . It was proved that Li_2O and other ceramics does not induce severe degradation of mechanical strength of austenitic stainless steel under the conditions of this examination.

8.2.2.2 Test between Beryllium and Austenitic Stainless Steel [8.2-3]

The compatibility of beryllium with austenitic stainless steel (316SS, 316L) was studied at the temperature between 400°C and 700°C for the period up to 6000 hours. Noticeable interaction between beryllium and the austenitic stainless steel was observed at temperatures higher than 600°C. The interaction is characterized by the double reaction layers formed by mutual diffusion of beryllium and elements of the stainless steel. The growth rate of the reaction zone was controlled by the beryllium diffusion.

The oxidation behavior of beryllium in the moist helium gas flow(partial pressure of water, 1kPa) was investigated at the temperature range between 550°C and 750°C by the continuous weight-gain measurement with the microbalance method.

The oxidation at the temperature below 550°C was protective, i.e., rate -decreasing with time, but at 600°C and above eventually breakaway oxidation occurred. From the temperature dependence of duration of the protective oxidation, it is expected that oxidation of beryllium will be protective over 10000 hours in the temperature range of 500°C and below which is adopted in the current breeding blanket design.

References

- [8.2-1] H. Yoshida, et al., JAERI-M 92-116 (1992)
- [8.2-2] H. Yoshida, et al., "Integrity and Compatibility study of Blanket Materials, Advance in Ceramics", Fabrications and Properties of Lithium Ceramics III.
- [8.2-3] H. Yoshida, et al., "Beryllium Compatibility in the Solid Blanket Concept", *ibid.*

8.3 Out-of reactor testing

Current Japanese breeding blanket concept for ITER consists of three breeder layers, nine multipliers and five cooling panels. The breeder layers and multiplier layers contain about 1mm diameter spheres of Li_2O and Be, respectively. In order to meet the design requirements of tritium release efficiency and material temperature restrictions, the configuration and dimensions of the blanket should be decided to achieve the optimum temperature profile in the radial direction. Thus,

basic data about pebble bed thermal conductivity, packing fraction and coolant water flow rate distribution are indispensable for reliable design of the blanket. On this view point, the following preliminary experiments were carried out this year prior to EDA.

- i) Cooling water distribution experiment
- ii) Pebble bed packing experiment
- iii) Pebble bed thermal conductivity experiment

Each experimental results are summarized as follows.

With respect to the cooling water distribution experiment [8.3-1], the experimental apparatus was fabricated so that three parallel test sections with orifices and pipes can be tested in the ITER condition (100 °C, 1.5 MPa maximum). The experimental values of pressure loss of test sections showed good agreement with the estimated values by Colebrook's equation.

With respect to the pebble bed packing experiment [8.3-2], 1/1 scale breeder layer canning models were fabricated and Al_2O_3 pebble packing experiments were performed. As the result, it was certified that the vibration of the canning was one of the candidate methods to get high packing fraction if the vibration condition was appropriately selected. Also, it was observed that the effective weight loaded on the bottom of the canning showed good agreement with the estimated value by Jannsen's equation, which was less than 1 % of the whole weight of the pebbles.

With respect to the pebble bed thermal conductivity experiment, real breeder material was used for the experiments. The experimental result of 1mm diameter Li_2O pebble bed is shown in Fig.V.8.3-1. In this figure, the estimated values by Yagi-Kunii's, Okazaki's and Schlunder's equations. Measured value was about 0.9 W/m.K and agreed to the estimation by Yagi-Kunii's equation.

References

- [8.3-1] H.Yoshida.et.al., JAERI-M.92-070.(1992).
- [8.3-2] M.Enoeda.et.al., JAERI-M.92-104.(1992).

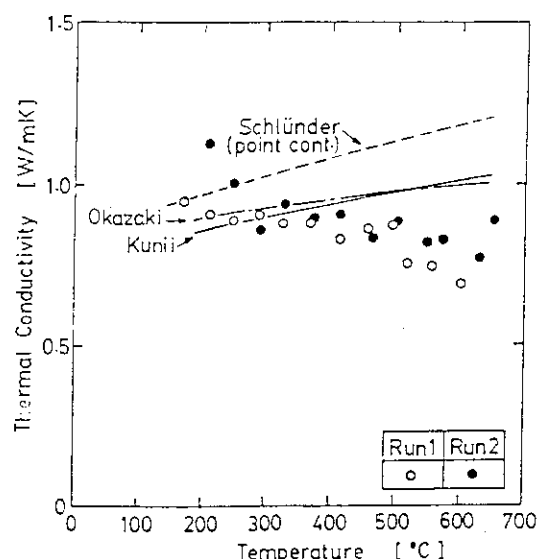


Fig V.8.3-1 Effective thermal conductivity of 1mm ϕ Li_2O sphere packed bed. (48% packing, stagnant He)

8.4 Design of tritium breeding blanket [8.4-1]

Design efforts were continued to refine the layered pebble bed blanket [8.4-2] proposed by Japanese team during ITER/CDA. Schematic drawing of the three breeder layer blanket is shown in Fig.V.8.4-1. Neutronics/thermal analyses were performed to investigate the optimal layered configuration. Since the ITER driver blanket is expected to be operated under various operation

modes, a series of thermal analyses were performed to define the allowable power variation from the normal condition and to investigate the transient temperature variation under the pulsed operation modes (i.e. $T_{\text{burn}}/T_{\text{dwell}} = 400/200$ s in the physics phase, and $= 2300/200$ s in the technology phase). Static and dynamic stress analyses were performed by the finite element method to clarify stress distribution and deformation of blanket box structure under the plasma also performed and necessity of some stiffening structure was indicated.

Blanket fabrication and assembly process is another important issue to realize large scale (over ten meter height) structure which requires a tolerance to order of millimeter. The present status of the two key fabrication technologies was examined ; joining method including hot isostatic pressing (HIP) and electron or laser beam welding ; pebble loading method which enables uniform and high density packing.

Design study of DEMO blanket was also performed. Research and development items required for DEMO blanket were clarified, keeping the DEMO reactor such as SSTR [8.4-3] in mind. Preliminary conceptual design of DEMO blanket test module to be installed in the ITER test port was performed and basic neutronics and thermal performances were evaluated.

References

- [8.4-1] H.Takatsu et al., to be published as JAERI-M (1992)
- [8.4-2] D.Smith.et.al., ITER Documentation Series, No.29, ITER Blanket, Shield and Material Data Base. IAEA (1991)
- [8.4-3] Y.Seki et al., JAERI-M 91-081 (1991)

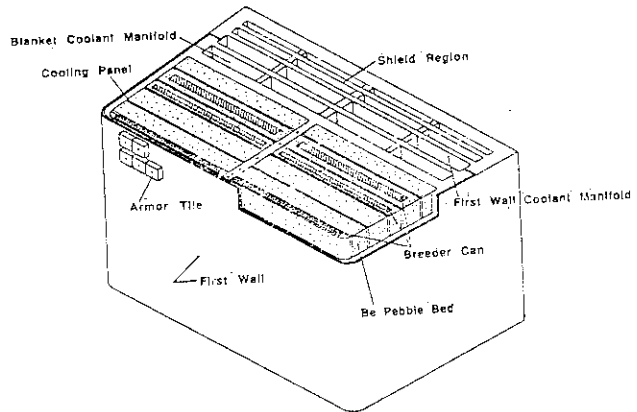


Fig V.8.4-1. Schematic view of layered pebble bed blanket

VI. NEXT STEP FOR JAERI TOKAMAK PROGRAM

1 International Thermonuclear Experimental Reactor (ITER)

1.1 Introduction

International Thermonuclear Experimental Reactor (ITER) was initiated at summit meetings of governmental leaders so as to develop an experimental fusion reactor through the united efforts. The overall programmatic objective of ITER is to demonstrate the scientific and technological feasibility of fusion energy.

In response to the summit initiatives, joint design work on ITER Conceptual Design Activities (CDA) under the auspice of the IAEA by four Parties, Japan, the United States, the Soviet Union and the European Community was conducted from April 1988 to December 1990. As a result, the feasible design concepts, the widest possible technical basis and the future R&D program were successfully developed. The four Parties agree to proceed the next step, Engineering Design Activities (EDA), which requires about 1200 professional man years for design and \$750M for technology R&D. Before starting EDA, Japanese scientific and technical review was finished.

1.2 ITER CDA review

The National Review Committee has conducted a technical review of the ITER Conceptual Design, pursuant to the charges given to the Committee by the Fusion Council.

The draft text of Agreement on Engineering Design Activities (EDA) for ITER specifies that technical objectives of ITER shall be reviewed internationally immediately after the start of the EDA on the basis of the Conceptual Design Report (CDR). It also specifies that the review results shall be submitted to the ITER Council within three months. Preparing for such an international review, the committee was set up under Fusion Council of Japan to conduct a national review of the ITER Conceptual Design.

The above text stipulates that "The overall programmatic objective of ITER is to demonstrate the scientific and technological feasibility of fusion energy. ITER would accomplish this objective, (1) by demonstrating controlled ignition and extended burn of deuterium-tritium plasmas, with steady state as an ultimate goal, (2) by demonstrating technologies essential to a reactor in an integrated system, and (3) by performing integrated testing of the high-heat-flux and nuclear components required to utilize fusion power for practical purposes"

The Committee was charged, based on the CDR, to review the detailed technical objectives along with technical approaches to determine the best practical way to achieve the programmatic objective of ITER. In particular, the following tasks were emphasized:

- (1) A review should be made on whether the results of the design described in the CDR are technically adequate to accomplish the overall programmatic objective of ITER. Specific ways for improvement, if any, should be identified.
- (2) Critical areas should be clarified where plasmas performances and reactor technology development anticipated in the CDR have high technical uncertainties. Ways to reduce these uncertainties should be identified. A review should be made on the flexibilities in the design which allow the introduction in the future of advanced of features and new possibilities and the improvement of plasma performances during operation. Specific ways for improvement, if any should be identified.
- (3) A review should be made on whether the operation and research programme described in the CDR are technically adequate to accomplish the overall programmatic objective of ITER. Specific ways for improvement, if any, should be identified.

The Committee had three meetings on Sept. 26, Oct. 23 and Nov. 29, and extensive discussions were held to determine the most practical approaches to meet the ITER programmatic objectives. The results and recommendations are summarized as follows:

1. The design described in the CDR is generally appropriate to accomplish the overall programmatic objectives of ITER. Regarding the choice of aspect ratio, a comparative study of the reactor types with a high and a low aspect ratio leads to a conclusion that the low aspect ratio adopted in the CDR should be chosen as reference.
The introduction of non-inductive current drive is judged appropriate for controlling disruptions and current profiles, to establish an extended burn in hybrid operation mode. It is also essential to the study of steady state operation with fully non-inductive current drive.
2. Areas where improvement could be made over the design described in the CDR and areas where effort should be made to reduce the existing uncertainties are identified. It is judged that the accomplishment of the overall programmatic objectives in ITER will be enhanced by taking proper action to overcome the issues in these areas.
 - (i) Staged operation programme is introduced to reduce risks due to uncertainties and incorporate new technologies developed during the operation in proper steps. The entire operation is divided into the first and the second phase each lasting for 8-9 years, redefining the corresponding physics phase (about 6 years) and the technology phase (about 12 years) described in the CDR. The first phase should be assigned not only to plasma physics research, but also to engineering testing under low neutron fluence.
 - (ii) Studies on extended burn of deuterium H-mode plasmas with low impurity concentration will be made in the first phase, preceded by simulated studies in the physics R&D. In particular, since plasma confinement and purity are significantly affected by the choice of

plasma facing materials, replacement of plasma facing components should be planned several times in the first phase.

- (iii) In order to establish the extended burn operation required in engineering testing, studies should be made on the frequency, impact, and control of disruptions in the first phase experiment with hydrogen and deuterium plasmas in ITER as well as in the physics R&D. Therefore, the full heating and current drive system should be installed at the beginning of the first phase. This is also important from the view point of achieving high availability in the second phase, i.e. 10% or a higher value.
- (iv) The steady state operation by fully non-inductive current drive at high fusion power should be studied in ITER. To meet the need in this operation, the design should be made flexible enough to allow change of divertor materials and modification of divertor structures, as needed, and an effective supplementary R&D should be implemented in this area as well.
- (v) Test of tritium breeding blankets under neutron irradiation should be made in the first phase for the reliability in their functions and structural strengths. It is appropriate then to proceed to the installation of full tritium breeding blankets, after evaluating the results obtained in the first phase, before the beginning of the second phase and to start full production of tritium.

Tests of nuclear components such as power-producing blankets are made under low neutron fluence in the first stage, and under high neutron fluence in the second phase. The minimum neutron fluence for the test is 0.7MWa/m^2 . During the later stage of the second phase a functional demonstration test of electric power generation should be made using the modules of power-producing blankets.

1.3 ITER Engineering Design Activities (EDA)

1.3.1 Physics R&D

The physics R&D program for the ITER Engineering Design Activity Phase has been established and, in many areas, R&D activity is being prepared to perform. The program covers all of the R&D needs to provide the design activity with the support for the optimization of the ITER design and eventually for the completion of the data base necessary for making the decision to start ITER construction. The program covers the following five areas and subdivided in 22 tasks, supplemented by subtasks, which are more specific database for ITER: 1) Power and particle exhaust physics, 2) Disruption control and operational limits, 3) Enhanced confinement, 4) Optimization of operational scenario and long-pulse operation, and 5) Physics of a burning plasma. The most crucial problems, to validate the ITER design concept and complete the physics data base required for starting ITER construction, in practical terms, are:

- 1) The development of active control method, in experiments prototypical for ITER, to demonstrate that a dense and cold divertor plasma ($T_e \leq 30\text{eV}$) is reliably formed, that the peak heat flux onto the divertor plate can be kept below about 10 MW/m^2 , and that helium exhaust conditions corresponding to a fractional burnup larger than several % with reasonable pumping speed can be ensured;
- 2) A characterization of disruptions which allows to specify their consequences for the plasma-facing components, and evidence that the number of disruptions to be expected allows an acceptable lifetime of these components;
- 3) The demonstration that steady-state operation in an enhanced confinement mode (in particular, in the ELMy H-mode) with satisfactory plasma purity is possible, and provision of the scaling of energy confinement for this mode which allows prediction of the performance of ITER with satisfactory accuracy;
- 4) Insurance that the presence of an appreciable population of fast ions does not jeopardize plasma performance in ITER.

Broad contributions to the program are proposed from JT-60U, JFT-2M and other facilities in Japan. The coverage of the program is generally satisfactory, while further efforts on the edge plasma in ITER-relevant divertor configurations and operating conditions are being enhanced.

1.3.2 Technology R&D

A wide range of the technology R&D is inevitably required to bridge from the present technology to the realization of ITER construction. A plan of long-term technology R&D for the period of the Engineering Design Activities(EDA) has been discussed and developed during the Conceptual Design Activities (CDA). The plan is focused on the R&D necessary to support a decision to be taken by the end of EDA to start ITER construction. In this plan, a wide range of international collaboration is expected to be maximized to best use the required resources and to minimize unnecessary duplication of effort.

The plan includes R&D for nine major systems of ITER; Superconducting Magnets, Containment Structures, Assembly & Maintenance, Current Drive and Heating, Plasma Facing Components, Blanket, Fuel Cycle, Structural Materials and Diagnostics. For each system, the R&D objectives, the tasks, the schedule and costs, and the needed facilities have been clarified.

It is suggested that all major testing programs can be conducted in existing facilities with some modifications, but a few new facilities may be required to conduct large scale model tests(scalable model tests) of center solenoid, toroidal field magnet, containment structure/assembly & maintenance, neutral beam, fuel cycle and blanket (in-pile and out-of-pile). These scalable model test facilities are to be built in a Party and used as an international common test facility in which several scalable models fabricated by Parties are tested together.

Based on the long-term technology R&D plan developed in CDA, the task sharing by four Parties will be discussed during the early phase of EDA and defined in the manner of equal contribution taking into account technological potential and interests. However, preliminary discussion on task sharing by four Parties has been made for the critical tasks, which are urgent and require a long lead time for the development, and the Parties agree to start immediately preparatory work for construction (or modification) of common test facilities and development of scalable models and their components listed below. These tasks will be worked out in the respective Task Agreements to be drawn up forthwith after the signing of Protocol 1.

- 1) Design of Central Solenoid Model Coil
- 2) Design of Toroidal Field Model Coil
- 3) Design of Central Solenoid Test Facility
- 4) Design of Toroidal Field Magnet Test Facility
- 5) Design of Neutral Beam Test Facility
- 6) Development and Test of Electrostatic Accelerator
- 7) Design of Electrostatic Quadrupole Accelerator
- 8) Development of Fabrication Methods for Ceramic Blanket Models
- 9) Design and Preparatory Work of In-Pile Blanket Test Facility
- 10) Fabrication and Testing of LiPb Blanket Channel
- 11) Critical Elements Study of Vacuum Vessel

2. Fusion Experimental Reactor(FER)

2.1. Role of FER and ITER[2.1-1]

The basic objectives of the next step large fusion device, which is an experimental reactor are to solve physics and technological issues and to supply data necessary to proceed to DEMO reactor without any further intermediate steps. The DEMO will demonstrate significant electric power generation steadily at a Q value of about 30, with a neutron wall load of about 3MW/m^2 and will be operated to a neutron fluence of the order of 10MWa/m^2 . Then the discussion will be on what is the acceptable range for the programmatic and technical objectives of the experimental reactor? For the past four years, the FER (Fusion Experimental Reactor) and ITER conceptual designs have been developed as realistic experimental reactor candidates to proceed to construction, the former in a domestic effort and the latter in four parties' international collaboration.

In 1990, the Fusion Council of Japan has set up a Review Committee on Technical Issues of Fusion Research and discussed and evaluated the technical designs of FER and ITER as well

Based on the long-term technology R&D plan developed in CDA, the task sharing by four Parties will be discussed during the early phase of EDA and defined in the manner of equal contribution taking into account technological potential and interests. However, preliminary discussion on task sharing by four Parties has been made for the critical tasks, which are urgent and require a long lead time for the development, and the Parties agree to start immediately preparatory work for construction (or modification) of common test facilities and development of scalable models and their components listed below. These tasks will be worked out in the respective Task Agreements to be drawn up forthwith after the signing of Protocol 1.

- 1) Design of Central Solenoid Model Coil
- 2) Design of Toroidal Field Model Coil
- 3) Design of Central Solenoid Test Facility
- 4) Design of Toroidal Field Magnet Test Facility
- 5) Design of Neutral Beam Test Facility
- 6) Development and Test of Electrostatic Accelerator
- 7) Design of Electrostatic Quadrupole Accelerator
- 8) Development of Fabrication Methods for Ceramic Blanket Models
- 9) Design and Preparatory Work of In-Pile Blanket Test Facility
- 10) Fabrication and Testing of LiPb Blanket Channel
- 11) Critical Elements Study of Vacuum Vessel

2. Fusion Experimental Reactor(FER)

2.1. Role of FER and ITER[2.1-1]

The basic objectives of the next step large fusion device, which is an experimental reactor are to solve physics and technological issues and to supply data necessary to proceed to DEMO reactor without any further intermediate steps. The DEMO will demonstrate significant electric power generation steadily at a Q value of about 30, with a neutron wall load of about 3MW/m^2 and will be operated to a neutron fluence of the order of 10MWa/m^2 . Then the discussion will be on what is the acceptable range for the programmatic and technical objectives of the experimental reactor? For the past four years, the FER (Fusion Experimental Reactor) and ITER conceptual designs have been developed as realistic experimental reactor candidates to proceed to construction, the former in a domestic effort and the latter in four parties' international collaboration.

In 1990, the Fusion Council of Japan has set up a Review Committee on Technical Issues of Fusion Research and discussed and evaluated the technical designs of FER and ITER as well

as their physics and technological bases which have been achieved in the past decade. The Council concluded that both FER and ITER designs are judged appropriate to meet the technical objectives of the next step in a long range Japanese fusion research program, and that these devices could surely be realized if adequate R&D efforts will be made.

Thus these two devices are judged to be within the acceptable range of the next step, but are characterized as follows :

- 1) The FER is to be the minimum-sized domestic device with the highest technical reliability in its construction.
- 2) The ITER is to be the maximum-sized international tokamak device with the maximum jump in the technology from the present level of achievement.

Major parameters of the two devices are compared in Table VI.2.1-1.

Table VI.2.1-1. Major parameters of FER and ITER

Item	FER	ITER
Fusion power	400 MW	1000 MW
Major radius	4.7 m	6.0 m
Minor radius	1.6 m	2.15 m
Vertical elongation, κ	2	2
Plasma volume	480 m ³	1100 m ³
Plasma current	15 MW	22 MW
Toroidal magnetic field	5.2 T	4.85 T
TF coil stored energy	23 GJ	40 GJ
Heating power	80 MW	120 MW
Annual tritium consumption	0.9 kg/y	5.5 kg/y
Cryostat structure	Concrete	Metal
Total weight of the reactor	15,000 ton	24,000 ton

From the technological point of view, no essential difference exist between these two devices except for a few points. One is an appreciable difference in size, typically characterized by the total weight of the tokamak reactor (15000 ton for the FER versus 24000 ton for the ITER), and the other is the absence of the tritium breeding blanket in the FER, since the FER intends to achieve the least minimum neutron fluence of 0.3-0.4MWa/m² to develop DEMO relevant blanket. Thus almost all the technologies essential to a power reactor can be demonstrated in an integrated system by either one of these devices.

From the physics point of view, as discussed in the reference[2.1-2], the FER design study shows that the FER will satisfy the high Q burning requirement ($Q \sim 20$ at the enhancement factor of 2 over the L-mode confinement, plasma current of 15MA), while it will be operated steadily by the non-inductive current drive at the same Q value of 5 and at the same plasma current of 15MA as ITER, since the FER design is optimized to maintain the important mission of the long burn, and the steady state operation required in the next step.

References

- [2.1-1] Shinzaburo Matsuda, "Status and Plans for Japanese FER/ITER Studies", Fusion Technology, Vol. 21, 1370, May 1992.
- [2.1-2] S.Matsuda et al, "Conceptual Design Study of the Fusion Experimental Reactor (FER)", Plasma Physics and Controlled Nuclear Fusion Research 1990., IAEA-CN-53/G-2-2, Thirteenth Conference Proceedings, Washington D.C. 1-6 October. 1990, published as Nuclear Fusion Supplement 1991, Vol. 3, 547.

2.2 FER Design

In 1991, the segmentation scheme of the FER blanket was investigated by using CAD(computer aided design). A new segmentation scheme was devised which enables the independent withdrawal of the inboard blanket without the withdrawal of the outboard blanket. Repair and maintenance scheme of the overall FER reactor facility was revised to be consistent with the reactor building design which is shown in Fig. VI.2.2-1. The reactor building design used the electrically insulated iron bars to prevent the corrosion due to the induced eddy current formation.

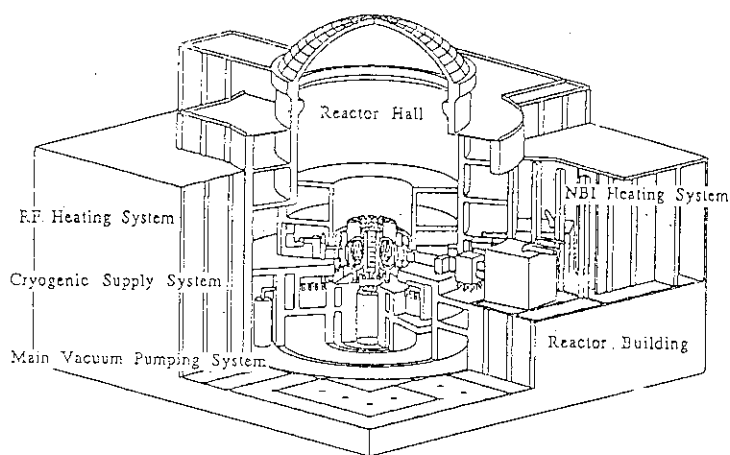


Fig. VI.2.2-1 Overview of the FER Reactor Building

In relation to the preparation for the siting of a fusion experimental reactor in Japan, safety and environmental aspects evaluations as well as the safety system design were carried out. The radwaste processing building size was estimated and its place in the plant layout was designed.

3. Fusion Reactor Design

3.1 Introduction

Fusion reactor design and related activities are conducted to clarify the goal of fusion research, i. e. attractive reactor concepts in terms of safety, environmental and economic aspects. The basic concept of the Steady State Tokamak Reactor, SSTR[3.1-1] which was developed in 1990 as a realistic reactor concept, has been improved this fiscal year, to have better environmental, safety and economic characteristics.

References

- [2.1-1] Shinzaburo Matsuda, "Status and Plans for Japanese FER/ITER Studies", Fusion Technology, Vol. 21, 1370, May 1992.
- [2.1-2] S.Matsuda et al, "Conceptual Design Study of the Fusion Experimental Reactor (FER)", Plasma Physics and Controlled Nuclear Fusion Research 1990., IAEA-CN-53/G-2-2, Thirteenth Conference Proceedings, Washington D.C. 1-6 October. 1990, published as Nuclear Fusion Supplement 1991, Vol. 3, 547.

2.2 FER Design

In 1991, the segmentation scheme of the FER blanket was investigated by using CAD(computer aided design). A new segmentation scheme was devised which enables the independent withdrawal of the inboard blanket without the withdrawal of the outboard blanket. Repair and maintenance scheme of the overall FER reactor facility was revised to be consistent with the reactor building design which is shown in Fig. VI.2.2-1. The reactor building design used the electrically insulated iron bars to prevent the corrosion due to the induced eddy current formation.

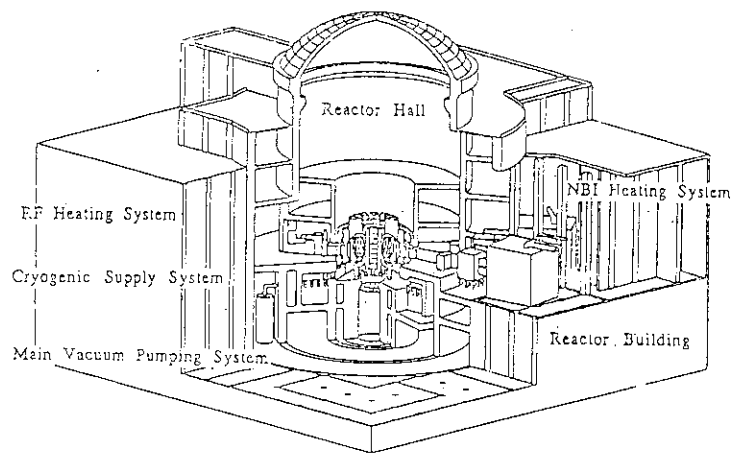


Fig. VI.2.2-1 Overview of the FER Reactor Building

In relation to the preparation for the siting of a fusion experimental reactor in Japan, safety and environmental aspects evaluations as well as the safety system design were carried out. The radwaste processing building size was estimated and its place in the plant layout was designed.

3. Fusion Reactor Design

3.1 Introduction

Fusion reactor design and related activities are conducted to clarify the goal of fusion research, i. e. attractive reactor concepts in terms of safety, environmental and economic aspects. The basic concept of the Steady State Tokamak Reactor, SSTR[3.1-1] which was developed in 1990 as a realistic reactor concept, has been improved this fiscal year, to have better environmental, safety and economic characteristics.

References

- [3.1-1] Y. Seki, M. Kikuchi et al, "The Steady State Tokamak Reactor", Plasma Physics and Controlled Nuclear Fusion Research 1990., IAEA-CN-53/G-I-2, Thirteenth Conference Proceedings, Washington D.C. 1-6 October, 1990, published as Nuclear Fusion Supplement 1991, Vol. 3, 473.

3.2 Steady State Tokamak Reactor(SSTR) Design

The SSTR improved concept which has higher safety and economic characteristics is called the SSTR-2 design. The improvement is being achieved by employing helium cooled plasma facing components and solid breeder blanket made of Ti-Al alloy as shown in Fig. VI.3.2-1.

Improved safety aspects of helium cooling compared with the water cooling are no pressure rise due to coolant phase change and minimal chemical reactions. The higher net thermal efficiency of about 40% will be achieved. In order to improve heat transfer capability, fine particles ($\sim 50\mu\text{m}$ diameter) of SiC are introduced in the helium primary coolant. The divertor plate is also cooled by solid-gas mixture coolant impinged at the back of the striking point to increase thermal capacity and to improve the heat transfer capability.

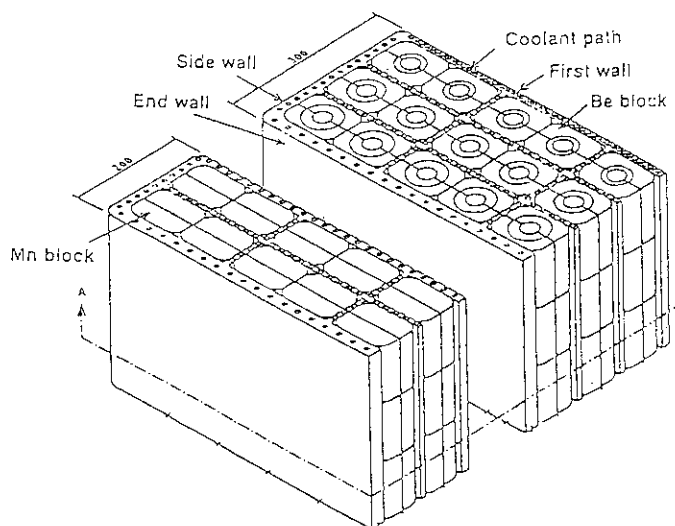


Fig. VI.3.2-1 Solid particulate suspended helium cooled SSTR-2 blanket made of titanium aluminide

In place of the low activation F82H ferritic steel, Ti-Al metallic compound (titanium aluminide) is used as the main structural material for plasma facing components and blanket. Ti-Al is selected for high temperature strength and reduced activation at 10 years after irradiation.

Helium cooling and Ti-Al structure resulted in a relatively high tritium breeding ratio which enables minimal use of beryllium which will result in less tritium inventory.

The future prospect of fusion power reactors is shown in Table VI.3.2-1. By the extrapolation from ITER and SSTR, the reduction of tritium and activation products inventory could be expected if the components development and materials development are achieved as expected. Safety characteristics are improved by the use of helium coolant in place of water. Furthermore the improved thermal efficiency will result in reduced thermal pollution.

References

- [3.2-1] S. Mori et al., "Solid Particulate Cooled Blanket for SSTR", Fusion Technology, Vol. 21, 1748, May 1992.

Table VI.3.2-1. Comparison of safety and environmental parameters for ITER, SSTR and SSTR-2

Item	ITER	SSTR	SSTR-2
Fusion power	1 GW	3 GW	4.5 GW*
Tritium inventory	6 kg	5 kg	3 kg*
Activation product inventory	$\sim 10^9$ Ci, SS-316	$< 10^9$ Ci, Reduced activation steel	$<< 10^9$ Ci, Ti-Al, SiC
Primary coolant	Water	Water	Helium
Coolant inlet/outlet temperature	60°C~100°C	285°C/325°C	400°C/700°C
Thermal efficiency	-	~30%	~40%

* Target value.

3.3 Safety Analyses

A comprehensive safety evaluation methodology[3.3-1] which aims to identify and to quantitatively estimate the dominant risks for designing safe fusion reactor plant was devised and a code development was continued.

It is programmed to be executable on an engineering work station (EWS) and simplified as much as possible to attain quick response. Utilizing the capability of EWS, the fusion reactor model is shown in layers so as to accurately depict the details of the model as required. In addition the code can provide clear show the calculated plant conditions such as tritium leakage map using a graphic display system. As a result, an extensive design options can be studied to find a rational fusion reactor concept with respect to safety.

References

- [3.3-1] M. Yamauchi, S. Kobayashi, Y. Seki and F. Kasahara, "Comprehensive Safety Evaluation Methodology for Fusion Reactor", Fusion Technology, Vol. 21, 2058, May 1992.

APPENDICES

A.1 Publication List (April 1991 - March 1992)

A.1.1 List of JAERI-M report

- 1) Nagashima K. and Sakasai A., "Numerical Analysis of Gas Puff Modulation Experiment on JT-60", JAERI-M 92-057.
- 2) Nagashima K. and Fukuda T., "Experimental Evidence of Off-diagonal Transport Term and the Discrepancy Between Energy/Particle Balance and Perturbation", JAERI-M 91-208.
- 3) Shimizu K., Shimada M., Takizuka T., "Simple Divertor Model for Transport Analysis Based on Experimental Data", JAERI-M 91-161.
- 4) Kubo H., "Spectroscopic Studies in JT-60", JAERI-M 91-135.
- 5) Hamamatsu K., Fukuyama A. and Azumi M., "Enhancement of Fusion Output by High Energy Ions during Additional Heating", JAERI-M 91-156.
- 6) Hirayama T., Sugie T., Sakasai A., et al., "Neoclassical Transport Analysis of Titanium Impurity in Plasmas with Strongly Peaked Density Profiles", JAERI-M 91-169.
- 7) Tsuji S., Hosogane N., K. Itami K., et al., "Improved Divertor Confinement Observed in JT-60", JAERI-M 91-195.
- 8) Tsuji S., Neyatani Y., Hosogane N., et al., "Diamagnetic Measurements in JT-60/JT-60U", JAERI-M 91-196.
- 9) Nishitani T., Takeuchi H., Barnes C.W., et al., "Absolute Calibration of the Neutron Yield Measurement on JT-60 Upgrade", JAERI-M 91-176.
- 10) Kardaun O., Miura Y., Matsuda T., et al., "Introduction to SAS on VAX", JAERI-M 91-098.
- 11) Tamai H., Mori M., Shoji T., et al., "Observation on effect of ergodic magnetic limiter for an ohmic heating plasma on JFT-2M tokamak", JAERI-M 91-110.
- 12) Miura Y., Mori M., Matsuda T., et al., "Figure Output Program for JFT-2M Experimental Data", JAERI-M 91-190.
- 13) Yamauchi T., Dimock D., Tolnas E., et al., "The JFT-2M TV Thomson Scattering System", JAERI-M 03-409.
- 14) Matsukawa M., Hosogane N., Ninomiya H., "JT-60U Configuration Parameters for Feedback Control Determined by Regression Analysis", JAERI-M 91-206.
- 15) Kurihara K. and Kimura T., "Tokamak Plasma Shape Identification Based on the Boundary Integral Equations", JAERI-M 92-075 (1992) (in Japanese).
- 16) Kawai M., "Modifications of the JT-60 NBI Magnetic System for the JT-60U", JAERI-M 91-223 (in Japanese).
- 17) Uehara K., Nagashima T., Ikeda Y., et al., "Conceptual Design of Fusion Experimental Reactor(FER/ITER)-Lower Hybrid Wave System", JAERI-M 91-182.
- 18) Yamamoto T., Tuneoka M., Sakamoto K., et al., "Conceptual Design of Fusion Experimental Reactor(FER/ITER)-Electron Cyclotron Wave System-", JAERI-M 91-194.
- 19) Fujii T., "Review of ICRF antenna Development and Heating Experiments up to Advanced Experiment I, 1989 on the JT-60 Tokamak", JAERI-M 92-037.
- 20) Yoshida K., Hasegawa M., Okuno K., et al., "Conceptual Design of SC Magnet System for ITER(I)", JAERI-M 91-120.
- 21) Koisumi K., Hasegawa M. and Yoshida K., "Conceptual Design of SC Magnet System for ITER(II)", JAERI-M 91-121.
- 22) Hasegawa M., Okuno K., Takahashi Y., et al., "Conceptual Design of SC Magnet System for ITER (III)", JAERI-M 91-122.
- 23) Kato T., Yoshida K., Hiue H., et al., "Conceptual Design of SC Magnet System for ITER (IV) -Power Supply and Cryogenic System-", JAERI-M 91-123.
- 24) Nakajima H., Nishi M., Egusa S., et al., "Conceptual Design of SC Magnet System for ITER (V) -Material-", JAERI-M 91-124.
- 25) Yoshida K., Sugimoto M., and Tsuji H., et al., "Conceptual Design of SC Magnet System for ITER(VI) -R&D Proposals-", JAERI-M 91-125.
- 26) Joseph R. ARMSTRONG, "Experimental Investigation of Cooling Perimeter and Disturbance Length Effect on Stability of Nb₃Sn Cable-in-Conduit conductors", JAERI-M 92-013.
- 27) Okumura Y., Watanabe K., "Design of a High Brightness Ion Source for the Basic Technology Accelerator(BTA)", JAERI-M 92-024.
- 28) Suzuki S., Akiba M., Araki M., et al., "Electron Beam Irradiation Experiments of First Wall Mock-Ups for Fusion Experimental Reactors (I)", JAERI-M 91-085.

- 29) Sakamoto K., Macbara S., Watanabe A. et al., "Initial Experiment of Focusing Wiggler of millimeter Wave free electron laser on LAX-1", JAERI-M 91-036.
- 30) Saigusa M. "Evaluation of Mode purity of ordinary and extraordinary modes by fixed elliptically polarized wave for ECH and ECCD", JAERI-M 91-131.
- 31) Kimura H., Saigusa M. et al., "Conceptual Design of Fusion Experimental Reactor (FER/ITER) - Ion cyclotron Wave System", JAERI-M 91-094.
- 32) Tsuneoka M., Fujita H., Nagashima T., "Design of JAERI Gyrotron Test Facility", JAERI-M 92-045.
- 33) Yamanishi T., Kinoshita M., Okuno K., et al., "Experimental Study for Cryogenic Distillation Column with N₂-Ar System", JAERI-M, 91-149
- 34) Shibamura K., Honda T., Kawamori N., et.al., "Japanese Contributions to Containment Structure Assembly & Maintenance and Reactor Building for ITER", JAERI-M 91-080.
- 35) Kimura H., Saigusa M., Saito Y., et.al., "Conceptual Design of Fusion Experimental Reactor (FER/ITER) - Ion Cyclotron Wave System -", JAERI-M 91-094.
- 36) Kuroda T., Yoshida H., Takatsu H., et. al., "Japanese Contributions to Blanket Design for ITER", JAERI-M 91-133.
- 37) Nakazato T., Mizoguchi T., Shimomura Y., et. al., "Study on Operational Capability of ITER", JAERI-M 91-209.
- 38) Azumi M., Hasegawa M., Kameari A., et. al., "Japanese Contribution of ITER RF Systems Design during CDA", JAERI-M 92-041.
- 39) Maki K., Kosako K., Seki Y. and Kawasaki H., "Nuclear Group Constant Set FUSION-J3 for Fusion Reactor Nuclear Calculations Based on JENDL-3", JAERI-M 91-072 (1991) (in Japanese).
- 40) Maki K., Kawasaki H., Kosako K. and Seki Y., "Nuclear Heating Constant KERMA Library - Nuclear Heating Constant Library for Fusion Reactor Group Constant Set FUSION-J3 -", JAERI-M 91-073 (1991) (in Japanese).
- 41) Fusion Reactor System Laboratory, "Concept Study of the Steady State Tokamak Reactor (SSTR)", JAERI-M 91-081 (1991).
- 42) Seki Y., Kawasaki H., Yamamuro N., Iijima S., "Revised Graphs of Activation Data for Fusion Reactor Applications", JAERI-M 91-109 (1991).
- 43) Yamamoto T., Tsuneoka M., Sakamoto K. et al., "Conceptual Design of Fusion Experimental Reactor (FER/ITER) -Electron Cyclotron Wave System-", JAERI-M 91-194 (1991).
- 44) Kuroda T., Yoshida H., Takatsu H.Takatsu., et al, "Japanese Contributions to Blanket Design for ITER", JAERI-M 91-133.
- 45) Nishio S., Sato K., Matsuoka F., et al., "Conceptual Design and Technology Development of Containment Structure Fusion Experimental Reactor (FER)", JAERI-M 91-089.
- 46) Shibamura K., Honda T., Kanamori N., et al., "Japanese Contributions to Containment Structure, Assembly & Maintenance and Reactor Building for ITER", JAERI-M 91-081.

A.1.2 List of papers published in Journals

- 1) Sato M., Nagashima A., Ishida S. et al., "Faraday rotation and elliptization of electron cyclotron emission on reactor-grade tokamak plasma", Jpn J Appl. Phys. **30** (1991) L1989
- 2) Kamada Y., Hosogane, N., Yoshino, R., et al., "Study of the Density Limit with Pellet Fuelling in JT-60", Nucl. Fusion **31** (1991) 1827.
- 3) Kamada Y., Ozeki, T. and Azumi, M., " Central Magnetohydrodynamic Activity in Pellet-fuelled JT-60 Plasmas" Phys. Fluids **B 4** (1992) 124.
- 4) Kikuchi M., Conn R.W., Najmabadi F., et al., Fusion Engineering and Design **16** (1991) 253.
- 5) Kikuchi M., Seki Y., Oikawa A., et al., Fusion Engineering and Design **18** (1991) 195.
- 6) Ide S., Imai T., Usigusa, K., et al., "Investigation of the Wave Spectrum Gap in the JT-60 LHCD Plasma", Nucl. Fusion, **32** (1992) 282.
- 7) Nakamura H., Hirayama T., Koide Y., et al., "Helium Ash Exhaust Studies with Core Fuelling by a Helium Beam:L-mode Divertor Discharges with Neutral-Beam heating in the JT-60", Phys.Rev.Lett. **67** (1991) 2658.
- 8) Shimada, M., Kubo, H., Itami, K., et al., "Remote Radiative Cooling in JT-60", J. Nucl. Mat. **176 & 177** (1990) 122.
- 9) Ishida S., Koide Y., Ozeki T., et al., "Observation of a Fast Beta Collapse during High Poloidal-Beta Discharges in JT-60", Phys. Rev. Lett. **68** (1992)1531.
- 10) Shimizu K., Yoshino R., Kamada Y., et al., "Simulation Study of Pellet Fuelled Plasmas in JT-60", Nucl. Fusion **31** (1991) 2097.
- 11) Shimizu K., Hosogane N., Shirai H., et al., "Simulation of High Ion Temperature Mode in JT-60", J. Phys. Soc. Jpn. **61** (1992) 560.

- 12) Nemoto M., Ushigusa K., Imai T., et al., "Interaction of Lower Hybrid Wave with Fast Ions Injected by Neutral Beam on the JT-60 Tokamak", *Phys. Rev. Lett.* **67** (1991) 70.
- 13) Itoh K., Sanuki H., Itoh S., et al., "Effect of the Radial Electric Field of Alpha Particle Loss in Tokamaks", *Nucl. Fusion* **31** (1991) 1405.
- 14) Hirayama T., Shirai H., Yagi M., et al., "Ion Anomalous Transport Study of L-mode Plasmas in JT-60 Tokamak", *Nucl. Fusion* **32** (1992) 89.
- 15) Tani K., Azumi M. and Devoto R. S., "Numerical Analysis of 2D MHD Equilibrium with Non-inductive Plasma Current in Tokamaks", *J. of Computational Phys.*, **98** (1992) 332.
- 16) Tani K., Yoshino R., Tuda T., et al., "Ripple-Assisted Fueling in Tokamak Reactors", *Fusion Tech.* **21** (1992) 103.
- 17) Itoh S. I. and Tani K., "Report on first Workshop on Alpha Physics in TFTR", *Kakuyugo-Kenkyu*, **65** (1991) 581 (in Japanese).
- 18) Tani K., Takizuka T. and Azumi M., "Recent Studies of Ripple Losses of Alpha Particles", *Kakuyugo-Kenkyu*, **66** (1991) 35 (in Japanese).
- 19) Azumi M. and Wakatani M., "Macroscopic and microscopic Instability", *Kakuyugo-Kenkyu*, **66** (1991) 494 (in Japanese).
- 20) Takeda T., "On Theory of Cold Fusion," *Genshiryoku Kogyo* **37** (1991) 40 (in Japanese).
- 21) Kishimoto Y., Oda H., Shiho M., "Origin of Parasitic Wave in Raman Regime Free Electron Laser," *Nucl. Instr. Methods A* **304** (1991) 632.
- 22) Yamagiwa M., Kimura H., "D-³He Fusion Yield with Higher Harmonic ICRF Heating of ³He Beams," *Nucl. Fusion* **31** (1991) 1519.
- 23) Matsushita S., Narusawa M., Kurita G., et al., "Parallelization of Nonlinear MHD PLasma Simulation," *Johoshori-Gakkai Ronbunshi* **33** (1992) 360 (in Japanese).
- 24) Matsumoto H., Burrell K.H., Carlstrom T., et al., "Suppression of the Edge Turbulence at the L, H Transition in DIII-D", *Plasma Phys. and Contr. Fusion*, **34** (1992) 615.
- 25) Neyatani Y., Shimada M., et al., "Scaling of Edge Magnetic Fluctuations in DIII-D L-Mode", *Jpn. J. Appl. Phys.*, **30** (1991) 1868.
- 26) Doyle E.J., Groebner R.J., Matsumoto H., et al., "Modifications in Turbulence and Edge Electric Fields at the L-H Transition in the DIII-D Tokamak", *Phys. Fluids B* **3** (1991) 2300.
- 27) Konoshima S., Stambaugh R., Matsumoto H., et al., "Study of Steady H-mode Discharge on DIII-D", *Japan Society of Plasma Science and Nuclear Fusion Research*, **66** (1991) 413 (in Japanese).
- 28) Uehara K., "Dynamical Picture of Current Drive Phenomena in Tokamaks", *Phys. Fluids B* **3** (1991) 26001.
- 29) Leonard A., Howard A., Hyatt A., et al., "Effects of the H-mode Power Threshold of JFT-2M", *Nucl. Fusion* **31** (1991) 1511.
- 30) Itoh S.-I., Itoh K., Fukuyama A., et al., "Edge Localised Mode Activity as a Limit Cycle in Tokamak Plasma", *Phys. Rev. Lett.* **67** (1991) 2485.
- 31) Ida K., Itoh S.-I., Itoh K., et al., "Density Peaking in the JFT-2M Tokamak Plasma with Counter Neutral-Beam Injection", *Phys. Rev. Lett.* **68** (1992) 182.
- 32) Nakajima T., Takaya I., Akiyama T., et al., "Study on hydrogen-isotope retention with collector probes in JFT-2M scrape-off layer", *J. Nucl. Mat.* **179-181** (1991) 349.
- 33) Miura Y., Shoji T., Mori M., et al., "Steady State H-mode by Ergodic Field on JFT-2M", *Kaku Yugo Kenkyu* **66** (1991) 267 (in Japanese).
- 34) Ogiwara N., Maeno M., "Large Amounts of Gas Release just after Disruptive Discharged in the JT-60 Tokamak", *J. Nucl. Mater.*, **176&177** (1990) 792.
- 35) Hiratsuka H., Kawasaki K., Miyo Y., et al., "A four-pellet Pneumatic Injection System in JT-60", *Fusion Eng. Design*, **13** (1991) 417.
- 36) Ando T., Takatsu H., Nakamura H., et al., "Heat Load on Divertor Plate of JT-60 during Normal and Abnormal Operations", *Fusion Eng. Design*, **15** (1991) 39.
- 37) Neyatani Y., Horie T., Ando T., "Design and Structural Analysis of the JT-60 Upgrade Vacuum Vessel", *Plasma Devices and Operations*, **1** (1991) 183.
- 38) Horiike H., Ando T., Kushima T., et al., "Design and Development of JT-60 Upgrade Vacuum Vessel and First Wall", *Fusion Eng. Design*, **16** (1991) 285.
- 39) Matsuoka M., "Static Analysis of Voltage Stability of the Intermediate Electrode in a Two-Stage Ion Accelerator", *Trans. IEE Japan*, **111-B** (1991) 807 (in Japanese).
- 40) Kuriyama M., "Operations of Neutral Beam System in JT-60", *Plasma devices and Operations*, **1** (1991) 127.
- 41) Ikeda Y., Imai T., Seki M., et al., "Development and Operation of JT-60 LHRF Launchers", *Plasma Devices and Operations* **1** (1991) 155-181.
- 42) Murakami Y., Abe T., et al., "Development of turbo-viscous pump with ceramic rotor assembly and oil-free driving unit", *J. Vac. Sci. Technol.* **A9** (1991) 2053.

- 43) Hiroki S., Abe T., Murakami Y., "Development of a quadrupole mass spectrometer using the second stable zone in Mathieu's stability diagram", *Rev. Sci. Instrum.*, **62** (1991) 2121.
- 44) Yoshida K., Isono T., Takahashi Y., et al., "The Stability Margin and Propagation Velocity of the Nb₃Sn Demo Poloidal Coil (DPC-EX)", *Advances in Cryogenic Engineering* **37** (1992) 315.
- 45) Sugimoto M., Yoshida K., Hasegawa M., et al., "Mechanical Test of superconducting Magnet System for Fusion Experimental Reactor", Elsevier Science Publishers B.V.(1991) 1530.
- 46) Tsuji H., "The Japan Atomic Energy Research Institute and the Development of Superconducting Magnets for Nuclear Fusion", *ISTEC Journal* **4** (1991).
- 47) Takahashi Y., Yoshida K., Ando T., et al., "Experimental results of the Nb₃Sn demo Poloidal Coil (DPC-EX)", *Cryogenics* **31** (1991) 640.
- 48) Kato T., Kamiyauchi Y., Tada E., et al., "Development on a Large Helium Turbo-Expander with Variable Capacity", *Cryogenic Engineering Congerence* (1991).
- 49) Nakajima H., Yoshida K., and Tsuji H., et al., "The Charpy Impact Test as an Evaluation of 4 K Fracture Toughness", *Advances in Cryogenic Engineering (Materials)*, **38** (1992) 207.
- 50) Ando T., Takahashi Y., Nishi M., et al., "AC Losses in a Multifilamentary Nb₃Al/Cu Composite Superconductor made by a Jelly Roll Process", *Advances in Cryogenic Engineering (Materials)*, **38** (1992) 813.
- 51) Ando T., Takahashi Y., Okuno K., et al., "AC Loss Results of the Nb₃Sn Demo Poloidal Coil (DPC-EX)", *IEEE* (1992) 206.
- 52) Tanaka S., Ohara Y., Yamamoto S., "Beam Profile Controller in Neutral Beam System", *Fusion Tech.* **19** (1991) 531.
- 53) Watanabe K., Araki M., Dairaku M., et al., "Production of a 95 % Proton Yield Beam in a Semi-cylindrical Plasma Generator", *Rev. Sci. Instrum.* **62** (1991) 2142.
- 54) Tanaka S., Yamamoto S., Araki M., et al., "Design and Experimental Results of a new Electron Gun 1 using a Magnetic Plasma Generator", *Rev. Sci. Instrum.* **62** (1991) 761.
- 55) Akiba M., Tanaka S., Seki M., "Application of Electron Beam for High Heat Flux Test Facility", *J. Atomic Energy Society of Japan*, **33** (1991) 447.
- 56) Seki M., Akiba M., Araki M., et al., "Thermal Shock Tests on Various Materials of Plasma Facing Components for FER/ITER", *Fusion Engineering and Design* **15** (1991) 59.
- 57) Yamazaki S., Seki M., Araki M., et al., "High Heat Flux Test on First Wall Materials", *ibid.* 17.
- 58) Seki M., Guseva M., Vieider G., et al., "ITER Related R&D on Low-Z Plasma-facing Materials for Divertor and First Wall", *J. Nuclear Mater.*, **179-181** (1991) 1189.
- 59) Vieider G., Cardella A., Akiba M., et al., "ITER Plasma Facing Components, Design and Development", *Fusion Engineering and Design* **16** (1991) 23.
- 60) Akiba M., Bolt H., Watson R., et al., "The Development of Divertor and First Wall Armor Parts at AERI, Sandia N. L. and KFA Julich", *ibid.* 23.
- 61) Ioki K., Akiba M., Yamada M., et al., "Development of Conductively Cooled First Wall Armor and Actively Cooled Divertor Structure for ITER/FER", *ibid.* 293.
- 62) Akiba M., Takatsu, Kuroda T., et al., "Development of Plasma Facing Components at JAERI", *Fusion Engineering and Design* **18** (1991) 99.
- 63) Laan J., Akiba M., Hassanein A., et al., "Prediction for Disruption Erosion of ITER Plasma Facing Components: a Comparison of Experimental and Numerical Results", *ibid.* 135.
- 64) Kitamura K., Akiba M., Araki M., et al., "Experimental and Analytical Studies on Residual Stress in the Tungsten-copper Duplex Structure for a Divertor Application", *ibid.* 173.
- 65) Akiba M., Araki M., Suzuki S., et al., "Performance of JAERI Electron Beam Irradiation Stand", *Plasma Devices and Operations*, **1** (1991) 205.
- 66) Teramoto T., Saito M., Suzuki S., et al., "Preliminary Fatigue and Fracture Tests of Two Stainless Steels after High Heat Load Application using Various Heat Sources", *ibid.* 331.
- 67) Bolt H., Akiba M., Benz A., et al., "Investigation of Carbon and Boron-carbon Materials under High Transient Surface Heat Loads", *Tanso*, **150** (1991) 285.
- 68) Nishimura T., Denda T., Suzuki S., et al., "Crack Propagation Tests of First Wall Materials by Cyclic Irradiation of Electron Beam", *Fusion Engineering and Design* **16** (1991) 357.
- 69) Maebara S., Tsuneoka M., Yokokura K. et al., "Improvement of 1MW Long-Pulse Klystron for Fusion Application", *Plasma Devices and Operations*, **1** (1991) 141.
- 70) Uda T., Okuno K., Matsuda Y., et al., "High Concentration Tritium Gas Measurement with Small Volume Ionization Chambers for Fusion Fuel Gas Monitors", *Journal of Nuclear Science & Technology*, **28** (1991) 447.
- 71) Okuno K., Uda T., O'hira S., et al., "Development of In-Situ Gas Analyzer for Hydrogen Isotopes in Fusion fuel Gas Processing", *ibid.*, 509.

- 72) Uda T., Okuno K., O'hira S., et al., "Preliminary study of Isotopic Methane Analysis by Laser Raman Spectroscopy for In-Situ Measurement at Fusion Fuel Gas Processing", *ibid.*, 618.
- 73) Yamanishi T., Enoda M., Naruse Y., et al., "Experimental study Separation Characteristics of Cryogenic Distillation Columns with H-D-T System", *Fusion Technology*, **20** (1991) 419.
- 74) Yamanishi T., Okuno K., Naruse Y., et al., "Liquid-Vapour Equilibrium in Binary Systems for He in nH₂, HD, and nD₂ under ordinary pressure", *J. Phys. Chem.*, **95** (1992) 2285.
- 75) Penzhorn R., Anderson J., Naruse Y., et al., "Technology and Component for a Closed Tritium Cycle", *Fusion Engineering & Design*, **16** (1991) 141.
- 76) Konishi S., Inoue M., Hayashi T., et al., "Early experiments of JAERI fuel cleanup system at the tritium systems test assembly", *ibid.*, **18** (1991) 33.
- 77) Konishi S., Inoue M., Hayashi T., et al., "Development of JAERI Fuel Cleanup System for Tests at the Tritium Systems Test Assembly", *Fusion Technology*, **19** (1991) 1595.
- 78) Okuno K., O'hira S., Naruse Y., et al., "Permeation Behavior of Deuterium Implanted into 304SS", *ibid.*, **19** (1991) 1607.
- 79) Hirata K., Ida T., Mitsui J., et al., "Separation of Hydrogen Isotopes by Advanced Thermal Diffusion Column Using Cryogenic-Wall", *ibid.*, **19** (1991) 1645.
- 80) Uda T., Okuno K., O'hira S., et al., "Application Study of Laser Raman Spectroscopy to In-Situ Gas Analysis for Fusion Fuel Processing Systems", *ibid.*, **19** (1991) 1651.
- 81) Hayashi T., Konishi S., Yamada M., et al., "Development of Large Oil-free Roughing Pump for Tritium service", *ibid.*, **19** (1991) 1663.
- 82) Konishi S., Yoshida H., Naruse Y., et al., "Tritium Experiments on Components for Fusion Fuel Processing at the Tritium Systems Test Assembly", *ibid.*, **19** (1991) 1668.
- 83) Walthers C. R., Jenkins E. M., Naruse Y., et al., "Continued Studies of Co-Pumping of Deuterium and Helium on Single, 4K Activated Charcoal Panel", *ibid.*, **19** (1991) 1811.
- 84) Okamoto M., Naruse Y., Okuno K., "Overview of Tritium Work in Japan", *Fusion Technology*, **21** (1992) 187.
- 85) Nakamura T., Hirata K., Yamanishi T., et al., "Experimental Separation characteristics of Thermal Diffusion Columns Using H-D-T system", *ibid.*, **21** (1992) 942.
- 86) Hirata K., Nakamura T., Matsumoto A., et al., "Separation of Hydrogen Isotopes by the "Cryogenic-Wall" Thermal diffusion Column", *ibid.*, **21** (1992) 937.
- 87) Uda T., Okuno K., Naruse Y., "Application of Laser Raman Spectroscopy to Isotopic Methanes Analysis in Fusion Fuel Gas Processing System", *ibid.*, **21** (1992) 436.
- 88) Hayashi T., Amano J., Okuno K., et al., "Release Behavior of Decay Helium from Zirconium-Cobalt Tritide", *ibid.*, **21** (1992) 845.
- 89) Konishi S., Hayashi T., Inoue M., et al., "Fabrication and Installation of the JAERI Fuel Cleanup System", *ibid.*, **21** (1992) 999.
- 90) O'hira S., Nakamura H., Konishi S., et al., "On-Line Tritium Process Analysis by Laser Raman Spectroscopy at TSTA", *ibid.*, **21** (1992) 465.
- 91) Sherman R. H., O'hira S., Nakamura H., et al., "Radiochemical Reaction Studies of Tritium Mixed Gases by Laser Raman Spectroscopy at TSTA", *ibid.*, **21** (1992) 457.
- 92) Inoue M., Konishi S., Yamanishi T., et al., "Isotope Separation System Experiments at the TSTA", *ibid.*, **21** (1992) 293.
- 93) Barnes J.W., Konishi S., Inoue M., et al., "Experience with an International (Japanese-American) Fusion Fuel Processing Hardware Project", *ibid.*, **21** (1992) 262.
- 94) Yamanishi T., Okuno K., Enoda M., et al., "Experimental Study for Dynamic Behavior of Cryogenic Distillation Columns Separating H-D-T System", *ibid.*, **21** (1992) 948.
- 95) Ito H., Suzuki T., Takanaga T., et al., "Separation of Tritium Using Polyimide membrane", *ibid.*, **21** (1992) 988.
- 96) Horiike H., "Trends and Perspectives in First Wall Technology", *Fusion Eng. Design* **16** (1991) 275.
- 97) Shimomura Y., "The Future of ITER", *Kaku Yugo Kenkyu* **65** (1991) 636 (in Japanese).
- 98) Okazaki R., Tada E., Matsuda S., "Study of Nuclear Fusion Reactor", *J. JSME* **94** (1991) 1019 (in Japanese).
- 99) Yamamoto S., "Radiation Hardening Problems of Diagnostic Components for International Thermonuclear Experimental Reactor (ITER)", *Hoshasen* **17** (1991) 38 (in Japanese).
- 100) Yamamoto S., "ITER Workshop on Radiation Effects on Diagnostic Components", *J. Atomic Energy Soc. Jpn.* **34** (1992) 129 (in Japanese).
- 101) Yoshikawa M., "Fusion Research and Development Entering into a New Stage", *Energy Review* **12** (1992) 4 (in Japanese).
- 102) Fujisawa N., "Plasma Physics Basis for ITER Design", *ibid.*, **12** (1992) 11 (in Japanese).

- 103) Kuroda T., Koizumi K., "ITER Conceptual Design from the Engineering Point of View", *ibid.*, **12** (1992) 16 (in Japanese).
- 104) Matsuda S., Yamamoto S., "Prospects of ITER Engineering Design Activities", *ibid.*, **12** (1992) 21 (in Japanese).
- 105) Nishio S., Ando T., Ohara Y., et al., "Engineering Aspects of a Steady State Tokamak Reactor (SSTR)", *Fusion Engineering and Design* **15** (1991) 121.
- 106) Yamagiwa M. and Kimura H., "D-³He Fusion Yield with Higher Harmonic ICRF Heating of ³He Beams", *Nuclear Fusion* **31** (1991) 1519.
- 107) Mori S., Yamazaki S., Adachi J. et al., "Blanket and Divertor Design for the Steady State Tokamak Reactor (SSTR)", *Fusion Eng. Des.* **18** (1991) 249.
- 108) Shatalov G. E., Abdou M. A., Antipenkov A., et al., "Breeder and Test Blankets in ITER", *Fusion Eng. Des.* **16** (1991) 85.
- 109) Proust E., Anzidei L., Dall Donne M., et al., "Solid Breeder Blanket Design and Tritium Breeding", *ibid.* **16** (1991) 73.
- 110) Takatsu H., Tada E., Shibamura K., et al., "Conceptual Design Activity of International Thermo nuclear Experiment Reactor(ITER) and Related Engineering R&D", *J. Atomic Energy Soc. Jpn* **33** (1991) 737.
- 111) Kurasawa T., Slagle O. D., Hollenberg G. W., et al., "In-situ Tritium Recovery from Li₂O Irradiation in Fast Neutron Flux-BEATRIX-II First Results", *Fusion Technol.* **19** (1991) 931.
- 112) Baker D. E., Kurasawa T., Miller J. M., et al., "BEATRIX-II : In-situ Tritium Test Operation" *ibid.* **19** (1991) 1640.
- 113) Honda T., Lousteau D., Sadakov S., et al., "Philosophy and Concepts for ITER Maintenance", *Fusion Eng. and Design* **18** (1991) 205.
- 114) Adachi J., Nakano Y., Uehara H., et al., "Feasibility Study of Remote Erosion Measurement of First Wall for Fusion Experimental Reactor", *Fusion Eng. and Design* **18** (1991) 501.
- 115) Shibamura K., Honda T., Kondoh M., et al., "Design Study of an Armor Tile Handling Manipulator for the Fusion Experimental Reactor", *Fusion Eng. and Design* **18** (1991) 487.

A.1.3 List of papers published in conference proceedings

- 1) Sato M., Ishida S., Ise N., et al., "Effects of relativistic mass and polarization change on ECE measurement for a reactor-grade plasma", *Course and Workshop Diagnostics for Contemporary Fusion Experiments (Proc. International School of Plasma Physics, Varenna, Italy, 1991)* 803.
- 2) Kamada, Y., Yoshino, R., Nagami, M., et al., "Pellet Injection with Improved Confinement in JT-60", in *Plasma Physics and Controlled Nuclear Fusion Research (Proceedings of the 13th International Conf. Wasington, 1990) IAEA, Vienna, Vol.1, (1991)* 291.
- 3) Funahashi A., and JT-60 team, "The initial experiments on the JT-60 Upgrade tokamak", in *Proc. 18th European Conference on Controlled Fusion and Plasma Physics, Berlin, 1991*.
- 4) Neyatani Y., Hospgane N., Matsukawa M., et al., "Development of Magnetic Sensors in JT-60 Upgrade", *14th Symp. on Fusion Engineering 1991*, p.1183.
- 5) Kikuchi M., and JT-60 Team, "Overview of H mode Experiments in JT-60 Upgrade:, 3rd Workshop on H-mode Physics, JET Joint Undertaking, Abingdon, U.K. 10-12 June 1991.
- 6) Kimura H., Yamamoto T., Fujii T., et al., "Studies on Fast Wave Current Drive in the JAERI Tokamaks", *Proc. IAEA Technical Coimmittee Meeting on Fast Wave Current Drive in Reactor Scale Tokamaks, (Arles, 1991)*, 260.
- 7) Kimura H. and Fujii T., "Fast Wave Heating and Current Drive in JT-60/60U", *Proc. U.S.-Japan Workshop on RF Heating and Current Drive in Confinement Systems Tokamaks, (Nagoya, 1991)*, NIFS-PROC-10, 81.
- 8) Imai T., Kimura H., Kusama K., et al., "Lower Hybrid Current Drive and Higher Harmonic ICRF Heating Experiments on JT-60", in *Plasma Physics and Controlled Nuclear Fusion Research (Proceedings of the 13th International Conf. Wasington, 1990) IAEA, Vienna, Vol. 1(1991)* 645.
- 9) Imai T. and JT-60 Team, "Initial Results of LHCD in JT-60U and Limitation of the LHCD Application", *Proc. U.S.-Japan Workshop on RF Heating and Current Drive in Confinement Systems Tokamaks, (Nagoya, 1991)*, NIFS-PROC-10, 37.
- 10) Devoto R. S., Ide S., Imai T., et al., "Comparison of Lower Hybrid Current Drive Experiments in JT-60 with Theory", *Proc. of 9th Top Conf. on Radio-Frequency Power in Plasmas, Charleston, (1991)* .
- 11) Nakamura H., Sakasai A., Hirayam T., et al., "Status and Plan of Helium Ash Transport and Exhaust Experiments in JT-60U", *Proc. of second International Workshop on Helium Transport and Exhaust in Tokamak Experiments (Montrey, 1992)*.

- 12) Shimada M., "SOL/Divertor Performance during Auxiliary Heating/Current Drive in JT-60U", Proc. U.S.-Japan Workshop on RF Heating and Current Drive in Confinement Systems Tokamaks, (Nagoya, 1991), NIFS-PROC-10, 183.
- 13) Sugie T., Itami K., Nakamura H., et al., "Impurity control and Helium Exhaust Experiment in JT-60", in Plasma Physics and Controlled Nuclear Fusion Research (Proceedings of the 13th International Conf. Wasington, 1990) IAEA, Vienna, Vol. 1(1991) 385.
- 14) Ishida S., Kikuchi M., Hirayama T., et al., "High Poloidal-Beta Experiments with a Hot-Ion Enhanced Confinement Regime in the JT-60 Tokamak, in Plasma Physics and Controlled Nuclear Fusion Research (Proceedings of the 13th International Conf. Wasington, 1990) IAEA, Vienna, Vol.1, (1991) 195.
- 15) Ishida S., Koide Y. and Hirayama T., "Enhanced Toroidal Rotation in Hot-Ion Mode with Nearly-Balanced Neutral Beam Injection in JT-60", in Proc. 18th European Conference on Controlled Fusion and Plasma Physics, Berlin, 1991, Part I-165.
- 16) Hirayama T., Kikuchi M., Shirai H., et al., " Local Transport Analysis of L-mode Plasmas in JT-60", in Proc. 18th European Conference on Controlled Fusion and Plasma Physics, Berlin, 1991.
- 17) Carrera R., Anderson J.L., Tani K., et al., "Description of Fusion Experiment IGNITEX", in Plasma Physics and Controlled Nuclear Fusion Research (Proceedings of the 13th International Conf. Wasington, 1990) IAEA, Vienna, Vol.3, (1991) 567.
- 18) Fukuyama A., Itoh S-I., Itoh, K., et al., "Nonresonant Current Drive by RF Helicity Injection", in Plasma Physics and Controlled Nuclear Fusion Research (Proceedings of the 13th International Conf. Wasington, 1990) IAEA, Vienna, Vol.1 (1991) 855.
- 19) Ozeki T., Azumi M., S. Ishida S., et al., "Effects of Hollow Current Profiles on the Ideal MHD Stabilities in JT-60 High Betapoloidal Plasmas", Proc. of 33th APS meeting (Tampa, FL.,USA)
- 20) Shirai H., Hirayama T., Yagi M., et al., "Transport Analysis of JT-60 Plasmas", *ibid*
- 21) Aoyagi T., Terakado T., Takahashi M., et al., "Very Fast Feedback Control of Coil-Current in JT-60 Tokamak", Proc. Inter. Conf. on Acceraletor and Large Exp. Phys. Control Systems (Nov. 11-15, 1991, Tsukuba).
- 22) Tsunematsu T., Nakamura Y., Nishio S., et al., "Modeling of Vertical Plasma Motion," ITER Physics/Design Option Work Session (san Diego, USA).
- 23) Kishimoto Y., Yamagiwa M., Itoh K., et al., "Effect of Energetic Trapped Particle Generated by ICRF Wave on Internal Kink Mode," *ibid*.
- 24) Takizuka T., "Physics of Tokamak Reactor Plasma," 7th Summer Seminar on Fusion Reactor (Mito) (in Japanese).
- 25) Kishimoto Y., Tokuda S., Nakamura Y., et al., "Space Charge Modeling in 3-Dimensional Focusing Wiggler FEL," 13th Internat'l Free Electron Laser Conf. (Santa Fe, USA).
- 26) Takizuka T., "Physics of Divertor Plasma in a Tokamak," 2nd International Youth School on Plasma Physics and Controlled Fusion (Dagomys, USSR).
- 27) Takizuka T., and JT-60 team, "Energy Confinement in JT-60U," DIII-D/JT-60U Joint Physics Workshop (Naka).
- 28) Kurita G., Tuda T., Azumi M., et al., "Effect of External Helical Field on Rotating Magnetic Island," Proc. 1991 Workshop on MHD Computations (Nagoya) p.82 (in Japanese).
- 29) Takeda T., "Plasma Simulator METIS and MHD Computation," *ibid*. p.154 (in Japanese).
- 30) Nakamura M., Tokuda S., "Numerical Experiments of SELENEJ Code," *ibid*. p.174 (in Japanese).
- 31) Takizuka T., "Thermal Energy Confinement of L-Mode Tokamak Plasma," Workshop on Theory of Toroidal System (Nagoya) (in Japanese).
- 32) Oikawa A., Kikuchi M., Seki Y., et al., "Conceptual Design of the Steady State Tokamak Reactor", Proc. 14th IEEE/NPSS Symp. on Fusion Engineering, 1991 Vol.2 p.670.
- 33) Nagami M., Miya N., Nakajima S., et al., "Preliminary Design Study of a Steady State Tokamak Device", Bull. Amer. Phys. Soc., **36** (1991).
- 34) Matsumoto H., Stockdale R., et al., "Perturbative Particle Transport Study of DIII-D H-mode Plasma", *ibid.*, **36** (1991) p.2476.
- 35) Prater R., Kawashima H., et al., "Initial Fast Wave Current Drive Experiments on DIII-D", *ibid.*, **36** (1991) p.2324.
- 36) Kazumi H., Yoshioka K., Kinoshita S., et al., "Tuning Method for Multiple Transmission Line with Mutually Coupled Fast Wave Antennas in JFT-2M", in Proc. 18th European Conference on Controlled Fusion and Plasma Physics, Berlin, 1991.
- 37) Saigusa M., Yamamoto T., Kawashima H., et al., "Analysis of Coupling Properties of Antenna Array in JFT-2M", 9th Topical Conf. on Radio Frequency Power in Plasma, Tampa(U.S.A.) 1991.
- 38) Kawashima H., Yamamoto T., Saigusa M., et al., "Investigation of Fast Wave Current Drive at High Nz Four-Loop Antenna in JFT-2M Tokamak", *ibid*.

- 39) Kawashima H., Yamamoto T., Petty C.C., et al., "Optimization of Phased Four-Loop Antenna in JFT-2M Tokamak", IAEA Technical Committee Meeting on Fast Wave Current Drive in Reactor Scale Tokamaks, Arles(France), 1991.
- 40) Kimura H., Yamamoto T., Fujii H., et al., "Studies on Fast Wave Current Drive in the JAERI Tokamaks", *ibid.*
- 41) Kondo I., Horiike H., Neyatani Y., et al., "JT-60 Operation Results after its Modification for Higher Plasma Current with Single Null Open Divertor", Proc. 14th Symp. Fusion Eng., San Diego, 1991.
- 42) Neyatani Y., Hosogane N., Matsukawa M., et al., "Development of Magnetic Sensors in JT-60 Upgrade", *ibid.*
- 43) Uchikawa T., Horiike H., Ninomiya H., et al., "Fabrication of the Vacuum Vessel for JT-60 Machine Upgrade", *ibid.*
- 44) Yotsuya M., Horiike H., Neyatani Y., et al., "Design and Performance Tests of Gas Circulation Heating of T-60U Vacuum Vessel", *ibid.*
- 45) Takanabe K., Horiike H., Ninomiya H., et al., "Development of Slide Support for JT-60U Vacuum Vessel", *ibid.*
- 46) Ioki K., Ando T., Yamamoto M., et al., "Design and Fabrication of Divertor Base-Plate for JT-60U", *ibid.*
- 47) Ando T., Kodama K., Yamamoto M., et al., "Quality Evaluation of Graphites and Carbon/Carbon Composites during Production of JT-60U Plasma Facing Materials", 5th Int. Conf. on Fusion Reactor Mater., Clear Water, Florida (1991).
- 48) Fujita I., Ando T., Akiba M., et al., "Surface Analysis for JT-60 Graphite Divertor Tiles", 10th Int. Conf. on Plasma Surface Interactions in Controlled Fusion Devices, Monterey (1992).
- 49) Gotoh Y., Ando T., Saidoh M., et al., "Erosion Characteristics of Carbon Related Materials", *ibid.*
- 50) Jimbou R., Saidoh M., Ogiwara N., et al., "Retention of Deuterium Implanted into B₄C-overlaid Isotropic Graphites and Hot-pressed B₄C", *ibid.*
- 51) Kimura T. and JT-60 Team, "Initial Results from the JT-60 Upgrade", in Proceedings of the 14th Symposium on Fusion Engineering, San Diego, 1991, pp.860-866.
- 52) Yonekawa I., et al., "Development of a Man/Machine Interface System for the JT-60 Upgrade", in Proceedings of the 14th Symposium on Fusion Engineering, San Diego, 1991, pp.798-801.
- 53) Matsuzaki Y., Aoyagi T., Terakado T., et al., "New Digital Control Systems of Poloidal Field Power Supplies for JT-60 Upgrade". 16th Symp. on Fusion Technology (London, 1990) p.1482.
- 54) Isaka M., Sekiguchi S., "Management and control of Cooling Water in JT-60 second Cooling system" Symp. on Technology in Laboratories in National Institute for Fusion Science (Toki, 1991) p.283.
- 55) Ikeda Y., Ichige H., Takeshita A., Omori K., "Overhauls of Toroidal Motor -Generator with 4GJ Flywheel" Symp. on Technology in Laboratories in National Institute for Fusion Science (Toki, 1991) p.287.
- 56) Kuriyama M., "Design of a Negative-Ion Based NBI System for JT-60U", Proc of 14th Symp. on Fusion Enging., San Diego, (1991) 78.
- 57) Suzuki Y., "Long Pulse Operation of a H⁻ Source", IAEA TCM on Negative Ion Based Neutral Beam Injectors (JAERI/Naka) (1991) p93.
- 58) Matsuoka M., "Role of JT-60U N-NBI Program", *ibid.*, P244.
- 59) Kuriyama M., "Specification of JT-60U N-NBI", *ibid.*, p250.
- 60) Mizuno M., "Power Supply System for JT-60U N-NBI", *ibid.*, p259.
- 61) Yamamoto T., Imai T., Kimura H. and JT-60 team, "LH Current Drive and ICRF Heating Experiments and Developments of RF Systems for JT-60/U", Proceeding of 9th Topical Conference on Radio Frequency Power in Plasmas, Charleston SC (1991) 243.
- 62) Ikeda Y., Seki M., Imai T., et al., "A new LHRF multi-junction launcher with oversized waveguides for JT-60U", Proceeding of 14th Symp. on Fusion Technology, San Diego U.S.A. (1991).
- 63) Fujii T., Saigusa M., Moriyama S., et al., "Mechanical Design and Analysis of JT-60U ICRF Launcher", Proceeding of 14th Symp. on Fusion Technology, San Diego U.S.A. (1991).
- 64) Kato T., Kamiyauchi Y., Tada E., et al., "Development on a Large Helium Turbo-Expander with Variable Capacity", Cryogenic Engineering Conference 1991.
- 65) Kato T., Ishida H., Tada E., et al., "Development of a Large Centrifugal Cryogenic Pump", Cryogenic Engineering Conference 1991.
- 66) Nishi M., Ando T., Isono T., et al., "Development of a 240 mm bore-13T Superconducting Coil for Large Scale Conductor Testing", MT-12 Conference, 23-28 1991.
- 67) Egusa S., Sugimoto M., Nakajima H., et al., "Effects of Fabric type, Specimen size, and Irradiation Atmosphere on the adiation Resistance of Polymer Composites at 77 K", International Cryogenic Materials Conference 1991.
- 68) Takao T., Tsukamoto O. and Yoshida K., "Irregularity of Conductor and Stochastic Estimation of the Possibility of Preamature Quenches in Superconducting Magnet", Cryogenic Engineering Conf. 1991.

- 69) Tanaka H., Hasegawa K., Okumura Y., et al., "High Density Plasma Production in a Multicusp Plasma Generator with ECR", 14th Symp. on Ion Sources and Ion-Assisted Technology, Tokyo, Japan, (1991).
- 70) Inoue T., Hanada K., Mizuno M., et al., "Beam Optics in a Negative Ion Source with 250 keV Electro-Static Accelerator", *ibid.*
- 71) Inoue T., Hanada K., Mizuno M., et al., "R&D's on Negative Ion Source and Accelerator for High Energy NBI", 14th IEEE/NPSS Symp. on Fusion Engineering, San Diego, Sept. (1991).
- 72) Okumura Y., "Intense Positive and Negative Ion Sources for Fusion Application" Inter. Conf. on Evaluation in Beam Applications, Takasaki, Nov. (1991).
- 73) Ohara Y., "Negative Ion Beam Program at JAERI", IAEA Technical Committee Meeting on Negative Ion Based Neutral Beam Injectors, Naka Nov. (1991) 43.
- 74) Pamela J., Hanada K., Okumura Y., "D⁻ Production and acceleration in Joint CEA-JAERI Experiment at Cadarache" *ibid.* 75.
- 75) Okumura Y., Hanada K., Watanabe K., et al., "Production of 2 A, 100 keV D⁻ ion beams by Cesium Seeding in the Joint CEA-JAERI Experiment", *ibid.* 84.
- 76) Suzuki Y., Hanada K., Inoue T., et al., "Long Pulse Operation of a H⁻ Source", *ibid.* 93.
- 77) Watanabe K., Hanada K., Inoue T., et al., "High Energy Acceleration of H⁻ Ions", *ibid.* 184.
- 78) Inoue T., Hanada K., Akiba M., Araki M., Mizuno M., et al., "Steering of H⁻ Beamlet by Aperture Displacement", *ibid.* 189.
- 79) Mizuno M., Hanada K., Inoue T., "Power Supply System for JT-60U N-NBI", *ibid.* 259.
- 80) Yamazaki S., Seki M., Akiba M., et al., "Development of First Wall with Radiative Cooled Graphite Armor Tile", Proc. 16th SOFT, London, Sept. (1990) 302.
- 81) Araki M., Akiba M., Seki M., et al., "Recent Results of Developmental study on Plasma Facing Components at JAERI", *ibid.* 307.
- 82) Gotoh Y., Akiba M., Araki M., et al., "Felt-carbon-carbon composite/copper brazed Structures for Active Cooling Plasma Facing Components", *ibid.* 312.
- 83) Linke J., Akiba M., Araki M., et al., "Disruption Simulation Experiments in Electron and Laser Beam Facilities", *ibid.* 428.
- 84) Vieider G., Cardela A., Akiba M., et al., "ITER Plasma Facing Components, Design and Development", Proc. 2nd ISFNT, Karlsruhe, June (1991).
- 85) Akiba M., Bolt H., Watson R., et al., "The Development of Divertor and First Wall Armor Parts at JAERI, Sandia N. L. and KFA Julich", *ibid.*
- 86) Ioki K., Akiba M., Yamada M., et al., "Development of Conductively Cooled First Wall Armor and Actively Cooled Divertor Structure for ITER/FER", *ibid.*
- 87) Akiba M., Takatsu, Kuroda T., et al., "Development of Plasma Facing Components at JAERI", *ibid.*
- 88) Laan J., Akiba M., Hassanein A., et al., "Prediction for Disruption Erosion of ITER Plasma Facing Components: a Comparison of Experimental and Numerical Results", *ibid.*
- 89) Kitamura K., Akiba M., Araki M., et al., "Experimental and Analytical Studies on Residual Stress in the Tungsten-copper Duplex Structure for a Divertor Application", *ibid.*
- 90) Linke J., Akiba M., Araki M., et al., "Disruption Simulation Experiments on First Wall Candidates", *ibid.*
- 91) Teramoto T., Saito M., Suzuki S., et al., "Preliminary Fatigue and Fracture Tests of Two Stainless Steels after High Heat Load Application using Various Heat Sources", *ibid.*
- 92) Toyoda M., Yamazaki S., Suzuki S., et al., "Crack Propagation Tests of First Wall Materials by Cyclic Irradiation of Electron Beam", *ibid.*
- 93) Araki M., Akiba M., Suzuki S., et al., "Thermal Cycling Tests of Plasma Facing Components for Fusion Experimental Reactor at JAERI", Proc. 14th SOFE, San Diego, Sep. (1991).
- 94) Akiba M., Araki M., Ando T., et al., "Thermal Shock Tests of Carbon Materials with High Power Beam", Proc. Inter. Conf. on Evolution in Beam Applications, Takasaki, Japan, Nov. (1991).
- 95) Akiba M., Araki M., Suzuki S., et al., "Experimental and Analytical Studies on Carbon Based Materials with High Thermal Conductivity", Proc. 5th Inter. Symp. on Materials, Clearwater, US, (1991).
- 96) Diegele E., Jakeman R., Suzuki S., et al., "Structural Analysis of a First Wall Component Results of Benchmark Calculations", *ibid.*
- 97) Tanabe T., Akiba M., Araki M., et al., "High Heat Load Test of Molybdenum", *ibid.*
- 98) Suzuki S., Akiba M., Araki M., et al., "Development of Divertor Modules for Fusion Experimental Reactors", Proc. 2nd Japan Inter. SAMPE Symposium and Exhibition, Chiba, Japan (1991).
- 99) Saigusa M., Yamamoto T., Kawashima H. et al., "Analysis of Coupling Properties of Antenna Array in JFT-2M", 9th Topical Conf. on Radio Frequency Power in Plasmas, Charleston, SC (1991) 193.
- 100) Shiho M., Maebara S., Watanabe A. et al., "JAERI Millimeter Wave FEL Experiments with a Focusing Wiggler", Nucl. Instr. and Methods in Phys. Res. A304 (1991) 141.

- 101) Sakamoto K., Ohasa K., Kasperek W. et al., "Quasi-Optical Antenna for a Whispering Gallery Mode Using a Double Reflector", Work shop on High power Microwave Generation and Applications Varenna, Italy, Sep. 9-17 (1991) 605.
- 102) Sakamoto K., Kishimoto Y., Watanabe A. et al., "MM Wave FEL Experiment with Focusing Wiggler", Work shop on High power Microwave Generation and Applications Varenna, Italy, Sep. 9-17 (1991) 597.
- 103) Tsuneoka M., Fujita H., Nagashima T. et al., "Design and Testing of Power Supply for The High Power Gyrotron", The 14th IEEE/NPSS Symp. on Fusion Engineering, San Diego CA, Sep. 30-Oct. 3, 1991.
- 104) Kishimoto Y., Oda H., Shiho M. "Origin of Parasitic Wave in Raman-regime Free Electron Laser", Nucl. Instr. and Methods in Phys. Res. A304 (1991) 632.
- 105) Kimura H., Yamamoto T., Fujii T. et al., "Studies on Fast Wave Current Drive in the JAERI Tokamak", IAEA Technical Committee Meeting on Fast Wave Current Drive in Reactor Scale Tokamaks, Arles, France Sep. 23-25 1991.
- 106) Yamamoto T., Imai T., Kimura H. et al., "LH Current Drive and ICRF Heating Experiments and Developments of RF System for JT-60U", 9th Topical Conf. on Radio Frequency Power in Plasmas, Charleston, SC (1991).
- 107) Kuroda T., Anzidei L., Dall Donne M., et. al., "Solid Breeder Blanket Design and Tritium Breeding", Proc. 2nd Int. Symp. Fusion Nucl. Tech., Karlsruhe, 1991.
- 108) Honda T., Lousteau D., Maisonnier D., et. al., "Philosophy and Concepts for ITER Maintenance", *ibid.*
- 109) Kimura H., Nakazato T., Fukuyama J., "Analysis of Fast Wave Current Drive for ITER", Proc. IAEA Tech. Commit. M. on Fast Wave Curr. Drive in Reactor Scale Tokamaks, Arles, (1991).
- 110) Yamamoto S., "Japanese Irradiation Test Program for ITER Diagnostic Components", ITER Workshop on Rad. Effects on Diag. Components, St.Petersburg, 1991.
- 111) Matoba T., "Requirements for Radiation Hardening of Diagnostic Components", *ibid.*
- 112) Kikuchi M., Conn R.W., Najmabadi F. and Seki Y., "Recent Directions in Plasma Physics and Its Impact on Tokamak Magnetic Fusion", Proc. 2nd.Int. Symp. on Fusion Nucl. Technol., Fusion Engineering and Design 16 (1991) 253.
- 113) Kikuchi M., Seki Y., Oikawa A., et al., "Conceptual Design of the Steady State Tokamak Reactor (SSTR)", Proc. 2nd.Int. Symp. on Fusion Nucl. Technol., Karlsruhe, June (1991).
- 114) Mori S., Yamazaki S., Nishio S., et al., "Blanket and Divertor Design for the Steady State Tokamak Reactor (SSTR)", Proc. 2nd.Int. Symp. on Fusion Nucl. Technol. Fusion Engineering and Design 18 (1991) 249.
- 115) Suzuki Y., Yamada M., Kikuchi M., et al., "A Conceptual Design of a Low Resistance Vacuum Vessel for Steady State Tokamak Reactor", Proc. 2nd.Int. Symp. on Fusion Nucl. Technol., Karlsruhe, June (1991).
- 116) Sharafat S., Cheng E.T., Kunugi T., et al., "ARIES-I Fusion Power Core Engineering", Proc. 2nd Int. Symp. on Fusion Nucl. Technol., Karlsruhe, June (1991).
- 117) Seki Y., "Safety and Environmental Prospects for Fusion Power Reactors", IEA International Conference on Technological Responses to Global Environmental Challenges, Kyoto, 6-8 November (1991).
- 118) Hasan M. Z. and Kunugi T., "Liquid-Metal Heat Transfer for the First Wall and Limiter/Divertor Plates of Fusion Reactors", Proc. AIChE Symposium Series No. 238, Vol. 87 (1991) 67.
- 119) Hasan M. Z. and Kunugi T., "Effects of Circumferentially Varying Heat Flux on the Liquid-Metal Thermal-Hydraulic Design of Plasma Facing Components of Fusion Reactors", Proc. 14th IEEE Symposium on Fusion Engineering, San Diego, Sept. 30- Oct. 4 (1991).
- 120) Oikawa A., Kikuchi M., Seki Y. and SSTR Design Team, "Conceptual Design of the Steady State Tokamak Reactor (SSTR)", Proc. 14th Symposium on Fusion Engineering, San Diego, Sept. 30- Oct. 4 (1991).
- 121) Shibamura K., Kondo M., Kakudate S., et al., "Recent Developments in Remote Maintenance for Fusion Experimental Reactor in JAERI", Proc. 14th IEEE Symposium on Fusion Engineering, San Diego, Sept. 30- Oct. 4 (1991).
- 122) Kimura H., Yamamoto T., Fujii T., "Studies on Wave Current Drive in the JAERI Tokamaks", Proc. IAEA Technical Committee Meeting on Fast Wave Current Drive in Reactor Scale Tokamaks, Arles, September (1991).
- 123) Nishio S., Takatsu H. and Sugihara M., "Transient Electromagnetic Analysis on Tokamak Device", Proc. Japan-CIS Joint Seminar on Electromagnetomechanical Phenomena in Structures, (1991) (to be published in Supplement of Int. J. of Applied Electromagnetics in Materials).
- 124) Nishio S., Miura H., Mori S. and Suzuki T., "Experimental Study of Electromagneticdynamics on Fusion Reactor", Proc. Japan-CIS Joint Seminar on Electromagnetomechanical Phenomena in Structures, (1991) (to be published in Supplement of Int. J. of Applied Electromagnetics in Materials).
- 125) Kimura H., Yamamoto T., Fujii T., "Studies on Wave Current Drive in the JAERI Tokamaks", Proc. IAEA Technical Committee Meeting on Fast Wave Current Drive in Reactor Scale Tokamaks, Arles, September (1991).
- 126) Yoshida H., Ohara A., Nakamura H. et al., "Beryllium Compatibility Study of Blanket Materials", Ceramic Transactions. 27 (1991) 157.

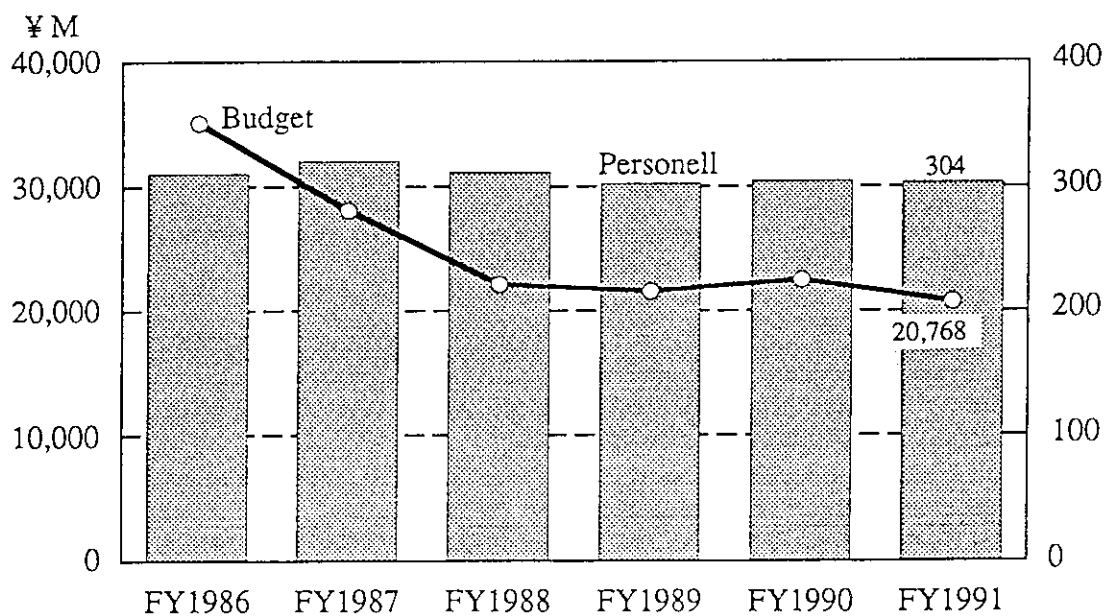
- 127) Yoshida H., Tanaka S., Enoeda M. et al, "Integrity and Compatibility Study of Blanket Materials", *ibid.* 27 (1991) 175.
- 128) Kurasawa T., Slagle O. D., Hollenberg. G. W., et al, "In situ Tritium Recovery from Li_2O Irradiated in a Fast Neutron Flux: BEATRIX-II Phase I-Temperature Gradient Specimen", *ibid.* 27 (1991) 299.
- 129) Watanabe H., Kurasawa T., "A Technique for In-Situ Tritium Recovery Experiment of Breeder Materials", *Proceeding of 3rd Asian Symposium on Research Reactor*, Hitachi Ibaraki, Japan Nov 11- 14 (1991) 253.

A.1.4 List of other reports

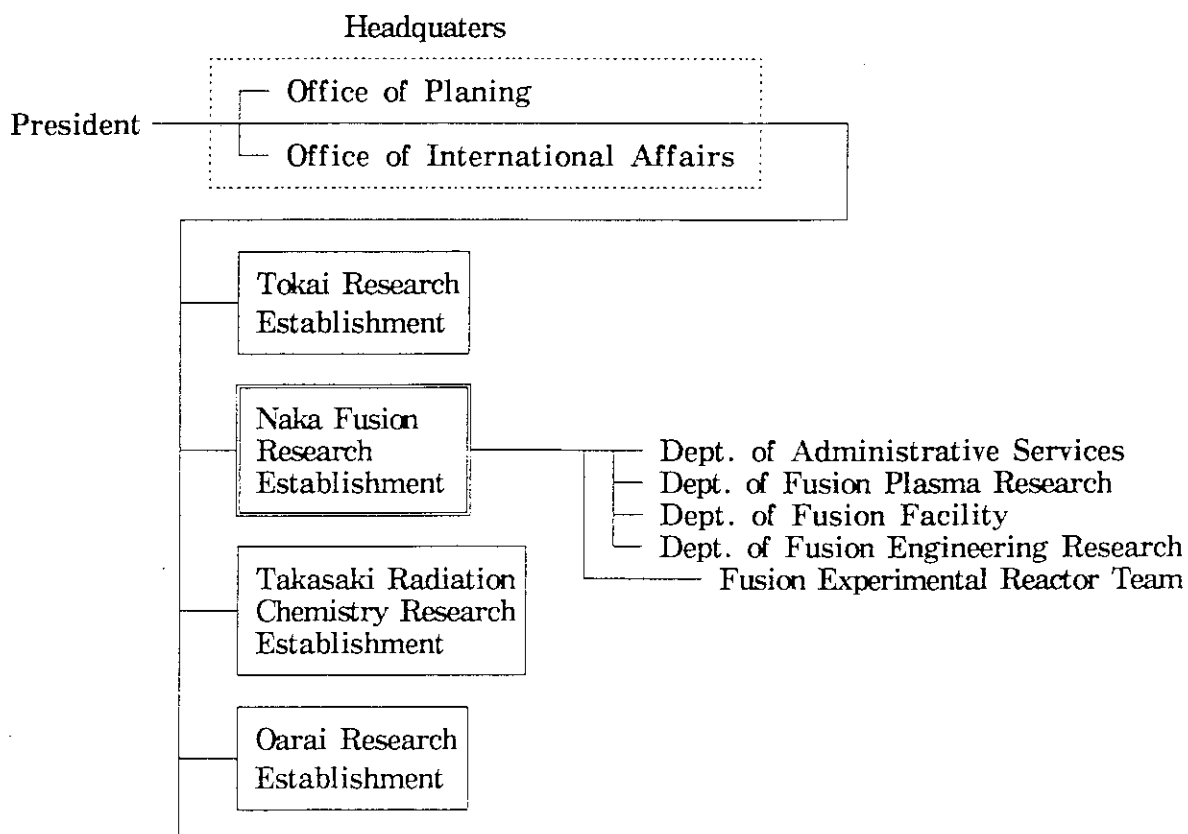
- 1) Kamada, Y., Snider, R.T., Taylor, T.S., et al., "Sawtooth Frequency Studies in DIII-D Tokamak" GA-A20611, General Atomics 1992.
- 2) Ishida S. (Coordinator) , "Interferometry and Polarimetry", in Report for ITER CDA Diagnostic Design), IAEA, Vienna, 1991, ITER Documentation Series, No.33, p.61.
- 3) Montalvo E., Carrera R., Tani K., et al., " Alpha Confinement in an Ohmically Heated Ignition Tokamak", Texas University Report CFER-485.
- 4) Carrera R., Arslanoglu R., Tani K., et al., " The Ignition Concept for a Fusion Ignition Experiment", Texas University Report CFER-488.
- 5) Hirayama T., "Numerical Scheme for Solving Stiff Equation and Impurity Transport Analysis of Pellet Fuelled Plasmas", NIFS-PROC-9 pp.95-109 (1992).
- 6) Philippon R., Groebner R., Matsumoto H., "Two-Stage Turbulence Suppression and EXB Plasma Flow Measured at the L-H Transition", GA-A20516(May. 1991).
- 7) Sinder R., DIII-D Team, "The DIII-D Tokamak and Energy Confinement at Low q", GA-A20556 (Aug. 1991).
- 8) Ida K., Itoh S.-I., Itoh K., et al., "Density Peaking in the JFT-2M Tokamak Plasma with Counter Neutral Beam Injection", NIFS-83 (1991).
- 9) Miura Y., Okana F., Suzuki N., et al., "Rapid Change of Hydrogen Neutral Energy Distribution at L/H Transition in JFT-2M H-mode", NIFS-134 (1991).
- 10) Ida K., Hidekuma S., Kojima M., et al., "Edge Poloidal Rotation Profiles of H-mode Plasmas in the JFT-2M Tokamak", NIFS-124 (1991).
- 11) Ando T., "Present Status of Developments of Superconducting Magnet Systems in JAERI", 7th US-JAPAN Workshop.
- 12) Yoshida K., Okuno K., Ando T., et al., "Developments of coils and conductors for ITER at JAERI", 7th US-JAPAN Workshop.
- 13) Young K. M., Mukhovatov V. S., Yamamoto S., et. al., "Summary Report ITER Workshop on Radiation Effects on Diagnostic Components", ITER/SU/91/TE/DG-1, 1991.
- 14) Kimura H., "ITER Current Drive Requirements", NIFS-PROC-10, (1992)150.
- 15) Sugihara M., Murakami Y., Kimura H., et. al., "Consistent of Current Drive and Divertor Conditions for Steady State and Hybrid Operation in ITER", *ibid.*, 200.

A.2 Personnel and Financial Data

A.2.1 Change in number of personnel and annual budgeted (FY1986-1991)



A.2.2 Organization chart (March 31, 1992)



A. 2. 3 Scientific staffs in the Naka Fusion Research Establishment (March 31, 1992)

Naka Fusion Research Establishment

SHIKAZONO Naomoto (Director General)

SEKIGUCHI Tadashi (Scientific Advisor)

TANAKA Masatoshi (Scientific Advisor)

TOMABECHI Ken (Scientific Advisor)

MIYAMOTO Goro (Scientific Advisor)

Department of Administrative Services

YAMAMOTO Takao (Director)

Department of Fusion Plasma Research

TAMURA Sanae (Director)

KISHIMOTO Hiroshi (Deputy Director)

HINO Shuhji (Administrative Manager)

Tokamak Program Division

KITSUNEZAKI Akio (Head)

KONOSHIMA Shigeru

NAGAMI Masayuki

OIKAWA Akira

MATSUMOTO Hiroshi

NAKAJIMA Shinji(*28)

TOYOSHIMA Noboru

MIYA Naoyuki

NISHITANI Takeo

USHIGUSA Kenkichi

Plasma Analysis Division

AZUMI Masafumi (Head)

HAGINOYA Hirofumi

SATO Minoru

HAMAMATSU Kiyotaka

OZEKI Takahisa

TANI Kenji

YAGI Masahiro

WAN Jan Ping(*90)

TSUCHIYA Satoru(*85)

HIRAYAMA Toshio

SAITO Naoyuki

TSUGITA Tomonori

SAKATA Nobuya

AOYAGI Tetsuo

OHSHIMA Takayuki

SHIRAI Hiroshi

TSUJI Shunji

Large Tokamak Experiment Division I

FUNAHASHI Akimasa (Head)

KITAMURA Shigeru

UNO Sadanori

FUKUDA Takeshi

ISEI Noriaki

KIKUCHI Mitsuru

NAGASHIMA Keisuke

NEYATANI Yuzuru

OHZEKI Masahiro

SHITOMI Morimasa

URAMOTO Yasuyuki

YOSHIDA Hidetoshi

NAGAYA Susumu

WOLFE Sean(*89)

GUNJI Hideo

ISHIDA Shinichi

KOIDE Yoshihiko

DE HAAS Johannes(*90)

NINOMIYA Hiromasa

SAKUMA Takeshi

TAKAHASHI Toranosuke

YAMASHITA Osamu

YOSHINO Ryuji

SUNAOSHI Hidenori

CHIBA Shinichi

HOSOGANE Nobuyuki

KAMADA Yutaka

KONDOH Takashi

NAITO Osamu

NUMAZAWA Susumu

SATO Masayasu

TSUKAHARA Yoshimitsu

Large Tokamak Experiment Division II

FUNAHASHI Akimasa (Head)

ASAKURA Nobuyuki

ITAMI Kiyoshi

MIURA Sanae(*84)

NEMOTO Masahiro

SHIMIZU Katsuhiro

TOBITA Kenji

IDE Shunsuke

KAWANO Yasunori

NAGASHIMA Akira

SAKASAI Akira

SUGIE Tatsuo

VAN BLOCKLAND Arjen(*89)

IMAI Tsuyoshi

KUBO Hirotaka

NAKAMURA Hiroo

SHIMADA Michiya

TAKEUCHI Hiroshi

Plasma Theory Laboratory

TAKEDA Tatsuoki (Head)

KAWANOBE Mitsuru(*49)

NAKAMURA Masatoshi(*68)

TOKUDA Shinji

YAMAGIWA Mitsuru

KISHIMOTO Yasuaki

NAKAMURA Yukiharu

TSUNEMATSU Toshihide

KURITA Gen-Ichi

TAKIZUKA Tomonori

TUDA Takashi

Experimental Plasma Physics Laboratory

MAEDA Hikosuke (Head)

AIKAWA Hiroshi

KAWASHIMA Hisato

MORI Masahiro

OGAWA Hiroaki

SEIKE Takamitsu(*79)

TAMAI Hiroshi

HOSHINO Katsumichi

MAENO Katsuki

MIURA Yukitoshi

OGAWA Toshihide

SHIINA Tomio

UEHARA Kazuya

KAWAKAMI Tomohide

MATSUDA Toshiaki

ODAJIMA Kazuo

OHASA Kazumi

SHOJI Teruaki

YAMAUCHI Toshihiko

Department of Fusion Facility

TANAKA Yuji (Director)

OHTA Minoru (Deputy Director)

Fusion Facility Administration Division

HINO Shuhji (General Manager)

JT-60 Facility Division I

SHIMIZU Masatsugu (Head) (To December)

KONDO Ikuo (Head) (From January)

AKASAKA Hiromi

AKIBA Kenichi(*79)

MATSUKAWA Makoto

HONDA Mitsuteru(*38)

HUMPHREYS David(*6)

ICHIGE Hisashi

IKEDA Yukiharu

ISAJI Nobuaki(*39)

ISAKA Masayoshi

KAWAMATA Youichi

KIMURA Toyoaki

KURIHARA Kenichi

TAKAHASHI Minoru

MUTOH Mitugu

NAGASHIMA Toshiyuki

NOBUSAKA Hiromichi(*28)

OMORI Kenichiro

OMORI Shunzo

OMORI Yoshikazu

YONEKAWA Izuru

SEIMIYA Munetaka

ARAKAWA Kiyotsugu

MATSUZAKI Yoshimi

TANI Takashi

TERAKADO Tsunehisa

TOTSUKA Toshiyuki

YAGYUU Jyunichi

YAMAGISHI Koujiro

YASUDA Taizou(*28)

JT-60 Facility Division II

KONDO Ikuo (Head) (to December)

SHIMIZU Masatugu (Head) (from January)

ANDO Toshiro

HONDA Masao

JIMBOU Ryutaro

KOIKE Tsuneyuki

MIYO Yasuhiko

SAIDOH Masahiro

SUNAOSHI Hidenori

TSURUMI Satoshi

ARAI Takashi

HORIIE Hiroshi

KAMINAGA Atsushi

MIYACHI Kengo

NAKAFUJI Takashi

SASAJIMA Tadashi

TAKASAKI Manabu

YAMAMOTO Masahiro

HIRATSUKA Hajime

HOSHI Shizuo

KODAMA Kozo

MIYAKE Kazuyuki

OGIWARA Norio

SASAKI Noboru

TANAKA Takejiro

YOSHIOKA Yuji

RF Facility Division

YAMAMOTO Takumi(Head)

ANNOH Katsuto

KITAI Tatsuya(*28)

NIHONMATU Yuuju(*28)

SHINOZAKI Shinichi

TAKAHASHI Shunji

TERAKADO Masayuki

FUJII Tsuneyuki

KIYONO Kimihiro

SAWAHATA Masayuki

SUGANUMA Kazuaki

TAKASA Akira

YOKOKURA Kenji

IKEDA Yoshitaka

MORIYAMA Shinichi

SEKI Masami

SUZUKI Norio

TAKAYASU Toshio

NBI Facility Division

KUNIEDA Shunsuke(Head)

AKINO Noboru

ITO Masaru(*31)

KOMATA Masao

MIZUNO Makoto

OHUCHI Yutaka

SUZUKI Yasuo(*28)

USUI Katsutomi

KURIYAMA Masaaki(Duputy Head)

EBISAWA Noboru

KAWAI Mikito

KOIZUMI Junichi(*4)

MOGAKI Kazuhiko

OOHARA Hiroshi

SHIMIZU Kazuhiko(*57)

YAMAZAKI Takesi(*28)

ITOH Takao(To November)

KASHIMURA Takanori(*30)

MATSUOKA Mamoru

OHGA Tokumichi

SATO Fujio(*28)

USAMI Hiroji(*86)

JFT-2M Facility Division

SUZUKI Norio (Head)
 HASEGAWA Koichi
 KIKUCHI Kazuo
 SAITO Masaya (*30)
 TANI Takashi

HONDA Atsushi
 KOMATA Masao
 SHIBATA Takatoshi
 TOKUTAKE Toshikuni

KASHIWA Yoshitoshi
 OKANO Fuminori
 SUZUKI Sadaaki

Department of Fusion Engineering Research

SHIMAMOTO Susumu (Director)

KANAZAWA Tetsuo (Administrative Manager)

Plasma Engineering Laboratory

MURAKAMI Yohio(Head)
 ABE Tetsuya
 HIROKI Seiji

KASAI Satoshi
 OBARA Kenjiro

HAMAZAKI Masanori(*1)

Superconducting Magnet Laboratory

TSUJI Hiroshi (Head)
 ANDO Toshinari
 HIYAMA Tadao
 YASUKAWA Yukio(*58)
 WADAYAMA Yoshihide(*2)
 MIYAKE Akihiro(*14)
 TAKAHASHI Tsuyoshi(*2)
 NAKAJIMA Hideo
 HANAWA Hiromi(*30)

NISHI Masataka
 KAWANO Katsumi
 TAKAHASHI Yoshikazu
 KATO Takashi
 SUGIMOTO Makoto
 HOSONO Fumikazu(*87)
 TSUKAMOTO Hideo(*2)
 SEKI Shuichi(*30)

SASAKI Tomoyuki(*4)
 YOSHIDA Kiyoshi
 KOIZUMI Norikiyo
 IWAMOTO Shuichi (*23)
 EBISU Hideki(*18)
 OKUNO Kiyoshi
 OSHIKIRI Masayuki

NBI Heating Laboratory

OHARA Yoshihiro(Head)
 AKIBA Masato
 HANADA Masaya
 Smid Ivica(*88)
 OKUMURA Yoshikazu
 TANAKA Masanobu(*2)
 YOKOYAMA Kenji

ARAKI Masanor
 IIDA Kazuhiro
 ISE Hideo (*16)
 SUZUKI Satoshi
 TANAKA Shigeru

DAIRAKU Masayuki
 INOUE Takashi
 NAKAMURA Kazuyuki
 TANAKA Hideki(*59)
 WATANABE Kazuhiro

RF Heating Laboratory

NAGASHIMA Takashi(Head)
 SHIHO Makoto
 SAIGUSA Mikio
 WATANABE Akihiko(*40)

TSUNEOKA Masaki
 MAEBARA Sunao
 FUJITA Hideo(*25)

SAKAMOTO Keishi
 KASUGAI Atsushi
 KIKUCHI Masaya(*25)

Tritium Engineering Laboratory

NARUSE Yuji (Head)
 AMANO Junzo(*23)
 HIRATA Kazuhiro(*29)
 ITO Hideki(*16)
 KURASAWA Toshimasa
 OBATA Hiroyuki(*16)
 OKUNO Kenji
 WATANABE tetsurou(*16)
 YOSHIDA Hiroshi

ENOEDA Mikio
 HONMA Takashi
 KAJIURA Souji(*2)
 MATSUDA Yuji
 OHARA Atsushi(*4)
 SHU Wei Min(*35)
 YAMADA Masayuki

HAYASHI Takumi
 INOUE Masahiko(*23)
 KONISHI Satoshi
 NAKAMURA Hirofumi
 OHIRA Shigeru
 SUZUKI Takumi
 YAMANISHI Toshihiko

Reactor Structure Laboratory

SHIMAMOTO Susumu (Head)
 TADA Eisuke
 SHIBANUMA Kiyoshi
 SATO Satoshi
 OKA Kiyoshi

OBARA Kenjiro
 KURASAWA Toshimasa
 KANAMORI Naokazu(*2)
 NAKAHIRA Masataka

NISHIO Satoshi
 KAKUDATE Satoshi
 TERAKADO Takuya (*31)

Fusion Reactor System Laboratory

SEKI Yasushi (Head)
AOKI Isao

Fusion Experimental Reactor Team

MATSUDA Shinzaburo(Head)
FUJISAWA Noboru
HOTTA Masataka (*58)
KOIZUMI Kouichi
MATOBA Tohru
OKAZAKI Takashi (*2)
SAJI Gen (*7)
SEKI Shogo
SHIMOMURA Yasuo
YAMAMOTO Shin

HASHIMOTO Toshiyuki(*16)
KANO Yoshinori(*83)
KONDOH Mitsunori(*4)
MURAKAMI Yoshiki (*4)
OOKAWA Yoshinao
SATO Satoshi
SHIBUI Masanao(*4)
SUGIHARA Masayoshi

HORIIKE Hiroshi
KIMURA Haruyuki
KURODA Toshimasa (*16)
NOMURA Yukio (*17)
SASAKI Takashi(*15)
SAWA Masafumi (*14)
SHIMIZU Katsusuke (*23)
TAKATSU Hideyuki

- *1 General Atomics, USA
- *2 Hitachi Ltd.
- *3 Lawrence Livermore National Laboratory, USA
- *4 Toshiba Corp.
- *5 Max-Planck Institute für Plasmaphysik, FRG
- *6 Massachusetts Institute of Technology, USA
- *7 Mitsubishi Atomic Power Industry Inc.
- *8 The University of Tokyo
- *9 Nagoya University
- *10 Okayama University
- *11 Kyoto University
- *12 Hiroshima University
- *13 Institute für Reaktorbauelemente, KfK, FRG
- *14 Ishikawajima-Harima Heavy Industries, Ltd.
- *15 Mitsubishi Electric Co., Ltd.
- *16 Kawasaki Heavy Industries
- *17 Hazama-gumi Ltd.
- *18 Kobe Steel Ltd.
- *19 Oak ridge National Laboratory, USA
- *20 Century Research Center Corp.
- *21 Northwestern Laboratory
- *22 Institute of Plasma Physics, Nagoya University
- *23 Mitsubishi Heavy Industry Ltd.
- *24 NAIG Nuclear Research Laboratory
- *25 Japan Atomic Industrial Forum
- *26 Central Research Institute for Electric Power
- *27 NEC Co.
- *28 Kaihatsu Denki Co.
- *29 Sumitomo Heavy Industry Co.
- *30 Nuclear Engineering Co., Ltd.
- *31 Tomoe Shokai
- *32 Ibaraki Kohsan
- *33 Tokyo Nuclear Service Co., Ltd.
- *34 ULVAC Co.
- *35 Kyushu University
- *36 Contract Researcher
- *37 Princeton Plasma Physics Laboratory, USA
- *38 LITEC Co., Ltd.
- *39 Japan Expert Clone Corp.
- *40 Nissei Sangyo Co., Ltd.
- *41 JET Joint Undertaking, UK
- *42 Hodaka Seiki Ltd.
- *43 Sumitomo Electric Industry Co.
- *44 Nikon Corp.
- *45 National Laboratory for High Energy Physics
- *46 Tsukuba University
- *47 Los Alamos National Laboratory, USA
- *48 Japan Radiation Engineering Co.
- *49 MEITEC Co., Ltd.
- *50 Osaka University
- *51 Imperial College, UK
- *52 Institute of Research Hydro-Quebec, Varenns, Canada
- *53 KFA-IPP, FRG
- *54 Ewic Engineering Co., Ltd.
- *55 ORC Manufacturing Co., Ltd.
- *56 Koike Sanso Kogyo Co., Ltd.
- *57 Hitachi Sanso Co., Ltd.
- *58 Fuji Electric Co., Ltd.

- *59 Nissin Electric Co., Ltd.
- *60 Sandia National Laboratories, USA
- *61 JGC Corp.
- *62 Tokyo Institute of Technology
- *63 Nuclear Research Center Karlsruhe, FRG
- *64 Argonne National Laboratory, USA
- *65 ITER Team
- *66 Yokohama National University
- *67 Nihon Software Kaihatsu, Inc.
- *68 Kanazawa Computer Service Corp.
- *69 University of California at Los angeles, USA
- *70 University of Texas, USA
- *71 Varian Company Co., Ltd.
- *72 Nagaoka University of Technology
- *73 Denki Kogyo Co., Ltd.
- *74 The NET Team
- *75 National Institute for Fusion Science
- *76 I. V. Kurchatov Institute of Atomic Energy
- *77 Keio University
- *78 Mitsubishi Cable Industries, Ltd.
- *79 Nippon Advanced Technology Co., Ltd.
- *80 Hamamatsu Photonics KK
- *81 University of California at San Diego, USA
- *82 University of Maryland
- *83 Atomic Data Service Corp.
- *84 Nihon Houshasen Engineering Co., Ltd.
- *85 ACE
- *86 Hitachi works
- *87 Hitachi Cable, Ltd.
- *88 Austrian Research Center Seibersdorf
- *89 STA Fellowship
- *90 JAERI Fellowship